

# Fractal Aggregation in Relation to Formation and Properties of Particle Gels

*Aan mijn ouders*

Promotoren: dr. ir. P. Walstra,  
hoogleraar in de zuivelkunde

dr. B. H. Bijsterbosch  
hoogleraar in de fysische- en kolloïdchemie

Co-promotor: dr. T. van Vliet  
universitair hoofddocent in de levensmiddelen-  
natuurkunde

01108301-32

L.G.B. Bremer

# Fractal Aggregation in Relation to Formation and Properties of Particle Gels

**Proefschrift**

ter verkrijging van de graad van  
doctor in de landbouw- en milieuwetenschappen,  
op gezag van de rector magnificus,  
dr. H.C. van der Plas,  
in het openbaar te verdedigen  
op woensdag 22 januari 1992  
des namiddags te vier uur in de aula  
van de Landbouwwuniversiteit te Wageningen

01108301-32  
01108301-32  
01108301-32

# Table of Contents

## I Introduction

1.1 General introduction.....	1
1.2 Factors controlling gelation .....	4
1.3 Outline of this thesis.....	8
1.4 References .....	10

## II Theory of Fractal Aggregation

2.1 Introduction .....	12
2.2 Computer simulations.....	14
2.3 The model.....	17
2.4 Some consequences of the model.....	20
2.4.1 The critical volume fraction .....	20
2.4.2 Permeability .....	22
2.4.3 Geometric structure and correlation function.....	24
2.4.4 Turbidity and (light) scattering.....	25
2.5 References .....	28

## III Materials and methods

3.1 Materials .....	30
3.2 Preparation of the gels.....	32
3.3 Permeability measurements.....	35
3.4 Determination of the geometry of the gel network.....	36
3.4.1 Confocal scanning laser microscopy.....	36
3.4.2 Correlation analysis .....	38
3.4.3 The grid method.....	39
3.5 Turbidity measurements .....	42
3.5.1 The change in turbidity during aggregation.....	42
3.5.2 Turbidity measurements on gels .....	44
3.6 References .....	45

## IV Formation and Geometric Structure of Particle Gels

4.1 Aggregation experiments.....	47
4.1.1 Casein particles.....	47

## Stellingen

- 1 Doordat percolatiemodellen voorbij gaan aan de beweeglijkheid van deeltjes en clusters en doordat de meeste modellen gebaseerd op de Smoluchowski-vergelijkingen geen rekening houden met de ruimtelijke opbouw van vlokken, resulteert het gebruik van deze modellen voor de beschrijving van gelvorming door deeltjes vaak in misverstanden en soms in onzin.

Dit proefschrift

- 2 De door percolatiemodellen voorspelde algemene kritieke volumefractie beneden welke gatering niet mogelijk is, bestaat niet in het fractale model en wordt in de praktijk niet gevonden.

Dit proefschrift, hoofdstukken 2 en 4, stelling 1

- 3 De bewering dat een gel alleen kan ontstaan indien de exponent,  $\tau$ , in de frequentieverdeling van het aantal deeltjes per cluster,  $N(n) \propto n^{-\tau}$ , groter is dan 2 is onjuist. In de praktijk zal een monodisperse cluster grootteverdeling gatering juist in de hand werken.

J.E. Martin and B.J. Ackerson, *Phys. Rev. A*, **31**, 1180, (1985)

Dit proefschrift, hoofdstukken 2 en 4, stelling 1

- 4 De halveringstijd, d.w.z. de tijd waarin het aantal deeltjes door vlokking is afgenomen tot de helft van het initiële aantal, wordt vaak ten onrechte vloktijd genoemd.

Dit proefschrift, hoofdstuk 6, stelling 1

- 5 Volgens Kendall et al. streven clusters naar maximalisatie van hun vrije energie.

K. Kendall, N. McN. Alford, W.J. Clegg and J.D. Birchall, *Nature*, **339**, 130, (1989)

- 6 De hoeveelheid treinsegmenten van geadsorbeerde polymeer moleculen is gevoeliger voor de adsorptie-energie dan de staartsegmentdichtheid dat is.

G.P. van der Beek, M.A. Cohen Stuart and T. Cosgrove, *Langmuir*, **7**, 49, (1991)

- 7 De bijdrage van texture profile analysis (TPA) aan een goede karakterisering van de mechanische eigenschappen van levensmiddelen is eerder negatief dan positief geweest.
- 8 In tegenstelling tot de moderne chemie kan men de fysische chemie de chemie van de toekomst noemen.  
W. Ostwald, *Zeitschrift für Physikalische Chemie*, 1, 1, (1887)
- 9 Een grote feitenkennis werkt remmend op het verrichten van onderzoek.
- 10 Het is onmogelijk om naar het verleden te reizen of in de toekomst te kijken. Iedereen kijkt in het verleden en reist naar de toekomst.
- 11 De regel dat je gewicht moet liggen onder het aantal kilo's verkregen door je lengte in meters in het kwadraat met 25 te vermenigvuldigen gaat uit van personen met een effectieve fractale dimensionaliteit van 2 en is dus oppervlakkig.
- 12 Reologische metingen met ondeugdelijke apparatuur zijn altijd "constant stress" experimenten.
- 13 Dit is een van de weinige stellingen over het oostblok die ten tijde van de promotieplechtigheid met zekerheid te verdedigen valt.

Leon Bremer

**Fractal Aggregation in Relation to Formation and Properties of Particle Gels**

Wageningen, 22 januari 1992

4.1.2 Polystyrene particles .....	48
4.1.3 Emulsions.....	53
4.1.4 Haematite particles.....	54
4.2 Permeability.....	55
4.3 Confocal scanning laser microscopy.....	60
4.4 Turbidity measurements .....	71
4.5 References .....	76

## **V Rheological Properties of Particle Networks**

5.1 Introduction .....	77
5.2 The modulus of gels with stretched strands.....	81
5.2.1 Introduction.....	81
5.2.2 The model.....	82
5.2.3 Extensional deformation.....	87
5.3 On the fractal nature of acid casein gels.....	89
5.3.1 Introduction.....	89
5.3.2 Theory .....	91
5.3.3 Materials and methods .....	95
5.3.4 Results.....	97
5.3.5 Discussion .....	99
5.3.6 Appendix.....	102
5.4 Rheological behaviour of gels of polystyrene particles.....	105
5.4.1 Introduction .....	105
5.4.2 Materials and methods .....	105
5.4.3 Results.....	107
5.4.3.1 Formation and ageing of the gels .....	107
5.4.3.2 Strain sweep measurements.....	109
5.4.3.3 Dynamic moduli versus frequency .....	111
5.4.3.4 Dynamic moduli versus volume fraction.....	112
5.4.4 Discussion .....	114
5.5 References .....	119

## **VI Aggregation Kinetics Related to the Observation of Instability**

6.1 Introduction .....	121
6.2 Diffusion limited aggregation.....	123
6.3 Complications .....	125
6.3.1 Floccs instead of smooth spheres.....	125
6.3.2 Interactions between particles.....	128
6.3.3 Polydispersity.....	130

6.3.4 The effective volume fraction.....	131
6.3.5 Velocity gradients .....	133
6.3.6 Sedimentation.....	135
6.4 Some aggregation times .....	138
6.5 Reaction limited aggregation.....	147
6.6 Floc break up and rearrangements .....	151
6.7 Conclusions.....	154
6.8 References .....	157

## **VII Factors Disturbing Gelation and Altering Gel Structure**

7.1 Introduction .....	159
7.2 Gravity.....	159
7.2.1 Effects of sedimentation and creaming.....	159
7.2.2 Collapse of the network under its own weight.....	163
7.2.3 Changes of the rheological properties of the gel.....	165
7.3 Velocity gradients .....	168
7.4 Rearrangements.....	170
7.4.1 Rearrangement of clusters of colloidal particles.....	170
7.4.2 Rearrangements after gelation, microsineresis.....	175
7.6 References .....	180
General Reflections and Suggestions for Further Research .....	181
List of symbols.....	184
Some terms and abbreviations used in this study.....	188
Summary.....	189
Samenvatting .....	194
Curriculum vitae .....	200
Nawoord.....	201



# I Introduction

## 1.1 General introduction

To gel or not to gel, that is the question on which this work is meant to give the clue. Sometimes aggregation of colloidal particles leads to a gel, and sometimes to a sediment. In spite of the tremendous importance of this difference, not in the last place for industrial purposes, still not much is known about the factors determining whether a system containing colloidal particles will gel or not. In general, aggregation leads to rather irregular-shaped aggregates which, potentially, may completely occupy the available volume, leading to a gel. Factors like sedimentation, velocity gradients in the aggregating dispersion and rearrangements of the flocs may, however, disturb this process. The ability to gel varies widely among different colloidal systems. Plastic fats (fat crystals in oil) and pulp particles in beverages like orange juice [1], gel at very low concentrations whereas emulsions seldom form a gel unless their volume fraction exceeds about 0.2.

The term 'gel' has traditionally been used rather loosely for various combinations of substances. Gels formed by the aggregation of particles may be mentioned as one of them, but even within this group, the gel properties vary widely as may be illustrated by comparing two members of this group; orange juice and silica gel! Another group of gels is constituted by networks consisting of long, flexible macromolecules, partially cross-linked by covalent bonds, microcrystalline domains, entanglements or other linkages. These gel types have traditionally been subject to more extensive studies, which resulted in the classical theory of gelation of Flory [2] and Stockmayer [3], and in percolation theories [4]. These theories have also been applied to particle networks [5 - 7] and they are even successful in fitting experimental results. For being successful it is, however, necessary to introduce some misty factors like a critical volume fraction (corresponding to a percolation threshold) and appropriately chosen polyfunctional structural elements [7]. For gels that are formed by the aggregation of particles the critical volume fraction is mainly dependent on the accuracy of the measurement and on factors like

convection currents in the sample. Consequently, the use of these theories does not contribute to a better understanding and insight in the formation of a particle network. A third group of gels is composed of fairly small, amphiphilic molecules which may associate into a gel. These types of gels are well ordered and also called liquid crystalline phases. A concentrated dispersion of (electrostatically) repulsive colloidal particles, may also be classified in this group because it exhibits a similar, well ordered structure. In this gel type the particles are not connected geometrically, but there is strong repulsive interaction which leads to a high packing density of the 'effective' hard-spheres whose interaction size is considerably larger than the particle geometrical size [8, 9].

Due to this huge variety of gels it is difficult to give a general definition of a gel [10]. Flory did spend a few pages of text in an introductory lecture [11] reviewing different definitions and general properties of gels. A gel may be defined as a continuous three-dimensional network of connected molecules or particles in a continuous liquid phase [12]. This definition would, however, exclude concentrated dispersions of repulsive particles, which are not connected geometrically. IUPAC (1972) says 'A gel is a colloidal system with a finite, usually rather small, yield stress. Materials such as silica gel which have passed a gel stage during preparation are improperly called gels. The term xerogel is used for such dried out open structures; and also for dried out compact macromolecular gels such as gelatin or rubber. The term aerogel is used when the openness of the structure is largely maintained'.

The one feature identified almost universally as an essential characteristic of a gel is its solid-like behaviour, a gel is characterized as having a yield stress at the considered time scale. Even this characteristic is, however, somewhat arbitrary; most people do not think of orange juice as being a solid [1], and on the other hand, cheese, which may also be classified as a gel, sometimes does not have a yield stress [13]. A better characteristic of solid-like behaviour is the preponderance of elastic over viscous properties which varies widely among different gels. Since both the yield stress and the ratio between the elastic and viscous properties are dependent on the time scale, it is possible that a material is a gel on a short, but fluid-like on a longer time scale.

Gelation of colloidal particles or polymers is characterized by a transition from a liquid to a solid state. At the 'gel point' there is a critical state between liquid and solid. For the determination of the gel point a criterion is needed to distinguish whether the system is liquid, before the gel point, or solid, after the gel point. The most simple approach is to define the gel point as the point where elastic properties become just preponderant over viscous properties; i.e.  $\tan \delta$  becomes smaller than one. With this definition, the gel point is dependent on the frequency of the measurement,  $\omega$ . Another definition of the gel point is the point where a permanent, three dimensional network is just formed. However, the detailed structure of a network may change continuously and one might disagree about how long the network must keep the same structure to call a system a gel. Winter and Chambon used another criterion which enabled an accurate determination of the instant of gelation of permanent gels [14, 15]. They found that linear viscoelasticity reduces to a simple, universal power law behaviour in which  $G$  scales like  $\omega^n$  after the gel point. The relaxation exponent,  $n$ , may vary between 0 and 1. At the gel point  $\tan \delta$  is independent of the frequency  $\omega$ .

The type of gels considered in this thesis are so-called particle gels in which a network formed after the aggregation of colloidal particles causes the solid-like properties. This group of gels may be divided in several subtypes, according to the properties of the particles (e.g. anisotropy), the gelation being reversible or not, and changes after gelation like syneresis. In this thesis any system that aggregates into a space-filling network is designated gel as distinct from a sediment which is not space-filling, but according to most other definitions also a gel. An important geometrical difference which particle gels show in comparison with macromolecular gels is the length of their strands relative to their thickness. In a typical macromolecular gel, the chains are, in general, thin compared to their length and can assume numerous conformations due to Brownian motion. The main cause of resistance against permanent deformation is a decrease in the number of possible conformations, i.e., a decrease in entropy. The modulus of elasticity is then proportional to  $kT$  for these gels (rubber theory). For the relatively thick strands of a particle network the value of  $kT$  per strand is negligible in comparison with the energy involved in the deformation of atomic or physical bonds in the

strand. Deformation of a particle gel is thus, mainly, an enthalpic process. A consequence of this difference is that the linear region, i.e. the region over which stress and strain are proportional, is much smaller in the case of particle gels [12]. Moreover, a particle gel is mostly much shorter, i.e. it fractures at a smaller deformation. Another property on which many particle gels may be distinguished from both other types, is the ability to swell. Both macromolecular gels and liquid crystalline phases are, in general, capable of swelling in the presence of a liquid such as water, benzene, etc. (good solvent). In general, irreversible particle gels do not show this behaviour because of their enthalpic nature (unless the building blocks swell).

The classification of a gel is not always simple. For example casein, which is extensively used in this work, consists of macromolecules. These macromolecules are, however, associated into particles which may aggregate and form a particle network.  $\beta$ -lactoglobuline and bovine serum albumin gels look, on electron micrographs, sometimes like particle networks [16 - 18]. They may nevertheless behave somewhat like macromolecular gels. On the other hand pectin gels are macromolecular gels with stiff chains and deformation leads here mainly to enthalpic changes. Gels made of clay particles may either be classified in the group of particle networks, or in the liquid crystalline group, depending on whether the particle-particle interactions are attractive or repulsive. Often commercial products like food-stuffs and pharmaceutical or cosmetic articles, such as ointments or creams, consist of more than one gel type. For example, some whipped emulsions consist of a network of aggregated particles which is stable due to a liquid crystalline gel phase at the oil-water interface of the emulsion droplets [19].

## **1.2 Factors controlling gelation**

There is still hardly any general, quantitative knowledge about conditions controlling the gelation of particles, but many factors promoting or hindering gelation are known:

- Particle interactions. One of the most extensively studied subjects in colloid chemistry is that of the interactions between particles. The classical factors in the description of interactions are the van der Waals attraction and the electrostatic repulsion. A quantitative description has been given in the well-known DLVO theory [20, 21]. This theory predicts that coagulation may occur in a so called secondary minimum, where the separation of two aggregated particles is relatively large (about 5 nm, non-touching), or in a primary minimum at very small separations (about 1 nm, touching). The depth of the secondary minimum, i.e. the interaction free energy, can be estimated and is often considered low compared to the primary minimum. Secondary minimum flocculation may thus result in weak, flexible bonds. At short separations, less than about 1-2 nm, short range interactions like hydration forces are effective [22]. These short range interactions are not incorporated in the DLVO theory and the position (and thus the depth) of this minimum cannot be predicted. Slight alterations in the effective distance of closest approach have a large effect on the energy of interaction. This distance is not only determined by general factors like the salt concentration, but also by rather specific characteristics of the system of interest like the presence of surface irregularities. Moreover, DLVO theory only considers interaction forces normal to the surface; the particles are, theoretically, free to move lateral. In practice, interaction forces lateral to the surface hinder rolling, slipping and rotation of particles with respect to each other. Again, the presence of surface irregularities is important, but difficult to quantify. The strength of the bonds may increase with time [23, 24] and fusion or sintering of the particles may occur leading to an increase of the stiffness of the flocs.

Another type of interactions occur in the case of particles with adsorbed polymers. Protruding loops and tails of the polymer may adsorb on other particles if there is some free surface available on the particles. This process is called bridging flocculation.

Interaction forces affect the strength and the stiffness of the flocs and thereby their ability to form a gel. Weak flocs rearrange easily into more compact structures which may settle before they fill the system. A network of weak flocs may collapse due to gravity or coarsen due to bond-breaking inside the network. Stiff, irreversible bonds or the presence of a

limited amount of reactive places on the particles hinder rearrangement of the flocs or the gel network and thus promote gelation. In addition to the interaction forces between the particles, the stiffness of the particles themselves may affect the stiffness of flocs and gel network and thus the ability to gel.

- Geometric structure of aggregates and particles. Traditionally, particle gels have often been modelled as consisting of 'strings of beads'. The formation of strings of particles promotes gelation and it has been shown that attachment of new particles at the ends of a string is sometimes, energetically, favourable [25]. These simple models enable a quantitative description of gel formation and of properties like pore size [26] and modulus of elasticity [27, 28]. The most simple version of these models, a cubic array of strands, predicts, however, pore sizes which are much too small and moduli which are much too high compared with experimental data. Moreover, a linear relationship between the modulus and the particle concentration has been derived from these models, but has never been found in practice. In order to make these models practically applicable, the introduction of correction factors, which consider a fraction of particles not contributing to the strands and some degree in randomness of the spatial distribution of the strands, is necessary.

Substantial progress in the understanding of aggregation and gelation phenomena has been made since the development of numerical simulation of the aggregation and the introduction of the concept of fractal geometry [29]. The previous 'string of beads' models are characterized by a dimensionality of 1 in the terms of a fractal model. Mostly, aggregation does not lead to strings, but to more or less open, on average spherical flocs. The volume fraction of particles in the floc decreases with increasing size. These flocs may be characterized by a higher, so called fractal dimensionality as will be clarified later on. The geometric structure of the aggregates is a very important factor to which much attention will be paid in this thesis.

In addition to the geometric structure of the flocs, the size and anisotropy of the primary particles is important. Small particles have, in general, a higher probability to form a gel because disturbances of the

gelation have less effect on small flocs. Anisometry of the particles leads to more ramified flocs and thus promotes gelation.

- Disturbances of the gelation; factors like shear or convection currents and sedimentation. It is well known that velocity gradients, for example caused by stirring, may prevent gelation. On the other hand, small convection currents caused by temperature gradients, may prevent sedimentation and thus promote gelation. Gelation is more likely if the disturbances are small or if the system is not very sensitive to them, e.g. small particles and a small density difference between the particles and the medium.

- Kinetics of aggregation and gelation, the time needed to form a space-filling structure. Rapid aggregation promotes gelation because it decreases the time in which the flocs may sediment, cream or rearrange to more compact flocs. Flocs which are formed due to diffusion limited aggregation tend to have a more open, ramified structure than flocs formed during slow aggregation. Another major kinetic factor is the evolution of the cluster size distribution; a narrow size distribution has a higher probability to gel than a broad distribution because the resulting network is more homogeneous and thus stronger. A high volume fraction of the particles increases the probability of gelation because the time needed to fill the system and the effect of disturbances is relatively small, and because the gel is relatively strong and resistant against uniaxial compression.

- Size, shape and properties of the vessel. If a network does not adhere to the wall of the container it may exhibit uniaxial compression under its own weight [30]. If the size of the vessel is not large enough compared to the size of the particles no network can be formed simply because there is not enough material (this will be shown later on).

All these factors may be interrelated which makes gelation an intricate subject. It would be a hopeless task to describe all factors, not to mention to quantify them. It is well known that, for instance, the salt concentration or the temperature affect the interaction between particles or the kinetics of aggregation. Less is known, however, about the influence of the geometric structure of the aggregates on the kinetics of

aggregation (and vice versa) and about many other factors which, nevertheless, may have a great effect on gelation (e.g. lateral interaction forces, kinetics of sintering, convection currents).

After the gel has been formed there are more complications. Characteristic for a particle network is the possibility of the formation of numerous additional bonds if the particles in the strands would have the opportunity to approach particles in other strands. This process, presumably, occurs mainly shortly after the gel point is reached; the process itself causes the rigidity of the network to increase, which, in turn, soon makes it much more difficult for still more bonds to be formed. In other words, such a rearrangement may stop itself, and the gel may reach a meta-stable stage, but before this stage the gel may have changed substantially. Moreover, some gels do not reach such a stage at all and are subject to syneresis; the network tends to shrink due to the formation of extra bonds between the strands, thus expelling the continuous phase. Syneresis is supported by external factors like deformation of the gel. Quite often aggregation leads, in first instance, to a network which is, however, unstable and collapses due to syneresis or gravity. If the gel is fixed to the walls of a container there is no possibility to expel the continuous phase. In that case micro-syneresis may occur which will lead to a coarsening of the network [31]. Extensive micro-syneresis may occur when the interaction energy keeping the particles in a strand together is not very high compared to  $kT$ , because initially some bonds have to break in order to give the particles in the strands the opportunity to form more new bonds.

### **1.3 Outline of this thesis**

The question whether an aggregating system will gel or not is much too comprehensive to be solved in general. It would even be a hopeless task to try and deal with all the combinations of factors controlling gelation. The main factors dealt with in this thesis are the effects of the geometric structure of the flocs and the kinetics of aggregation on the gelation and on the properties of the gel that may have been formed. Less attention is paid to the nature of the particle-particle interactions. Many



experimental results and ideas of other research-workers have been examined with a 'fractal view' and form an essential part of this thesis (e.g. [31 - 34]). The 'infrastructure' of the thesis has been affected by some publications which are fully incorporated.

In chapter II a short literature review is given on computer simulations of particle aggregation which have been performed under numerous different 'input' conditions. The results of these simulations are compared with experimental results from literature. Using the concept of fractal geometry a model is developed which describes the formation and geometric structure of a gel. Some consequences of this model will also be discussed, for instance that the size of the container relative to the size of the aggregating particles may be an important parameter. Furthermore, some consequences of this model for the resulting gel properties like permeability and turbidity are discussed.

In chapter III materials and methods are described; first of all the preparation of the gels. Further, attention is paid to permeability measurements, confocal scanning laser microscopy and turbidity measurements. The results are compiled and discussed in chapter IV. It was found that some systems are able to gel at an extremely low volume fraction of particles.

Chapter V deals with the rheology of particle gel networks. Models are derived which relate the stiffness (modulus of elasticity) and the strength (stress at which fracture occurs) to the volume fraction of the particles. Gels formed with casein, respectively polystyrene latex, particles are tested and the similarities and differences are described. It was found that gels built with the same material but with different geometric structure differ substantially (orders of magnitude) in stiffness.

In chapter VI the kinetics of aggregation and gelation are described. Traditionally, mainly the first steps of the aggregation process have received attention. In this chapter, however, attention is paid to later stages, up to gelation. The essential question is; how long will it take before the aggregation can be perceived, be it because of gelation, sedimentation, or the appearance of visible flocs. It will be shown that the evolution of the geometric structure of the flocs has a strong effect on this time.

Chapter VII pays attention to factors which disturb gelation. The effect of (gravitational) forces and velocity gradients is described (semi) quantitatively. This chapter contains also speculations on the relation between the interactions of the particles and the ability to gel and gel properties. The rate of disaggregation and rearrangement may be an important factor which is, however, hardly understood.

#### 1.4 References

- 1 T. van Vliet and A.C.M. van Hooydonk, in *Proceedings of the 9th International Congress on Rheology*, Mexico, eds. B. Mena, A. Garcia-Rejon and C. Rangel-Nafaile, Universidad Nacional Autonoma de, 1984, **4**, 115
- 2 P.J. Flory, *J. Amer. Chem. Soc.*, 1941, **63**, 3083
- 3 W.H. Stockmayer, *J. Chem. Phys.*, 1943, **11**, 45
- 4 D. Stauffer, A. Coniglio and M. Adam, *Adv. Pol. Sci.*, 1982, **44**, 103
- 5 M. Gordon, in *Integration of Fundamental Polymer Science and Technology*, ed. L.A. Kleintjens and P.J. Lemstra (Elsevier, Amsterdam, 1985)
- 6 M. Tokita, R. Niki and K. Hikichi, *J. Chem. Phys.* 1985, **83**, 2583
- 7 M. Tokita, *Food Hydrocolloids*, 1989, **3**, 263
- 8 E. Dickinson, *Chemistry & Industry*, 1 October 1990, 595
- 9 D.W. Benzing and W.B. Russel, *J. Colloid Interface Sci.*, 1981, **83**, 163
- 10 P.H. Hermans, in *Colloid Science Vol II*, ed. H.R. Kruyt (Elsevier, Amsterdam, 1949)
- 11 P.J. Flory, *Faraday Discussions of the Chemical Society*, 1974, **57**, 7
- 12 P. Walstra, T. van Vliet and L.G.B. Bremer, in *Proc. Conf. on Food Polymers, Gels and Colloids*, ed. E. Dickinson (Royal Soc. of Chem., Cambridge, 1990), 369
- 13 H. Luyten, *Ph.D. Thesis*, (Wageningen Agricultural University, The Netherlands 1988)
- 14 H.H. Winter and F. Chambon, *J. Rheol.*, 1986, **30**(2), 367
- 15 F. Chambon and H.H. Winter, *J. Rheol.*, 1987, **31**(8), 683
- 16 D.M. Mulvihill, D. Rector and J.E. Kinsella, *Food Hydrocolloids*, 1990, **4**, 267
- 17 M. Stading and A. Hermanson, *Food Hydrocolloids*, 1990, **4**, 121
- 18 S. Poole, S.I. West and J.C. Fry, *Food Hydrocolloids*, 1987, **1**, 301
- 19 J.M.M. Westerbeeck, *Ph.D. Thesis*, (Wageningen Agricultural University, Netherlands 1989)
- 20 B.V. Deryagin and L.D. Landau, *Acta Physico Chim. U.R.S.S.*, 1941, **14**, 633
- 21 E.J.W. Verwey and J.Th.G. Overbeek, in *Theory of the Stability of Lyophobic Colloids*, (Elsevier, Amsterdam, 1948)
- 22 J.N. Israelachvili, *Intermolecular and Surface Forces* (Academic Press, London, 1985)
- 23 G. Frens and J.Th.G. Overbeek, *J. Colloid Interface Sci.*, 1971, **36**, 286
- 24 G. Frens and J.Th.G. Overbeek, *J. Colloid Interface Sci.*, 1972, **38**, 376
- 25 L. Thomas and K.H. McCorkle, *J. Colloid Interface Sci.*, 1971, **36**, 110

- 26 M.P. Tombs, *Faraday Discussions of the Chemical Society*, 1974, **57**, 158
- 27 C.J. Nederveen, *J. Colloid Sci.*, 1963, **18**, 276
- 28 H. Kamphuis, R.J.J. Jongschaap and P.F. Mijnlief, *Rheol. Acta*, 1984, **23**, 329
- 29 F. Family and D.P. Landau (eds.), *Kinetics of Aggregation and Gelation*, (North-Holland, Amsterdam, 1984)
- 30 T. van Vliet and P. Walstra, in *Food Colloids*, eds. R.D. Bee, P. Richmond and J. Mingins (Royal Soc. of Chem., Cambridge, 1989)
- 31 H.J.M. van Dijk, *Ph.D. Thesis*, (Wageningen Agricultural University, The Netherlands, 1982)
- 32 S.P.F.M. Roefs, *Ph.D. Thesis*, (Wageningen Agricultural University, Netherlands 1986)
- 33 H.J.C.M. van den Bijgaart, *PhD. Thesis*, Wageningen Agricultural University, The Netherlands, 1988
- 34 P. Zoon, *PhD. Thesis*, Wageningen Agricultural University, The Netherlands, 1988

## II Theory of Fractal Aggregation

### 2.1 Introduction

In the past 10 years many scientists and mathematicians have worked on problems concerning 'order in chaos' and 'fractals'. A fractal has, in general, a sprawling tenuous pattern. As a fractal is magnified it reveals repetitive levels of detail, so that a similar structure exists on all scales; a fractal is scale invariant. Mandelbrot [1] pointed out that many disorderly objects in nature have this property. Well-known examples are coastlines; accretion of metal particles in an electrolytic bath, mountain ranges and several properties or processes varying with time, such as the weather. All these examples, which are of a bewildering complexity, can be described by surprisingly simple equations. The quantitative measure of how a fractal scales is expressed by the fractal dimensionality which is an universal property, i.e., it is independent of many details of how the object is formed. The dimensionality is related to behaviour at large scales where fluctuations are averaged out. As a consequence, a simple model, neglecting most of the complexity of a real system, may nevertheless be useful in describing the scaling properties of the system. In many fields these models are of limited interest; for instance, in meteorology one is interested in the fluctuation itself, i.e. the weather on one particular day. Fractal models are, however, very useful in describing aggregation, gelation and gel properties [2,3]. In these cases one is not interested in the spatial coordinates of a particular particle, but in the overall properties of the system.

An example of a fractal, which may be used to model a floc, is given in figure 2.1. Considering the number of particles forming the fractal, a string of beads model is characterized by a dimensionality of 1, because a magnification of the scale by a factor  $X$  results in a change of the number of particles by a factor  $X^1$ . By the same argument, the dimensionality of a plane filled with particles is 2; increase of the scale by a factor  $X$  results in a change in the number of particles with a factor  $X^2$ . The fractal in figure 2.1 has a fractal dimensionality which equals  $\log_5/\log_3$  (approximately 1.46) which is a fraction of the Euclidian dimension. This

explains the term fractal dimensionality. The scaling behaviour does not apply to all length scales in a real system. The fractal in figure 2.1 is characterized by an upper cut-off length ( $R$ ) which equals the radius of the cluster and a lower cut-off length ( $a$ ), equal to the radius of the primary particles. The fractal dimensionality ( $D$ ) does apply to length scales between  $a$  and  $R$ .

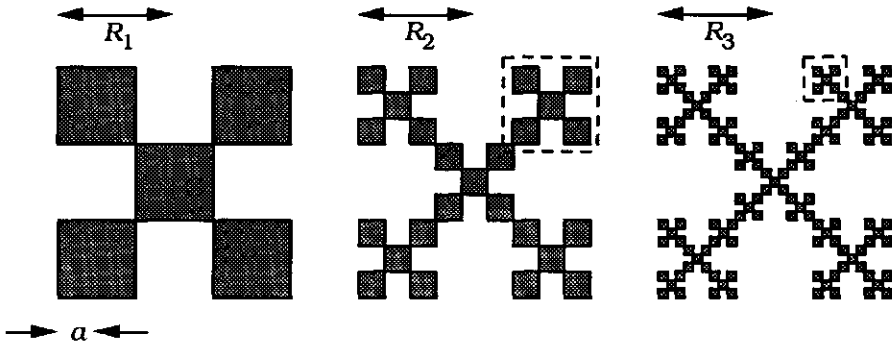


**Fig. 2.1** Examples of two-dimensional deterministic fractals of various size and magnification. The fractals may be used to model a floc.

For the number of particles in a fractal floc  $N_p$  we may write [3]:

$$N_p = \left(\frac{R}{a}\right)^D \quad (2.1)$$

A property of a three-dimensional fractal floc is that its density decreases as its size increases because  $D$  is smaller than 3. Real flocs are, in general, fractals in a statistical sense. These stochastic fractals are not exactly scale invariant like the deterministic fractals of fig. 2.1., i.e., a part of a stochastic fractal is not an exact copy of the fractal itself. However, on average a part of a stochastic fractal shares statistical properties with the fractal itself. Examples, taken from the work of Weitz et al. [2, 4], are shown in fig. 2.2. These are projections of (3 dimensional) clusters of gold particles which exhibit a very ramified, fractal structure. Eqn. 2.1 does apply to these flocs. Parts of the large floc in fig. 2.2 that are magnified have on average the same geometric structure as the smaller flocs and as the large floc itself. Aggregation of clusters leads automatically to the

repetitive levels of detail that are characteristic for fractals because small clusters aggregate into larger clusters that on their turn aggregate further.

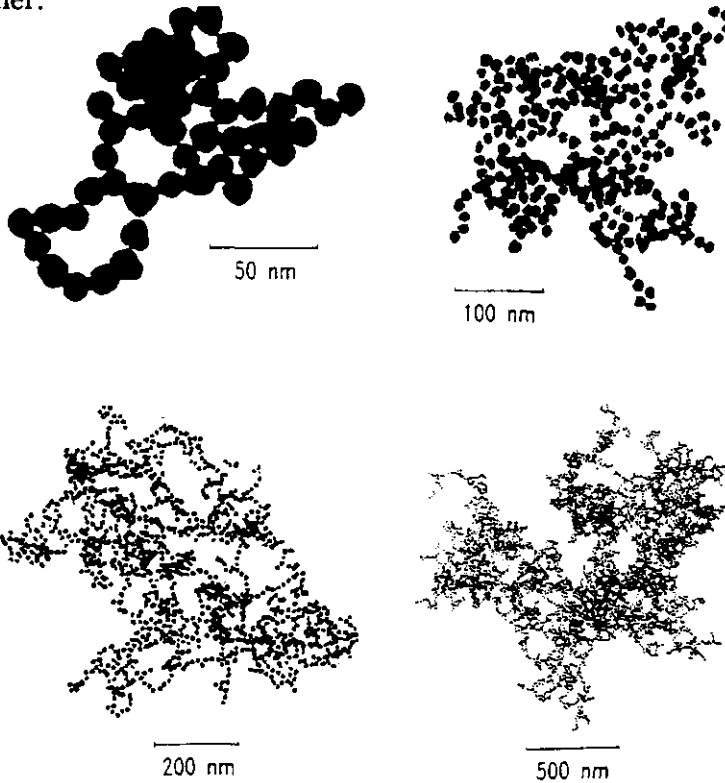


**Fig. 2.2** *Electron micrographs of clusters of gold particles with varying sizes at varying magnifications (taken from Weitz et al [2]). The projections of the three-dimensional clusters, and the clusters themselves are stochastic fractals.*

## 2.2 Computer simulations

Much of the present understanding of the relation between aggregation mechanisms and the resulting structure of the flocs is based on the results of computer simulations. The earliest computer simulation models by Vold [5, 6] and Sutherland [7] investigated particle-cluster aggregation via linear trajectories. The resulting structures are porous,

but uniform on sufficiently long length scales; i.e., the fractal dimensionality (almost) equals the Euclidian number of dimensions. This implies a rather high volume fraction of particles in the flocs. Simulated flocs which look more like the examples in figure 2.2 were obtained by Sutherland [8, 9] using cluster-cluster aggregation via linear trajectories. The concept of fractal geometry was, however, not used at that time.

Considerable interest in the simulation of aggregation has been generated by the discovery by Witten and Sander [10] that particle-cluster aggregation via Brownian trajectories leads to flocs with a well-defined fractal dimensionality which has a value of about 1.7 in 2-dimensional simulations and 2.4 in 3 dimensions. These values are independent of many details of how the floc is formed; for instance a small sticking probability, which is a simple representation of a (high) activation energy, leads to the same dimensionality at long length scales. The branches of the aggregate (small length scales) are, however, thickened. Also changes in the length of the Brownian steps (flights) does not change the dimensionality on scales larger than the Brownian steps. On smaller scales,  $D$  may vary from the long scale value to the Euclidian value which also is obtained for linear trajectories [11].

The particle-cluster models are, in general, not realistic in describing the aggregation of colloidal particles. A more realistic model which investigates cluster-cluster aggregation has been introduced, independently, by Meakin [12] and Kolb et al [13]. There is not much difference between 'Sutherlands' clusters and the new, so-called Diffusion Limited Cluster Aggregation (DLCA) clusters, because the effect of Brownian motion is negligible in comparison with the effect of cluster to cluster addition. The DLCA model is, however, very useful because it is possible to introduce numerous details on how aggregation proceeds, and because the kinetics of aggregation and the floc size distribution can be followed. A simplified simulation in which clusters are grown by consecutive diffusion of two equal sized clusters towards each other is called a hierarchical or monodisperse model. The dimensionality obtained with this model is only slightly lower than  $D$  in the case of a polydisperse model. Values obtained for  $D$  are; about 1.43 in 2-dimensional and about 1.75 in 3-dimensional simulations. These values are, again, insensitive to some details of the model, such as the way in which the cluster diffusion

coefficient depends on the number of particles in the cluster [14, 15] (provided that smaller clusters diffuse at least as rapidly as larger clusters). The fractal dimensionality in these models is, however, sensitive to the introduction of a low sticking probability [16, 17]. If this probability is thus low that, effectively, all mutual bonding configurations are sampled before aggregation of the clusters, the so-called Chemically or Reaction Limited Cluster Aggregation model (CLCA or RLCA) applies. This model results in an increase of  $D$  up to about 1.55 in 2-dimensional and 2.0 in hierarchical, 3-dimensional simulations. A low sticking probability has also a huge effect on the kinetics of aggregation. Ball et al. [18] pointed out that RLCA leads to an exponentially increasing cluster radius and a power-law cluster size distribution.  $D$  is significant higher (about 2.1) if the polydispersity of the cluster size distribution is taken into account (The process looks somewhat like particle-cluster aggregation due to the wide variation in cluster size). Probably there is a feed-back mechanism between the cluster size distribution and the fractal dimensionality [18]. The kinetics of aggregation and gelation is discussed further in chapter VI.

Other important complications, which have been studied, are the effect of random bond breaking [19] and rotational diffusion [20]. Random bond breaking does not (or hardly) affect the dimensionality, the flocs are however more compact at short length scales. Rotational diffusion decreases the fractal dimensionality of cluster-cluster aggregates [16]; the effect is, however, small in most realistic simulations. The introduction of particle-particle interaction forces in the model has, in general, no influence on the structure on large scales but it may affect the short range structure [21, 22]. Recently, simulations in which rearrangements after the cluster to cluster addition are allowed have been performed [23, 24]. These rearrangements lead to an increase of the dimensionality up to about 2.3, depending on the extent of freedom to rearrange. Similar results have been reported by Adachi and Ooi [25] who used table-tennis balls to model a floc instead of simulation on a computer. These models may be useful to predict the behaviour of flocs with flexible bonds, like flocs consisting of emulsion droplets or particles which are aggregated in the secondary minimum.



There are numerous experimental results which are in perfect agreement with computer simulations. In addition to the electron micrographs of Weitz et al. [4], small angle X-ray scattering [26] and light scattering [26 - 28] have often been used. Most simulations and experiments were carried out at low concentration. The discussion of fractal-type structures in non-dilute systems is much more complicated, due to the interpenetration of the clusters and the formation of a gel state. These gels are homogeneous on the macroscopic scale, but heterogeneous and possible of a fractal nature on smaller scales. Kolb et al. [29] have suggested that higher volume fractions of particles should lead to a higher dimensionality, owing to an increase in interpenetration between the developing clusters, leading to a dimensionality of 3 in the case of gelation. Simulations of aggregation in concentrated systems resulted in an increase of the effective fractal dimensionality with increasing concentration [21].

### 2.3 The model

The model is described on a lattice, although this is not an essential feature. Each lattice site is occupied with either a particle or a volume element solution. A fractal structure on the lattice is expressed by Eqn. 2.1. Here,  $R$  is the radius of the fractal and  $a$  is the radius of one lattice site which can be equal to the radius of one primary particle if a lattice site is of the same size as the particle size.  $D$  is the fractal dimensionality. In a real system  $R$  and  $a$  are not well defined, the aggregates are in general not spherical and the primary particles are not always monodisperse. One may, however, consider the system to be characterized by an upper ( $R$ ) and a lower ( $a$ ) cut-off length, between which scaling limits fractal geometry applies. The average radius of the primary particles is used as the lower cut-off length. This is not necessarily true but it turns out to be a good choice for most gels (see further on).

It is obvious that the total number of lattice sites that have been taken up by an aggregate ( $N_a$ ) equals  $(R/a)^3$  for a 3-dimensional lattice.

$$N_a = \left(\frac{R}{a}\right)^3 \quad (2.2)$$

The volume fraction of particles in an aggregate ( $\phi_a$ ) can thus be expressed by:

$$\phi_a = \frac{N_p}{N_a} = \left(\frac{R}{a}\right)^{D-3}, \quad (2.3)$$

implying, since  $D < 3$ , that  $\phi_a$  decreases as  $R$  increases. The fractal clusters thus grow until they jointly occupy the total liquid volume, at which moment a gel is formed. This implies that the fractal dimensionality of the aggregating clusters is retained in the gel (albeit with a slight modification: see later on), while at a scale  $\gg R$ , the gel is homogeneous and has, of course, a dimensionality of 3. Mathematically, the sum of all sites occupied by the individual fractal aggregates  $\sum N_{a,t}$  will be equal to the total number of lattice sites in the gel ( $N_t$ ):

$$\sum N_{a,t} = N_t \quad (2.4)$$

and:

$$\sum \phi_{a,t} N_{a,t} = \phi_0 N_t \quad (2.5)$$

Here  $\phi_0$  is the overall volume fraction of the particles and  $N_t$  is the total number of aggregates. Combination of the equations 2.1 to 2.4 leads to:

$$\phi_0 = \frac{\sum R_i^D}{a^{D-3} \sum R_i^3} = \left(\frac{R_g}{a}\right)^{D-3} \quad (2.6)$$

where  $R_g$  is the 3-D average radius of the clusters in the gel;

$$R_g = \left[ \frac{\sum R_i^3}{\sum R_i^D} \right]^{\frac{1}{3-D}}$$

After gelation it is thus possible to define  $R$  more precisely.

The model leads to a gel built of fractal clusters. Because fractals are scale invariant, the gel may also be scale invariant, i.e., a gel formed from a system with a high volume fraction of particles may resemble a gel with a low particle concentration, only the scale will be different. In order to be scale invariant the cluster size distribution in the gel needs to have the same form, whatever the particle volume fraction. The existence of so-called self-preserving cluster size distributions has been observed by Swift and Friedlander [30], long before the introduction of fractals. The idea of self-preserving cluster size distributions has recently become of interest in dynamic scaling theories and is connected to the idea of fractal geometry [18].

The appearance of a gel may vary considerably with the volume fraction of the disperse phase. Laying and McBain [31] distinguished between a 'gel' which is turbid, consisting of coagulated particles, and a 'jelly' like gelatin which is transparent. This difference is, however, only based on a difference in dimension of the building blocks. Von Weimarn [32] showed that there is a gradual transition from transparent 'jellies' to flaky, coagulated 'gels' if the concentration of the disperse phase decreases. Eqn. 2.6 gives a quantitative relation between the overall volume fraction and the scale, i.e. the average size of the clusters in a gel, given a fixed value of the fractal dimensionality. According to some computer simulations, however, the effective fractal dimensionality will increase with increasing volume fraction due to an increase in interpenetration between the clusters [21]. This is in contradiction with the property of scale invariance of the fractal clusters. The form of a small cluster will resemble the form of a larger cluster and the relative interpenetration is thus independent of cluster size and, according to Eqn. 2.6, also of the volume fraction. Interpenetration may thus lead to a gel with, on a scale smaller than  $R$ , a fractal dimensionality somewhat higher than that of the original clusters, but independent of the volume fraction; this agrees with experimental results (see further on). A reason why computer simulations may lead to different results is the limited number of particles used in these simulations. The total scale of the simulation experiment is often far smaller than the scale on which the gel is homogeneous.

The structure of the aggregates is not expected to be fractal at very short distances, due to particle impenetrability and to interactions between non-bonded particles [21]. Consequently, the model may not be valid at very high volume fractions, since in that case the clusters contain only a small number of particles at gelation. Although a single small floc is not fractal, a large collection of these flocs may nevertheless show statistical fractal behaviour. At very low volume fractions sedimentation may disturb the gelation, since the flocs become very large and thus may sediment; moreover, in such large tenuous flocs the pliability of the strands may not be negligible any more, permitting rearrangement of the floc structure (chapter VII).

## **2.4 Some consequences of the model**

### *2.4.1 The critical volume fraction*

In contrast with percolation models the fractal model does not anticipate a general critical volume fraction for gelation to occur. The only result of a lower volume fraction will be a coarser gel (Eqn. 2.6). In practice, however, there will be some critical volume fraction, be it because of disturbances like velocity gradients or sedimentation or due to syneresis [33]. Even if there is no disturbance at all there will be some lower limit because the scale on which the gel is heterogeneous can never exceed the size of the container (figure 2.3). In this case, the ratio between the size of the container and the size of the primary particles will determine the critical volume fraction. In most experiments this effect is not important because convection and sedimentation will disturb gelation already at far higher volume fractions. However, the effect may be important if the size of the container is very small, like it is for the aggregation of fat crystals in an emulsion of oil in water, where part of the oil crystallizes. The ratio between the size of the emulsion droplets and the fat crystals inside them determines whether the droplets are solid-like (gelled) and thus may aggregate or liquid-like and thus fuse (coalescence). In accordance with this, it has been observed that an emulsion which contained large crystals in the droplets was stable

whereas an emulsion with small crystals in the oil phase but with the same droplet size and crystalline fat concentration was unstable [34]. Solid-like droplets aggregate readily because protruding fat crystals may penetrate into other droplets leading to so called partial coalescence [34].

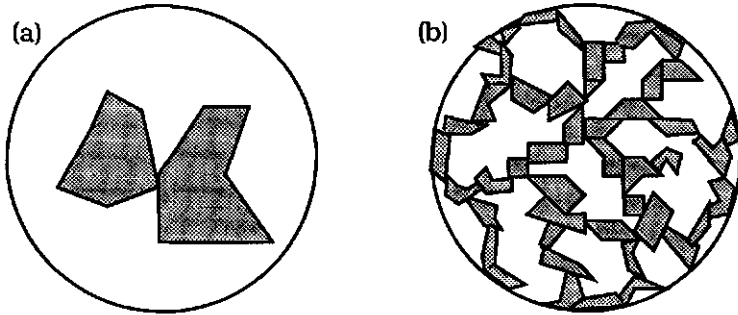


**Fig. 2.3** Two emulsion droplets with large (a) and small (b), aggregated fat crystals. The fat concentration in both droplets is similar. In droplet (a) no network can be formed because the ratio between the size of the droplet and the size of the crystals is not small enough.

A simple approximation of the critical volume fraction of particles that is needed to occupy the system at given  $D$ ,  $R_d$  and  $a$  would be  $(R_d/a)^{D-3}$  where  $R_d$  is the radius of the container (droplet) and  $a$  the radius of the primary particles (fat crystals). A gel will just be formed if the size of a floc that contains all primary particles equals the size of the container. In practice, the situation is more complicated due to the effects of the boundary of the container. Various situations may be considered or simulated on a computer:

- 1 - Moving boundaries; particles that cross the boundary of the container are transferred to the other side (computer simulation).
- 2 - Particles do not stick to the wall of the container.
- 3 - Particles stick to the solid wall of the container. The density of the gel close to the wall will be high (section 4.3).
- 4 - Particles stick to a liquid-liquid interface and are able to diffuse laterally after attachment; a two-dimensional surface gel may be formed.

Two-dimensional computer simulations on a  $20 \times 20$  lattice showed that the simple approach of a surface fraction that should be higher than

$(R_d/a)^{D-2}$  to form a gel is only applicable in the case of moving boundaries. In the case of particles that stick or do not stick to the wall of the container (situations 2 and 3) a higher surface fraction was needed to obtain percolation, i.e., a connection between two opposite walls (results not shown).

#### 2.4.2 Permeability

In the case of a laminar flow through a matrix generally Darcy's law is obeyed. For the tube in figure 2.4 we may write

$$Q_f = B_p A_c \frac{\Delta P}{\eta l} \quad (2.7)$$

- $Q_f$  = flow rate ( $\text{m}^3 \text{s}^{-1}$ )
- $B_p$  = permeability coefficient ( $\text{m}^2$ )
- $\Delta P$  = pressure difference ( $\text{N m}^{-2}$ )
- $\eta$  = viscosity of the flowing liquid ( $\text{N m}^{-2} \text{s}$ )
- $A_c$  = pore size area of the gel ( $\text{m}^2$ )
- $l$  = height of the gel (m)

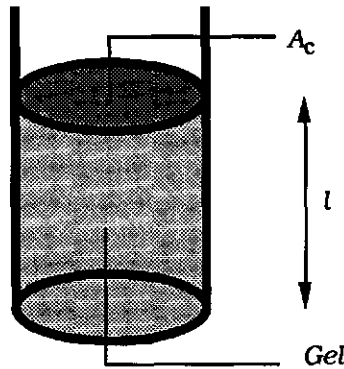


**Fig. 2.4** Tube filled with a gel with pore size area  $A_c$  and height  $l$ .

The flow rate through one fractal structural element, due to a constant pressure gradient, will scale like (as in Poiseuille's law)

$$Q_f \propto R^4 \quad (2.8)$$

The flux through the gel in case of a constant pressure gradient will thus scale like

$$Q_f \propto \sum Q_{f,i} \propto \sum R_i^4 \quad (2.9)$$

if the number of pores in the gel were constant. The absolute size of the pore surface area ( $A_c$ ) of the gel scales like  $A_c \propto R_f^2$ . This, in combination with Eqn. 2.9, leads to the following relation between the size of the fractal clusters in a gel and the permeability coefficient ( $B_p$ ) of that gel as defined by Darcy's law:

$$B_p \propto \frac{Q_f}{A_c} \propto R_{42}^2 \quad (2.10)$$

If the cluster size distribution is self-preserving during the aggregation process then  $R_{42} \propto R_{3D}$  and Eqns. 2.6 and 2.10 can be combined to yield:

$$B_p = \frac{R_g^2}{K} = \frac{a^2}{K} \phi_0^{2/(D-3)} \quad (2.11)$$

where  $K$  is a constant, comparable with the tortuosity factor in the Kozeňy-Carman equation.  $K$  is dependent on the cluster size distribution and on the ratio between the effective hydrodynamic radius of the clusters and the radius of the clusters in a gel,  $R_g$ .

Equation (2.11) describes a relation between the structure of the gel (expressed in an effective fractal dimensionality  $D$ ), the volume fraction of the particles in the gel, the size of these particles and the permeability of the gel. Measurements of the permeability of gels of varying particle concentration can thus provide information about the effective fractal dimensionality.

Darcy's law is applicable in the case of laminar, so-called creeping flow. If the flow rate is too high, inertial forces become important, leading to turbulence.  $Q$  is no longer proportional to  $\Delta P$  in that case. The crossover from laminar to turbulent flow is generally given by the Reynolds number,  $Re$ ;

$$\text{Re} = \frac{v\rho_1 p}{\eta} \quad (2.12)$$

- $v$  = liquid flux ( $\text{m s}^{-1}$ ) =  $Q/A_c$   
 $\rho_1$  = density of the flowing liquid ( $\text{kg m}^{-3}$ )  
 $p$  = characteristic pore radius, here taken equal to  $R_g$  (m)

In the case of flow through porous media Re should not exceed a certain critical value, which varies from 0.1 to 75 depending on the porous medium [35].

#### 2.4.3 Geometric structure and correlation function.

As has been stated before, aggregation may lead to a scale invariant gel consisting of fractal clusters. The relation between the scale on which the gel is heterogeneous, expressed in  $R_g$ , and the volume fraction has been given by Eqn. 2.6. It will thus be easy to estimate the effective fractal dimensionality by comparing the geometric structure of gels with varying volume fractions of particles.

A quantitative description of the density fluctuations of a cluster or in a gel can be given by a correlation or distribution function. The so-called density-density correlation function  $C(r)$  is given by

$$C(r) = \frac{\langle \rho(x)\rho(x+r) \rangle}{\bar{\rho}^2} \quad (2.13)$$

where  $\langle \dots \rangle$  represents averaging over all orientations and all positions,  $x$ , in the gel and  $\bar{\rho}$  is the average density in the gel. Actually  $\rho(x)$  is the local weight concentration of the particles on position  $x$  and  $\bar{\rho} = \phi_0 \rho_p$  where  $\rho_p$  is the density of the material of the particles. If the gel is isotropic it is no longer necessary to average over all orientations. A 1-dimensional 'section' through the gel is enough to calculate the correlation function if there are enough particles on that line to average out the fluctuations in density. The density-density correlation function is, on length scales longer than  $a$ , equal to the radial distribution function  $g(r)$  which is a measure for the probability that there is, on a distance  $r$  from any particle, another particle.



The mass of the particles contained in a sphere of the gel with radius  $R$  can be obtained by integration of the density-density correlation function:

$$M_p = \bar{\rho} \int_0^R 4\pi r^2 C(r) dr \quad (2.14)$$

For a fractal, the mass,  $M_p$ , equals  $(R/a)^D \times \frac{4}{3}\pi a^3 \times \rho_p$  (the number of primary particles multiplied by their mass). This, in combination with Eqn 2.14, leads to a relation between the correlation function,  $C(r)$  and the length scale,  $r$  ( $r > a$ ):

$$C(r) = \frac{D}{3\phi_0} \left(\frac{r}{a}\right)^{D-3} \quad (2.15)$$

The fractal dimensionality is thus accessible from an image through the slope of a log-log plot of  $C(r)$  versus  $r$  if  $r$  lies between the lower cut-off where fractal behaviour starts,  $a$ , and the upper cut-off length, the size of the flocs in the gel,  $R_g$ . At larger length scales the gel is homogeneous and the correlation function will thus be independent of  $r$ .

#### 2.4.4 Turbidity and (light) scattering

Scattering techniques constitute a powerful method of studying fractal structures. Often, the angular dependence of the scattering of laser light, X-rays or neutrons is employed. It has recently been shown that the value of the fractal dimensionality is also accessible through measurements of the wavelength dependence of the turbidity [36].

In the angular dependence measurements the power-law decay of the structure factor,  $S(q)$ , as a function of the so called wave vector ( $q$ ) is studied in order to obtain the fractal dimensionality [26]. In the region where  $1/R \ll q \ll 1/a$  fractal behaviour applies.  $S(q)$  is proportional to the Fourier transform of the correlation function (Eqn. 2.15). In an isotropic system in three dimensions [37, 38];

$$S(q) = 1 + \left(\frac{4}{3}\pi a^3\right)^{-1} \phi_0 \int_0^\infty |C(r) - 1| \frac{\sin(qr)}{qr} 4\pi r^2 dr \quad (2.16)$$

substitution of  $q^{-1}d(qr)$  for  $dr$ ,  $q^{-1}(qr)$  for  $r$  and  $C(r)$  of Eqn. 2.15 in Eqn. 2.16 provides:

$$S(q) = 1 + D(qa)^{-D} \int_0^\infty (qr)^{D-1} \frac{\sin(qr)}{qr} d(qr) \propto (qa)^{-D} \quad (2.17)$$

where  $q = \frac{4\pi n_0}{\lambda} \sin\left(\frac{\theta}{2}\right)$

$\theta$  is the scattering angle,  $\lambda$  is the wavelength (in air) and  $n_0$  the refractive index of the medium.

In turbidity measurements one integrates over a broad range of  $q$  and Eqn. 2.17 will thus not be valid in most cases. If the scaling region is finite and bounded by both upper ( $R$ ) and lower ( $a$ ) cut-off lengths another structure factor can be derived [37].

$$S(q) = \frac{D\Gamma(D-1)\sin[(D-1)\arctan(qR)]}{(qa)^D [1 + 1/(q^2 R^2)]^{(D-1)/2}} \quad (2.18)$$

Where  $\Gamma(D-1)$  is the gamma function of  $(D-1)$ . The upper cut-off length has been introduced via a cut-off function  $h(r) = \exp(-r/R)$  that may be multiplied with the function  $|C(r) - 1|$  in Eqn. 2.16. The cut-off function,  $h(r)$ , is introduced to avoid the edge effects due to the finite size of the clusters and approaches 1 if  $r \ll R_g$  and 0 if  $r \gg R_g$ . Eqn. 2.18 is valid over a broad range of  $q$ 's.

Using the Rayleigh-Gans-Debye theory one may calculate the dissipation function,  $Q$ , which is the factor by which the turbidity calculated from Rayleigh scattering must be multiplied. In the case of spherical particles

$$Q = \frac{3}{8} \int_\alpha^\pi \frac{9(\sin(qa) - qa \cos(qa))^2 S(q) \sin\theta (1 + \cos^2 \theta)}{(qa)^6} d\theta \quad (2.19)$$

where  $\alpha$  is the acceptance angle of the spectro-photometer [39]. The change of the turbidity ( $\tau$ ) with the wavelength ( $\lambda$ ) depends on the dependence of  $Q$  on the wavelength. From

$$\tau = HCMQ \quad (2.20)$$

with

$$H = \frac{32\pi^3 n_0^2 \left(\frac{dn}{dC}\right)^2}{3N_A \lambda^4} \quad (\text{kg}^{-2} \text{ m}^2 \text{ mol}),$$

$N_A$  Avogadro 's number ( $\text{mol}^{-1}$ ),  $dn/dC$  the specific refractive index increment ( $\text{kg}^{-1} \text{ m}^3$ ),  $M$  the molecular weight ( $\text{kg mol}^{-1}$ ) and  $C$  the concentration ( $\text{kg m}^{-3}$ ), the derivative

$$\beta = \frac{d \log Q}{d \log \lambda} = 4 - \gamma + \frac{d \log \tau}{d \log \lambda} \quad (2.21)$$

can be obtained [36].

$\gamma$  is often assumed to be  $-0.2$  for proteins [36] and is a result of the wavelength dependence of the refractive index.

$$\gamma = 2 \frac{d \log \left( n_0 \frac{dn}{dC} \right)}{d \log \lambda} \approx -0.2 \quad (2.22)$$

Now  $Q$  can be calculated and  $\beta$  can be obtained from its wavelength dependence.  $\beta$  will tend asymptotically towards the input fractal dimensionality for very large clusters [36]. When the fractal dimension is known, information can be obtained about the size of the clusters ( $R$ ) [3].

Fig. 2.5 shows that the acceptance angle of the spectro-photometer is very important; the lower limit of the integration in Eqn. 2.19 is set at the value of the acceptance angle.

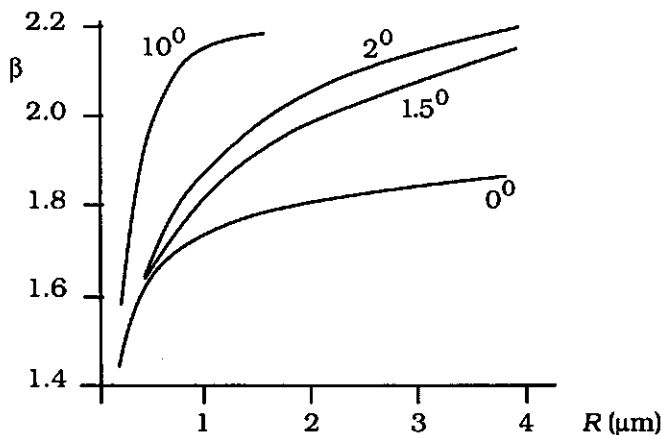


**Fig. 2.5** The wavelength exponent  $\beta$  ( $= d \log Q / d \log \lambda$ ) calculated as a function of the cluster radius  $R$  for various angles of acceptance;  $D = 2.27$ ,  $a = 50$  nm and  $n = 1.33$ .

The value of  $\beta$  is slightly dependent on the wavelength because the log-log plot of  $Q$  as a function of the wavelength is not completely linear.  $\beta$  is calculated by assuming  $\log Q$  to be linear with  $\log \lambda$  between 400 and 800 nm wavelength.

#### 2.4.5 Rheology and kinetics

The previous gel properties (permeability, correlation function, turbidity) are strictly dependent on the geometric structure after gelation. This structure is, however, affected by the interactions between the particles during gelation. Rheological properties of the gel network depend both on the geometric structure, and on the interaction forces in and among the particles. Interaction forces are also important for rearranging processes occurring after the gelation. The rheological properties of particle networks will be described in chapter V and the kinetics of aggregation and gelation in chapter VI.

## 2.5 References

- 1 B.B. Mandelbrot, *The Fractal Geometry of Nature* (Freeman, New York, 1982)
- 2 F. Family and D.P. Landau (ed.), *Kinetics of Aggregation and Gelation* (North-Holland, Amsterdam, 1984)
- 3 L.G.B. Bremer, T. van Vliet and P. Walstra, *J. Chem. Soc. Faraday Trans 1*, 1989, **85**, 3359
- 4 D.A. Weitz and M. Oliveria, *Phys. Rev. Lett.* 1984, **52**, 1433; D.A. Weitz, J.S. Huang, M.Y. Lin and J.Sung, *Phys. Rev. Lett.*, 1984, **53**, 1657; 1985, **54**, 1416
- 5 M.J. Vold, *J. Colloid Sci.*, 1959, **14**, 168
- 6 M.J. Vold, *J. Colloid Sci.*, 1963, **18**, 684
- 7 D.N. Sutherland, *J. Coll. Int. Sci.*, 1966, **22**, 300
- 8 D.N. Sutherland, *J. Coll. Int. Sci.*, 1967, **25**, 373
- 9 D.N. Sutherland and I. Goodarz-Nia, *Chem. Eng. Sci.*, 1971, **26**, 2071
- 10 T.A. Witten and L.M. Sander, *Phys. Rev. Lett.*, 1981, **47**, 1400
- 11 P. Meakin, in ref. (2), p 91
- 12 P. Meakin, *Phys. Rev. Lett.*, 1983, **51**, 1119
- 13 M. Kolb, R. Botet and R. Jullien, *Phys. Rev. Lett.*, 1983, **51**, 1123
- 14 P. Meakin, *Phys. Rev. B*, 1984, **29**, 2930
- 15 P. Meakin, *J. Chem. Phys.*, 1985, **82**, 3786
- 16 M. Kolb and R. Jullien, *J. Phys. Lett. (Paris)*, 1984, **45**, 977
- 17 P. Meakin and Z.R. Wasserman, *Phys. Lett. A*, 1984, **103**, 337
- 18 R.C. Ball, D.A. Weitz, T.A. Witten and F. Leyvraz, *Phys. Rev. Lett.* 1987, **58**, 274
- 19 P. Meakin, *J. Chem. Phys.*, 1985, **83**, 3645
- 20 P. Meakin, *J. Chem. Phys.*, 1984, **81**, 4637
- 21 G.C. Ansell and E. Dickinson, *Phys. Rev. A*, 1987, **35**, 2349
- 22 P. Meakin, *J. Coll. Int. Sci.*, 1990, **134**, 235
- 23 P. Meakin and R. Jullien, *J. Chem. Phys.*, 1988, **89**, 246
- 24 R.C. Ball, *personal communication*
- 25 Y. Adachi and S. Ooi, *J. Coll. Int. Sci.*, 1990, **135**, 374
- 26 D.W. Shaeffer, S.E. Martin, P. Wiltzius and D.S. Cannell, *Phys. Rev. Lett.*, 1984, **52**, 2371
- 27 P.W. Rouw and C.G. de Kruij, *Phys. Rev. A*, 1989, **39**, 5399
- 28 M.Y. Lin, R. Klein, H.M. Lindsay, D.A. Weitz, R.C. Ball and P. Meakin, *J. Coll. Int. Sci.*, 1990, **137**, 263
- 29 M. Kolb, R. Jullien and R. Botet, in *Scaling Phenomena in Disordered Systems*, ed. R. Pynn and A. Skjeltrop (Plenum, New York, 1985), p. 71
- 30 D.L. Swift and S.K. Friedlander, *J. Coll. Sci.*, 1964, **19**, 621
- 31 M.E. Laying and J.W. McBain, *Kolloid Zeitschrift*, 1924, **35**, 18
- 32 P.P. von Weimarn, *Kolloid Zeitschrift*, 1925, **36**, 175
- 33 H.J.M. van Dijk and P. Walstra, *Neth. Milk Dairy J.*, 1986, **40**, 3
- 34 K. Boode, *Ph.D. Thesis*, (Wageningen Agricultural University, The Netherlands, in preparation)
- 35 A.E. Scheidegger, *The physics of flow through porous media*, (Oxford University press, London, 1960)
- 36 D.S. Horne, *Faraday Discuss. Chem. Soc.*, 1987, **83**, 259
- 37 J. Teixeira, in *On Growth and Form*, ed. H.E. Stanley and N. Ostrowsky (Nijhoff, Dordrecht, 1986), p. 145
- 38 P.W. Rouw, *Ph.D. Thesis*, (Utrecht University, Netherlands, 1988)
- 39 P. Walstra, *J. Coll. Int. Sci.*, 1968, **27**, 443

## III Materials and methods

### 3.1 Materials

All low molecular weight substances used were analytical grade. The low-heat skim-milk powder was a commercial product (Krause, Heino) and the sodium caseinate powder was supplied by the Netherlands Institute of Dairy Research (NIZO). The casein concentration in the dried skim-milk powder was 28.6 wt.% and in the sodium caseinate powder 93.0 wt.%. A more complete composition has been given elsewhere [1]. Dispersions of the powders were prepared with demineralized water. A standard skim-milk with a somewhat higher solids content than in normal bovine skim-milk was made by dispersing 120 g skim-milk powder in 1 kg water. The protein concentration was varied by ultrafiltering standard skim-milk in a concentrator equipped with a hollow fibre cartridge with a cut-off of 10,000 Daltons (Amicon). The ultrafiltrate, the skim-milk and the concentrate could be mixed in order to obtain the required protein concentration. In this way the concentration of low molecular weight electrolytes was kept constant, independent of the protein concentration. A standard sodium caseinate dispersion contained 50 g Na-caseinate powder and 0.1 mole NaCl per kg dispersion. Other protein concentration were obtained by diluting the standard sodium caseinate solution with a 0.1 M NaCl solution. Both standard dispersions were stirred at least 24 h at 30 °C before use. To prevent bacterial growth 200 ppm  $\text{NaN}_3$  was added as a preservative.

Casein is the main component involved in the structure of gels made from milk [2]. Casein includes a family of different casein molecules, whose common characteristic is that they are insoluble at pH 4.6. Under the natural conditions of milk (and in skim-milk dispersions) they are associated into large spherical particles, the so-called casein micelles. Casein micelles consist of water, casein, salts (mainly calcium and phosphate) and some minor components [2]. Sodium caseinate dispersions do not contain calcium phosphate which is essential for the integrity of casein micelles. These dispersions are translucent at the natural pH of milk. At lower pH, however, the casein associates into

particles and the dispersion becomes opaque. These particles are slightly smaller than the particles in a skim-milk dispersion at similar conditions.

Polystyrene particles of 220 and 395 nm radius were prepared by the method of Goodwin et al. [3]. The latex with particles of 70 nm radius was kindly supplied by AKZO Research and the latex with particles of 35 nm radius was home-made by adding 5 g palmitic acid per kg as a surfactant.  $K_2S_2O_8$  was used as initiator ( $0.8 \text{ g kg}^{-1}$ ) and  $KHCO_3$  ( $1.0 \text{ g kg}^{-1}$ ) as the electrolyte. In the case of surfactant-free latices, the styrene concentration was varied in order to obtain various particle sizes [3] and was lower than 0.9 M. In the case of latex with palmitic acid and the AKZO latex, the styrene concentration was 3 M. The synthesis conditions and the radius of the particles are compiled in table 3.1.

**Table 3.1** Radius and polymerization conditions of the latices.

$a$ (nm)	[Styrene] (g/kg)	[ $K_2S_2O_8$ ] (g/kg)	T	Surfactant
35	300	0.85	70 °C	5 g/kg palmitic acid
70	300	0.88	70 °C	8.4 g/kg Na-dihexyl sulfosuccinate
220	40	0.80	85 °C	none
395	80	0.80	60 °C	none

After synthesis the latices were purified by means of micro-filtration or dialysis against demineralized water (millipore super Q quality). In the case of the 35 nm particles 0.16 M NaCl was used because this latex would otherwise gel due to the relatively large interaction size at low salt concentrations (gel type: concentrated dispersion of repulsive particles).

Other colloids that were used are haematite ( $\alpha\text{-Fe}_2\text{O}_3$ ) particles of 34 nm radius, synthesized by the method of Penners [4] and emulsions of bromated salad oil. The bromated oil was made by (slow) addition of bromine to salad oil. The density of the oil could be matched to that of the water in this way. The emulsions were prepared from a pre-emulsion, consisting of 350 g of a solution containing  $30 \text{ g kg}^{-1}$  sodium caseinate and 150 g of oil. The emulsion was recycled during 20 minutes at constant pressure and temperature in a Rannie high-pressure homogenizer. The size of the emulsion droplets could be adjusted by

varying the homogenization pressure. After preparation the excess sodium caseinate was removed by means of micro filtration against a 0.1 M NaCl solution.

### 3.2 Preparation of the gels

Casein gels were prepared in three different ways;

- 1) quiescent warming up a sodium caseinate solution or skim-milk dispersion of pH 4.6 from 4 to 30 °C.
- 2) slow acidification of a sodium caseinate solution with glucono- $\delta$ -lactone (GDL), a slowly hydrolyzing acid precursor, at 30 °C.
- 3) addition of 500 ppm rennet (Leeuwarder kaasstremsel, strength 10000 SU) to skim-milk at 30 °C.

These three methods, which are described in more detail in the following paragraphs, yield gels with different properties.

Acidification in the cold was performed according to the method of Roefs [1]. Upon acidification of skim-milk, the calcium phosphate, which is essential for the integrity of the casein micelles at pH 6.65 (the pH of milk), dissolves together with part of the casein. At pH 5.2 the calcium phosphate is completely dissolved but still most of the casein is associated. At lower pH (4.6) the casein becomes fully associated again in particles which are stable in the cold (below 10 °C at the present salt concentration). The average diameter of the particles is ca. 120 nm and is more or less independent of pH, but the structure of the casein particles at pH 4.6 and 6.65 is different and they are kept together by, at least partly, different interaction forces [5].

In order to prepare sodium caseinate gels, the concentration NaCl of the sodium caseinate dispersions was increased to 0.14 M because at lower concentrations some aggregation already occurred during the acidification. Upon acidification in the cold (<4 °C), pH 4.6 solutions of sodium caseinate also tend to self-associate and form particles of about 50-100 nm which are stable at NaCl concentrations higher than roughly 0.1 M. At higher temperatures and salt concentration less than about 0.2 M the casein particles are not stable any longer. They will aggregate into larger clusters and finally form a gel.



The second type of gel, the GDL-induced gel, was prepared by adding 0.165 g GDL (dissolved in a 0.1 M NaCl solution) per gram sodium caseinate powder in the solution. This amount of GDL yielded a final pH of 4.6 after 24 h at 30 °C. GDL is an acid precursor which slowly hydrolyses thus forming gluconic acid. Emulsions prepared with sodium caseinate as emulsifier, were destabilized in the same way. In order to prepare GDL-induced skim-milk gels the amount of GDL per gram skim-milk powder was 0.102 g, again at 30 °C.

The third gel type, the rennet-induced gel, was made by adding 500 ppm rennet, a proteolytic enzyme, to a skim-milk dispersion. The casein micelles are stabilized by one of the casein compounds, called  $\kappa$ -casein. The  $\kappa$ -casein is thought to form a hairy layer round the micelles, thus stabilizing the system by steric repulsion [2]. The rennet splits off the hydrophilic part of the  $\kappa$ -casein. The resulting paracasein micelles are unstable which leads to aggregation and gelation (fig. 3.1). This method is only suitable for skim-milk, no Na-caseinate gels were prepared in this way.

To enable making gels from polystyrene latex particles under quiescent conditions, i.e., slow acidification by GDL, the latex particles were first covered with palmitate. For this purpose a dialysis tube filled with latex was placed in a solution of 1 g palmitic acid in 5 litre 0.16 M NaCl at 80 °C. The pH was adjusted at 11 by adding NaOH. After 24 h the tube was removed and dialyzed in a solution of 0.16 M NaCl and 0.01 M  $\text{Na}_2\text{HPO}_4$  at 80 °C for at least 5 days, in order to remove the excess sodium palmitate. The NaCl/ $\text{Na}_2\text{HPO}_4$  solution was refreshed every day (totally at least 4 times). The last NaCl/ $\text{Na}_2\text{HPO}_4$  solution was used to vary the volume fraction of the latex particles. Gels were made by adding 4 g GDL per 100 g latex independent of its volume fraction. This led to gelation within a few minutes because the latex was only stable at high pH, probably due to the electrostatic repulsion of the carboxyl groups of the palmitate. This procedure led to quiescent aggregation and gelation of the latex. The gelation at low volume fractions occurred faster than at high volume fractions, due to the buffering of the palmitate on the surface which led to a slower decrease of the pH in the case of high  $\phi_0$  (more palmitate). As may be expected this effect was especially noticeable in the case of small particles (large surface area and thus more palmitate).

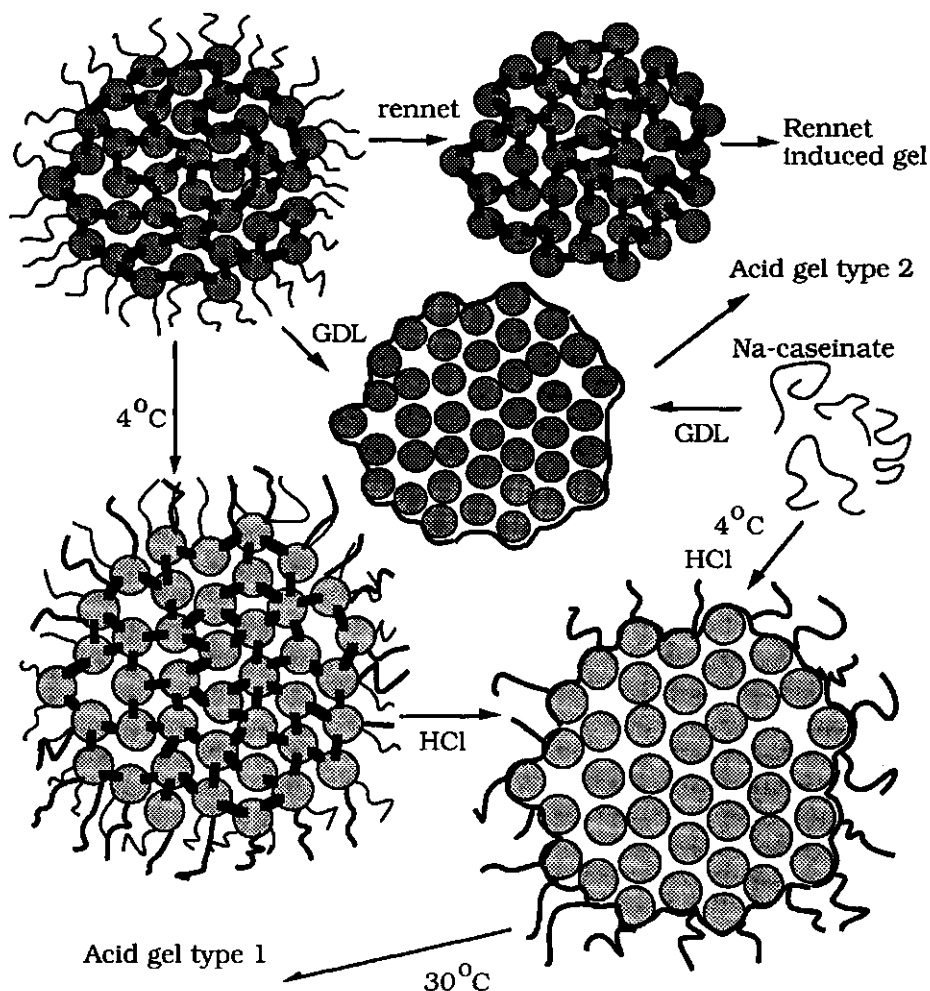


**Fig. 3.1** Formation of gels from casein micelles, highly schematic. Casein micelles can be destabilized by: 1) Rennet which cuts the stabilizing  $\kappa$ -casein. The colloidal calcium-phosphate remains in the micelles, 2) The addition of GDL, the  $\kappa$ -casein becomes uncharged and loses its effect of steric repulsion and 3) Acidification in the cold: part of the  $\beta$ -casein goes into solution and has a stabilizing effect. After warming up the dispersion the  $\beta$ -casein becomes fully aggregated again and the casein micelles will aggregate.

In addition to quiescent aggregation experiments traditional coagulation experiments were performed (coagulation = aggregation due to electrolyte addition). The sediment volume or the gelation was studied

for polystyrene and haematite sols at various volume fractions and salt concentrations (i.e. aggregation rates). The turbidity course with time was recorded and related to the structure of the flocs and to the kinetics of aggregation (section 3.5.1).

### 3.3 Permeability measurements

For the permeability measurements a method developed by van Dijk [6, 7] was used. Gels were made in glass tubes which were open at both ends. The tubes were placed in a thermostated measuring vat made of clear plexiglass (figure 3.2). The pressure difference over the gel,  $\Delta P$ , could be adjusted by varying the depth of the gel in the measuring vat. The liquid flux  $v$  ( $Q_f/A_c$ ) could be measured by reading the level of the percolating liquid at regular time intervals with the help of a travelling microscope.

The permeability coefficient,  $B_p$ , can be calculated using Eqn. 2.7 (Darcy's Law). The pressure difference equals:

$$\Delta P(t) = -\rho_1 g(h(\infty) - h(t)) \quad (3.1)$$

Substitution in 2.7 leads to

$$B_p = \frac{\eta l v(t)}{\rho_1 g(h(\infty) - h(t))} \quad (3.2)$$

$v(t)$  equals  $\frac{d(h(\infty) - h(t))}{dt}$  and Eqn. 3.2 can be integrated:

$$B_p = \frac{1}{t_2 - t_1} \int_{h(\infty) - h(t_1)}^{h(\infty) - h(t_2)} \frac{\eta l \, d(h(\infty) - h(t))}{\rho_1 g(h(\infty) - h(t))} = \frac{\eta l \{\ln[h(\infty) - h(t_1)] - \ln[h(\infty) - h(t_2)]\}}{\rho_1 g(t_2 - t_1)} \quad (3.3)$$

The liquid flux varied from  $3 \times 10^{-8}$  to  $5 \times 10^{-6}$  m s<sup>-1</sup>. Assuming a large value of  $p = 20 \mu\text{m}$  in Eqn. 2.12 provides a maximum value of  $Re = 10^{-4}$  and there was thus no risk for turbulent flow. The measured permeability coefficients for acid-induced casein and polystyrene gels did

not change with time and were independent of the pressure gradient  $\Delta P/l$  for pressure gradients smaller than about  $10^4 \text{ Pa m}^{-1}$ . It is thus unlikely that the pressure gradient induced changes in the gel structure like it did during permeability measurements on rennet induced skim-milk gels at comparable values of  $\Delta P/l$  [7]. These gels were subject to micro-syneresis, which process was enhanced by the permeability measurement. Roefs found no increase in  $B_p$  for acid-induced casein gels at these pressure gradients either [1].

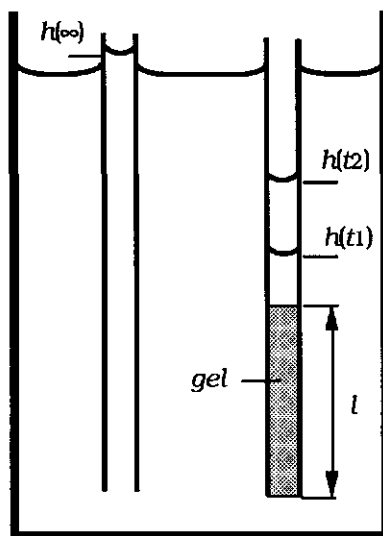


**Fig. 3.2** Schematic representation of permeability measurement.

### 3.4 Determination of the geometry of the gel network

#### 3.4.1 Confocal scanning laser microscopy

Electron microscopy has often been used in order to study the structural features of particle gels [1, 8 - 10]. This method has the drawback that the whole preparation procedure is very elaborate and that the fixation and dehydration may affect the gel texture. Confocal scanning laser microscopy is a rather new technique in which the sample, e.g. a fluorescent gel, is scanned by a focussed laser beam [11 - 14]. The amount

of fluoresced light is measured, via a normal microscope, by a photon multiplier. A simplified picture of the instrument is given in figure 3.3.

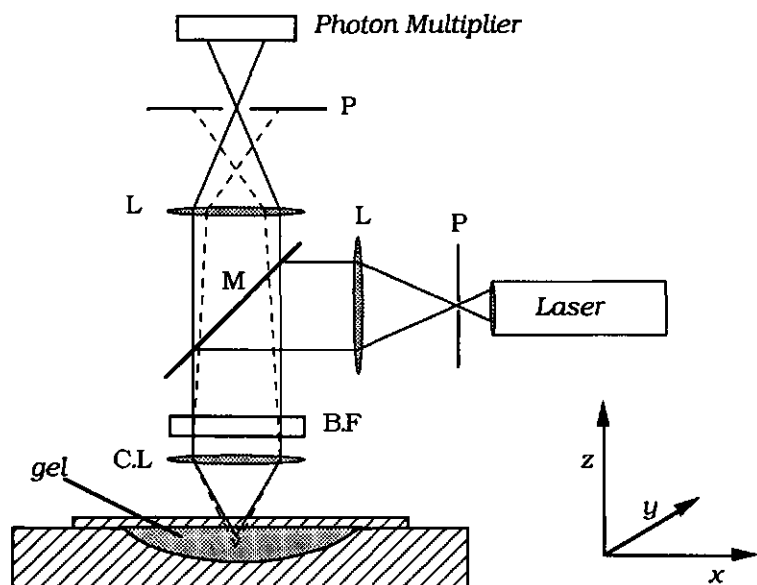


**Fig 3.3** Schematic representation of the Confocal Scanning Laser Microscope (not to scale) [12]. P is a pinhole, B.F a low pass blocking filter, M a dichroic mirror, L a lens and C.L. the collector confocal lens (objective). The dashed line represents fluoresced light from a point which is not in focus. The resolution in the z-direction depends on the size of the pinholes.

The sample can be moved in the z-direction which enables a series of pictures to be made and so a three-dimensional image of the gel network to be composed. The thickness of an optical section can be varied qualitatively by adjustment of the pinhole (Fig. 3.3). The pictures are shown on a monitor and are stored in a computer as an array of pixels which have a relative fluorescent intensity, expressed as an integer, ranging from 0 to 255. This intensity corresponds with the local density and is used in calculating the correlation function (Eqn. 2.13).

Skim-milk or sodium caseinate dispersions were made fluorescent by addition of fluorescein isothiocyanate (FITC) or rhodamine B. Gels of the fluorescent casein were made in special object glasses (figure 3.3),

using the standard methods. The dye concentration was roughly 0.2 g per kg dispersion. Other dye concentrations were tested in order to check whether the dye affects the geometry of the gel or the image obtained from CSLM. This appeared to be not the case; no difference was visible between similar gels with different dyes or dye concentrations, except, of course, differences in intensity and wavelength of the fluoresced light.

After gelation and ageing, the gels were studied with the confocal scanning laser microscope (Biorad) of the 'Technische en Fysische Dienst voor de Landbouw', (TFDL) at Wageningen. In one experiment GDL gels composed of four different sodium caseinate concentrations were studied; 10.3, 16.2, 25.5 and 40.0 g casein per kg dispersion. These concentrations were chosen in such a way that the cluster-size in the gel would differ by a factor of two for every concentration step, assuming a fractal dimensionality of 2.35 (Eqn. 2.6). In order to check the scale invariancy the thickness of the optical sections had to be adjusted in such way that a constant ratio existed between the thickness of the section and the size of the clusters in the gel. This was done by piling up several optical sections with known mutual distance (500 nm), thus creating a so called extended focus image. The thickness of this image should be less than the size of the clusters but much more than the thickness that a single section represents due to the limited resolution in the z-direction (roughly 500 nm). For the 40.0 g kg<sup>-1</sup> gel the image consisted of 2 sections and the thickness was thus roughly 1  $\mu\text{m}$ , the 25.5 g kg<sup>-1</sup> gel consisted of 4 sections leading to a thickness of 2  $\mu\text{m}$ . By stacking respectively 8 and 16 sections in the case of 16.2 and 10.3 g kg<sup>-1</sup> gels the image thickness was adjusted to 4 and 8  $\mu\text{m}$ . In addition to the GDL-induced gels, some gels made by acidification in the cold and rennet-induced gels after various ageing time were studied.

### 3.4.2 Correlation analysis

In section 2.4.3 the principles of correlation analysis have been described. The ensemble average in Eqn. 2.13 applies over all positions in the gel and over all orientations. Such an analysis would however be very time consuming and rather cumbersome, e.g. because the resolution in the z-direction is somewhat less than the lateral resolution. The intensity

of the fluoresced light reaching the detector decreases when it originates deeper inside the sample. Because the particle gels are probably isotropic a correlation analysis of one optical section is expected to yield the same information, provided the section is large and thin enough in comparison to the cluster size.

Calculation of the correlations functions was performed on a personal computer (Zenith, IBM AT compatible). Single optical sections were stored as a lattice of 384 horizontal and 256 vertical points, each point having a value,  $\rho$ , ranging from 0 to 255. This is an indirect measure for the local casein concentration and thus for the local density in the gel. One section took about 100 kbytes of memory. The regular pictures were composed of  $768 \times 512$  points but were compressed in order to save computer time and memory. Each time one horizontal line of 384 points, or local densities,  $\rho_{i,1}$  to  $\rho_{i,384}$  was read and the correlations were calculated according to:

$$C(r) = \frac{1}{256 \times 284 \times \bar{\rho}^2} \sum_{i=1}^{i=256} \sum_{j=1}^{j=284} \rho_{i,j} \rho_{i,j+r} \quad (3.4)$$

in which  $r$  was varied from 0 to 100 relative units of distance equal to the length of one lattice site.  $\bar{\rho}$  is obtained by calculating the average of all points in the lattice. The absolute value of one unit of distance, i.e. the length of one lattice site, is dependent on the magnification and in the case of the 10.3, 16.2, 25.5 and 40.0 g kg<sup>-1</sup> gels amounted to respectively 536, 268, 134 and 67 nm. These lengths were obtained by measuring the length of the reference bar in the micrographs relative to the length of the total micrograph which corresponds to 384 lattice sites. Thus, instead of the ensemble average over all positions in the gel and over all orientations the ensemble average over all positions in one plane of the gel and over one orientation was calculated.

### 3.4.3 The grid method

Another method to analyse the internal structure of the gels determines the self-similarity of the clusters explicitly [15]. A grid made of squares of length  $L$  was drawn over an optical section of a gel and a

histogram was established of the number of squares with  $n$  particles as a function of  $n$ . Because the particles were too small to be observed individually the intensity of the fluoresced light, which is supposed to be proportional to the number of particles, was used. On length scales where fractal behaviour applies the number of particles on a square,  $n_{i,L}$ , is proportional to  $L^{D_2}$  and counting the number of particles on a square as a function of its size enables thus the determination of  $D_2$ , which value characterizes the fractal nature of the two-dimensional image. Because the total number of particles in a two-dimensional picture is proportional to the surface fraction of the particles,  $\phi_s$ , the first moment of the histogram, i.e. the average number of particles per square  $\langle n_{i,L} \rangle$  is also proportional to  $\phi_s L^2$  on all length scales. The second moment of the histogram [15] equals

$$S_2(L) = \frac{1}{N_T} \sum_{i=1}^{N_T} n_{i,L}^2 = \langle n_{i,L}^2 \rangle \quad (3.5)$$

where  $N_T$  is the total number of squares that is used in the calculation and the subscripts  $i$  and  $L$  refer to the site and the length of the site considered. If the squares are large enough to contain a homogeneous part of the gel  $n_{i,L}$  is constant, i.e. all squares contain roughly the same amount of particles proportional to  $\phi_s L^2$ . In this case  $\langle n_{i,L}^2 \rangle = \langle n_{i,L} \rangle^2$  and  $S_2(L)$  thus scales like  $\phi_s^2 L^4$ . On smaller length scales where fractal behaviour applies  $n_{i,L}$  varies depending on the position of the square in the gel; a square located in a pore of the gel contains no particles whereas one in the centre of a cluster contains many particles. The number of particles in each square scales like  $L^{D_2}$  and the variation among various squares, i.e. the width of the histogram, increases for decreasing  $L$ , until  $L$  becomes smaller than the size of the primary particles. In the latter case a constant ratio, equal to  $\phi_s$ , exists between the number of squares located inside the particles and the total number of squares. Here the histogram consists of two peaks, one for the empty squares and one for the squares containing (a part of) the particles. In the empty squares  $n_{i,L} = 0$  and the other squares contain a part of a particle scaling like  $L^2$ . The fraction of the latter squares scales like  $\phi_s$  and the second moment of this histogram thus scales like  $\phi_s L^4$ .



The scaling behaviour of  $S_2(L)$  on length scales between  $2a$  and  $2R_g$  can be obtained considering the scale invariance characterizing the fractal nature of a gel. A gel may be considered to be built up of particles with radius  $a$  aggregated into fractal flocs with radius  $R_g$ , but also of flocs with diameter  $L$  which are aggregated into larger flocs with radius  $R_g$ . In the latter case a constant ratio may be assumed between the number of squares (diameter  $L$ ) containing a floc with diameter  $L$  and the total number of squares. This ratio equals the effective surface fraction of these flocs,  $\Phi_s(L)$ . The histogram is assumed to consist of two peaks, one with empty ( $n_{i,L} = 0$ ) and one with squares containing a floc. The amount of particles in the latter scales like  $\phi_{fs}(L)L^2$  where  $\phi_{fs}(L)$  is the surface fraction of the particles in the squares containing a floc. The number of particles in such a square scales like  $L^{D_2}$  and  $\phi_{fs}(L)$  like  $L^{D_2}/L^2 = L^{D_2-2}$ . Because the total number of particles is a constant the number of squares containing a floc scales like  $L^{-D_2}$  and their effective surface fraction,  $\Phi_s(L)$ , like  $L^{2-D_2}$ . The second moment of the histogram thus scales like  $\Phi_s(L) \times (\phi_{fs}(L)L^2)^2 \propto L^{2+D_2}$  on length scales where fractal behaviour applies (Eqn. 3.6).

$$S_2(L) \propto L^{2+D_2} \quad 2a < L < 2R_g \quad (3.6)$$

The smallest value chosen for  $L$  was equal to the length of one lattice site (section 3.4.2) and the largest value was 100 sites ( $100 \times 100$  pixels per square). For  $n_{i,L}$  the sum of the grey-values in square  $i$  was taken. The advantage of the grid method over correlation analysis was the much smaller amount of computer time needed to obtain  $D$ .

The grid method is well suited to analyse a three-dimensional image. In this case the volume has to be divided in boxes with length  $L$  and volume instead of surface fractions have to be used;  $\Phi(L) \propto L^{3-D}$  and  $\phi_f(L) \propto L^{D-3}$  and the second moment of the histogram scales like  $\Phi(L) \times (\phi_f(L)L^3)^2 \propto L^{3+D}$  if  $2a < L < 2R_g$  (Eqn. 3.7).

$$S_2(L) \propto L^{3+D} \quad 2a < L < 2R_g \quad (3.7)$$

It has been shown that the projection of a three-dimensional fractal is characterized by the same  $D$  as the fractal object itself if  $D < 2$  [15]. An image obtained with confocal scanning laser microscopy is something in between the cross-section and a projection of three-dimensional fractals. In order to calculate the mass of the particles on a cross-section the density-density correlation function may be integrated over 2 dimensions:

$$M_p \propto \int_0^R 2\pi r C(r) dr \propto \int_0^R r^{D-2} dr \propto R^{D-1} \quad (3.8)$$

In this equation,  $D$  is the fractal dimensionality of the original three-dimensional flocs and  $D-1$  that of a cross-section. A cross-section through a fractal object is thus characterized by a fractal dimensionality,  $D_2$ , which is 1 lower than that of the total floc;  $D = D_2 + 1$ .

### 3.5 Turbidity measurements

#### 3.5.1 The change in turbidity during aggregation

In order to study the stability of polystyrene latex and haematite sols at various electrolyte concentrations the change in turbidity as measured in a Zeiss PMQ II spectrophotometer was recorded on an x-t recorder. This enabled the acquisition of the initial value of  $d\tau/dt$ ,  $(d\tau/dt)_0$ , which is a relative measure of the aggregation rate. In all experiments  $d\tau/dt$  was measured 15 s after the addition of salt. For the large particles studied, the change of the turbidity was mainly due to doublet formation after 15 s. However, in the case of smaller particles the average floc contained already several particles after that time and now the change of the turbidity may depend not only on the aggregation rate but also on the evolution of the floc geometry. Measurement of  $(d\tau/dt)_0$  of small particles requires a stopped flow spectrophotometer [16 - 18]. The value of  $(d\tau/dt)_0$  increases as a function of electrolyte concentration until it reaches a maximum at the critical coagulation concentration, ccc. At higher electrolyte concentration the aggregation rate is diffusion limited.

In fig. 3.4 the turbidity is depicted as a function of time for various electrolyte concentrations and floc structures.

The maximum value of the turbidity,  $\tau_{\max}$ , can be related to the geometry of the flocs [19, 20]. If the Rayleigh Gans Debye theory applies, the dissipation function,  $\mathcal{Q}$ , in Eqn. 2.19 equals  $\tau/\tau_0$ . If the primary particles are very small ( $a \ll 1/q$ ), this equation reduces to

$$\mathcal{Q} = \frac{3}{8} \int_{\alpha}^{\pi} S(q) \sin \theta (1 + \cos^2 \theta) d\theta \quad (3.9)$$

This dissipation function is proportional to the structure factor,  $S(q)$ , given in Eqn. 2.18. The turbidity becomes independent of the size of the clusters if they are much larger than the wavelength of the light; the structure factor is of order  $(qa)^{-D}$  in that case and the relative value of  $\tau_{\max}$ ,  $\tau_{\max}/\tau_0$ , is thus dependent on the wavelength ( $\lambda \propto q^{-1}$ ), the size of the primary particles and the dimensionality of the clusters.

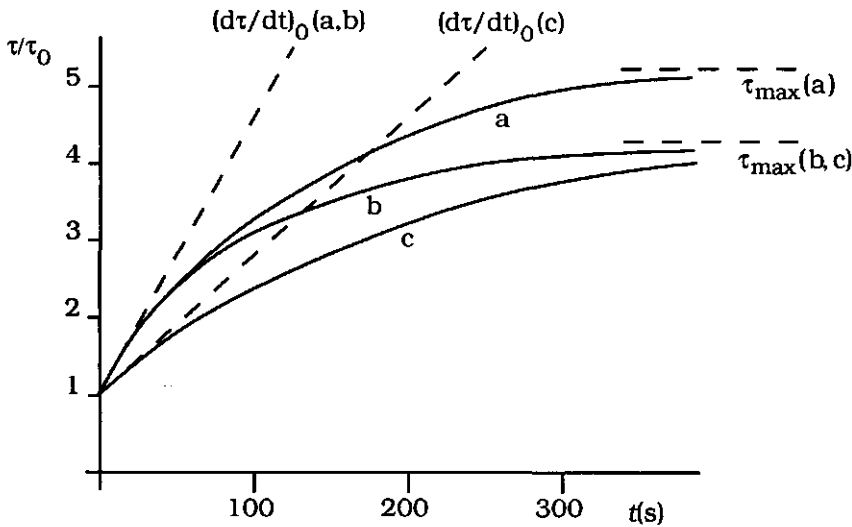


**Fig. 3.4** Presumed turbidity as a function of time after adding a coagulant; a)  $c_s = c_{cc}$  (critical coagulation concentration) and the flocs are relatively dense, b) high electrolyte concentration,  $c_s > c_{cc}$  and the flocs are ramified, and c)  $c_s < c_{cc}$  and the floc structure is like in b).  $(d\tau/dt)_0$  is independent of  $c_s$  if  $c_s \geq c_{cc}$ .

### 3.5.2 Turbidity measurements on gels

The turbidity measurements were carried out with a Zeiss PMQ II spectrophotometer with an attachment for turbidimetric analysis (figure 3.5) [21]; the angle of acceptance was 1.5 degrees.

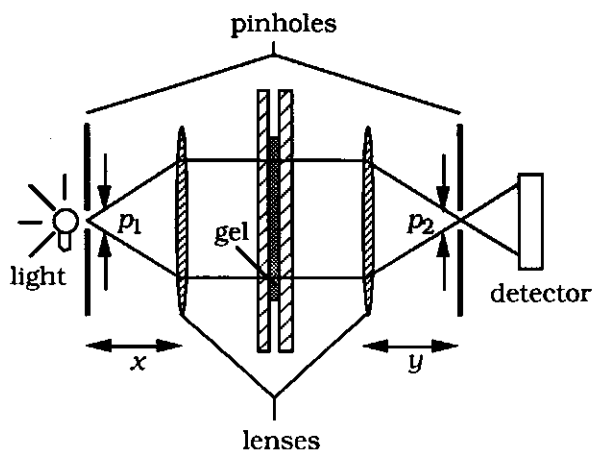


**Fig. 3.5** Schematic presentation of the turbidity measurement. The angle of acceptance equals  $(\tan(p_1/x) + \tan(p_2/y))/n_0$

The acid casein gels used in the turbidimetric analysis were prepared by acidification of sodium caseinate solutions with glucono- $\delta$ -lactone to a pH value of roughly 4.6. The turbidity was measured in optical cells with an optical path-length ranging from 0.152 to 4.95 mm, depending on the caseinate concentration in the gel. The gels were aged for 16 hours at room temperature. The measurements were carried out over the wavelength range 380 - 1700 nm.

In order to check the validity of the value  $-0.2$  of the term  $\gamma$  [22], the turbidity of a dispersion of very small particles showing pure Rayleigh scattering ( $\beta = 0$ , Eqn. 2.21) was measured. In this case the amount of scattered light would be proportional to  $\lambda^{-4}$  if the relative refractive index,  $m$ , were fixed [23]. The dependence of  $m$  on the wavelength was calculated using Eqn. 2.21:  $\gamma = 4 + d \log \tau / d \log \lambda$ . This measurement turned out to be impossible for casein particles because they were not

small enough to show Rayleigh scattering. For polystyrene particles of 35 nm radius  $\gamma$  turned out to be  $-0.25$ .

The effective fractal dimensionality was obtained from the turbidity spectra of the most dilute dispersion where the clusters are very large. Here  $\beta$  approached  $D = 4.2 + d \log \tau / d \log \lambda$ . At these low caseinate concentrations the gel was not strong enough to resist the gravitational force. It was necessary to gently shake these samples before every measurement.

The size of the fractal clusters in the gel ( $R_g$ ) was estimated by comparing the experimental  $\beta$  with fig. 2.5 (calculated  $\beta$ ) for an angle of acceptance of 1.5 degrees. This gave only a rough approximate of  $R_g$  which was very sensitive to experimental inaccuracy and to insufficiencies in the applied theory. Some measurements were performed at other angles of acceptance in order to check whether the dependence on this angle agrees with theoretical expectation.

The rennet induced gels were prepared by adding 500 ppm rennet to skim-milk dispersions. Skim-milk was concentrated (or diluted) by means of ultrafiltration of a standard skim-milk dispersion. These turbidity measurements were started as soon as possible after the gelation occurred.

### 3.6 References

- 1 S.P.F.M. Roefs, *Ph.D. Thesis*, (Wageningen Agricultural University, Netherlands 1986)
- 2 P. Walstra and R. Jenness, *Dairy Chemistry and Physics* (Wiley, New York, 1984)
- 3 J.W. Goodwin, J. Hearn, C.C. Ho and R.H. Ottewill, *Colloid and Polymer Sci.*, 1974, **252**, 464
- 4 N.H.G. Penners and L.K. Koopal, *Colloids and Surfaces*, 1986, **19**, 337
- 5 P. Walstra, *J. Dairy Sci.*, 1990, **73**, 1965
- 6 H.J.M. van Dijk, *Ph.D. Thesis*, (Wageningen Agricultural University, The Netherlands, 1982)
- 7 H.J.M. van Dijk and P. Walstra, *Neth. Milk Dairy J.*, 1986, **40**, 3
- 8 S. Henstra, and D.G. Schmidt, *Naturwissenschaften*, 1970, **57**, 247.
- 9 S. Henstra, and D.G. Schmidt, *Proc. 7th Int. Congress on Electron Microscopy*, Grenoble (1970). 387
- 10 V.R. Harwalkar and M. Kalab, *Journal of Texture Studies*, 1980, **11**, 35

- 11 H.T.M. van der Voort, G.J. Brakenhoff, J.A.C. Valkenburg and N. Nanninga, *Scanning*, 1985, **7**, 66
- 12 H.T.M. van der Voort, J.A.C. Valkenburg, E.A. van Spronsen, C.L. Woldringh and G.J. Brakenhoff, in *Correlative Microscopy in Biology: Instrumentation and Methods*, M.A. Hayat, Ed., Academic Press, London, 1987
- 13 H.T.M. van der Voort, PhD Thesis, (Amsterdam University, The Netherlands, 1989)
- 14 T. Wilson (ed.), *Confocal Microscopy*, Academic Press, London, 1990
- 15 D.A. Weitz and J.S. Huang, in *Kinetics of Aggregation and Gelation*, (North Holland, Amsterdam, 1984)
- 16 J.W.Th. Lichtenbelt, H.J.M.C. Ras and P.H. Wiersema, *J. Colloid Interface Sci.*, 1974, **46**, 522
- 17 J.W.Th. Lichtenbelt, C. Pathmamanoharan and P.H. Wiersema, *J. Coll. Int. Sci.*, 1974, **49**, 281
- 18 N.H.G. Penners and L.K. Koopal, *Colloids and Surfaces*, 1987, **28**, 67
- 19 S.A. Troelstra and H.R. Kruyt, *Kolloid-Beihefte*, 1943, **54**, 225
- 20 G. Frens, *Faraday Discuss. Chem. Soc.*, 1990, **90**, 143
- 21 P. Walstra, *J. Colloid Interface Sci.*, 1968, **27**, 443
- 22 D.S. Horne, *Faraday Discuss. Chem. Soc.*, 1987, **83**, 259
- 23 H.C. van de Hulst, *Light scattering by small particles* (Wiley, New York, 1957; Dover edn, 1981)

## IV Formation and Geometric Structure of Particle Gels

### 4.1 Aggregation experiments

In this section the results of simple aggregation experiments are described and discussed. The aim of these experiments is to obtain qualitative information about parameters affecting the gelation or the formation of a sediment. Parameters that have been varied are the size of the particles, their volume fraction, their density and their (surface) properties.

#### 4.1.1 Casein particles

In order to study the effect of the casein concentration on the gelation or aggregation of casein dispersions series of tubes with varying casein concentration were destabilized with GDL which slowly hydrolyses thus causing acidification, or rennet which cuts the hydrophylic protruding chains of the  $\kappa$ -casein (fig. 3.1). Results for sodium caseinate dispersions are compiled in table 4.1.

**Table 4.1:** Sodium caseinate with GDL (0.25 g per g caseinate powder, 30 °C)

casein concentration (g kg <sup>-1</sup> )	volume fraction (%)	description
> 1.8	> 0.48	continuous gel network which remains intact for at least 24 h at quiescent conditions.
0.5 - 1.8	0.14 - 0.48	segregation, in first instance a continuous network is formed which, in general, releases from one side of the wall of the tube leading to a cobweb like structure.
< 0.5	< 0.14	sediment on the bottom of the tubes and some cobweb like flocs on the wall.

The size of the clusters that would form a network at these concentrations can be estimated if we assume a dimensionality,  $D = 2.35$  and casein particles with radius  $a = 50$  nm (Eqn. 2.6). If  $\phi = 0.48$  % the size of the clusters,  $R$ , is 0.18 mm and if  $\phi = 0.14$ %,  $R = 1.2$  mm. Skim-milk dispersions gave a similar impression when they were destabilized with GDL; however, the volume fraction casein above which a gel is formed was slightly higher. At low volume fraction rennet-induced skim-milk gels showed a similar behaviour but at high volume fractions syneresis occurred occasionally. Syneresis led to a release of the network from the wall and a shrinking gel which retained its original shape. Whether syneresis on a macroscopic level occurs, presumably depends on the surface properties of the tube and on mechanical disturbances which may lead to release of the gel from the wall of the tube. The higher the casein concentration, the more often macroscopic syneresis occurred after ageing for 16 h at 30 °C. Rennet induced gels were stable for at most three days at 30 °C, after this time all rennet-induced gels were collapsed. The appearance of the remaining, collapsed casein network varied. The network shrank in one piece if the gel came free from the wall during the first stages of the ageing process; if no such release occurred, some dense flocs remained sticking to the wall of the container. Acid casein gels stayed stable for weeks.

#### 4.1.2 Polystyrene particles

The small polystyrene particles, radius 35 nm and 70 nm, were prepared by emulsion polymerization in the presence of surfactant (section 3.1). The dispersion with 35 nm particles, pH = 7, was stable at NaCl concentrations below 0.2 M for at least 2 days. At pH = 3, the particles were stable at NaCl concentrations below 0.08 M. Presumably, the palmitate used during the emulsion polymerization of these particles was not fully removed by the purification procedure and the carboxyl groups cause the particles to be negatively charged at pH 7. At pH 3 these weak acidic groups become uncharged and lose their stabilizing effect. The dispersion with 70 nm particles possessed roughly the same properties after they were covered with Na-palmitate (section 3.2).



Without being covered the particles were only stable at NaCl concentrations below 0.05 M. The critical coagulation concentration, ccc, – defined as the salt concentration above which the aggregation rate is diffusion limited – was roughly 0.18 M (fig. 4.1). The surfactant, N-dihexyl sulfosuccinate, was presumably largely removed by the purification procedure. The surface charge density caused by the  $-\text{SO}_4^-$  groups that stem from the initiator,  $\text{K}_2\text{S}_2\text{O}_8$ , is relatively low for small particles because they have a relatively large surface. This may be the reason for the low electrolyte concentrations at which these particles coagulate.

The larger polystyrene particles prepared without surfactant were stable at NaCl concentrations below 0.2 M, independent of the pH and the ccc was 0.4 M. These properties did not change after addition of Na-palmitate and it was impossible to destabilize the large particles by addition of GDL. Presumably, a high surface charge density caused by  $-\text{SO}_4^-$  groups hinders the adsorption of palmitate. These strong acidic groups are not neutralized by GDL. In Fig. 4.1, the rates of coagulation, expressed as  $d\tau/dt$ , are shown as a function of the electrolyte concentration for the 70 and 220 nm particles. The coagulation rate  $d\tau/dt$  is measured 15 s after the addition of salt.

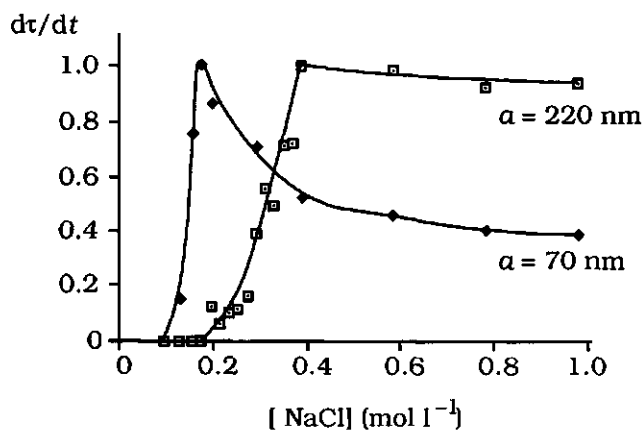


**Fig. 4.1** Relative apparent coagulation rates, expressed as  $d\tau/dt$  15 s after salt addition, for (almost) surfactant-free polystyrene sols with particle radii of 70 and 220 nm.

At salt concentrations higher than roughly 0.2 M the 70 nm particles show an *apparent* decrease of the coagulation rate as a function of the NaCl concentration. This decrease is due to the method of measurement;  $d\tau/dt$  is dependent on the coagulation rate, but also on the evolution of the floc geometry. Because the structure factor,  $S(q) \propto (qa)^{-D}$ , is larger for flocs with a higher fractal dimensionality (Eqn. 2.18 with  $qa \ll 1$  and  $qR \gg 1$ ), compact flocs provide a higher turbidity than ramified flocs containing the same amount of particles. Presumably, the flocs become more ramified at higher NaCl concentration. This hinders an accurate determination of the ccc by this method because it is uncertain whether the coagulation rate has attained the plateau level at the salt concentration where  $d\tau/dt$  is highest. For the 220 nm particles the rate of change of the turbidity is, after 15 s, mainly due to the formation of doublets and the geometric structure of the flocs is thus hardly reflected, resulting in a value of  $d\tau/dt$  independent of the salt concentration beyond the ccc.

The maximum turbidity of the dispersions,  $\tau_{\max}$ , was highest at electrolyte concentrations just below the ccc, indicating relatively compact flocs. At a higher concentration of monovalent electrolyte  $\tau_{\max}$  decreased as a function of  $c_s$  until it attains a constant level at high salt concentration ( $> 0.8$  M). This indicates that the flocs become more ramified as [NaCl] increases. Higher concentrations of monovalent counter ions lead presumably to stronger interparticle contacts. Low values of  $\tau_{\max}$  were also obtained by coagulation due to counter ions with higher valencies [1]. Here  $\tau_{\max}$  attained the same value as for high concentrations monovalent electrolyte but the level appeared to be independent of the electrolyte concentration beyond the ccc [1]. Polyvalent counter ions form presumably stronger interparticle contacts than monovalent ions.

The results of the study of the sediment volume of polystyrene latices are compiled in fig. 4.2 and table 4.2. For all surfactant-free latices the volume fraction of particles in the sediment,  $\phi_{\text{sed}}$ , varied from about 3 % at high salt concentration,  $c_s$ , to about 10 % at the ccc. These values are in agreement with the result of Buscall et al. [2] who observed that rapid aggregation of submicron spheres results in a space-filling network at a critical volume fraction of 5 %. The sediment volume was measured

40 h after salt addition. High sediment volumes and thus low values of  $\phi_{\text{sed}}$  (ramified flocs) correlated well with low values of  $\tau_{\text{max}}$ . The explanation of the apparent decrease of the coagulation rate as a function of  $c_s$  (fig. 4.1) is in agreement with the volume fraction of the 70 nm particles in the sediment. At  $c_s = 0.2$  M, both  $\phi_{\text{sed}}$  and  $d\tau/dt$  are relatively high and they decrease at higher  $c_s$ .

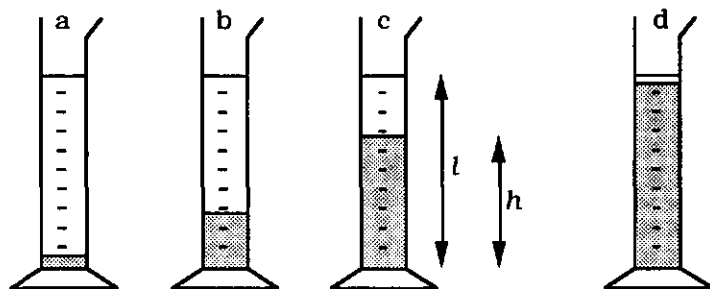


**Fig. 4.2** Determination of the relative sediment volume,  $v_s = h/l$  and the volume fraction of the particles in the sediment,  $\phi_{\text{sed}} = \phi_0/v_s$  for a polystyrene latex sol at various salt concentrations: a)  $[\text{NaCl}] = 0.1$  M (no aggregation, stored in the refrigerator for 2 weeks), b)  $[\text{NaCl}] = 0.4$  M, c)  $[\text{NaCl}] = 1$  M and d)  $[\text{MgCl}_2] = 0.5$  M.  $\phi_0 = 3\%$ ,  $a = 395$  nm

[NaCl]		70 nm		220 nm		395 nm	
$\phi_0(\%)$	$v_s$	$\phi_{\text{sed}}(\%)$	$v_s$	$\phi_{\text{sed}}(\%)$	$v_s$	$\phi_{\text{sed}}(\%)$	
0.11	1	0.16	6.3	N.S.	—	N.S.	—
0.11	3	0.42	7.1	N.S.	—	N.S.	—
0.11	10	1	gel	N.S.	—	N.S.	—
0.20	1	0.18	5.6	0.12	8.3	0.09	11.1
0.20	3	0.42	7.1	0.33	9.1	0.29	10.3
0.20	10	1	gel	1	gel	0.92	10.9
0.39	1	0.48	2.1	0.11	9.1	0.10	10.0
0.39	3	1	gel	0.31	9.7	0.29	10.3
0.39	10	1	gel	0.97	10.3	0.90	11.1
0.95	1	0.68	1.5	0.26	3.8	0.22	4.5
0.95	3	1	gel	0.88	3.4	0.69	4.3
0.95	10	1	gel	1	gel	1	gel

**Table 4.2**  $v_s$  and  $\phi_{\text{sed}}$  for various polystyrene latex sols, coagulated by various NaCl concentrations. Sediments were aged for 40 h. N.S. means no sedimentation within 40 h.

The present understanding of aggregation is mainly based on computer simulations, where two different regimes of irreversible aggregation are distinguished. In the diffusion limited regime [3, 4] all encounters result in attachment and the flocs exhibit an open, ramified structure ( $D = 1.8$ ). In the reaction limited regime [5, 6] many encounters must occur before attachment takes place. This results in denser flocs ( $D = 2.1$ ). The latter regime applies to aggregation at low  $c_s$  where electrostatic forces cause a repulsive energy barrier of several  $kT$  between approaching particles. At higher  $c_s$  the height of the barrier is reduced until it is completely eliminated at the ccc. At salt concentrations higher than the ccc, aggregation becomes diffusion limited. Consequently,  $\phi_{sed}$  is expected to decrease as a function of  $c_s$  until it reaches a constant, low value at the ccc. In practice, however, flocs that are formed at the ccc are relatively dense resulting in a high  $\phi_{sed}$  and  $\tau_{max}$  and only beyond the ccc become the flocs more ramified as a function of  $c_s$ . The variation in floc geometry beyond the ccc is presumably caused by a decreasing extent of rearrangement as a function of  $c_s$  [7]. Apparently, higher  $c_s$  results in stronger, stiffer flocs.

Gels of polystyrene particles with  $[NaCl] = 0.95$  M and  $\phi_0 = 10$  % formed a network which was much coarser and weaker than the original gel after they were redispersed by violently shaking them. Shaking sediments or gels with  $[NaCl] = 0.95$  M and  $\phi_0 = 3$  % resulted in more compact sediments after settling,  $\phi_{sed} \approx 10$  %. After shaking and settling, sediments with  $[MgCl_2] = 0.5$  M were less dense;  $\phi_{sed} \approx 6$  % ( $\phi_0 = 3$  %). All sediment volumes decreased slowly as a function of time, but the mutual relative differences between the sediments at various salt concentrations persisted. After 3 weeks the sediment volumes reduced to about 70 % of the volume obtained after 40 h.

Coagulation experiments of the palmitate-covered latices resulted in a coarse, space-filling network, even at low volume fraction ( $a = 70$  nm,  $\phi_0 = 1$  %). The coarseness of the network was a result of the mixing of the electrolyte and the sol. Immediately after the sol came into contact with electrolyte solution, gelation occurred leading to encapsulation of the electrolyte, and it was necessary to vigorously shake the mixture to obtain a homogeneous distribution of the electrolyte. Turbidity measurements resulted in  $\tau_{max}$  being similar for  $[NaCl] = 0.4$  and  $[NaCl] =$

1 M and lower than for the bare particles. Floccs made of palmitate-covered polystyrene particles are apparently much stiffer than floccs of bare particles leading to less rearrangement and more ramified floccs.

At quiescent conditions the palmitate-covered polystyrene particles of 35 and 70 nm radius formed a network at extremely low volume fractions. Even at  $\phi_0 = 0.0002$  a cobweb like network, with a mesh-size that could be perceived by the naked eye, was formed after aggregation of the 35 nm particles with GDL. If we assume a fractal dimensionality of 2.2, the radius of the clusters would be 1.5 mm (Eqn. 2.6) which is roughly equal to the experimental result. The aggregation of these large clusters occurs, of course, not due to their Brownian motion. Small velocity gradients in the dispersion presumably hinder settling of the floccs and cause orthokinetic aggregation (chapter VI). The density difference,  $\Delta\rho$ , between the palmitate-covered polystyrene particles and the medium was very small. After ageing for some days the network was somewhat coarser and often it became partly released from the wall of the container.

At higher volume fractions, 1 to 10 %, the quiescently aggregated system was more 'solid-like'; the gel could resist gravity (to some extent) without being stuck to the walls of a container. After stirring, the gels fractured into large floccs that expelled some liquid (showed some syneresis) thus forming a viscous dispersion. At volume fractions higher than 10 % the gels had a very short consistency, and stirring converted the system into a grainy mass.

#### 4.1.3 Emulsions

Emulsions of small droplets of bromated salad oil gelled at very low volume fractions ( $\phi_0 < 1\%$ ), at least if a small excess of casein was present. The density of the emulsion droplets was matched to the density of the continuous phase at 30 °C in order to prevent creaming. After micro filtration of the emulsions all casein that was not situated at the surface of the droplets was removed, and addition of GDL resulted in coalescence. An excess casein was thus needed to form a gel and it was uncertain whether a casein gel with emulsion droplets inside, or a gel of aggregated emulsion droplets was formed. Emulsions without free casein,

$a \approx 10 \mu\text{m}$  and  $\phi_0 = 10, 20$  and  $30 \%$ , to which a small amount of casein was added appeared to be stable 16 h after the addition of GDL. However, after gentle rocking the emulsions became stiff. The small amount of free casein,  $\phi = 0.3 \%$ , became attached to the surface of the droplets a short time after the destabilization by GDL. Further aggregation of these large droplets occurred due to small velocity gradients. The rocking of the emulsion caused velocity gradients which may have led to further aggregation or to an increase of the strength of the bonds between the droplets. The diameters of the clusters in the gels were, according to Eqn. 2.6 with  $D = 2.35; 0.69, 0.24$  and  $0.13 \text{ mm}$  for  $\phi_0 = 10, 20$  and  $30 \%$  respectively. This was in agreement with observations; the 10 % emulsion showed clear irregularities on a length scale somewhat smaller than 1 mm whereas both other gels appeared homogeneous. Aggregation of very large particles may thus lead to the formation of a fractal particle network in spite of the fact that these particles are much more sensitive to disturbances like sedimentation and velocity gradients.

#### 4.1.4 Haematite particles

Spherical haematite particles prepared by the method of Penners and Koopal [8] were destabilized by addition of various concentrations of NaCl. The particle volume fraction was 0.5 % in all samples,  $a$  was 34 nm and the pH was 4. At  $c_s$  above 0.08 M (the ccc [9]) haematite sols showed the same behaviour as the bare polystyrene particles: an increasing sediment volume at increasing salt concentration. The value of  $\phi_{\text{sed}}$  varied from roughly 16 % at 0.06 M to about 4 % at 1 M NaCl and 2 - 3 % at 0.5 M  $\text{Na}_2\text{SO}_4$ , measured 24 h after salt addition. The sample with  $[\text{NaCl}] = 0.05 \text{ M}$  appeared stable just like samples with lower salt concentration. However, during decanting the 0.05 M dispersion was more viscous and showed some gel-like blobs (3 days after salt addition). At low electrolyte concentrations, where slow aggregation occurs, Frens [10] reported very low values of  $\tau_{\text{max}}$  and gelation at  $\phi_0 = 2 \%$  [11]. He explained these results with anisotropic aggregation resulting in chains of particles. The repulsive energy barrier favours attachment of new particles at the ends of a string [12] and hinders rearrangement of strings into more compact structures. Amal et al. [13] found  $D$  of haematite aggregates to range from

2.3 for rapid, diffusion limited aggregation ( $[KCl] = 0.08 \text{ M} = \text{ccc}$ ) to 2.8 for slow, reaction limited aggregation ( $[KCl] = 0.05 \text{ M}$ ). They did not report on aggregation at higher salt concentrations nor on ramified flocs at low electrolyte concentration. The fractal dimensionality of 2.3 found at the ccc and thus at a condition of diffusion limited aggregation, is much higher than expected from computer simulations. This discrepancy is probably due to the large effect of rearrangements on the geometry of the flocs. At high electrolyte concentration or in the case of counter ions with a higher valency rearrangements are probably less pronounced leading to a lower value of  $D$ .

#### 4.2 Permeability

In fig. 4.3 permeability coefficients,  $B_p$ , of acid Na-caseinate and polystyrene latex gels are given as a function of the volume fraction of the primary particles,  $\phi_0$ . The volume fraction of the casein matrix was calculated by assuming the voluminosity of the casein particles to be 2.7 ml per g casein [14].

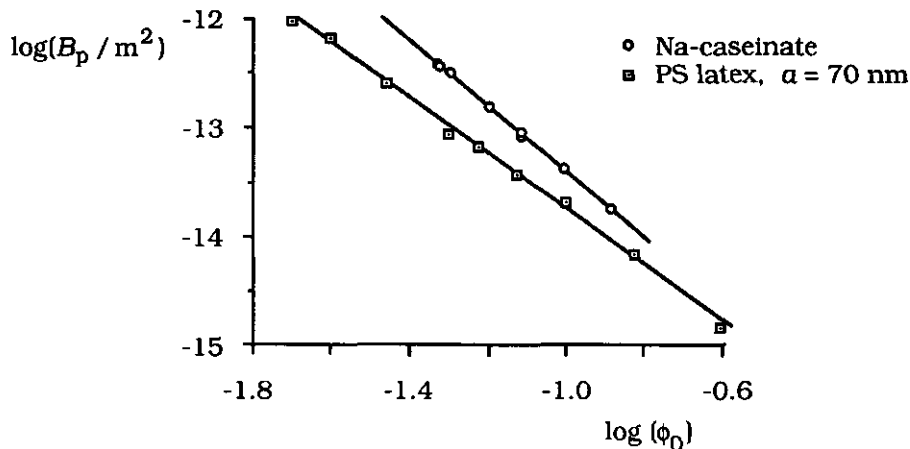


**Fig. 4.3** *Logarithm of the permeability coefficient as a function of the logarithm of the volume fraction of Na-caseinate and polystyrene latex gels formed by acidification with GDL and aged for 16 h at 30 °C before measurement at 30 °C.*

The slope of these log-log plots is  $-3.05$  in the case of the Na-caseinate gels and  $-2.54$  for gels made with polystyrene particles. All gels were aged for 16 h at  $30\text{ }^{\circ}\text{C}$ . Roefs et al. [15] reported a slope of  $-3.3$  for gels prepared by warming a skim-milk dispersion of pH 4.6 from 4 to  $30\text{ }^{\circ}\text{C}$  (type 1 gel). At similar volume fraction these gels have a higher permeability due to a larger size of the primary particles. The effective fractal dimensionalities of the clusters composing the gels, obtained with Eqn. 2.11, are 2.39 for type 1 skim-milk, 2.34 for type 2 Na-caseinate, and 2.21 for polystyrene latex gels.

The permeability of acid casein and polystyrene latex gels is time independent. No difference in permeability was found between gels that were aged for 2, or 18 h. Just after the gel point changes in geometric structure may occur, but it is impossible to study the permeability of gels at that early stage; the gels are not strong enough to resist the pressure gradient and it takes at least 20 minutes to determine the permeability of a gel. Therefore, reliable values of the permeability could only be obtained after the gel was aged for about 2 h.

Experiments with casein gels obtained by adding rennet to skimmed milk were performed by van Dijk and Walstra [16, 17]. They obtained, again in a plot of  $\log B_p$  versus  $\log \phi_0$ , an initial slope of  $-2.6$ , but the permeability increased as a function of time due to 'microsyneresis'. This is because rennet-induced casein gels tend to synerese, while during the permeability measurement macroscopic shrinking of the gel is impossible, since it is constrained in a tube. This causes rearrangements of the network on a microscopic scale. Consequently, local condensation of the network and the formation of wider pores elsewhere. Before extensive microsyneresis occurred, the effective fractal dimensionality was 2.23.

In order to fit the permeability data of the polystyrene latex gels the constant,  $K$ , in Eqn. 2.11 should be  $1.0 \times 10^2$  leading to  $B_p = R_g^2/100$ . It is not possible to obtain  $K$  for the casein gels because the casein particles have a rather broad size distribution and the volume fraction of the particles is not exactly known. However, substitution of  $K = 100$  in Eqn 2.11 enables the estimation of the average size of the casein particles. In order to fit the measurements  $a$  should be 88 nm in the case of skimmed milk gels and 59 nm in the case of Na-caseinate gels (voluminosity of



casein assumed to be  $2.7 \text{ ml g}^{-1}$ ). These sizes are in reasonable agreement with the results obtained by Roefs et al. [15], indicating that also in the case of casein gels the factor  $K$  is not far from 100, in spite of the difference in  $D$ .

The magnitude of  $K$  depends on the cluster size distribution and on the effective permeability of the individual clusters. The latter may be described in terms of the ratio between the hydrodynamic radius of the clusters composing the gel,  $R_h$ , as defined by the Stokes-Einstein relation and  $R_g$  (fig. 4.4)

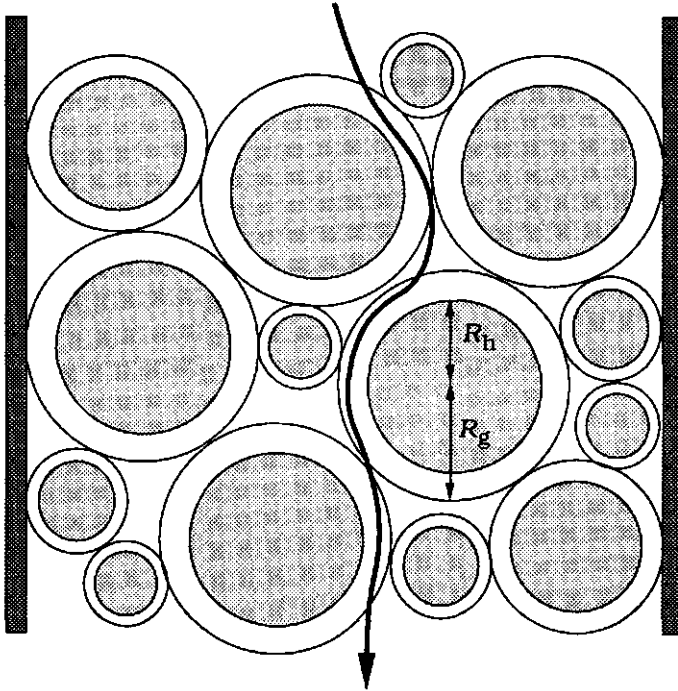


**Fig. 4.4** Highly schematic representation of a gel built up of spherical clusters with a hydrodynamic radius  $R_h$  and an effective radius in the gel  $R_g$ . The bold line shows a possible path for the percolating liquid.

The most widely used approach for the permeability of a porous medium is the so called Kozeňy-Carman equation in which the medium is represented by a bundle of tortuous, non-interconnecting channels of various width but of a definite length. The permeability is calculated from

the flow through the channels and expressed in terms of the specific surface area of the pores and the porosity of the medium [18]. For a structure built up of spheres the specific surface area may be converted into the volume surface average radius of the spheres,  $R_{32}$ , and one may write [16]

$$B_p = \frac{(1-\phi)^3 R_{32}^2}{45\phi^2} \quad (4.1)$$

However, the volume fraction of the spheres should be higher than 0.5. This condition is not met in the particle gels that have been studied since  $\phi_0$  varied from 0.02 to 0.25. However, if a particle gel is considered to be built up of spherical clusters with a hydrodynamic radius  $R_h$  and an effective radius  $R_g$  (fig. 4.4), Eqn. 4.1 may be valid because the effective volume fraction of the clusters with radius  $R_h$  is considerably higher than  $\phi_0$ . This effective volume fraction depends on the packing density of the spheres with radius  $R_g$  and on the ratio  $R_h/R_g$ . Assuming a packing density of 0.7, the effective volume fraction of the hydrodynamic spheres is  $0.7(R_h/R_g)^3$ . Substituting this value for  $\phi$  in Eqn. 4.1 and relating it to the empirical relation  $B_p = R_g^2/100$  leads to:

$$B_p = \frac{(1-0.7(R_h/R_g)^3)^3 R_h^2}{45(0.7(R_h/R_g)^3)^2} = \frac{1}{100} R_g^2 \quad (4.2)$$

The ratio  $R_g/R_h$  can be obtained from this equation and turns out to be 1.13.

A more direct approach is by use of the Brinkman equation which is based on a so called drag theory. The medium is assumed to consist of spherical particles kept in position by external forces. The permeability coefficient,  $B_p$ , is calculated from the damping force exerted by the particles on the liquid flowing around them and can be written as [18]:

$$B_p = \frac{R_h^2}{18} \left( 3 + \frac{4}{\phi} - 3\sqrt{\frac{8}{\phi} - 3} \right) \quad (4.3a)$$

Substitution of the empirical relation  $B_p = R_g^2/100$  and  $\phi = 0.7(R_h/R_g)^3$  yields  $R_g/R_h = 1.13$  again. Adachi and Kamiko used the Brinkman theory to study the sedimentation velocity of separate permeable flocs [19]. The ratio,  $F$ , between the resistance experienced by an impermeable sphere and that of a permeable sphere can be calculated from [19]

$$F = \frac{\left(\frac{R}{\sqrt{B_p}}\right)}{\left(\frac{R}{\sqrt{B_p}}\right) - \tanh\left(\frac{R}{\sqrt{B_p}}\right)} + \frac{3}{2\left(\frac{R}{\sqrt{B_p}}\right)^2} \quad (4.3b)$$

The permeability coefficient of a gel equals that of its smallest elements that possess on average the properties of the gel as a whole, i.e. elements with radius  $R_g$ . The factor  $\left(\frac{R}{\sqrt{B_p}}\right)$  in this equation may thus be obtained from the empirical relation  $B_p = R_g^2/100$ ; i.e.  $\left(\frac{R}{\sqrt{B_p}}\right) = 10$ . Substitution in Eqn. 4.3b yields  $F = 1.13$ . The hydrodynamic drag experienced by a sphere is linearly proportional to its radius (Stokes) and the ratio  $F$  thus equals the ratio  $R_g/R_h$ . Because a small variation in the ratio  $R_g/R_h$  results in a large change of the permeability, the ratio can be obtained with a high accuracy and rather independent of the model. On the other hand, it implies that expressions for the permeability of a particle gel are necessarily imprecise.

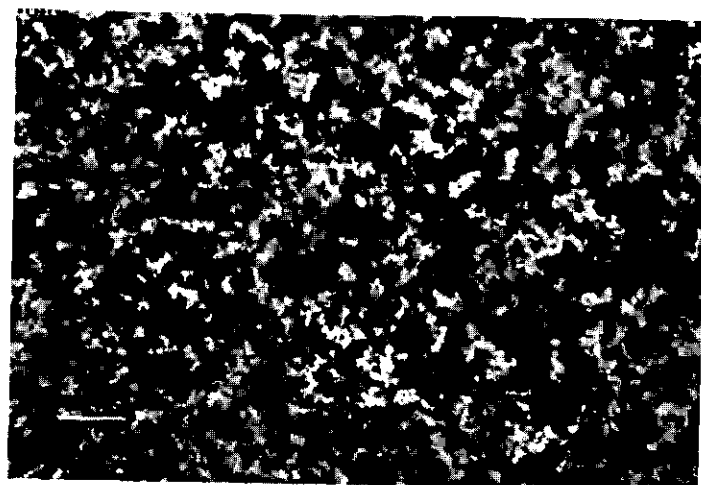
The ratio  $R_g/R_h$  is dependent on the dimensionality of the clusters; it should equal 1 in the case of  $D = 3$  and be higher at lower dimensionalities. The value of  $R_g/R_h$  is significantly smaller than expected for tenuous fractal flocs: For random polymer coils, the ratio between the hydrodynamic radius and the radius of gyration,  $R_h/R_{gyr}$ , calculated with the Kirkwood-Riseman theory, equals 0.665 [20]. The radius of gyration is substantially smaller than  $R_g$  and  $R_g/R_h$  thus is expected to be roughly 2. Chen and Meakin [21, 22] obtained values for  $R_h/R_{gyr}$  of 0.875 and 0.97 for simulated clusters with  $D = 1.78$  and 2.1 respectively. For ideal fractal flocs the radius of gyration can be related to  $R_g$  as will be shown later on;  $(R_{gyr}/R_g) = \sqrt{D/(2+D)}$  (Eqn. 6.10) [23]. The ratio  $R_g/R_h$  thus amounts to 1.67 and 1.44 for  $D = 1.78$  and 2.1 respectively. Amal et al. [13] estimated  $R_{gyr}$  of haematite flocs using static, and  $R_h$  by dynamic light scattering, and obtained a ratio which was roughly equal to 1 yielding  $R_g/R_h = 1.36$ . When using these values, the permeability of the gel would be much

higher than actually measured; substituting the value 1.36 for  $R_g/R_h$  in Eqn. 4.2 yields  $B_p = 1/17 R_g^2$  which is about 6 times higher than the experimental permeability. After the gel point rearrangements may have caused a decrease of  $R_g/R_h$  by internal cross-linking and interpenetration of the flocs. The difference between experimental and theoretical values of  $B_p$  can not be due to polydispersity of the flocs: in the case of a broad cluster size distribution the permeability would be even higher, because the largest pores predominantly determine the value of  $B_p$  ( $R_{42} > R_{3D}$ ).

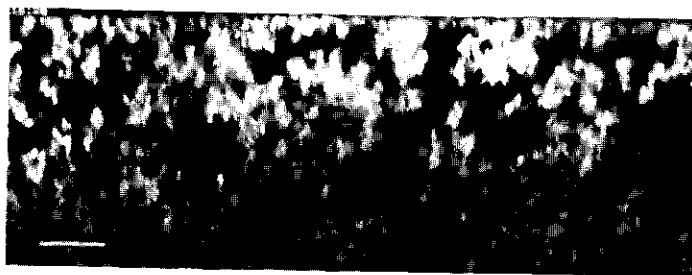
### 4.3 Confocal scanning laser microscopy

Optical sections of various skim-milk gels of casein concentration 2.7 % (m/m) are shown in figs. 4.5 and 4.6. The first of these figures shows two micrographs of an acid skim-milk gel, a section in the  $x$ - $y$  plane (fig. 4.5a) and a section in the  $x$ - $z$  plane (fig. 4.5b). Assuming a particle radius of 80 nm,  $D = 2.35$  and a voluminosity of 2.7 ml g<sup>-1</sup> results in a cluster radius of 4.5  $\mu$ m (Eqn. 2.6) which seems to agree with the micrographs. The section in the  $x$ - $z$  direction (fig. 4.5b) is obtained by scanning lines in the  $x$ -direction and shifting the sample over a distance of 100 nm in the  $z$ -direction after a line has been scanned. In total 300 lines have been scanned in this way and the total depth is thus 30  $\mu$ m. The magnification of the clusters is therefore higher in the  $z$ -direction which results in somewhat elongated clusters.

The  $x$ - $z$  section shows a higher casein density close to the glass surface. This implies small pores and clusters in the  $x$ - $y$  sections close to the glass wall. Sections have to be taken on a depth of at least one cluster diameter in order to be sure to observe a bulk-gel. The optical resolution and the apparent density gradually decrease upon penetrating deeper into the sample, due to scattering of the fluoresced light. This effect is dependent on the casein concentration; for 40 g/kg the maximum depth was roughly 20  $\mu$ m and for low concentrations (< 15 g/kg) it was bound by the focal distance of the objective. The resolution in the  $z$ -direction depends on the size of the pinhole (fig. 3.3) and is somewhat lower than that in the  $x$  or  $y$ -direction.



a)

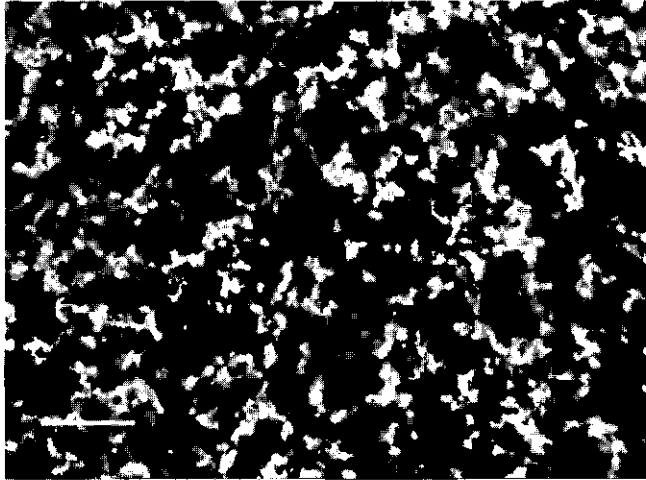


b)

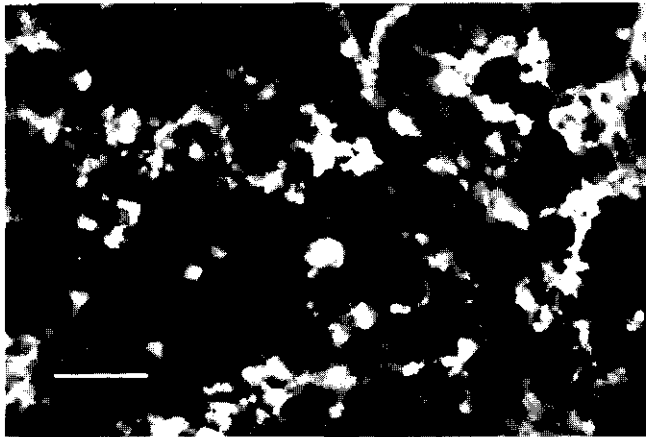
**Fig. 4.5** *Confocal Scanning Laser Micrographs of type 2 acid skim-milk gels with a casein concentration of 27 g/kg. The bars refer to 10  $\mu\text{m}$  in the x or y-direction. a) optical section in the x-y plane; b) optical section in the x-z plane, the total length of the z-axis is 30  $\mu\text{m}$ .*

The ageing of rennet-induced skim-milk gels is shown in fig. 4.6 where two sections of gels, aged for 1 and 18 h at 30  $^{\circ}\text{C}$  are depicted. The coarseness of the fresh gel is of the same order as in the case of the acid gel of fig. 4.5. However, the structure seems to be different; in the acid gels the clusters are packed rather loosely whereas the stress caused by microsineresis leads to aggregates connected by stretched strands in the case of rennet-induced gels. This variation in structure has a large effect on the rheological properties of the gel as will be shown in chapter V. After ageing for 18 h the coarseness of the rennet-induced gels has

increased dramatically (fig. 4.6b). The coarsening continues until after a few days the gel breaks up into small flocs sticking to the glass surface.



a)



b)

**Fig. 4.6** *Optical sections through rennet-induced skim-milk gels, aged for 1 h (a) and 18 h (b) at a temperature of 30 °C. The bars refer to 10 μm.*

The scale invariance of fractal aggregates implies that a large floc is similar to a small floc but on another scale. The geometric structure of a

gel with a high volume fraction will therefore be similar to that of a gel with a low  $\phi_0$  on another scale if the cluster size distribution is similar. In fig. 4.7 two micrographs of Na-caseinate gels are shown at different casein concentrations and magnifications. The fractal dimensionality obtained from the relation between  $R_g$  and  $\phi_0$  is 2.35 (Eqn. 2.6).

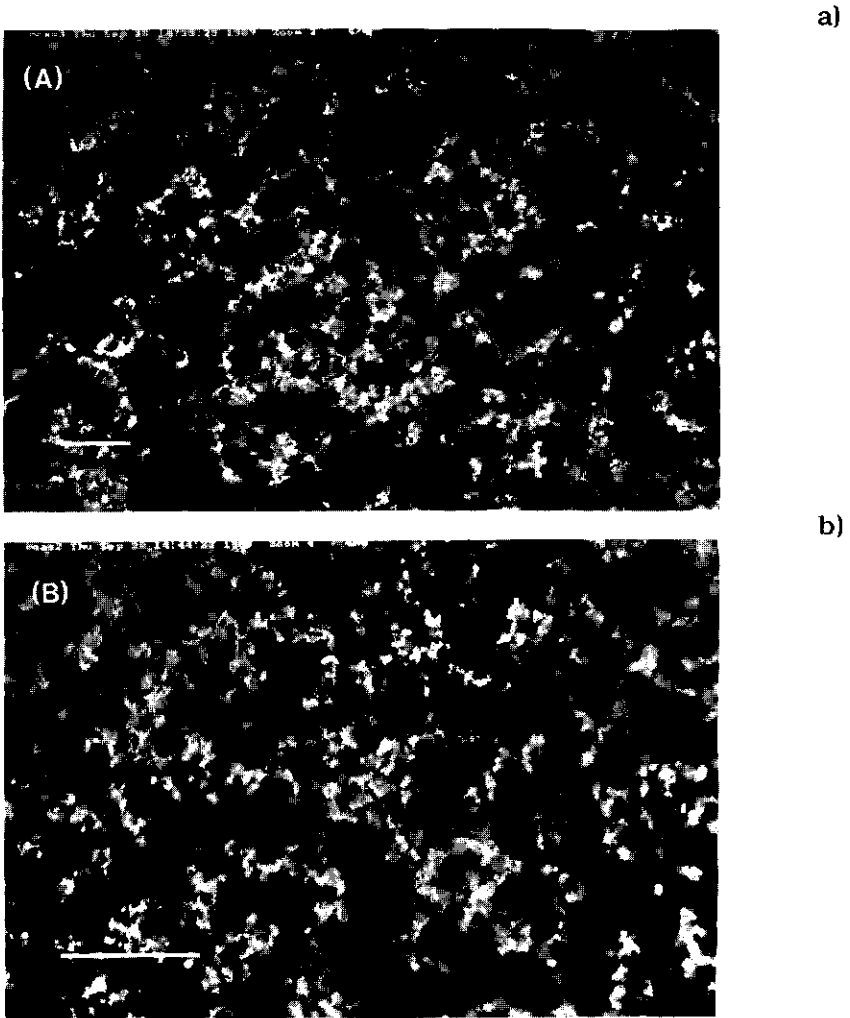


**Fig. 4.7** Confocal Scanning Laser Micrographs of acid Na-caseinate gels, a) casein concentration 16.2 g/kg, optical section thickness 4  $\mu\text{m}$ ; b) casein concentration 25.5 g/kg, optical section thickness 2  $\mu\text{m}$ . The bars refer to 10  $\mu\text{m}$ .

The fractal dimensionality is also accessible by applying correlation analysis to one single picture. In fig. 4.8  $\log C(r)$  has been plotted as a function of  $\log r$  for three casein concentrations which are chosen so that the expected cluster size for successive concentrations is always a factor 2 different if the dimensionality is 2.35 (Eqn. 2.6). The expected cluster sizes correspond reasonably well with the minima of the correlation functions in fig. 4.8. However, the slopes of the straight lines corresponding to  $D$  at length scales where fractal behaviour applies, were much lower than expected. Eqn. 2.15 predicts a slope of  $D - 3$  which equals  $-0.65$  if  $D = 2.35$ . However, the slopes in fig. 4.8 are  $-0.16$ ,  $-0.09$  and  $-0.04$  resulting in the unreasonable apparent dimensionalities  $D = 2.84$  for 16.2,  $D = 2.91$  for 25.5 and  $D = 2.96$  for 40 g/kg.

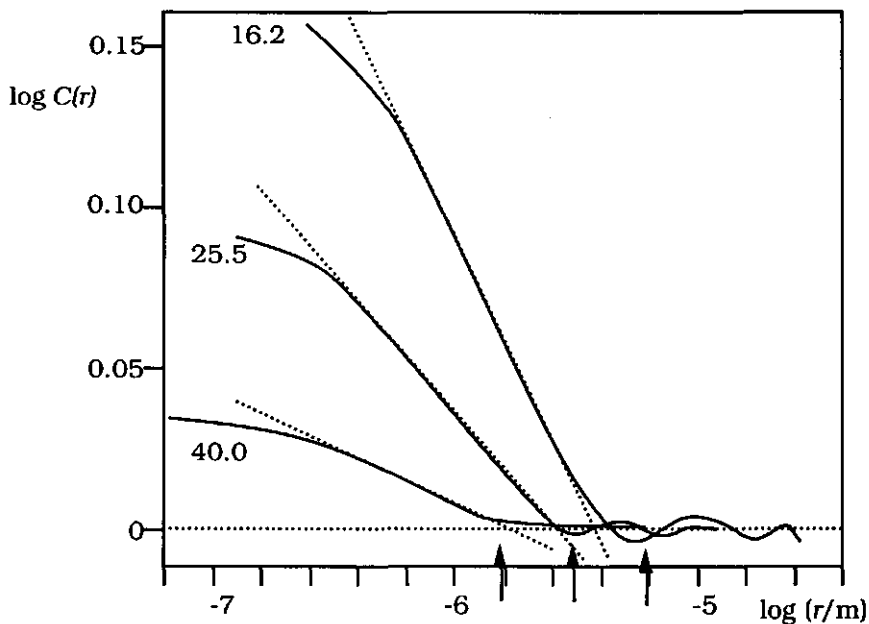


**Fig 4.8** Correlation functions deduced from micrographs of Na-caseinate gels with casein concentrations of 16.2, 25.5 and 40.0 g/kg. The arrows indicate the expected cluster sizes for  $a = 50$  nm,  $D = 2.35$  and a voluminosity of 2.7 ml per g casein. They amount to 1.5  $\mu\text{m}$ , 3.1  $\mu\text{m}$  and 6.2  $\mu\text{m}$ , respectively (Eqn. 2.6)



These high, concentration dependent values of the apparent  $D$  are caused by the limited resolution in the  $z$ -direction. A two-dimensional CSLM image is something in between a cross-section through the gel and a projection of the clusters present in a gel layer of a rather undefined thickness. The projection of a three-dimensional fractal floc is characterized by the same dimensionality as the floc itself if  $D < 2$  and 2 for any higher value of  $D$ . A cross-section through a three dimensional fractal floc is characterized by a dimensionality  $D - 1$  (section 3.4). The two-dimensional images are thus characterized by a fractal dimensionality between  $D - 1$  (real cross-section) and 2 (projection) if  $D$ , the fractal dimensionality of the three-dimensional clusters is larger than 2. Correlation analysis of the images yields thus values for the apparent fractal dimensionality between  $D$  and 3.

The dimensionality obtained from the curves shown in fig. 4.8 is dependent on the casein concentration because the resolution in the  $z$ -direction is more or less constant whereas the size of the fractal clusters is dependent on the casein concentration. At high concentrations the clusters are not very large compared to the resolution in the  $z$ -direction, the picture has therefore more the character of a projection of a layer than of a cross-section. At lower casein concentrations the clusters are bigger and the images get more and more the character of a cross-section, leading to a decrease in apparent dimensionality upon a decrease in casein concentration.

The conclusion is that for calculating  $D$  from the slope of the curves a correction has to be made for the finite thickness of the images. Figure 4.9 gives a histogram of the grey value distribution for the 25.5 g/kg casein gel. Since the volume fraction casein is roughly 6-7% the number of black sites, i.e., sites without casein, would be very high for a real cross-section. But, the histogram shows only a small number of sites without casein (grey level 0). This is due to the relatively thick optical section and to fluoresced light from sites which are out of focus and therefore spread out over the picture. If the volume fraction of casein is exactly known and the size of the particles is larger than the resolution of the microscope it would be possible to make a better reconstruction of the gel. In that case it would be possible to define a criterion, a minimum grey level value: any site with a lower grey value is supposed to be empty

and any location with a higher value full. This grey level should be chosen so that the surface fraction of primary particles on the picture equals  $\phi_0$ .

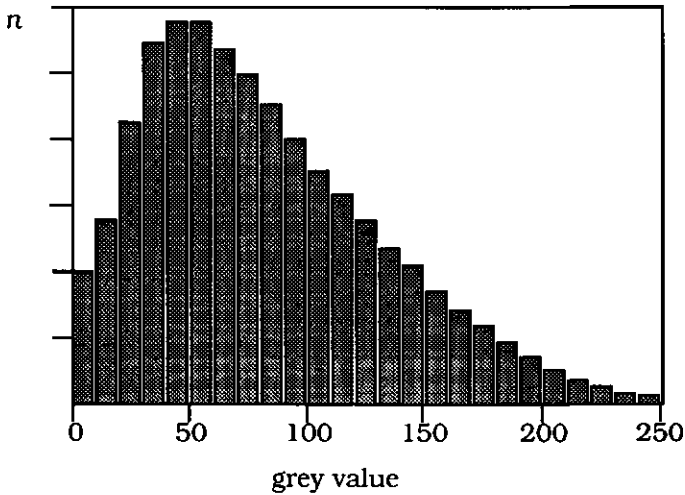


**Fig 4.9** Grey value distribution of an image of the 25.5 g/kg casein gel. The grey value is a measure for the number of casein particles that are present in a site, and  $n$  is a measure for the number of sites that have a particular grey value.

Actually, the size of the casein particles is smaller than the size of the sites that are scanned which makes the analysis more complicated. We subtracted from every grey value in the gel a value which was chosen in such way that the resulting picture had a surface fraction approximately equal to the volume fraction of the gel. Negative results were set 0 and the surface fraction was calculated by assuming a surface fraction 1 if all points had a grey value equal to the maximum value. In fig. 4.10 the surface fraction is plotted as a function of the value subtracted from all grey values in the case of the 25.5 g/kg casein gel. The volume fraction of the casein particles in the gel is about 7 % assuming a voluminosity of 2.7 ml/g ( $2.55 \% \times 2.7$ ). The value that has to be subtracted in order to obtain the appropriate surface fraction,  $\phi_s$ , is thus about 100. The original (apparent) surface fraction for all images was 30 - 35 %, independent of the casein concentration in the gel.

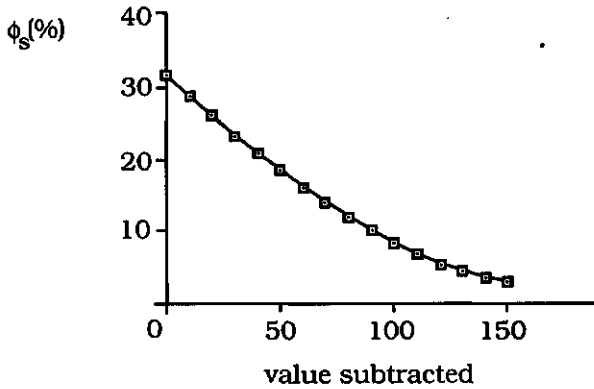


**Fig. 4.10** Typical example of the surface fraction as a function of the value subtracted from all grey values of the picture. This graph is derived from the same image as fig. 4.9.

The fractal dimensionality deduced from the correlation function of the modified images decreases gradually with an increasing diminishment of the grey values. It is however not very sensitive to this decrease since  $D$  varies roughly from 2.4 to 2.3 if the value subtracted varies from 80 to 130. For all images, these are the values that lead to a realistic surface fraction. The dependence of the apparent fractal dimensionality on the value subtracted is shown in fig. 4.11 where the second moment of the distribution of the amount of casein per square is plotted as a function of the size of the squares, both on a logarithmic scale (section 3.4.3). Since  $S_2(L)$  scales like  $L^{D_2+2}$ , resulting in high slopes, the second moment is normalized to  $S^*_2 = S_2(L)/(\langle n_{i,L} \rangle^2)$  in order to obtain relatively larger variations in the slope of the plots. Because  $\langle n_{i,L} \rangle^2$  scales like  $L^4$ , the slope of the lines in the  $\log L - \log S^*_2$  plots equals  $D_2 - 2$ . For the 3-dimensional flocs  $D$  is higher by an amount 1 ( $D = D_2 + 1$ ) and the slope is thus  $D - 3$  if the image represents a real cross-section. The grid method provides the same value of  $D$  as the correlation analysis but it is less (computer) time consuming.

The (apparent) surface fraction of the 16.2 g/kg image was 5 % after subtracting 100, and 3 % after subtracting 150 from all grey values of the image, and  $D$  was 2.39 and 2.20 respectively. The actual volume fraction of the gel, assuming a voluminosity of 2.7 ml/g, is  $1.6 \times 2.7 = 4.3$  %.

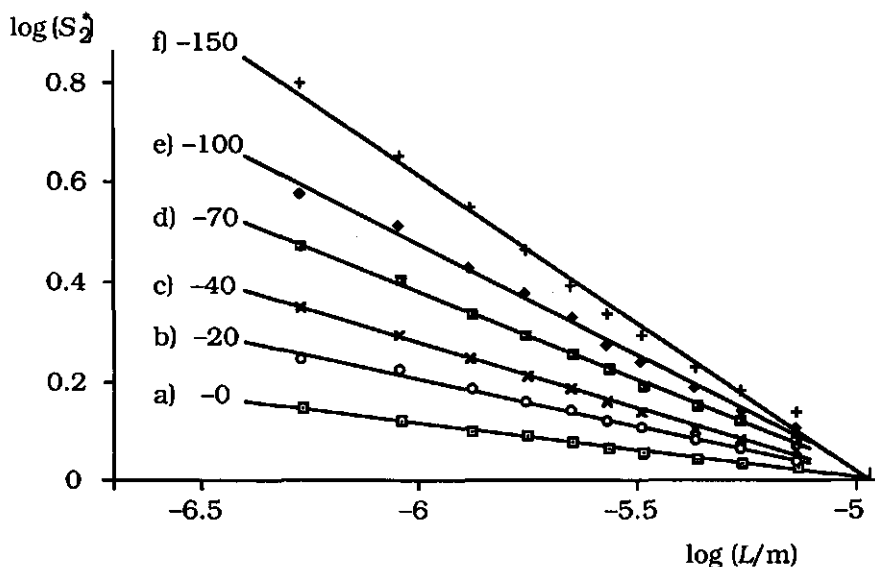


**Fig. 4.11** Second moment of the grey value distribution ( $S_2$ ), expressed as  $S_2^* = S_2(L)/\langle n_{i,L} \rangle^2$  as a function of the size of the squares ( $L$ , section 3.4.3) after subtraction of various values from the image of the 16.2 g/kg gel. The value subtracted is indicated near the figures. a) slope =  $-0.16$ ,  $D = 2.84$ , b) slope =  $-0.26$ ,  $D = 2.74$ , c) slope =  $-0.36$ ,  $D = 2.64$ , d) slope =  $-0.49$ ,  $D = 2.51$ , e) slope =  $-0.61$ ,  $D = 2.39$ , f) slope =  $-0.8$ ,  $D = 2.2$ . The lines cross at  $L = 10.8 \mu\text{m}$ ,  $R_g \approx 5.4 \mu\text{m}$ .

In fig. 4.12 the fractal dimensionality, obtained with the grid method, is plotted against the apparent surface fraction of the image. The surface fraction determines the maximum difference between  $\langle n_{i,L} \rangle^2 = (S_1(L))^2$  and  $S_2(L) = \langle n_{i,L} \rangle$ . The first scales like  $\phi_s^2 L^4$ , but the latter has a maximum if all material is concentrated in one fraction,  $\phi_s$ , of the squares while the other fraction is empty. This is so if  $L < a$  and in that case  $S_2(L)$  scales like  $\phi_s L^4$  (section 3.4.3, table 4.3). The maximum value of  $S_2^* = S_2(L)/\langle n_{i,L} \rangle^2$  is thus  $1/\phi_s$ . The slope of the lines in fig. 4.11 is expected to be  $\log \phi_s / (\log R - \log a)$  if straight lines are assumed between the points  $S_2^* = 1/\phi_s$  for  $L = 2a$  and  $S_2^* = 1$  for  $L = 2R$  on a log-log scale. Because  $\log R - \log a$  is roughly 2 for the 16.2 g/kg gel ( $a \approx 50 \text{ nm}$  and  $R \approx 5 \mu\text{m}$ ) the slope,  $D - 3$ , would equal  $\log \phi_s / 2$ . The curve  $D = 3 + \log \phi_s / 2$  is also shown in fig. 4.12.

**Table 4.3** Calculated examples of  $\langle n_{i,L} \rangle^2$  and  $\langle (n_{i,L})^2 \rangle$  for a total of 5 squares at various conditions. The value of  $S^*_2$  is lowest and equal to 1 if the local volume fraction, expressed by  $n$ , is equal in all squares. The value is maximum and equal to  $1/\phi_s$  if all material is concentrated on a fraction,  $\phi_s$ , of the squares.

	$n$					$\phi_s$	$\langle n_{i,L} \rangle^2$	$\langle (n_{i,L})^2 \rangle$	$S^*_2$	$L \gg$
$R$	0.2	0.2	0.2	0.2	0.2	0.2	0.04	0.04	1.00	
$a < L < R$	0.0	0.1	0.2	0.3	0.4	0.2	0.04	0.06	1.50	
$L \ll a$	0.0	0.0	0.0	0.0	1.0	0.2	0.04	0.20	5.00	
$L \gg R$	0.6	0.6	0.6	0.6	0.6	0.6	0.36	0.36	1.00	
$a < L < R$	0.1	0.3	0.7	0.9	1.0	0.6	0.36	0.48	1.33	
$L \ll a$	0.0	0.0	1.0	1.0	1.0	0.6	0.36	0.60	1.67	

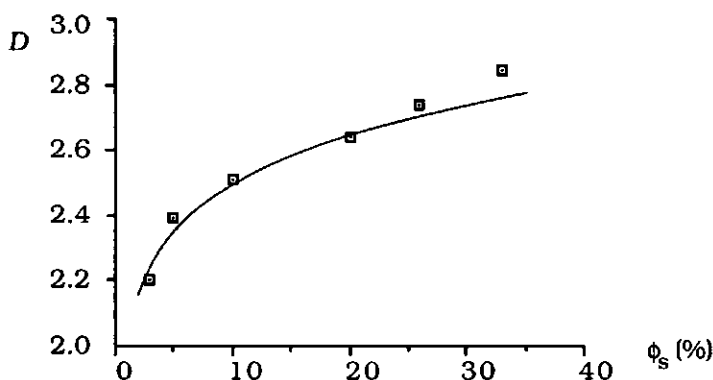


**Fig. 4.12**  $D$  obtained with the grid method as a function of the surface fraction of the particles in the images. The surface fraction was varied by subtracting various values from the grey values. At the actual volume fraction of the gel, 4.3 %,  $D \approx 2.35$ . The curve is a fit according to  $D = 3 + \log \phi_s / 2$ .

Extrapolation of the lines in fig. 4.11 to  $S^*_2 = 1/\phi_s$ , yields the length scale of the lower cut-off length,  $a$ , which was found to amount to roughly 50 nm.

Roughly similar correlation functions are found for each casein concentration, if the appropriate value was subtracted from all grey values resulting in a surface fraction equal to the actual volume fraction of the particles in the gel.  $D$  thus seems to be independent of the volume fraction  $\phi_0$ . In fig. 4.13 the correlation functions are plotted. These

functions are deduced from the images after subtraction of the appropriate number in order to obtain the right surface fraction. Instead of  $C(r)$ ,  $\phi_0 C(r)$  is plotted, which directly yields the probability that, on a distance  $r$  from any particle, another particle is situated. At a large distance from any particle this probability equals the volume fraction of the gel, but at shorter distances the probability is higher until it becomes 1 if  $r < a$ . The experimental lines become curved for a value of  $\log r = -6.5$  ( $r \approx 300$  nm) due to the limited resolution of the microscope. However, if the linear part is extrapolated, the probability indeed becomes 1 for  $r \approx 50$  nm, which is the average radius of the casein particles. The fluctuations with minima on distance  $R$  and  $3R$  may indicate a rather monodisperse cluster size distribution which can also be observed in the micrographs.

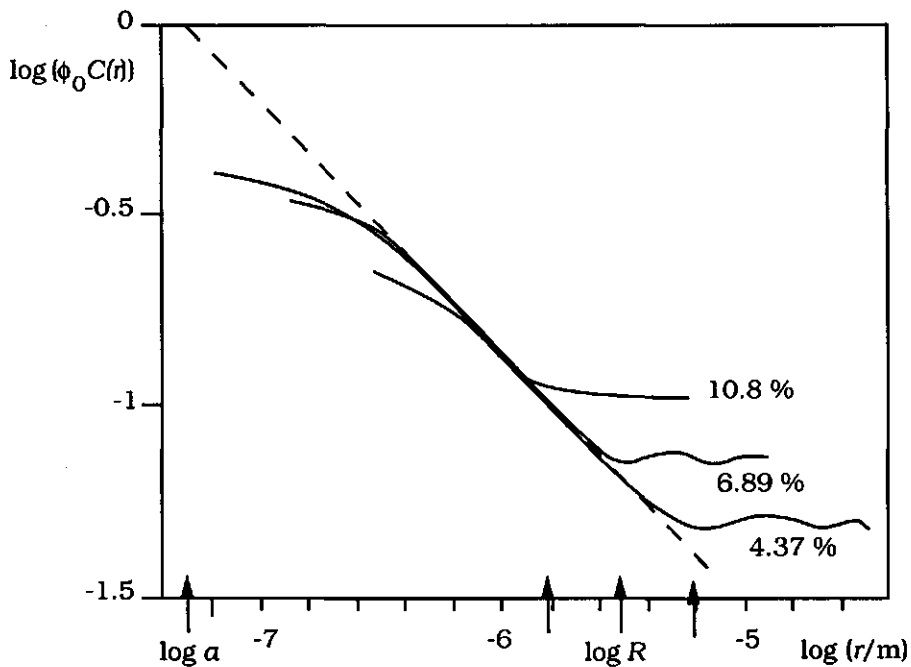


**Fig. 4.13** Correlation functions deduced from micrographs of the same Na-caseinate gels as in fig. 4.8 after subtraction of the appropriate value from all grey values in order to equalize the surface fraction of the images to  $\phi_0$ . The slope of the line, found by regression analysis of the linear region, equals  $-0.61$  resulting in a dimensionality  $D = 2.39$ .

#### 4.4 Turbidity measurements

The wavelength exponent,  $\beta$  in Eqn. 2.21, is calculated and depicted as a function of  $R$  in fig. 2.5. If the casein concentration is low, the clusters are large and the experimental value of  $\beta$  approaches the fractal dimensionality,  $D$ . The average fractal dimensionality, obtained from measurements of dilute (0.5 g/kg) aggregating Na-caseinate dispersions, was  $2.27 \pm 0.05$ . (The slope of the  $\log \tau - \log \lambda$  curves was  $-1.93 \pm 0.05$ ; 5 measurements.) Turbidity measurements of rennet-induced gels resulted in a higher effective fractal dimensionality,  $D = 2.4$ , [24, 25] measured a short time after the gelation.

All log-log plots of the turbidity as a function of the wavelength were of very high linearity with correlation coefficients  $> 0.9998$ . Fig. 4.14 gives some examples.

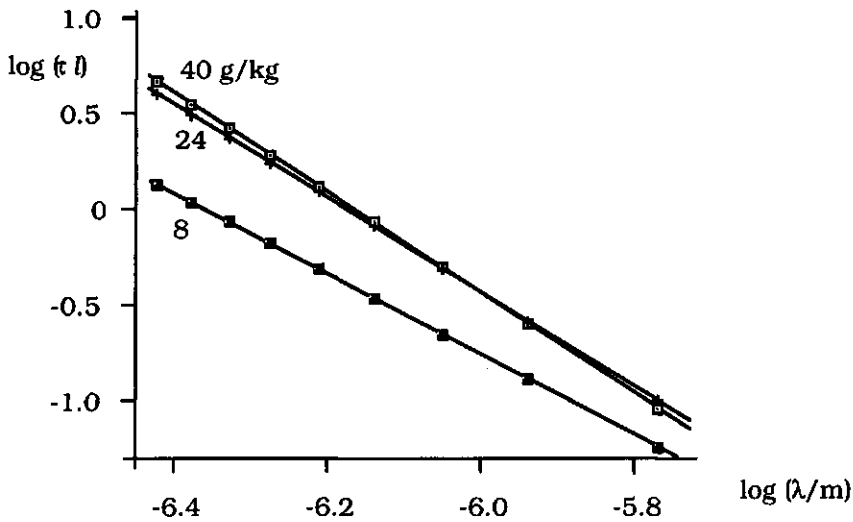


**Fig. 4.14** Turbidity ( $\tau l$ ) of acid type 2 Na-caseinate gels as a function of the wavelength ( $\lambda$ ) for different casein concentrations. The optical path-length,  $l$ , was 0.152 mm and the angle of acceptance  $1.5^\circ$ .

It is striking that the turbidity of a 40 and a 24 g/kg gel are roughly similar in spite of the difference in the number of scattering particles. The 40 g/kg gel becomes apparently homogeneous on length scales of the order of the wavelength that is used which causes a lower turbidity. This

is particularly the case at a wavelength of 1700 nm where the 24 g/kg gel has a higher turbidity than the 40 g/kg gel. The 8 g/kg gel has, at 380 nm wavelength, a turbidity that is almost 3 times lower than the 24 g/kg gel, in agreement with the Beer-Lambert law ( $\tau \propto C$ ). Results of the turbidity measurements at various casein concentrations are compiled in table 4.4.  $R_{cal}$  is calculated with Eqn. 2.6, assuming a voluminosity of 2.7 for the casein at the present conditions. Not too much value should be assigned to the absolute values of  $R$  obtained by comparison of the wavelength exponent  $\beta$  derived from the slope of the  $\log \tau - \log \lambda$  plot and the theoretical value in fig. 2.5.

**Table 4.4** Results of turbidity measurements.  $R$  is obtained from fig. 2.5 and  $R_{cal}$  from Eqn. 2.6 assuming a voluminosity of 2.7 ml g<sup>-1</sup>, and  $a = 50$  nm. c.c. is the correlation coefficient between  $\log \tau$  and  $\log \lambda$ .

$C$ (g/kg)	$\frac{d \log \tau}{d \log \lambda}$	$\beta$	$R$ ( $\mu\text{m}$ )	$R_{cal}$	c.c.
acid type 2 Na-caseinate gels					
1.8	-1.97	2.23	27.0	181.1	0.99996
5.4	-2.02	2.18	5.1	33.4	0.99997
8.0	-2.10	2.10	3.4	18.3	0.99998
16.0	-2.26	1.94	1.8	6.3	0.99981
24.0	-2.46	1.74	0.7	3.4	0.99982
40.0	-2.61	1.59	0.4	1.5	0.99992
rennet-induced skim-milk gels					
20.8	-1.94	2.26	---	---	0.99939
52.0	-2.07	2.13	---	---	0.99941

In fig 4.15 deviations from linearity are plotted for the log-log plot of  $\tau$  as a function of  $\lambda$  (determined) and the double-log plot of  $Q$  as a function of  $\lambda$  (calculated from theory), respectively. Fig 2.5 is calculated assuming a straight line between  $Q$  at 400 and 800 nm. Because both the experimental curve of  $\log \tau$  versus  $\log \lambda$  and the theoretical plot of  $\log Q$  versus  $\log \lambda$  are not completely straight, the deviations being opposite to each other, the experimental and theoretical values of  $\beta$  are uncertain. The absolute cluster size,  $R$ , obtained from fig. 2.5, varies strongly due to



small variations in  $\beta$  and is thus also uncertain and dependent on the range of wavelengths used for its estimation. The relative magnitude of  $R$  is, however, in fair agreement with  $R_{\text{cal}}$  over a large range of concentrations.  $R$  is about  $0.2 \times R_{\text{cal}}$  over the entire range. Another factor that may have frustrated the estimation of  $R$  is multiple scattering. The wavelength exponent  $\beta$  is strongly dependent on the angle of acceptance,  $\alpha$  (fig. 2.5). In practice  $\beta$  varied indeed,  $\beta$  being larger if  $\alpha$  was larger. The variation is however less than expected in fig. 2.5. This may be due to multiple scattering. At short wavelengths  $\tau l$  has values up to 5 which means that light scattered within an angle lower than  $\alpha$  has a very low probability to reach the detector without being scattered again. ( $\tau \times l = \ln(I_0/I)$  where  $I_0$  and  $I$  are the intensities of the incident and the transmitted beam, respectively).

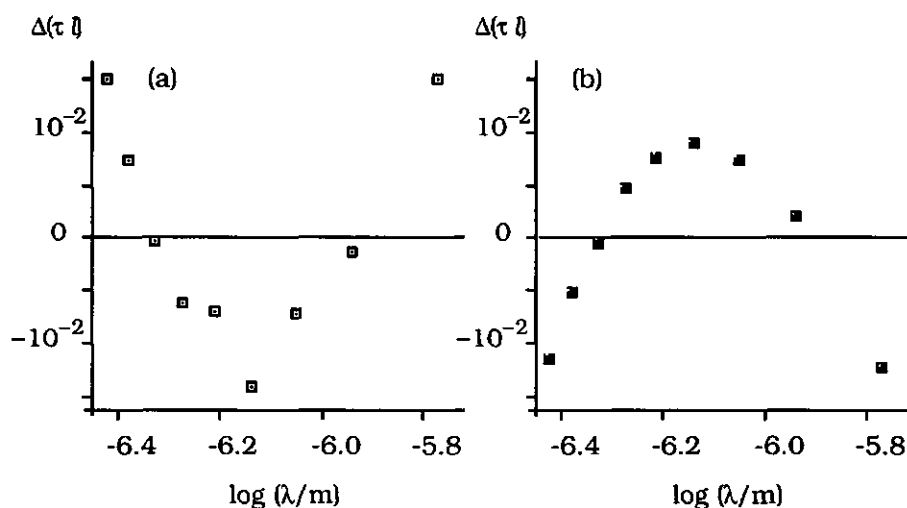


**Fig. 4.15** (a) Experimental and (b) theoretical deviations from linearity for the  $\log \tau - \log \lambda$  plot of a 16 g/kg acid Na-caseinate gel. The deviations,  $\Delta(\tau l)$ , are expressed in the same units as the turbidity in fig. 4.13.

The difference between the experimental and theoretical deviations from linearity may be due to: 1) the fact that the term  $\gamma$  (Eqn. 2.22) is not constant over the wavelength spectrum, 2) multiple scattering and 3) insufficiencies in the theory. It is uncertain which of these effects is dominating. Also the effect of the glass surfaces of the optical cells on the structure of the gels close to the surface may be important (section 4.3).

The agreement between turbidimetric results and theory is somewhat puzzling. For the Rayleigh-Gans theory to be applicable, the phase shift parameter  $2\pi n_0 R(m-1)/\lambda$  should be far below 1. Here  $m$  is the effective refractive index of the clusters relative to the medium [26]. For the fractal casein clusters this condition will always have been fulfilled, the phase shift parameter being at most 0.1. But, once a gel is formed, the condition would become  $\pi n_0 l(m-1)/\lambda \ll 1$  where  $l$  is the optical path length through the gel. Since we had  $l = 0.15 - 5$  mm, this condition was never fulfilled. Presumably, the destructive interference of scattered light due to the close proximity of the fractal clusters was negligible, at least for the lower concentrations where the clusters are large. In principle, these effects can be estimated by using a structure factor that is derived from the Fourier transform of the radial distribution function of the gel (obtained by CSLM) rather than that of individual flocs (fig. 4.16b).

Fig. 4.16a shows the difference between the theoretical correlation function that has been used to obtain Eqn. 2.18 and the experimental result obtained from CSLM. The boundaries of the clusters in the casein gel are more sharply defined than predicted from the theoretical correlation function (curve b). Lin et al. [27] compared various cut-off functions and found also sharper cut-off functions than  $\exp(-r/R)$  for computer-generated clusters.

The structure factors  $S(q)$  obtained from Eqn. 2.18 and from the Fourier transform of the experimental  $|C(r)-1|$  (Eqn. 2.16) turn out to be different at wave factors ( $q$ ) from 5 to  $5.5 \times 10^5 \text{ m}^{-1}$  (Fig. 4.16b). Wave factors that are studied in the turbidity measurements range from  $1.3 \times 10^5$  to  $10^7 \text{ m}^{-1}$  and from  $6 \times 10^5$  to  $4.4 \times 10^7 \text{ m}^{-1}$  for  $\lambda = 1700$  and  $380$  nm respectively. These wave factors are mainly larger than those where difference occurs. The destructive interference of scattered light due to the close proximity of the clusters is therefore negligible for the 16.2 g/kg gel. In principle, it is possible to predict all light scattering data from (three-dimensional) images of the gel. However, the optical resolution of CSLM images is not sufficient to obtain information about the small length scales (large  $q$ ).

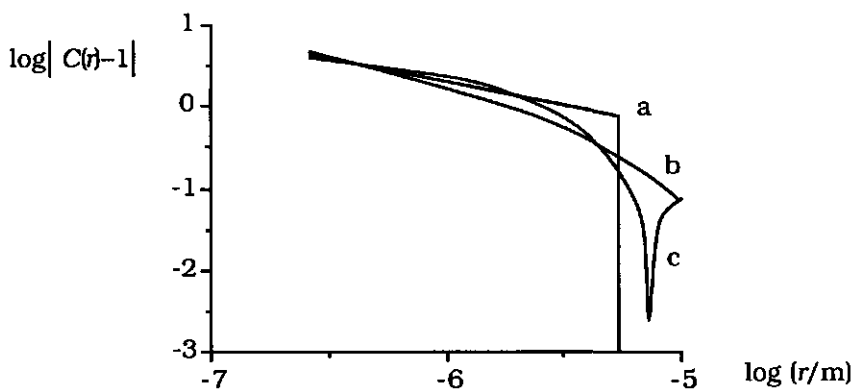


**Fig. 4.16a** Theoretical (a,b) and experimental (c) values of  $\log|C(r)-1|$  as a function of  $\log r$ :

$$\text{a. b) } |C(r)-1| = h(r) \left| \frac{D}{3\phi_0} \left(\frac{r}{a}\right)^{D-3} - 1 \right| \quad (4.4)$$

with  $R = 5 \mu\text{m}$ ,  $a = 50 \text{ nm}$ ,  $D = 2.4$ ,  $\phi_0 = 6.3 \%$ . The cut-off function is

a)  $h(r) = 0$  for  $r > R$ ,  $h(r) = 1$  for  $r < R$ , b)  $h(r) = \exp(-r/R)$ , and  
 c) experimental result obtained from the 16.2 g/kg Na-caseinate gel.

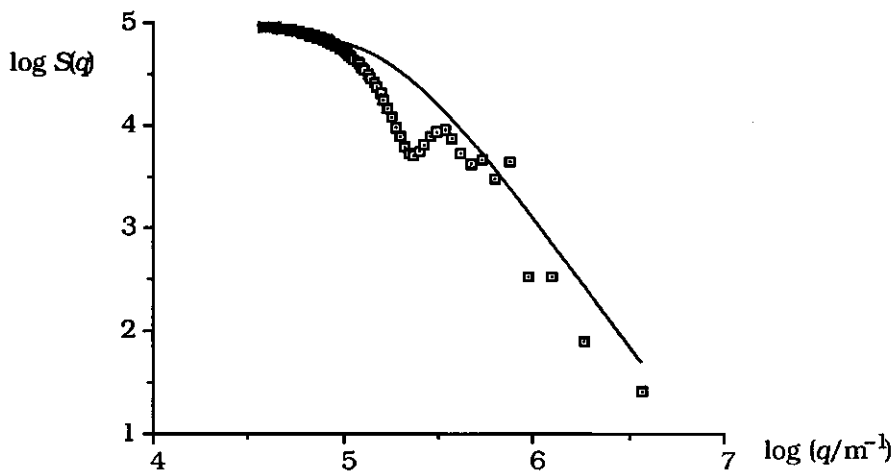


**Fig. 4.16b** Representation of the structure factor,  $S(q)$ , given by Eqn. 2.18 for  $D = 2.4$ ,  $R = 5 \mu\text{m}$  and  $a = 50 \text{ nm}$  (continuous line). The dots are obtained from the correlation function of a 16.2 g/kg Na-caseinate gel (Eqn. 2.16).

## Acknowledgement

We thank Siebe Henstra and El Bouw, TFDL Wageningen, for helpful discussion and assistance with the CSLM.

## 4.5 References

- 1 S.A. Troelstra and H.R. Kruyt, *Kolloid-Beihfte*, 1943, **54**, 225
- 2 R. Buscail P.D.A. Mills, J.W. Goodwin and D.W. Lawson, *J. Chem. Soc. Faraday Trans I*, 1988, **84**, 4249
- 3 P. Meakin, *Phys. Rev. Lett.*, 1983, **51**, 1119
- 4 M. Kolb, R. Botet and R. Jullien, *Phys. Rev. Lett.*, 1983, **51**, 1123
- 5 R. Jullien and M. Kolb, *J. Phys.*, 1984, **A17**, L639
- 6 R.C. Ball, D.A. Weitz, T.A. Witten and F. Leyvraz, *Phys. Rev. Lett.*, 1987, **58**, 274
- 7 Y. Adachi and S. Ooi, *J. Coll. Int. Sci.*, 1990, **135**, 374
- 8 N.H.G. Penners and L.K. Koopal, *Colloids and Surfaces*, 1986, **19**, 337
- 9 N.H.G. Penners and L.K. Koopal, *Colloids and Surfaces*, 1987, **28**, 67
- 10 G. Frens, *Faraday Discuss. Chem. Soc.*, 1990, **90**, 143
- 11 G. Frens, *personal communication*
- 12 L. Thomas and K.H. McCorkle, *J. Colloid Interface Sci.*, 1971, **36**, 110
- 13 R. Amal, J.A. Raper and T.D. Waite, *J. Colloid Interface Sci.*, 1990, **140**, 158
- 14 P. Walstra, *J. Dairy Research*, 1979, **46**, 317
- 15 S.P.F.M. Roefs, A.E.A. de Groot-Mostert and T. van Vliet, *Colloids and Surfaces*, 1990, **50**, 141
- 16 H.J.M. van Dijk, *Ph.D. Thesis*, (Wageningen Agricultural University, The Netherlands, 1982)
- 17 H.J.M. van Dijk and P. Walstra, *Neth. Milk Dairy J.*, 1986, **40**, 3
- 18 A.E. Scheidegger, *The physics of flow through porous media*, (Oxford University press, London, 1960)
- 19 Y. Adachi and M. Kamiko, *Proc. World Congress of Chem. Eng.*, Karlsruhe, 1991
- 20 C. Tanford, *Physical Chemistry of Macromolecules*, John Wiley, NY, 1961
- 21 P. Meakin, Z.Y. Chen and J.M. Deutch, *J. Chem. Phys.*, 1985, **82**, 3786
- 22 Z.Y. Chen, P. Meakin and J.M. Deutch, *Phys. Rev. Lett.*, 1987, **59**, 2121
- 23 F.E. Torres, W.B. Russel and W.R. Schowalter, *J. Colloid Interface Sci.*, 1991, **142**, 554
- 24 L.G.B. Bremer, T. van Vliet and P. Walstra, *J. Chem. Soc. Faraday Trans I*, 1989, **85**, 3359
- 25 D.S. Horne, *Faraday Discuss. Chem. Soc.*, 1987, **83**, 259
- 26 H.C. van de Hulst, *Light scattering by small particles* (Wiley, New York, 1957; Dover edn, 1981)
- 27 M.Y. Lin, R. Klein, H.M. Lindsay, D.A. Weitz, R.C. Ball and P. Meakin, *J. Colloid Interface Sci.*, 1990, **137**, 263

# V Rheological Properties of Particle Networks

## 5.1 Introduction

Various models have been developed to represent the three dimensional structure of particle networks and thereby to relate the macroscopic, rheological properties to microscopic properties; e.g., the strength of particle-particle bonds. The most simple model is the so-called 'ideal network model' in which all particles are arranged in a statistical network of chains that all contribute to the same extent to the rigidity of the network. This model implies that the rigidity of a gel would be proportional to the particle concentration. This dependency is not found in practice and another model, the 'aggregate network model' has been developed. In this model the particles are aggregated into agglomerates, which are connected by chains of particles. The mechanical strength of the network is mainly determined by the relatively few particles that link the agglomerates together. The fraction of the particles that are built into these links depends on their volume fraction; the lower the volume fraction, the smaller the fraction of particles built in strands. In order to relate rheological properties of a particle gel to the properties of the particles a (rough) estimate of the fraction particles in the stress carrying strands is required.

Aggregate networks of chains in three mutually perpendicular directions have been used to relate rheological gel properties to properties of the particles in the strands [1-4]. A more sophisticated transient-network model for concentrated dispersions of attracting particles has been introduced by Kamphuis et al. [5, 6]. They used an isotropic network model in which chains of particles are assumed to be constantly created and broken due to thermal actions and applied deformations. All these models are useful for concentrated dispersions. In gels made of dilute dispersions, however, the uncertainty about the fraction of the particles in the stress carrying strands prevents a successful application of these models.

The introduction of the concept of fractal geometry enabled a quantitative description of the geometric structure of flocs. A particle gel

consists of a collection of these flocs that jointly occupy the volume, thus forming a network. A floc may thus be considered the smallest structural element that possesses the properties of the gel. The modulus of a fractal floc has been calculated by Brown and Ball [7]. They show that the modulus of a floc scales like  $\phi^\mu$  where  $\phi$  is the volume fraction of the particles in the floc and  $\mu$  depends on the fractal dimensionality,  $D$ , and the so-called chemical length exponent. The latter is a measure for the dependence of the length of a stress carrying strand in a floc on the size of that floc. Values for  $D$  and the chemical length exponent have been obtained from computer simulations of aggregation and  $\mu$  is anticipated to be 3.5 in the case of diffusion, and 4.5 in the case of reaction limited cluster cluster aggregation. Buscall et al. [8] have compared these model calculations with experimental results on aggregate networks formed from polystyrene and silica particles. However, the quantitative agreement that they obtain may well be fortuitous as will be shown later on.



The fractal aggregate model that we develop and use in the sections 5.2 to 5.4 is based on the same ideas as the model of Brown and Ball. We consider the whole network instead of one floc. Due to the scale invariance of the fractal flocs and the self preserving floc size distribution during the aggregation process, particle gels are scale invariant in a sense; i.e., a gel formed from a concentrated dispersion resembles a gel formed from a dilute dispersion, only the scale is different. This scaling phenomenon is confirmed by CSLM micrographs (Chapter IV). The modulus of an aggregate network depends on the properties of the primary particles and on the geometric structure of the network. The effect of the geometric structure can be divided into two contributions: 1) The number of stress-carrying strands per unit area in a cross-section perpendicular to the direction of the applied force,  $N$  and 2) The magnitude of the microscopic deformation of the strands caused by the macroscopic (shear) strain,  $C_e$ , which depends on the position and length,  $L$ , of the stress-carrying strands.  $C_e$  is proportional to the elastic constant of individual strands. In a fractal network model these contributions can be related to the size of the fractal flocs in the gel,  $R_g$ , which, in turn, depends on the volume fraction of the particles,  $\phi_0$  (Chapter II).

We consider two different types of particle networks. In the first type the strands are stretched and thus straight. For these gels, a given shear results in a microscopic deformation inside the strands that is independent of the size of the clusters forming the gel. This model is described in section 5.2 [9]. However, in fractal flocs that arise from smaller flocs or particles that are attached to each other in a random way, the strands are not straight. This second type of gel, with curved strands, is described and compared with the first type in section 5.3 [10] and 5.4. The length of the stress carrying strands is assumed to be independent of the size of the flocs composing the gel in both gel types, i.e. the shortest path connecting 2 particles on a mutual distance much larger than  $R$  is independent of  $R$  and  $\phi_0$ . The model of Brown and Ball takes a chemical length exponent into account. However, this exponent is only slightly greater than 1 indicating that  $L$  is almost independent of  $R$ . Shih et al. [11] distinguish two regimes, a strong and a weak-link regime. In the strong link regime the elasticity of the gel is determined by the elasticity of the flocs (like in the other models) but in the weak link regime the elastic behaviour of the gel is dominated by the elastic constant of the interfloc links. This model may apply to gels with very small and stiff fractal flocs (high volume fraction). The number of interfloc links per unit cross sectional area is proportional to  $R^{-2}$ . Deformation of such gels result in a deformation of a number of interfloc links proportional to  $R^{-1}$  and the elastic constant of a string of these flocs,  $C_e$ , is thus proportional to  $R$ . The differences between the models are shown by means of a highly schematic representation of the networks in table 5.1.

The exponent  $x$  in table 5.1 is 0.262 for the Koch curve that is used as an example. The chemical length exponent, which is in this case the fractal dimensionality of the Koch curve, equals  $\log 4 / \log 3 = 1.262$ .

The number of stress carrying strands per unit area,  $N$ , is evidently proportional to  $R^{-2}$  in all models. For the straight strand model, the deformation of the strands in the case of a macroscopic extension is independent of  $R$  as can be concluded from table 5.1. The modulus of this gel type is therefore proportional to  $R^{-2}$  as will be shown in section 5.2.

Model	High $\phi$	Low $\phi$	
Straight strands [9, 10]			$N \propto R^{-2}$ $C_e \propto R^0$ $L \propto R^0$ $\mu = \frac{2}{3-D}$
Curved strands [10]			$N \propto R^{-2}$ $C_e \propto R^{-1}$ $L \propto R^0$ $\mu = \frac{3}{3-D}$
Brown and Ball [7, 8, 11]			$N \propto R^{-2}$ $C_e \propto R^{-2-x}$ $L \propto R^x$ $\mu = \frac{4+x}{3-D}$
Shih et al. [11]			$N \propto R^{-2}$ $C_e \propto R^1$ $L = -$ $\mu = \frac{1}{3-D}$

 Floc periphery     Stress carrying strand of particles

**Table 5.1.** Comparison of various fractal aggregate network models; highly schematic.  $N$  is the number of strands per unit of cross sectional area,  $C_e$  and  $L$  are the elastic constant and the length of a strand resp., and  $\mu$  the exponent in the relation between the modulus of a gel and the volume fraction;  $G \propto \phi_0^\mu$ .

The situation for the curved strands is more complicated. Assuming the straight parts of the strands in table 5.1 to be rigid, a deformation will result in a distortion of the angle between the straight chain parts. The magnitude of this distortion, and therefore the torque, is independent of



the size of the flocs. Because the length of these straight parts is proportional to  $R$ , the force needed to give a certain deformation scales, per strand, like  $R^{-1}$ . The modulus of the gel is in this case proportional to  $R^{-3}$  (section 5.3). Brown and Ball have obtained a modulus proportional to  $R^{-(4+x)}$  with their model, where  $x$  (the chemical length exponent minus 1) is found to be slightly more than 0 [7]. They assumed bending to occur between every particle in the strand. In this case the number of positions where bending occurs in a floc is proportional to  $R^{1+x}$ , and a deformation will result in a distortion, and thus a torque, scaling like  $R^{-1-x}$ . Here, the force needed to give a certain deformation scales, per strand, like  $R^{-2-x}$ .

Our experimental results are in agreement with either the model with straight or that with curved strands. In none of the gels agreement with the model of Brown and Ball nor with that of Shih et al. has been found. This may be due to internal cross linking which results in a gel consisting of fairly rigid agglomerates connected by flexible junctions [12].

## 5.2 The modulus of particle networks with stretched strands<sup>1</sup>

### 5.2.1 Introduction

A particle gel consists of a continuous three-dimensional network of connected particles, which is formed due to their aggregation in a continuous liquid phase. The strands of aggregated particles in such networks may become stretched by micro- syneresis, which occurs if a gel tends to synerese but has no possibility to do so because it is fixed to the walls of the container [13, 14]. This effect may lead to a coarsening of the network caused by some local breaking of bonds. In a gel which is subject to micro- syneresis all stress carrying strands will become straightened and energy uptake caused by macroscopic deformation will be due to an extension of strands in the gel network (fig. 4.6). For particle gels this is mainly an enthalpic process, in contrast with macromolecular gels where the energy storage is (mainly) entropic.

---

<sup>1</sup> The sections 5.2.1 and 5.2.2 have been published in *Rheologica Acta* [9]

Much theoretical work has been carried out to relate factors like the colloidal interaction forces between particles and the particle size to such rheological properties of particle gels as the shear modulus [1 - 6]. In addition to these properties, primarily determined by the particles, the geometric structure of the network is important for its rheological behaviour [5 - 12]. In the next session we present a simple model which relates the shear modulus of a particle gel to these particle properties and to the geometric structure of the gel network in the case of a network with stretched strands.

### 5.2.2 The model

The modulus of a gel is a measure of the amount of energy needed to deform the gel. This energy is stored or dissipated in the particle chains when they are deformed. If we define the collective effective length of the strands in the gel,  $L$ , (the backbone length), we can write for the amount of energy,  $E$ , stored in the gel due to a deformation, in the case of elastic strands:

$$E = \int_0^{\Delta L} f(\Delta L) dL \quad (5.1)$$

where  $f$  is the force needed to extend or compress the strands over a distance  $\Delta L$ , which is the sum of the absolute changes in strand length. If the measurements are done in the so-called linear region (i.e.  $df/dL$  is constant) we may write

$$E = \frac{1}{2} f \Delta L = \frac{1}{2} \frac{df}{dL} (\Delta L)^2 = \frac{1}{2} \frac{d^2 A}{dL^2} (\Delta L)^2 \quad (5.2)$$

where  $dA$  is the change in Gibbs energy. The force needed to extend or compress a strand depends on the nature of the particles and their interactions.

$E$  is the amount of energy stored in the gel due to deformation. For an experiment in shear in the linear region we may also write for  $E$  (fig. 5.1):

$$E = \frac{1}{2} F \Delta x = \frac{1}{2} \gamma \sigma V \quad (5.3)$$

where  $\gamma$  is the shear strain (equal to  $\Delta x/h$ ),  $\sigma$  the shear stress (equal to  $F/O$ ), and  $V$  the gel volume (equal to  $hO$ ).

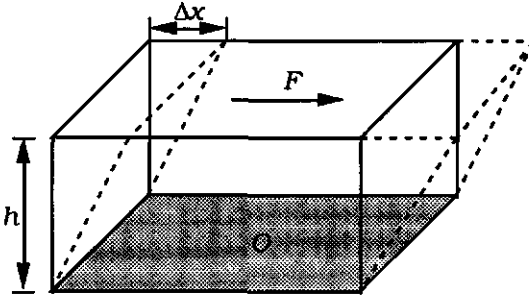


**Fig. 5.1.** Shear deformation of a gel caused by force  $F$ . The shear strain  $\gamma$  equals  $\Delta x/h$ , and the shear stress  $\sigma$  equals  $F/O$ .

Combination of equations (5.2) and (5.3) gives:

$$\gamma \sigma = \frac{(\Delta L)^2}{V} \frac{d^2 A}{dL^2} \quad (5.4)$$

The strands are built of linked particles and the deformation of the strands will thus lead to a deformation of the particles themselves, of the particle-particle bonds, or both. If we divide the strands in parts with a length equal to the radius of the particles ( $a$ ) then we may relate the average energy stored in one such part due to a deformation  $da$  of the particles, to the energy stored in the gel backbone due to the collective deformation  $dL$ :

$$\frac{d^2 A}{dL^2} = \frac{a}{L} \frac{d^2 A}{da^2} \quad (5.5)$$

Using equation (5.5) and a factor  $N$  which is defined as the effective strand length per unit of volume ( $N = L/V$ ) leads to

$$\gamma \sigma = \left( \frac{\Delta L}{L} \right)^2 N a \frac{d^2 A}{da^2} \quad (5.6)$$

The shear modulus,  $G$  equals  $\sigma/\gamma$ . Together with Eqn. (5.6) this gives:

$$G = N \frac{\left(\frac{\Delta L}{L}\right)^2}{\gamma^2} a \frac{d^2 A}{da^2} \quad (5.7)$$

The factor  $(\Delta L/L)^2/\gamma^2$  describes a relation between the deformation of the strands in the gel network and the macroscopic strain. For an isotropic gel with straight, i.e. stretched, strands this factor can be calculated. The length ( $l$ ) of a strand connecting two infinite large plates at a mutual distance ( $h$ ) can be written as  $\sqrt{x^2 + y^2 + h^2}$  (fig 5.2). The shear strain  $\gamma$  can be written as  $\Delta x/h$ . Differentiation of  $l$  to  $x$  yields:

$$\frac{dl}{dx} = \frac{x}{\sqrt{x^2 + y^2 + h^2}} \quad (5.8)$$

For strains in the linear region we may write  $\gamma h$  for  $dx$  and  $\Delta l$  for  $dl$ , we can thus write for the factor  $(\Delta l/l)/\gamma$ :

$$\frac{\Delta l/l}{\gamma} = \frac{hx}{x^2 + y^2 + h^2} \quad (5.9)$$

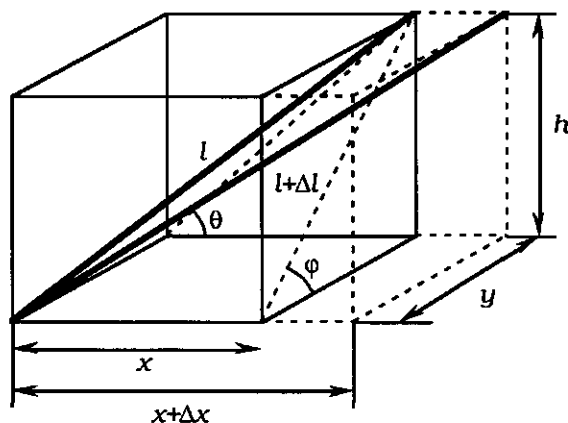


**Fig. 5.2.** Deformation of a strand with length  $l$ . The direction of the strand is determined by the angles  $\theta$  and  $\phi$ .

In an isotropic gel all strand directions have the same probability and we can thus obtain an average value for  $(\Delta l/l)/\gamma$  which equals  $(\Delta L/L)/\gamma$  by integration over all space angles. For  $x$  we can substitute  $h/\tan \theta$  and for  $y$  we can substitute  $h/\tan \phi$  (fig. 5.2). Integration gives:

$$\frac{\Delta L/L}{\gamma} = \left(\frac{2}{\pi}\right)^2 \int_0^{\pi/2} \int_0^{\pi/2} \frac{\cot \theta}{\cot^2 \theta + \cot^2 \phi + 1} d\theta d\phi =$$

$$\left(\frac{2}{\pi}\right)^2 \int_0^{\pi/2} -\frac{1}{2} \tan^2 \phi \ln(\sin^2 \phi) d\phi = \frac{2(1 - \ln 2)}{\pi}$$

Consequently,

$$\gamma = \frac{\pi}{2 - 2 \ln 2} \frac{\Delta L}{L} \tag{5.10}$$

If the particles are hard spheres, the modulus is mainly determined by the interaction forces between the particles and by their size instead of by the deformability of the particles themselves. Here we have to use the extension or compression of the distance between the particles,  $dH$ , (which corresponds to  $2da$ , fig. 5.3) instead of  $da$ .

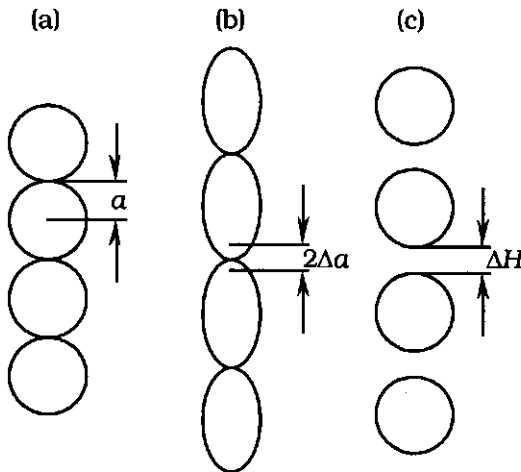


**Fig. 5.3.** Highly schematic picture of a strand with particles (radius  $a$ ) before (a) and after the exertion of a tensile force in the case of soft (b) and hard (c) particles. The picture is not to scale.

In the case of Van der Waals attraction and Born repulsion between hard spherical particles which as a first approximation may be modelled as a Lennard-Jones potential [6] we may write

$$\frac{df}{dH} = \frac{A_H a}{2H_0^3} \quad (5.11)$$

where  $A_H$  is Hamaker's constant and  $H_0$  the inter-particle distance at which attractive and repulsive forces are cancelled out. Because geometrically  $dH$  corresponds to  $2da$ , we may write for the factor  $d^2A/da^2$  in Eqn. (5.7)

$$\frac{d^2A}{da^2} = \frac{df}{da} = 2 \frac{df}{dH} = \frac{A_H a}{H_0^3} \quad (5.12)$$

If we assume that all particles are incorporated in the stress carrying strands (which is of course not realistic) then

$$N = \frac{3\phi_0}{2\pi a^2} \quad (5.13)$$

which may be used to derive a relation for  $G$  similar to those mentioned in literature ( $\phi_0$  is the volume fraction of particles)

$$G = \frac{6}{\pi^3} (1 - \ln 2)^2 \frac{A_H \phi_0}{H_0^3} \approx 0.018 \frac{A_H \phi_0}{H_0^3} \quad (5.14)$$

Kamphuis et al. have found, after a much more complicated derivation a similar relation, but with a factor  $1/(20\pi)$ , which is about 0.016. They, however, use only half of the strands because they assume a negligible compression modulus. Nederveen and Papenhuijzen obtain also similar relations but again with a different numerical term, for instance  $1/(6\pi) \approx 0.053$  [3], they use very simple models with strands in three mutually perpendicular directions which leads to another modulus than for an isotropic network.

Equation (5.7) is similar to the equation derived by van Vliet and Walstra [15]

$$G = NC \frac{d^2 A}{da^2} \quad (5.15)$$

if  $C = ((2-2\ln 2)/\pi)^2 a$ . They define  $N$  as the number of stress carrying strands per unit cross-section, but this is proportional to the length of the stress carrying strands per unit volume in the case of an isotropic gel with stretched strands.

If the network is formed out of a collection of clusters with a fractal nature (which is often the case) it is possible to relate  $N$  to the volume fraction of the particles [10, 16]. Then an expression is obtained in which  $G$ , for a particle network with stretched strands, is proportional to  $\phi_0^{2/(3-D)}$  [10]:

$$G = \left(\frac{2}{\pi}(1 - \ln 2)\right)^2 \frac{nA_H}{H_0^3} \phi_0^{2/(3-D)} \quad (5.16)$$

where  $n$  is the effective number of bonds that each cluster has with other clusters. For curved strands the dependence of  $G$  on  $\phi_0$  will still be stronger [10].

The model with hard spheres aggregated by Van der Waals attraction has been used in order to model gels of fat particles in oil (margarine) [3 - 6]. If the deformation of the particles is large compared to the deformation of the bonds, for instance after fusion or sintering of the particles then Young's modulus of the material in the particles will enter. Substitution of  $\pi a E$  for  $d^2 A / da^2$  (cylindrical strands) gives reasonable results in the case of casein gels [10]. The model is useful in translating particle properties to properties of the gel made of these particles and to relate the rheological properties to the geometric structure of the gel network.

### 5.2.3 Extensional deformation

It is possible to use the same approach to calculate the tensile or compression modulus, the so-called Young modulus  $E$ , of a network with stretched strands. In fig. 5.4 the deformation of a strand with length  $l$ , due to an uniaxial tensile force  $F$  that is exerted on the network, is depicted. The same equations as in 5.2.2 may now be written in order to

relate the macroscopic tensile or compression strain,  $\epsilon = \Delta h/h$ , to the deformation of the strands,  $\Delta L/L$ . The resulting integration that has to be solved is

$$\frac{\Delta L/L}{\epsilon} = \left(\frac{2}{\pi}\right)^2 \int_0^{\pi/2} \int_0^{\pi/2} \frac{1}{\cot^2 \theta + \cot^2 \varphi + 1} d\theta d\varphi$$

resulting in

$$\epsilon = \frac{\pi}{4 - \pi} \frac{\Delta L}{L} \quad (5.17)$$

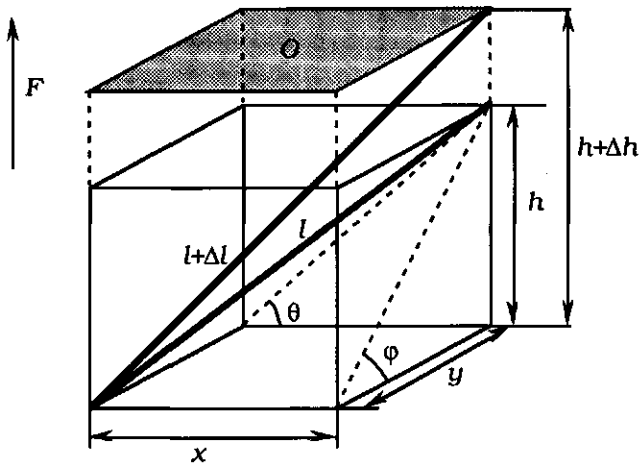


**Fig. 5.4.** Deformation of a strand with length  $l$  due to a tensile force  $F$ .

It is possible to relate the shear and the compression moduli that are calculated with this model:

$$E = \frac{(4 - \pi)^2}{(2 - 2 \ln 2)^2} G \approx 1.96G \quad (5.18)$$

In practice, however, compressive and tensile deformations are different from deformations in shear because the volume of the sample can be changed. This makes the model in case of extensional or compressive deformations unrealistic because the liquid in the gel network can not be



expelled or taken up freely. A measure for the change in volume is the Poisson ratio  $\mu_p$ .

$$\mu_p = \frac{1}{2} \left( 1 - \frac{dV}{V d\epsilon} \right) \quad (5.19)$$

With this ratio it is possible to relate the values for the different moduli (the shear, the Young and the bulk modulus). For isotropic, homogeneous materials we may write [17]

$$E = 2G(1 + \mu) \quad (5.20)$$

In our model  $d\epsilon = dV/V$  leading to  $\mu = 0$ . The resulting relation,  $E = 2G$  is close to the relation obtained in Eqn. (5.18).

### *Acknowledgement*

We are indebted to Dr. M.H. Hendriks for discussion and help concerning the mathematical aspects of section 5.2.2 and 5.2.3.

## **5.3 On the fractal nature of the structure of acid casein gels<sup>1</sup>**

### *5.3.1 Introduction*

The mechanical properties of dairy products like yoghurt, quarg and ymer are, to a considerable extent, determined by the geometric structure of the gel network formed after coagulation of the casein particles. These products are essentially casein gels, but they have widely varying (mechanical) properties [18 - 20]. The mechanical properties of a gel network are defined by three factors: the spatial distribution of the particles, the strength of the interaction forces between the particles and the structure of the particles themselves. In section 5.3 we compare two casein gels at essentially the same conditions (casein and salt composition) and, thus, with essentially equal particle-particle interactions and particle structure. Any difference in gel structure would

---

<sup>1</sup> The sections 5.3.1 - 5.3.5 have been published in *Colloids and Surfaces* [10].

thus be strictly due to the spatial distribution of the casein particles. Gel type 1 is made by warming a quiescent sodium caseinate dispersion of pH 4.6 from 4 to 30 °C. The casein particles are stable at low temperature but start to aggregate at about 10 °C. Gel type 2 is made by adding glucono- $\delta$ -lactone (GDL) to a casein solution of pH 6.7 at 30 °C; the GDL slowly hydrolyses in water thus causing a slow decrease in the pH. When the pH falls below about 5.0 the casein particles are no longer stable and they start to aggregate. For both gel types the final pH was 4.6, i.e., the isoelectric pH of casein. In spite of these similarities, the mechanical properties of both gel types are widely different, e.g., the shear modulus for a type 2 gel is an order of magnitude smaller than that of a type 1 gel (at casein concentrations comparable to those in milk [18]).

It has recently been shown [16] that acid casein gels can be described as a collection of aggregated fractal clusters which have an effective fractal dimensionality,  $D$ , of about 2.3. This description enables to present a quantitative picture of the spatial distribution of the casein particles. A cluster is of a fractal nature if a power-law dependence exists between the amount of casein particles in the cluster and the radius of the cluster and if the magnitude of this power, designated the fractal dimensionality, is below 3. This implies that the volume fraction of casein in any cluster will decrease with increasing cluster size. Because the overall volume fraction has a fixed value, there must be a relation between the volume fraction, the cluster size in the gel and the fractal dimensionality. This relation has been derived as [16]:

$$R_{3D} = a\phi_0^{1/(D-3)} \quad (5.21)$$

with

$$R_{3D} = \left( \frac{\sum R_i^3}{\sum R_i^D} \right)^{1/(3-D)}$$

Here  $a$  is the radius of the casein particles,  $R_{3D}$  a measure of the average radius of the aggregates which compose the gel, and  $\phi_0$  the volume fraction of casein particles in the system.

The volume fraction, and thus the voluminosity of the casein particles, has a large effect on the size of the clusters in the gel. Much has been published about the voluminosity of casein, which can be determined in various ways [21 - 23]. We conclude that the voluminosity

is roughly 2.5 ml per g casein at a temperature of 30 °C and 3.5 - 4.5 ml per g casein at 10 °C, at the present conditions. In addition to the temperature, the pH (fig 5.5) and the salt concentration affect the voluminosity.

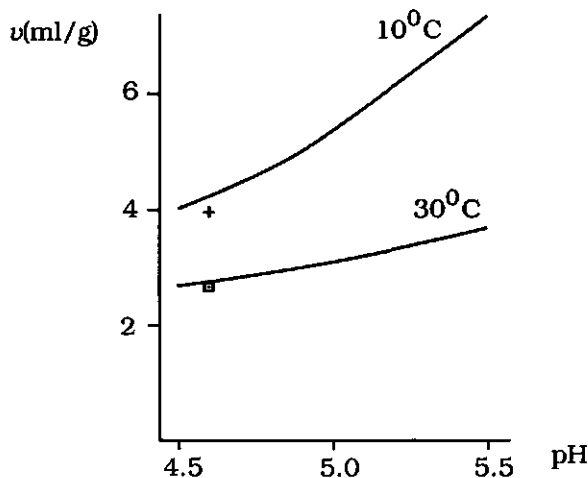


**Fig. 5.5.** Voluminosity of casein particles ( $\text{ml g}^{-1}$ ) as a function of the pH for casein dispersions at 10 and at 30 °C [22].

### 5.3.2 Theory

For the mechanical properties of a gel the sum of the length of the stress carrying strands per unit of volume,  $N$ , is an important variable [9]. If we assume the clusters to be scale invariant we can write

$$N = \frac{n \sum R_i}{\sum R_i^3} = nR_{13}^{-2} \quad (5.22)$$

where  $n$  is the collective length of the effective strands in a cluster relative to the radius of the cluster,  $(L_i/R_i)$ ; for scale invariant clusters this is assumed to be a constant factor which is, in case of straight strands, about equal to the effective number of bonds that each cluster has with other clusters. Aggregation in quiescent systems leads to rather monodisperse flocs because the relative small clusters diffuse faster than the large flocs and have thus a higher probability to aggregate. Because the

flocs are rather monodisperse,  $R_{13} \approx R_{3D}$ , and we can combine (5.22) with (5.21) to yield

$$N = n\alpha^{-2}\phi_0^{2/(3-D)} \quad (5.23)$$

In addition to  $N$ , the nature and the position of the strands in the network will determine the rheological properties of the gel. The strands are chains of connected casein particles, and in so far similar in both casein gels; also the nature of the casein particles and the interaction forces between the particles are similar. The position and the thickness of the strands may, however, vary and this may lead to variation in modulus among individual strands if the deformation is small enough. A relation between the (shear) modulus of a particle network ( $G$ ) and  $N$  is [9, 15]

$$G = NC \frac{d^2 A}{da^2} \quad (5.24)$$

where  $dA$  is the change in Gibbs energy when the radius of a particle in a strand is extended or compressed over a distance  $da$  and  $C$  is a characteristic length, determined by the geometry of the network, which relates the deformation of the strands in the gel to the macroscopic shear strain ( $\gamma$ ).

For both types of casein gels the interaction between the casein particles and the particles themselves are similar and the difference between gel type 1 and gel type 2 are thus to be caused by the geometry of the gel network. The mechanical properties of the material in the casein particles can be expressed by Young's modulus, ( $E$ ). For straight cylindrical strands of a thickness of  $2a$  we can write

$$\frac{d^2 A}{da^2} = \frac{df}{da} = \pi a E \quad (5.25)$$

where  $f$  is the force exerted on the strands and  $E$  is Young's modulus for the casein particles.

In case of an isotropic gel network with straight (stretched) strands it is possible to relate the deformation of the strands to the macroscopic

shear strain.  $C$  is derived to be approximately  $a/26$  [9] and thus independent of the particle concentration. For this type of gel we can derive, using Eqns. (5.22 - 5.25)

$$G = \frac{\pi\pi}{26} E\phi_0^{2/(3-D)} \quad (5.26)$$

For gels with curved strands, the situation is more complicated. In these type of gels, a relation between the macroscopic shear strain and the deformation of the casein particles in the strands is difficult to derive. We can, however, define an imaginary gel backbone which connects the clusters with straight rather than with curved strands.  $C$  is in this case again equal to  $a/26$ , but the length of the real strands is of course not equal to the length of the imaginary strands. In case of scale invariant clusters both lengths are however proportional. The factor  $d^2A/da^2$  is different for curved strands; it is obvious that a curved strand is easier to extend than a similar straight strand. For the average stress in a curved strand with a certain deformation  $\Delta L/L$  (fig. 5.6d) we can write

$$\sigma \propto \frac{\Delta f}{a^2} \quad (5.27)^*$$

In a curved strand (fig 5.6) the strain can attain the value [24]

$$\epsilon_{\max} = \frac{12aY}{X^2} \propto \frac{a}{R} \propto \frac{\Delta a}{R} \quad (5.28)$$

$Y$  and  $X$  are defined in fig 5.6 and are both proportional to the size of the clusters in the gel ( $R$ ). In the case of small strains we can derive a relation between  $d^2A/da^2$  and Young's modulus, using Eqns. (5.27) and (5.28):

$$E \equiv \frac{\sigma}{\epsilon} \propto \frac{R}{a^2} \frac{\Delta f}{\Delta a} = \frac{R}{a^2} \frac{d^2A}{da^2} \quad (5.29)$$

or

---

\*Eqn. 5.27 has been obtained assuming that the number of positions on a strand where bending occurs is independent of the size of the floc (Table 5.1). If this number is proportional to the size of the floc  $\sigma \propto \Delta f R/a^3$  and the model of Brown and Ball applies.

$$\frac{d^2 A}{da^2} \propto \frac{a^2}{R} E = a\phi_0^{1/(3-D)} E \quad (5.30)$$

Combination of Eqns. (5.23), (5.24) and (5.30) yields

$$G \propto nE\phi_0^{3/(3-D)} \quad (5.31)$$

where the factor  $n$  is, again, about equal to the number of effective cluster-cluster bonds. In our model we use cylindrical strands with a diameter of  $2a$ . This may give realistic results when the particles in the strands are more or less fused.

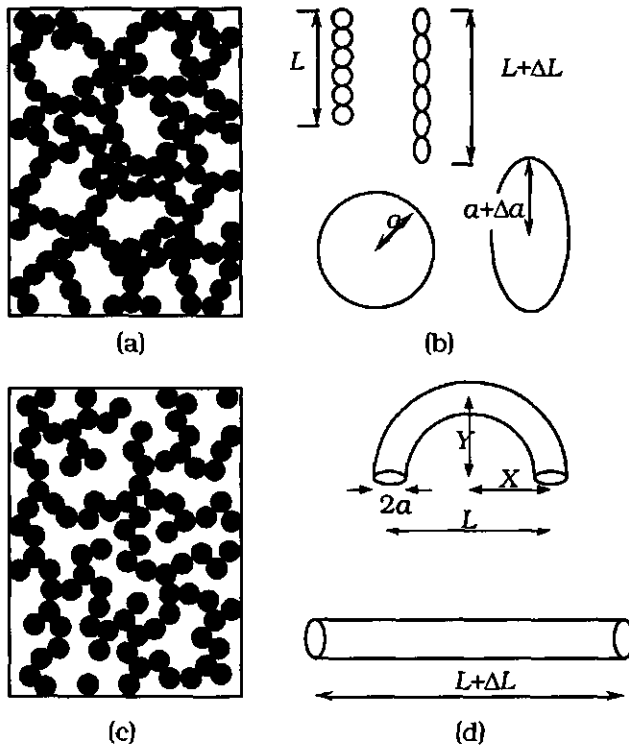


**Fig 5.6.** (a) Schematic picture of a casein gel with stretched strands. (b) Model strand of casein particles from fig. 5.6a, before and after a deformation of the gel. (c) Schematic picture of a casein gel with curved strands. (d) Model strand of casein particles from fig. 5.6c, before and after a deformation of the gel.

All these equations are only valid for small deformations, in the so-called linear region. For larger deformations the situation is different. The stress at which fracture occurs ( $\sigma_f$ ) is, as a first order approximation, proportional to the number of stress carrying strands. The strain at which fracture occurs ( $\gamma_f$ ) is dependent on the properties of the material in the particles, the bonds between these particles and on the extent to which a macroscopic shear strain leads to a deformation of the particles and bonds. Both  $\sigma_f$  and  $\gamma_f$  may depend on the deformation rate. Because the number of stress carrying strands is proportional to  $N$  we can write, as a first order approximation, for both gels with straight and curved strands

$$\sigma_f \propto \phi_0^{2/(3-D)} \quad (5.32)$$

if the material is not too brittle so that the curved strands can be stretched without fracture occurring. The strain at which fracture occurs,  $\gamma_f$ , will be larger for the gels with curved strands because the initial macroscopic shear strain hardly leads to deformation of the casein particles. Only after the strands are stretched, macroscopic deformation leads to a significant deformation of the particles. If the network strands are brittle, fracture may occur before the strands are stretched. In that case, the microscopic deformation ( $\epsilon$ ) is dependent on the size of the clusters in the gel (Eqn. 5.28), and thus on the volume fraction ( $\phi_0$ ); for such gels,  $\gamma_f$  will be less at a higher particle concentration.

### 5.3.3 Materials and methods

Type 2 gels were made by adding 0.165 g GDL per g sodium caseinate to a solution of sodium caseinate powder at 30 °C. The salt concentration in the solutions was kept constant at 0.14 M NaCl, independent of the sodium caseinate concentration. The final pH was always between 4.60 and 4.65. 16 - 20 h after the addition of GDL the dynamic moduli were measured in a concentric cylinder apparatus. The inner cylinder was oscillated sinusoidally and the resulting deformation was measured. A complete description of the method has been given elsewhere [18, 25]. The rheological data for the type 1 gels were taken from earlier work [18].

The measurements at large deformations were carried out with a Deer constant-stress rheometer. Gel type 2 was deformed by a sinusoidal shear stress (frequency 0.2 Hz). The stress was slowly increased until the gel fractured. The maximum deformation was measured as a function of the maximum shear stress for different casein concentrations. Creep measurements on gel type two were carried out by applying a constant stress in the range of 40 to 140 Pa to a gel with a concentration of 31.0 g casein per kg. Each gel was tested only once at one shear stress. A part of the gels was made in the same way as the gels used for the measurements at small deformations. Most gels tested at large deformations were made, however, by adding 0.33 g of GDL per g sodium caseinate powder. In this case we measured 2.5 h after the addition of GDL and the pH of these gels was 4.53 - 4.60. The creep measurements on gel type 1 were taken, again, from earlier work [18]. These measurements were performed on acid skim-milk gels instead of sodium caseinate gels. This caused slightly different interactions between the casein particles because the ionic composition was different in case of gels made of skim-milk. The casein particles were also somewhat larger. Both properties caused sodium caseinate gels, in general, to be somewhat stronger than skim-milk gels of the same casein concentration. This was probably of quite limited significance compared to the large differences in dynamic shear modulus for small deformations between the gel types, so that we could safely compare both results.

The voluminosity of the casein particles  $v$  (in ml per gram casein) was determined from the mass of the pellet of a sample of known casein concentration after centrifugation at 45000 g for 1 hour. For sodium caseinate, this method is only suitable at pH 4.6; at higher pH, where the casein molecules are not aggregated into casein particles, an ultra centrifuge would be required. Some samples were gelled before their voluminosity was determined, and the pellet was formed by collapse of the gel network rather than by settling of individual particles. This did not influence the results significantly, because a gelled and a non-gelled sample gave identical voluminosities at 10 °C. An absolute value of the voluminosity could not be obtained by this method, because the result depended slightly on speed and time of centrifugation. The (relative) values, however, were useful to explain the difference between the gel



types. Other methods can yield other voluminosities, especially if they take into account the 'hairy' character of the surface of the casein particles [21]. These values are probably less significant for our purpose because there is no significant hairy layer if particles are aggregated.

### 5.3.4 Results

Results on the storage modulus  $G'$  and the loss modulus  $G''$  as a function of the casein concentration are shown in fig 5.7, for type 1 gels and type 2 gels. The slope of the log - log plots is 2.6 in case of type 1, and 4.6 in case of type 2 gels. The slopes of the  $G'$  plots are slightly higher than those of  $G''$ . The moduli of the type 1 gels are, especially for the lower casein concentrations, much higher than those of the type 2 gels. The fractal dimensionality gathered from these curves is 2.24 for type 1 gels using Eqn. (5.26) (straight strands) and 2.35 for type 2 gels using Eqn. (5.31) (curved strands). The frequency dependence of the dynamic moduli is roughly similar for all acid casein gels tested. At 30 °C, both  $G'$  and  $G''$  increase with the angular frequency  $\omega$  as  $G \propto \omega^{0.15}$  over the whole range that has been tested (from  $10^{-3}$  to  $10^1$  rad/s [18, 20]).

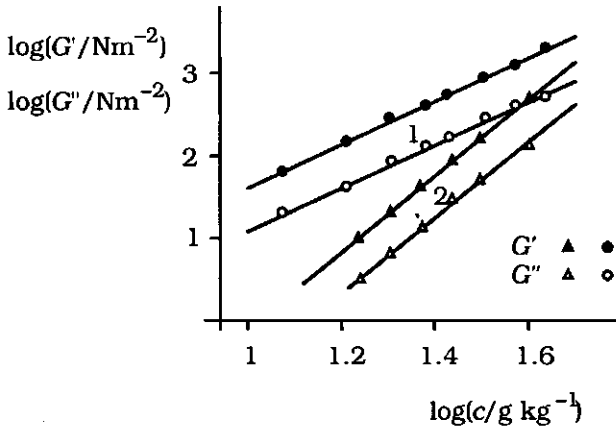


**Fig. 5.7.** Storage  $G'$  and loss modulus  $G''$  as a function of the casein concentration of acid gels (pH 4.6) made of Na-caseinate for type 1 and type 2 gels. Both gels were aged for about 16 h at 30 °C before they were measured at the same temperature at an angular frequency of 1 rad s<sup>-1</sup>.

In fig 5.8 the (maximum) shear strain of type 2 casein gels of various concentrations is depicted as a function of the shear stress brought on by an oscillating stress with a frequency of 0.2 Hz. The fracture shear strain  $\gamma_f$  is about 1.1, independent of the casein concentration. Fig 5.9 is derived from the same set of results. Here the log of the fracture stress ( $\log \sigma_f$ ) is depicted as a function of the log of the casein concentration. The result is a straight line with a slope of 2.46, leading to an effective fractal dimensionality of 2.19 (Eqn. 5.32).

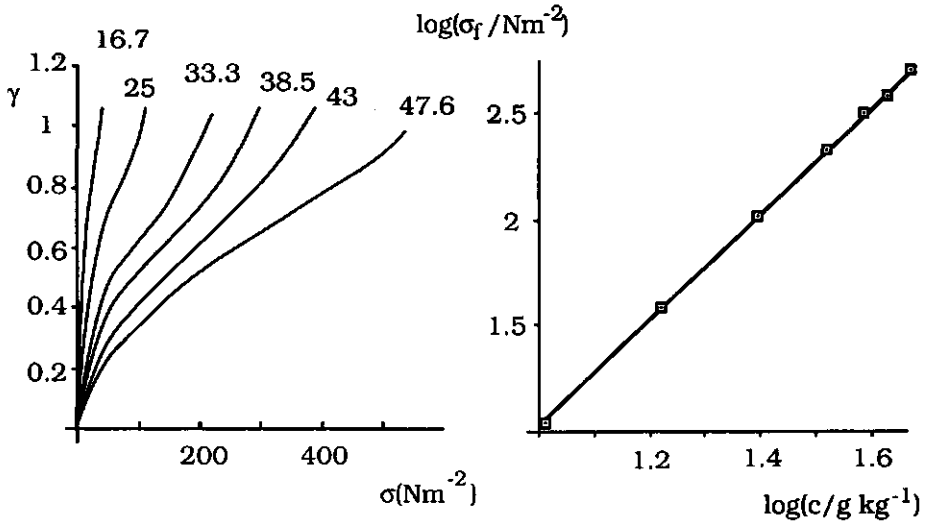


**Fig. 5.8.** Stress-strain relationship for type 2 acid casein gels. Measured is the maximum strain caused by an oscillating shear stress at a frequency of 0.2 Hz or  $1.25 \text{ rad s}^{-1}$ . The concentration of Na-caseinate ( $\text{g kg}^{-1}$ ) is indicated.

**Fig. 5.9.** Fracture stress, derived from fig. 5.8, as a function of the casein concentration of a type 2 acid casein gel.

Results of the creep measurements are in fig 5.10. The casein concentration is 34.2  $\text{g/kg}$  for the type 1 and 31.0  $\text{g/kg}$  for the type 2 gels. The most obvious difference between both gel types is the shear strain at which fracture occurs,  $\gamma_f$  having a value of 0.5 - 0.6 for type 1 and 1.1 - 1.2 for type 2 gels, independent of the loading time. The difference in  $\sigma_f$  is not so clear; the type 1 gels are a little bit stronger but have a somewhat higher casein concentration. In general, Na-caseinate

gels are stronger than gels made up of skim-milk at the same casein concentration. That in our measurement the type 1 gel exceeds the type 2 gel in strength may thus be caused by the difference in gel type. Probably, type 1 gels have a slightly higher  $\sigma_f$  than type 2 gels under similar conditions.

The amount of water kept per gram casein is for the cold (10 °C) acid sodium caseinate dispersion 3.2 ml, for the casein gel at the same temperature it is also 3.2 ml/g and for the casein gel at 30 °C it is 2.0 ml/g. If we assume that 1 g of casein has a volume of 0.7 ml we obtain a voluminosity of 2.7 ml/g for casein at 30 °C and 3.9 ml/g at 10 °C. These points are also shown in fig 5.5, which gives the results of more extended studies of  $\nu$  of casein particles [22, 23].

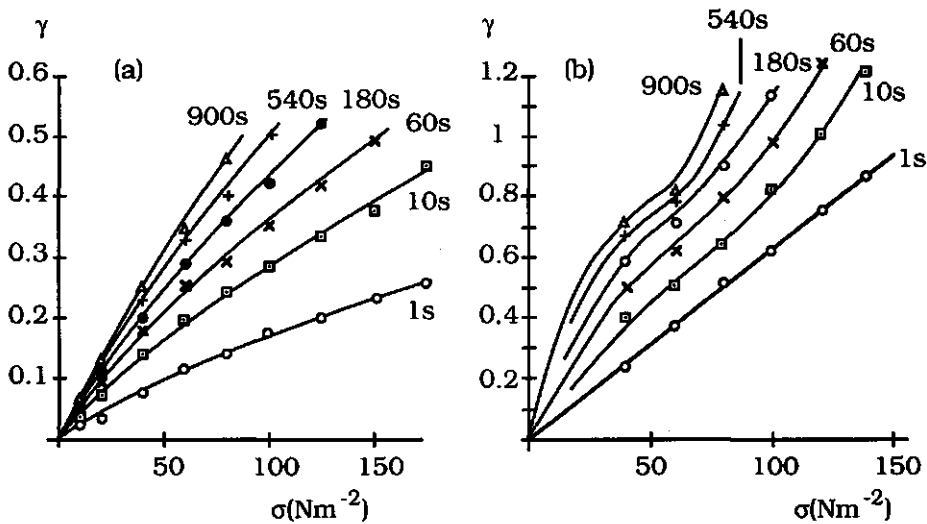


**Fig. 5.10.** Shear deformation as a function of shear stress derived from creep measurements for: (a) type 1 gels made of skim-milk; and (b) for type 2 Na-caseinate gels. Each gel was tested only once at a constant stress. The loading time is indicated.

### 5.3.5 Discussion

Both casein gels are formed by the aggregation of casein particles under quiescent conditions and their structures are expected to be

similar when the gel is just formed. For type 1 gels, gelation starts at a lower temperature and thus at a higher voluminosity of the casein particles. For these gels the effective volume fraction is thus higher at the same casein concentration. If we assume an incipient voluminosity of 3.9 ml/g for type 1 and of 2.7 ml/g for type 2 we calculate that  $N_1 = 2.43 N_2$  (Eqn. (5.23) with  $D = 2.35$ ).  $N$  is thus higher for type 1 gels but the factor 2.43 is probably an over-estimation. It is difficult to estimate the real  $N$  because it is affected by several factors. For type 1 gels the rate of the voluminosity change [26], the heating rate, the temperature where aggregation and gelation starts, the aggregation rate and the final temperature are important variables [18]. The temperature at which gelation starts is dependent on the salt concentration, the aggregation rate and the heating rate. For type 2 gels  $N$  will be defined by the rate of pH change, the pH at which the gelation starts, the final pH and possibly the rate of voluminosity change (although only a very limited voluminosity change is allowed after gelation because otherwise a type 1 gel arises). In both gels  $N$  is time dependent because new bonds will still be formed and old bonds may be broken after the gelation. This may be one of the reasons why the stiffness of the casein gels increases with time [18, 27]. Another reason may be an increase in the factor  $d^2A/da^2$ , due to fusion of the particles or due to the strands becoming more straightened.

$N$  particularly affects the fracture stress  $\sigma_f$  (Eqn. 5.32), which is thus expected to be higher for type 1 gels. This is in agreement with the observations,  $\sigma_f$  being slightly higher for type 1 gels (fig 5.9). However, more differences are involved than the difference in gel type. Type 1 gels were made up of skim-milk (casein concentration 34.2 g/kg) and type 2 gels of sodium caseinate (casein concentration 31.0 g/kg). The interactions between the particles may be slightly different for either gel because of the difference in ionic strength and composition.

At very high volume fractions, one anticipates not much difference between the modulus of the gels with the straight (type 1) and the gels with the curved strands (type 2). If we extrapolate the lines in figure 5.7, we obtain a point where both gel types have the same moduli; approximately at  $\phi_0 = 0.35$ . At this volume fraction the ratio  $R/a$  is about 5 (Eqn. 5.21) and the strands in the network are thus only a few particles long and hardly curved. The power law behaviour of  $G$  versus  $\phi_0$  is not

expected to persist up to very high volume fractions, because then the size of the clusters becomes very small, and fractal behaviour should thus not apply to the individual clusters. In our experiments the power law behaviour does persist up to rather high volume fraction, at least up to  $\phi_0 = 0.15$  ( $R/a = 18$ ). Apparently, the clusters show already a fractal behaviour at  $R/a = 18$ .

As expected, at lower volume fractions gels with straight strands are stiffer than gels with curved strands and the difference increases with decreasing volume fraction, as follows from the results of the dynamic moduli  $G'$  and  $G''$  (fig 5.7).

The absolute value for Young's modulus,  $E$ , of the material in the strands that we calculate from our results (fig. 5.7), assuming that  $D = 2.35$  and  $n = 3$  [Eqn. 5.26], is larger than  $10^6 \text{ N m}^{-2}$ , and thus significantly higher than  $10^5 \text{ N m}^{-2}$ , which is about Young's modulus of a very young Gouda cheese [28]. Gouda cheese has about the same casein concentration in water as the strands, about 30 wt%. Probably, Gouda cheese is more inhomogeneous than the material in the strands, leading to lower moduli.

The results at higher deformations, figs. 5.8 - 5.10, are also in agreement with the model. The casein particles are so flexible that no fracture occurs before the strands in a type 2 gel are stretched. The deformation of the casein particles is still rather low at this point, particularly for gels with large clusters (low casein concentration). The macroscopic strain, however, has reached a considerable value. After the point at which most strands are stretched the deformation of the material in the strands increases progressively with increasing macroscopic shear strain. For type 1 gels this happens from the beginning and for type 2 gels after a certain shear strain has been reached. The difference in shear strain at which fracture occurs between both gel types ( $1.2 - 0.6 = 0.6$ ) provides information about the degree to which the strands are curved. It is obvious that not all strands are stretched at the same time, the macroscopic deformation not being distributed equally over all casein strands. It is thus difficult to anticipate the strain at which fracture occurs, even if we have sufficient information about the properties of the casein strands. Fracture of materials is an intricate subject [29] and we can only compare different 'fractal gels' because they are scale invariant.

This implies that the average position of the strands in the gel network, and thus their deformation, is independent of the casein concentration.

The fractal dimensionality of casein gels is known from other measurements (table 5.2) and is about 2.35. There must be a transition from a gel with curved to a gel with straight strands and for the plot of  $\log G$  versus  $\log \phi_0$  we thus expect a slope ranging from  $2/(3-D)$  for a typical type 1 gel to  $3/(3-D)$  for a typical type 2 gel. However, we found lower slopes for the type 1 casein gel, and also for  $\log \sigma_f$  versus  $\log \phi_0$  of both casein gels (fig 5.9). This may be not surprising, because Eqn. 5.32 is only a first order approximation and type 1 gels undergo many changes before they are transformed, and not all these changes have to be independent of the volume fraction. For instance, the stretching of the strands leads to a larger deformation of the material in the strands in the case of smaller clusters (and thus at higher  $\phi_0$ ) because  $a/R$  (Eqn. 5.28) is then relatively large. This may also be the explanation for the low slope in fig. 5.9.

According to our model,  $G$  is independent of the particle size  $a$ . In most experiments, however, one finds that smaller particles lead to stronger gels. Buscall has found for polystyrene latex gels that  $G$  is about proportional to  $a^{-2}$  [8]. This is probably due to the scale invariance not persisting on the scale of the size of the particles. The relative degree to which fusion has occurred after a certain time is dependent on the size of the particles. Only if the fusion occurs very fast or if the gel is aged for a very long time, we expect the modulus to be independent of  $a$ . This may have been the case in the gels of Nederveen [3] who obtained roughly the same modulus for gels with 100 nm and with 4  $\mu\text{m}$  particles (fat crystals in oil).

**Table 5.2** The effective fractal dimensionality of the clusters in a casein gel as a result of different types of measurements.

	Type 1	Type 2
Permeability - volume fraction	2.39	2.36
Shear modulus - volume fraction	2.24	2.36
Fracture stress - volume fraction	2.2	2.19
Turbidity - wavelength		2.27
Cluster size in the gel - volume fraction (microscopy)	2.35	2.35

### 5.3.6 Appendix

In this appendix some additional information on the rheological properties of casein gels, that has not been published in [9] (sections 5.2.1 and 5.2.2) or [10] (sections 5.3.1 - 5.3.5), is given.

The evolution of a type 2 gel into a type 1 gel may be the result of a decrease in the voluminosity of the particles or of a stretching of the strands due to micro-syneresis. The first mechanism is expected in the case of casein gels made by acidification in the cold, because there is a considerable decrease in voluminosity of the casein particles after gel formation. However, the other mechanism can not fully been excluded because the particles that are formed from the Na-caseinate in the cold may be different from the particles formed at 30 °C [30] and it cannot be ruled out that some microsyneresis occurs before the gel reaches the higher temperatures. Measurements of the dependence of the loss tangent on temperature and frequency of both acid casein gel types gave similar results at high casein concentrations [18], indicating similar properties of the casein particles and their interactions.

In table 5.3 various rheological properties of type 1 [18] and type 2 [31] acid casein gels are compiled.

Property	type 1 gel	type 2 gel
$\frac{d \log G'}{d \log \phi_0}$	2.6	4.7
$\frac{d \log G''}{d \log \phi_0}$	2.6	4.4
$\tan \delta (30 \text{ }^\circ\text{C})$	0.26 independent of $\phi_0$ independent of $\omega$	0.26 - 0.37 decreasing with increasing $\phi_0$ decreasing with increasing $\omega$

**Table 5.3** *Compilation of some differences in rheological properties between type 1 and 2 acid casein gels.*

Roefs found for type 1 acid skim-milk gels  $\tan \delta$  to be 0.26, independent of  $\phi_0$  and  $\omega$  [18]. For a type 2 acid skim-milk gel, casein concentration 26 g/kg,  $\tan \delta$  was also 0.26 and independent of  $\omega$  [18]. Schrijvers obtained the same result for a type 2 Na-caseinate gel with a high casein concentration ( $> 40$  g/kg). At lower casein concentrations  $\tan \delta$  increased and became a (slightly) decreasing function of  $\omega$  [31]. A plausible explanation of these differences will be given in section 7.2.

Experimental data on the modulus of acid skim-milk gels as a function of the casein concentration give curved lines in a log-log plot [16, 18]. The casein concentration had been varied by means of ultra-filtration thus keeping the concentration of all components except that of the casein micelles and dissolved proteins approximately constant. During acidification, however, the calcium phosphate of the casein micelles goes into solution, resulting in a higher salt concentration at higher casein concentrations. This leads to different interactions at different casein concentrations and curved lines instead of the straight lines for Na-caseinate gels (fig. 5.7) where the interactions between the particles are independent of the casein concentration. Measurements on acid skim-milk gels in which the casein concentration has been varied by dissolving different amounts of skim-milk powder in demineralized water result in even more strongly curved lines.

Experimental data on rennet induced skim-milk gels give straight lines in a double logarithmic plot of the storage and loss moduli as a function of the casein concentration [25]. The slope of the curves is 2.4, indicating a gel with stretched strands and an effective fractal dimensionality of 2.2. In these rennet induced casein gels the salt concentration is constant because the calcium phosphate stays in the casein micelles fig (3.1). The properties of the particles and their interactions is therefore different from those of the particles in acid casein gels. Rennet induced gels are subject to (micro-) syneresis [13, 14] which causes stretching of the strands.

The skim-milk gels used in this thesis were made of low-heat skim-milk powder. Heating of milk alters the properties of casein because of adsorption of heat-denaturated whey proteins [32]. Gels made by quiescent acidification of high-heat skim-milk powder with GDL are presumably type 1 gel, i.e., gels with stretched strands [33].



## 5.4 Rheological behaviour of gels of polystyrene particles

### 5.4.1 Introduction

The rheological behaviour of aggregate networks has found new interest after the introduction of the concept of fractal geometry of gel networks. Particle networks can be modelled as a collection of interconnected fractal clusters. This model is shown to be very useful to describe the formation and the properties of casein gels. Casein gels are particle gels, although the particles themselves consist of associated macromolecules. In the case of skim-milk the casein micelles have an intricate and variable structure, depending on pH, salt concentration, temperature, etc. (fig. 3.1). For Na-caseinate the gel formation is a 2 stage process in which the casein molecules first associate into particles which subsequently aggregate thus forming flocs and a gel. Gels of spherical monodisperse polystyrene particles are formed directly due to their aggregation. This system has the advantage that the volume fraction can be determined precisely and that the particles are monodisperse and is therefore especially suitable to study the fractal nature of particle gels.

### 5.4.2 Materials and methods

The preparation of the polystyrene latices and the method by which the gels have been prepared are described in the sections 3.1 and 3.2. The rheological measurements at  $\phi_0 > 0.5\%$  were carried out with a Bohlin VOR rheometer. In this apparatus an outer cylinder was oscillated sinusoidally and the resulting torque on the inner cylinder was measured via a torsion bar. Three types of measurements were performed. First the gel formation and ageing were followed at a small deformation  $\gamma \approx 1\%$  and a frequency of 1 Hz ( $6.28 \text{ rad s}^{-1}$ ). After ageing for 2 h the frequency was varied from 10 to 0.01 Hz and back to 10 Hz. Finally, a so-called 'strain-sweep' measurement was performed at a frequency of 1 Hz. In this experiment the amplitude of the oscillation (and thereby the strain) was gradually increased until fracture occurred.

The formation of gels with a volume fraction of 12 % was studied at varying strains in order to check the reproducibility and the effect of deformations on the gel properties and ageing.

For the lower volume fractions a parallel-plate rheometer without bearings was used [34]. This apparatus consisted of a ferro-magnetic disk which floated on the dispersion. The disk was centred by a magnetic field until its position was fixed because a gel had formed. After ageing for 16 h, a torque was imposed on the disk by means of a rapidly rotating magnet (fig. 5.11). The torque,  $T_q$ , was varied between  $10^{-8}$  and  $10^{-5}$  N m by changing the distance between the disk and the rotating magnet. The thickness of the gel layer,  $d$ , was about 5 mm and the radius of the disk,  $R_d$ , was 47.5 mm.

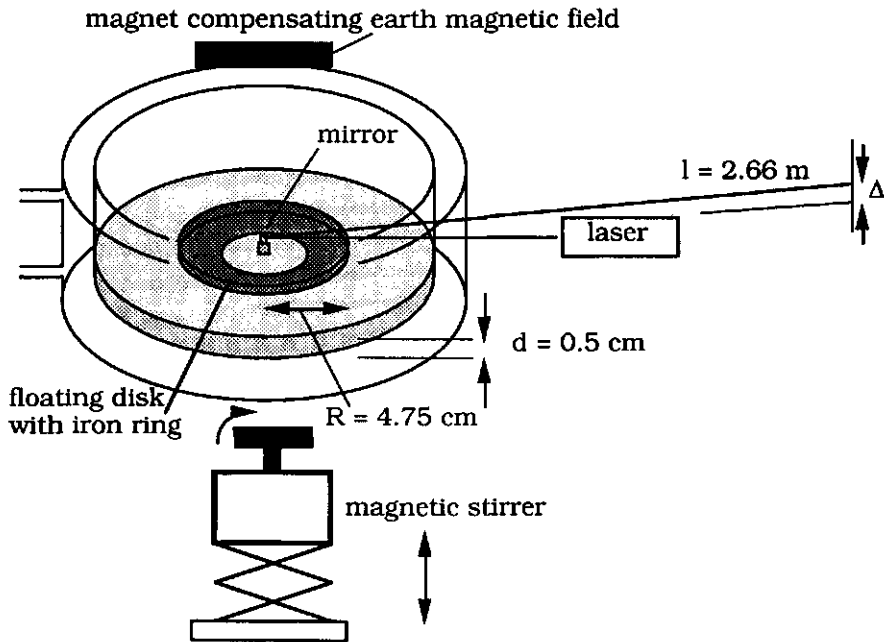


**Fig. 5.11** Schematic presentation of the floating disk rheometer (not to scale). The angle of distortion is  $\alpha = \Delta/(2l)$ .

The angular distortion,  $\alpha$ , was measured via a mirror on top of the disk and a laser beam. After applying a deformation the distance between the disk and the rotating magnet was increased to the maximum value ( $T_q < 10^{-10}$  Nm). In the case of relatively small deformations ( $\gamma < 0.2$ ) the

disk turned back to its initial position. A static shear modulus,  $G$ , was calculated according to [35]

$$G = \frac{2dT_q}{\pi\alpha R_d^4} \quad (5.33)$$

This equation applies to the distortion of a cylinder and is thus not exact for the floating disk because the gel outside the cylinder beneath the disk is not taken into account. The reproducibility of these measurements was not very good and the modulus obtained from different experiments, performed at the same volume fraction, varied by a factor 2 to 3.

### 5.4.3 Results

#### 5.4.3.1 Formation and ageing of the gels

In fig. 5.12 - 5.15 the formation and ageing of the gels of varying volume fractions are followed by measuring  $G'$ . Gelation occurs within a few minutes at low  $\phi_0$  to 40 minutes at  $\phi_0 = 0.35$ . This difference is due to the buffering of the palmitate on the surface of the particles which leads to a slower decrease of the pH in the case of high  $\phi_0$  (more palmitate).

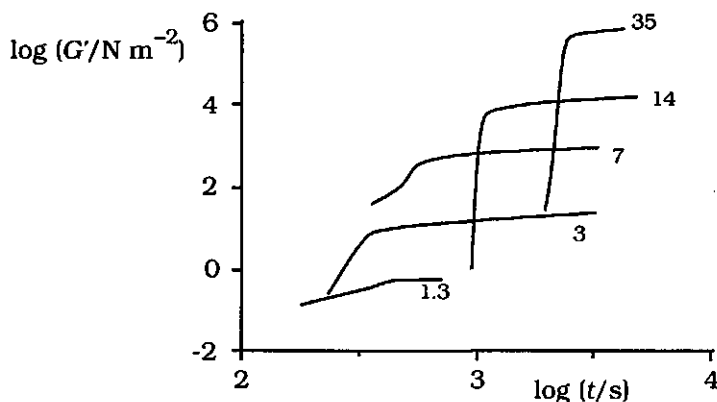


**Fig. 5.12** Logarithm of the storage modulus  $G'$  of various polystyrene latex gels plotted as a function of the logarithm of the time after addition of GDL. Ageing temperature = 20 °C and  $\omega = 1$  Hz (6.28 rad s<sup>-1</sup>). The volume fraction, expressed as a percentage, is indicated near the curves.

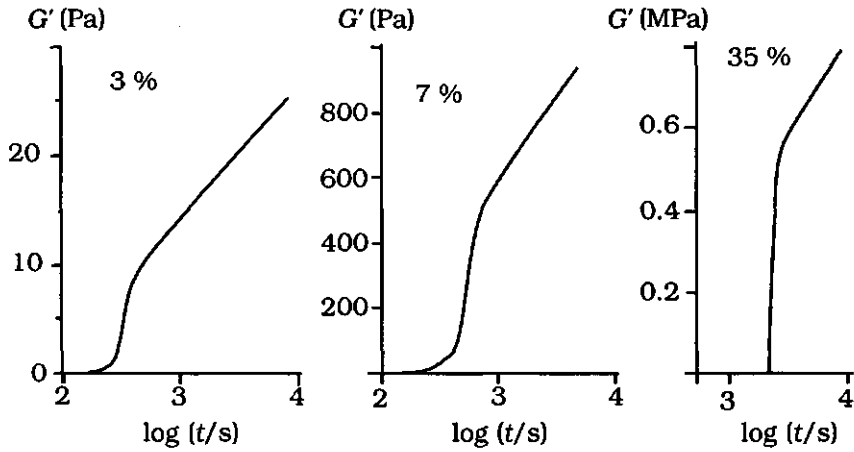


**Fig. 5.13** Storage modulus  $G'$  plotted as a function of the logarithm of the time after addition of GDL.

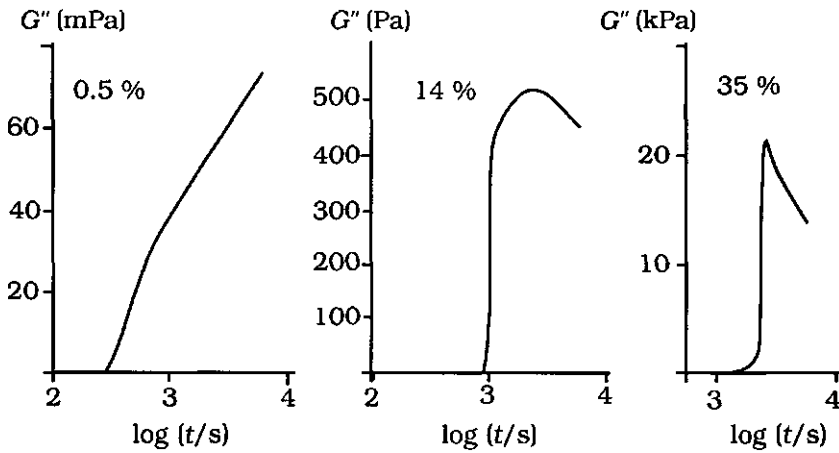


**Fig. 5.14** Loss modulus  $G''$  for various volume fractions plotted as a function of the logarithm of the time after addition of GDL.  $T = 20^\circ\text{C}$ ,  $\omega = 1\text{ Hz}$ .

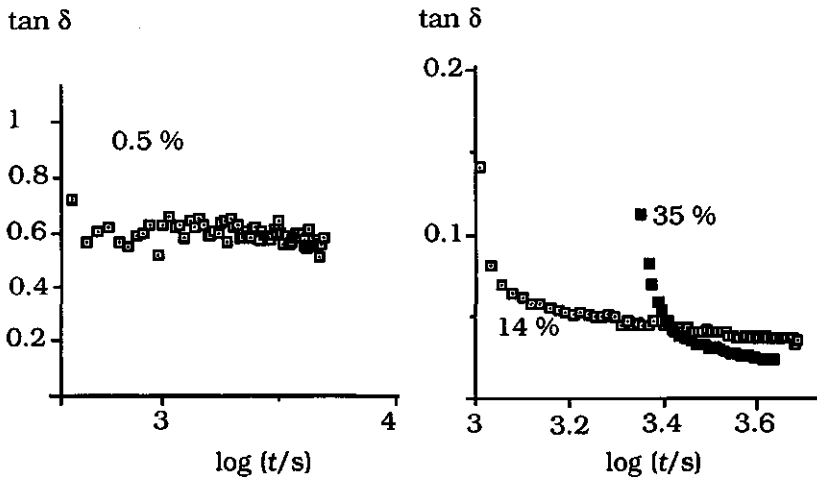


**Fig. 5.15** Loss tangent  $G''/G'$  for various volume fractions plotted as a function of the logarithm of the time after addition of GDL.  $T = 20^\circ\text{C}$ ,  $\omega = 1\text{ Hz}$ .

At very low volume fractions ( $< 3\%$ )  $G''$  and  $G'$  both increase as a function of time and the loss tangent remains roughly constant. At higher  $\phi_0$ ,  $G'$  increases and  $G''$  and  $\tan \delta$  decrease as a function of ageing time. The relative rate of the increase of  $G'$ ,  $dG_r / d \log t$ , is independent of  $\phi_0$ .  $G_r(t)$  is defined as  $G'(t)$  divided by the storage modulus 3000 s after gelation. The slope of the straight part of curves of  $G_r$  versus  $\log t$  was  $0.6 \pm 0.1$ . The loss tangent is smaller for a higher  $\phi_0$ .

#### 5.4.3.2 Strain sweep measurements

Results of strain sweep measurements are compiled in fig. 5.16 and 5.17. The linear region, i.e. the region where stress and strain are proportional, is small; the shear strain should be smaller than 1%. Gels with a volume fraction below 0.02 were studied at a shear strain of 5% which led to a slightly higher  $G'$  and a slightly lower  $G''$  than at smaller strains. The shear strain at which fracture occurs is, for gels made of polystyrene particles, dependent on the volume fraction and is higher at lower  $\phi_0$ .

During a strain sweep experiment  $G''$  and  $\tan \delta$  first decrease whereas  $G'$  increases. The decrease of  $G''$  and  $\tan \delta$  become less pronounced if the gel is aged for a longer time.

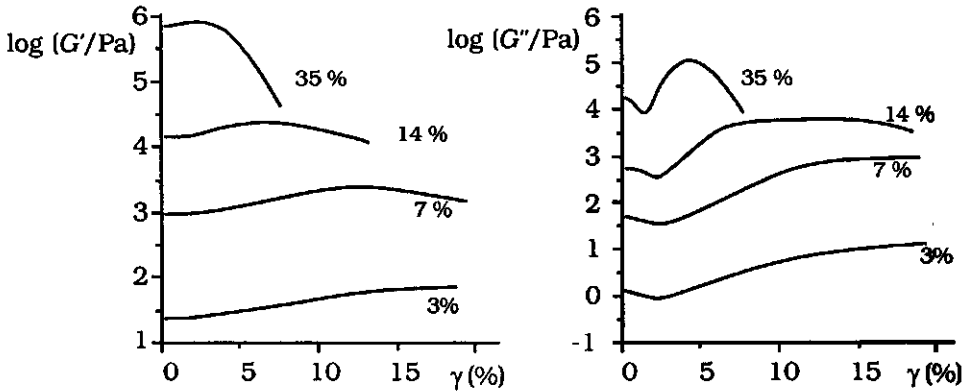


**Fig. 5.16** Logarithm of the apparent storage and loss moduli of polystyrene latex gels plotted as a function of the shear strain. The volume fraction is indicated near the curves. The minimum strain was 0.1 %

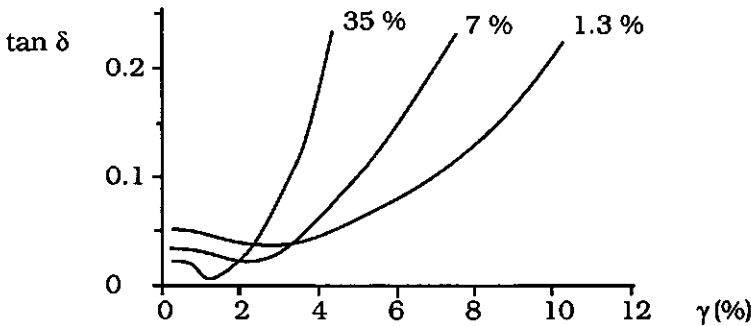


**Fig. 5.17** The loss tangent of various latex gels as a function of the shear strain  $\gamma$  in a so-called strain-sweep experiment. The volume fraction is indicated near the curves. The minimum strain was 0.1 %.

At larger strains, i.e. 2 - 3 %,  $G''$  increases until macroscopic fracture occurs. After macroscopic fracture occurs  $G'$  and  $G''$  decrease strongly. For a volume fraction of 0.35 macroscopic fracture starts at a strain of 4 %, for  $\phi_0 = 0.14$  at  $\gamma = 8$  % and for  $\phi_0 = 0.07$  at  $\gamma = 13$  %. At lower  $\phi_0$  no macroscopic fracture occurs (maximum strain was 20 %).

### 5.4.3.3 The dynamic moduli as a function of frequency

In fig. 5.18 the results of measurements at varying  $\omega$  are compiled for various volume fractions.

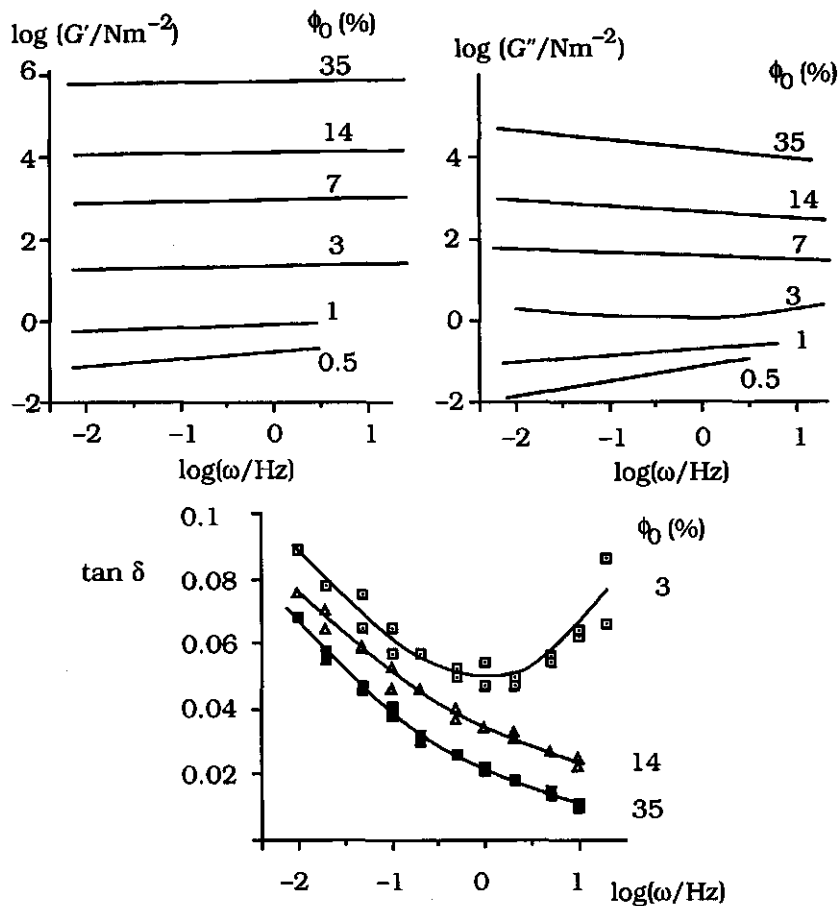


**Fig. 5.18** Storage modulus  $G'$ , loss modulus  $G''$  and  $\tan \delta = G''/G'$ , as a function of the angular frequency  $\omega$ . Measuring and ageing temperature were  $20^\circ\text{C}$ . The gels were aged for 2 h. The initial volume fraction is indicated near the curves.

The dependence of  $G'$  on  $\omega$  varies from  $G' \propto \omega^{0.16}$  for  $\phi_0 = 0.5\%$  to  $G' \propto \omega^{0.02}$  for  $\phi_0 = 35\%$  and of  $G''$  from  $G'' \propto \omega^{0.37}$  for  $\phi_0 = 0.2\%$  to  $G'' \propto \omega^{-0.24}$  for  $\phi_0 = 35\%$ . The cross-over from decreasing loss moduli as a function of

$\omega$  to increasing  $G''$  occurs at  $\phi_0 = 3\%$ . At the same volume fraction we also found the cross-over from increasing to decreasing  $G''$  as a function of ageing time.

#### 5.4.3.4 The dynamic moduli as a function of the volume fraction

In fig. 5.19 the logarithm of the storage and loss moduli, measured at two different angular frequencies, are depicted as a function of the logarithm of the volume fraction. The straight lines for  $\log G'$  versus  $\log \phi_0$  have a slope of 4.18 for  $\omega = 10$  and 4.21 for  $\omega = 0.01$  Hz and Eqn. (5.31) yields  $D = 2.28$ . The slope is independent of the ageing time of the gels. The curves of  $\log G''$  versus  $\log \phi_0$  become curved below a certain volume fraction; for low  $\phi_0$  and high  $\omega$ ,  $G''$  is relatively high. The slope of the straight part of these curves is 4.08, yielding  $D = 2.26$ . The slope of the curves of  $\log G''$  versus  $\log \phi_0$  decreases slightly as a function of ageing time.

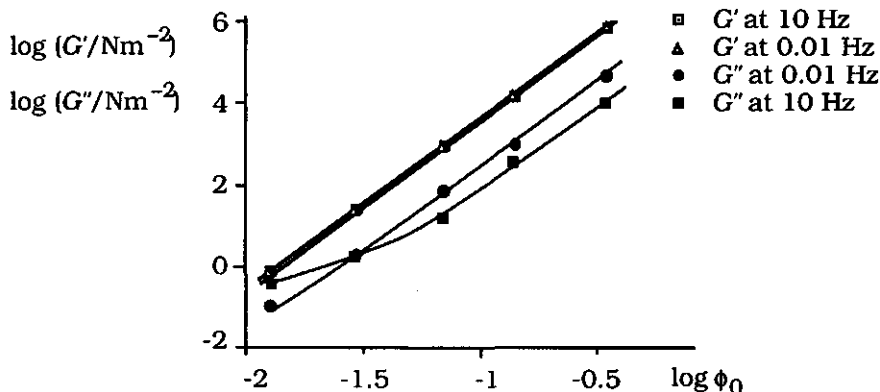


**Fig. 5.19** Storage modulus  $G'$  and loss modulus  $G''$  as a function of  $\phi_0$  for  $\omega = 0.01$  and  $\omega = 10$  Hz. The slope of the  $G'$  curves is 4.18 at 10 Hz and 4.21 at 0.01 Hz, the correlation coefficient is 1.000. The average slope of the  $G''$  curves is 3.67 at 10 Hz and 4.08 at 0.01 Hz, with correlation coefficients of 0.989 and 0.999, respectively.

Results of some measurements with the floating disk rheometer are compiled in fig. 5.20. The modulus,  $G$ , calculated with Eqn. 5.33, is plotted as a function of the angle of distortion,  $\alpha$  and the maximum strain.



The maximum strain,  $\gamma_m$ , is the strain of the gel under the outer side of the disk and is thus equal to  $\alpha R_d/d$ . The strain in the part of the gel that is below the central region of the disk is smaller.

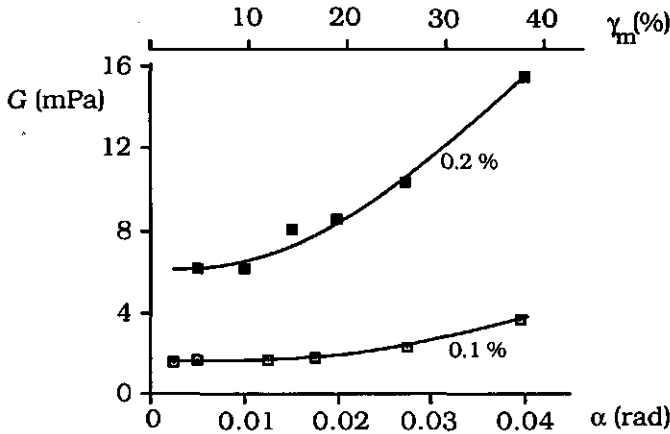


**Fig. 5.20** Shear modulus as a function of the deformation. The initial volume fraction of the polystyrene latex particles is indicated near the curves.

In fig. 5.21  $\log G$  is depicted as a function of  $\log \phi_0$  for particles with radii of 35 and 70 nm. A range of 9 decades in  $G$  is covered for the smallest particles. It is seen that a bend in the curve occurs at  $\phi_0 = 0.015$ . Below the bend, the slope is 2.46, and Eqn. (5.26) yields  $D = 2.19$ ; above the bend, the slope is 4.12 for  $a = 35$  nm, Eqn. (5.31) yielding  $D = 2.27$ , and 4.02 for  $a = 70$  nm, yielding  $D = 2.25$ . Concentration series measured with the floating disk rheometer ( $0.001 < \phi_0 < 0.02$ ) at a maximum shear deformation,  $\gamma_m$ , of 10 %, ageing time 16 h and with the Bohlin VOR ( $0.005 < \phi_0 < 0.35$ ,  $\gamma = 1$  %, ageing time 1 - 2 h) are combined in the figure. At volume fractions below 0.001 the modulus measured with the floating disk rheometer is roughly constant. This is probably due to the presence of a surface gel. At the water-air interface a film consisting of aggregated polystyrene particles develops during gel formation. The volume fraction of the particles in this film is much higher than in the bulk. The same phenomenon was observed on CSLM micrographs of casein gels in the vicinity of the glass surface (chapter 4). The relative contribution of the surface gel to the resistance against distortion is

presumably negligible at volume fractions above 0.1 %. If we assume a thickness of 1 particle diameter (70 nm) for the surface film its shear modulus can be estimated. In that case, the shear stress is roughly  $\sigma_f \approx T_q/2\pi R_d^2 h$  where  $h$ , the thickness of the film is 70 nm, and the strain is roughly  $\gamma_f \approx \alpha R_d/b$  where  $b \approx 0.03$  m is the distance between the floating disk and the wall of the container with the gel. At volume fractions lower than 0.1 %, a torque,  $T_q \approx 1.2 \times 10^{-8}$  N m results in a distortion,  $\alpha \approx 8 \times 10^{-3}$ . The shear modulus of the film is thus roughly  $\sigma_f/\gamma_f \approx 1$  kPa. The effect of a surface film can be estimated by measuring the torque with disks of different size. The contact area of the disk with the bulk gel and thus the torque would scale like  $R_d^2$  and of the torque for a surface gel like  $R_d$ .

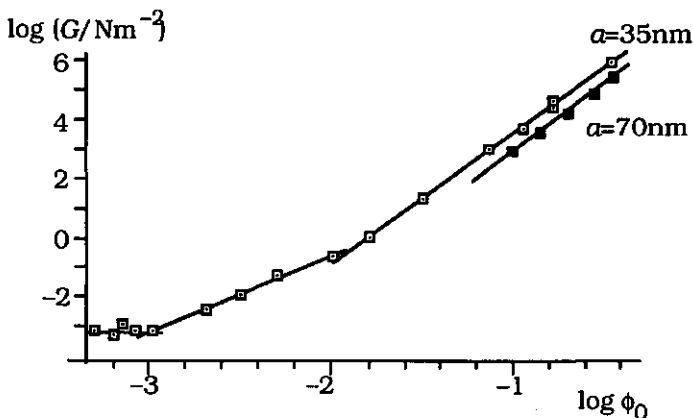


**Fig. 5.21**  $\log G$  depicted as a function of  $\log \phi_0$  for particles with radius,  $a = 35$  and  $70$  nm.

#### 5.4.4 Discussion

The formation of gels of polystyrene particles occurs rapidly after the latex becomes unstable. Permeability measurements (Chapter IV) show that the geometric structure of a gel that is aged for 16 h does not change as a function of time (range of volume fractions studied; 2 to 25 %,  $a = 70$  nm). The permeability of each gel was measured 2 and 16 hours after gelation and no significant differences were found. The ageing of polystyrene latex gels is therefore mainly due to changes at the level of

the particle-particle bonds. These changes are independent of  $\phi_0$ ; the loss tangent and its dependence on  $\omega$  are thus expected to be independent of  $\phi_0$ . For type 1 acid casein gels this is found in practice, but for polystyrene latex gels  $\tan \delta$  depends on  $\phi_0$ . The reason for this phenomenon lays in the formation and breaking of new bonds due to the deformation of the gel (explained in section 7.2). At high  $\omega$  and low  $\phi_0$  dissipation of energy is mainly due to the viscous flow of water through the gel and between the particles. This is the reason why plots of  $\log G''$  versus  $\log \phi_0$  (fig. 5.19) and plots of  $\log G''$  versus  $\log \omega$  (fig. 5.18) have a bend at low volume fraction and high frequency. Below the bend the contribution of the energy that is dissipated due to relaxation of the particle-particle bonds becomes small compared to the dissipation due to viscous flow. Eventually,  $G''$  becomes larger than  $G'$  at low  $\phi_0$  and high  $\omega$  because more energy is dissipated due to viscous flow through the network than stored in the network. At these conditions it is arbitrary whether the network may be called 'gel' (chapter I).

Plots of  $\log G'$  versus  $\log \phi_0$  give straight lines with a slope that does not depend on the ageing time nor on the angular frequency for  $\phi_0 > 0.015$ . The slope of these lines was  $4.1 \pm 0.2$  and the fractal dimensionality is thus  $2.27 \pm 0.04$  according to Eqn. 5.31 and  $2.02 \pm 0.05$  according to the model of Brown and Ball. The latter value is in agreement with computer simulations, but not with the dimensionality obtained with other methods, e.g. permeability measurements ( $D = 2.21$ , chapter IV). Buscall et al. [8] and Shih et al. [11] obtained similar experimental results for the dependence of the modulus of various particle gels on the initial volume fraction of the particles. Buscall et al. used larger polystyrene particles,  $a = 165$  to  $a = 480$  nm, which were coagulated into a network after addition of salt. The critical volume fraction needed to obtain a space filling network was about 0.05, probably because of the shear that must have been applied to mix the polystyrene dispersion with the salt solution and due to sedimentation of the flocs.

The bend that occurs in the curve of  $\log G$  versus  $\log \phi_0$  (fig. 5.21) is presumably due to syneresis occurring at low  $\phi_0$ , converting the gel with curved into one with straight, stretched strands. This is in agreement with the idea that longer and thinner strands are more prone to breaking, thereby exhibiting syneresis [36]. Another contribution to the difference

in slopes may have been the difference in the method of measuring  $G$ . At low  $\phi_0$  (floating disk rheometer) the ageing time was longer and the strain at which  $G$  was measured was higher. Probably these differences affect the absolute value of  $G$ , but hardly the slope of the curve.

The strain at which fracture occurs in polystyrene latex gels is small and depends on the volume fraction of the particles in the gel (fig. 5.17). For casein gels this is not the case, macroscopic fracture occurs at shear strains,  $\gamma_f$ , of 0.5 - 0.6 for gels with stretched and 1.1 - 1.2 for gels with curved strands, virtually independent of  $\phi_0$ . The strands of polystyrene particles fracture at a  $\gamma$  where they cannot yet be straightened, presumably because polystyrene particles are more rigid than casein micelles. Shih et al. [11] assumed that linear elastic behaviour vanishes if the deformation becomes so large that the weakest bonds break. The force exerted on a strand,  $F_s$ , due to a deformation,  $\gamma$ , depends on the elastic constant of the strands,  $C_e$  (table 5.1);  $F_s \propto \gamma C_e$ . Assuming that a constant force, independent of  $\phi$ , is needed to break a strand Shih et al. derived

$$\gamma_f \propto R^{2+x} \propto \phi_0^{(2+x)/(D-3)} \quad (5.34)$$

using the model of Brown and Ball. Their experimental results on boehmite alumina gels showed power law behaviour for the dependence of  $G'$  and  $\gamma_f$  on  $\phi_0$ ;  $G' \propto \phi_0^{4.1}$  and  $\gamma_f \propto \phi_0^{-2.1}$  yielding  $D = 2$  and  $x = 0.1$  according to the model of Brown and Ball.

Similar relations can be derived for the straight strand model,

$$\gamma_f \propto R^0 \propto \phi_0^0 \quad (5.35)$$

and for the curved strand model,

$$\gamma_f \propto R^1 \propto \phi_0^{1/(D-3)} \quad (5.36)$$

Eqn. 5.35 is in accordance with the experimental results on casein gels. Applying Eqn. 5.36 to the experimental results of Shih et al. yields  $D = 2.5$  whereas Eqn. 5.31 yields  $D = 2.3$ . Results of  $\log \gamma_f$  as a function of  $\log \phi_0$  for polystyrene latex gels are plotted in fig. 5.22.

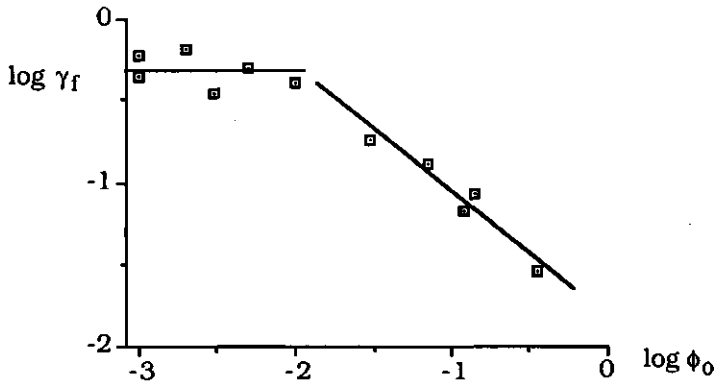


**Fig. 5.22**  $\log \gamma_f$  depicted as a function of  $\log \phi_0$  for polystyrene particles with radius 35 nm.

For  $\gamma_f$  the shear deformation where the value of the modulus,  $G$ , just starts to decrease is taken (this is another  $\gamma_f$  than obtained in the creep measurements in section 5.3.4). The slope of the straight line for volume fractions higher than 1 % is  $-0.75$  yielding  $D = 1.7$ . The model of Shih et al. fits the experimental results even worse (yielding the impossible values  $D = 2.4$  and  $\alpha = -1.5$ ). Presumably the fracture behaviour and non-linearity are more complicated than assumed in these models. However, the observation that the strain at which fracture occurs is independent of  $\phi_0$  for low, and a decreasing function of  $\phi_0$  for high volume fractions is in qualitative agreement with the idea that the strands become stretched at low  $\phi_0$  (due to microsineresis).

Results of strain sweep measurements show a minimum in  $\tan \delta$  at small strains (fig. 5.17). Presumably, the bonds between the particles increase in strength or in number due to the applied deformation. This leads to an increase of  $G'$  and a relatively much larger decrease of  $G''$ ; because the particles are pressed onto each other they 'stick' better, presumably due to an increase of the contact surface, leading to less relaxation of bonds. The depth of the minimum of  $\tan \delta$  and  $G''$  obtained for strain sweep measurements decreases if the gel had been aged longer. This is in accordance with the idea that the contact surface between particles increases due to deformation of young gels; in aged gels the contact surface is already increased due to sintering. At larger

deformations  $G'$  and  $G''$  increase because the strands become more and more stretched.

Deformations may affect the rheological properties of gels. In order to study the effect of the oscillating deformation that is imposed on the system during the gel formation, gelation under various strains is studied (fig. 5.23). No difference in properties is found for gels that are formed at strains smaller than 1 %. These small deformations have no significant effect on the properties of the particle-particle bonds nor on the gel structure.

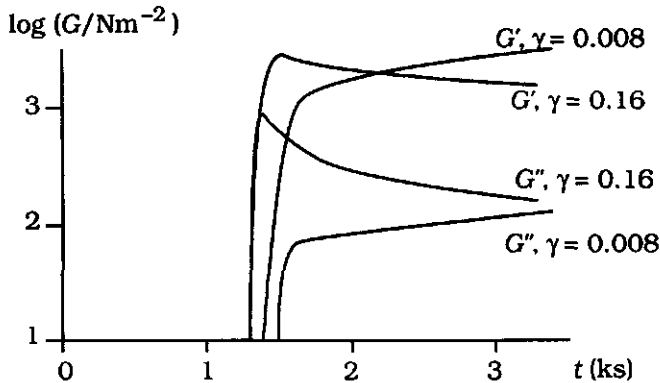


**Fig. 5.23** *Logarithm of the apparent storage and loss moduli of polystyrene latex gels as a function of time. The magnitude of the maximum strain applied during the gelation is indicated near the curves.  $\phi_0 = 0.12$ .*

If a gel is formed at a strain of 0.16 and the strain is decreased after gel formation, the storage modulus decreases roughly by a factor 5. The results of strain sweep measurements of gels that are formed at a strain of 0.008 and 0.16 are depicted in fig. 5.24. Presumably, strands become oriented if large deformations are imposed on the system during gel formation. Probably, strands that provide a 'short connection' between both cylinder walls of the rheometer have a high probability to break, which makes the stress carrying strands on average longer. This is in accordance with the observation that the strain at which fracture occurs is larger if gelation occurs while the system is subject to large oscillating deformations. If the strain decreases the strands dangle rather loosely in the gel and the storage modulus decreases. This effect may be the reason

for the poor reproducibility of the measurements with the floating disk rheometer. During the gelation the disk is centred by a magnetic field but small variations in its position may still be possible. This may have led to non-reproducible variations in strain history.

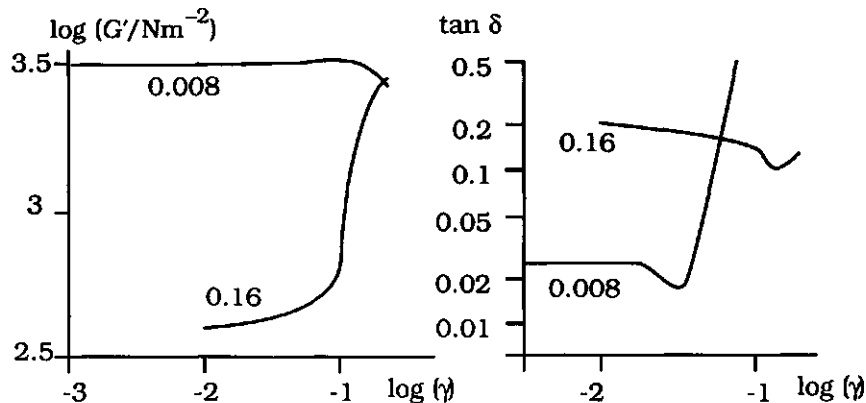


**Fig. 5.24** Strain sweep experiments of the gels from fig. 5.23. Strain sweep measurements were performed after the gels were formed and aged for 2 h at the indicated shear strain. The volume fraction of particles was 12 % and the temperature was 20 °C.

#### Acknowledgement

We gratefully acknowledge Dr. J. Lichtenbelt and Dr. B. Reuvers of Akzo research in Arnhem for helpful discussion, the opportunity to use their Bohlin VOR rheometer and for assistance with the measurements.

#### 5.5 References

- 1 T. van Vliet, *Interactions between adsorbed macromolecules*, Ph.D. Thesis, Wageningen Agricultural University, The Netherlands, 1977.
- 2 M. van den Tempel, *J. Coll. Sci.*, 1961, **16**, 281
- 3 C.J. Nederveen, *J. Colloid Sci.*, 1963, **18**, 276
- 4 J.M.P. Papenhuijzen, *Rheol. Acta.*, 1972, **11**, 73
- 5 H. Kamphuis, R.J.J. Jongschaap and P.F. Mijnlief, *Rheol. Acta*, 1984, **23**, 329
- 6 H. Kamphuis, R.J.J. Jongschaap, *Colloid & Polymer Sci*, 1985, **263**, 1008
- 7 W. D. Brown, PhD Thesis, Department of Physics, University of Cambridge, U.K., 1987
- 8 R. Buscall P.D.A. Mills, J.W. Goodwin and D.W. Lawson, *J. Chem. Soc. Faraday Trans I*, 1988, **84**, 4249

- 9 L.G.B. Bremer and T. van Vliet, *Rheologica Acta*, 1991, **30**, 98
- 10 L.G.B. Bremer, B.H. Bijsterbosch, R. Schrijvers, T. van Vliet, and P. Walstra, *Colloids and Surfaces*, 1990, **51**, 159
- 11 W.H. Shih, W.Y. Shih, S.I. Kim, J. Liu and I.A. Aksay, *Physical Review A*, 1990, **42**, 4772
- 12 R.C. Ball, personal communication
- 13 P. Walstra, H.J.M. van Dijk and T.J. Geurts, *Neth. Milk Dairy J.*, 1985, **39**, 209
- 14 H.J.M. van Dijk and P. Walstra, *Neth. Milk Dairy J.*, 1986, **40**, 3
- 15 T. van Vliet and P. Walstra, *Neth. Milk Dairy J.*, 1985, **39**, 115
- 16 L.G.B. Bremer, T. van Vliet and P. Walstra, *J. Chem. Soc. Faraday Trans I*, 1989, **85**, 3359
- 17 M. Reiner, *Advanced Rheology*, Lewis H.K., London, 1971
- 18 S.P.M.F. Roefs, *Structure of Acid Casein gels*, Ph.D. Thesis, Wageningen Agricultural University, The Netherlands, 1986
- 19 S.P.F.M. Roefs, A.E.A. de Groot-Mostert and T. van Vliet, *Colloids and Surfaces*, 1990, **50**, 141
- 20 S.P.F.M. Roefs and T. van Vliet, *Colloids and Surfaces*, 1990, **50**, 161
- 21 P. Walstra, *J. Dairy Research*, 1979, **46**, 317
- 22 D.F. Darling, in *The effect of polymers on dispersion properties*, ed. Th.F. Tadros (Acad. Press London, 1982)
- 23 A.C.M. van Hooydonk, H.G. Hagedoorn and I.J. Boerrigter, *Neth. Milk Dairy J.*, 1986, **40**, 281
- 24 R.J. Roark, *Formulas of stress and strain*, Mc Graw, 1965
- 25 P. Zoon, T. van Vliet and P. Walstra, *Neth. Milk Dairy J.*, 1988, **42**, 103
- 26 H.J.C.M. van den Bijgaart, T. van Vliet, P. Walstra and P. Zoon, *Neth. Milk Dairy J.*, 1989, **43**, 85
- 27 S.P.F.M. Roefs and T. van Vliet, in *Advances in rheology: 4; Applications*, ed. B. Mena, A. Garcia-Rejon and C. Rangel-Nafaile (Universidad Nacional Autonoma de Mexico, 1984), p. 249
- 28 H. Luyten, *Ph.D. Thesis* (Wageningen Agricultural University, Netherlands, 1989)
- 29 A.G. Atkins and Y-W. May, *Elastic and plastic fracture*, (Ellis Horwood limited, Chichester, 1985)
- 30 J. Visser, A. Minihan, P. Smits, S.B. Tjan and I. Heertje, *Neth. Milk Dairy J.*, 1986, **40**, 351
- 31 R. Schrijvers, *MSc. Thesis* (Wageningen Agricultural University, the Netherlands, 1989)
- 32 J. Mottar, A. Bassier, M. Joniau and J. Baert, *J. Dairy Sci.*, 1989, **72**, 2247
- 33 C. Keetels, *MSc. Thesis* (Wageningen Agricultural University, The Netherlands, 1989)
- 34 T. van Vliet, A.E.A de Groot-Mostert and A.Prins, *J. Phys. E.*, 1981, **14**, 745
- 35 R.W. Whorlow, *Rheological techniques*, Ellis Horwood Ltd., 1980
- 36 T. van Vliet, H.J.M. van Dijk, P. Zoon and P. Walstra, *Colloid Polymer Sci.*, 1991, **269**, 620



# VI Aggregation Kinetics Related to the Observation of Instability

## 6.1 Introduction

There is an ongoing interest, both practical and fundamental, in the stability of colloidal dispersions. These systems are considered stable if they undergo no perceptible, i.e. often visible, change on a specified time scale. The rate of bond formation is usually considered to be the determining factor for the time that a system stays stable. However, other factors like the structure of the flocs and the precision of the observation determine whether changes of the system are perceptible and are as such important for the assessment of the stability.

In an unstable dispersion bonds between the particles are formed which leads to their aggregation followed by the formation of visible flocs, sedimentation, creaming or gelation. The rate of bond formation has received considerable attention in literature. Most often the approach is based on Smoluchowski's equations [1, 2]:

$$\frac{dc_k}{dt} = \frac{1}{2} \sum_{i+j=k} K_{i,j} c_i c_j - c_k \sum_{j=1}^{\infty} K_{k,j} c_j \quad (6.1)$$

These equations can be solved in some cases, depending on the choice of the concentration independent collision kernel  $K_{i,j}$  [1-6], leading to a complete expression for the time-dependent number concentration of the clusters,  $c_k(t)$ . The choice of  $K_{i,j}$  is dependent on the aggregation mechanism. In his theory of rapid, perikinetic aggregation, Smoluchowski considered any particle as a 'sink' for the particles colliding with it. He obtained the collision rate by calculating the diffusion of particles to such a sink. The obtained collision kernel,  $K_{i,j}$ , is roughly constant, independent of the size of the particles. If there is an energy barrier for aggregation the collision rate slows down. In that case a retardation factor,  $W$ , which is the ratio between the rate of rapid and slow aggregation can be defined. Fuchs [7] developed a theory considering diffusion to take place in a force field from which  $W$  can be calculated.

Spatial effects can never be accounted for in Smoluchowski's equations, because they only distinguish between clusters with different numbers of particles, regardless of their geometric structure. Nevertheless, Smoluchowski's equations often give results which are in agreement with practical observations and computer simulations if the proper collision kernel has been chosen [8] and if the effective volume fraction is low.

The rate of bond formation is not the only factor affecting the aggregation time, i.e. the time after which aggregation becomes visible. Also the geometric structure of the flocs is important because it determines when sedimentation or gelation starts or when the flocs are large enough to be observed with the naked eye. Flocs can often be described as so-called fractal structures. A floc is fractal if a power-law dependence exists between the number of particles in a floc,  $i$ , and the radius of that floc,  $R_i$ . The power is the so called fractal dimensionality,  $D$ . For an ideal floc with fractal behaviour on the length scales between  $a$  and  $R_i$  we may write

$$i = \left( \frac{R_i}{a} \right)^D \quad (6.2)$$

$a$  is the radius of the particles in the floc. Fractal flocs are scale invariant, i.e., small cluster resemble large clusters on another scale. In practice, the value of  $D$  varies from 1.7 - 1.8 in the case of rapid aggregation into rigid flocs, to 3 in the case of immediate coalescence of the aggregating particles. The whole range of intermediate values has been reported as well (e.g. [9 - 13]). The effect of the geometric structure of the flocs on the aggregation time is huge. If we compare a rapidly aggregating system where tenuous flocs are formed with a coalescing system with, initially, the same concentration and size of the particles, the rate of bond formation is equal for both cases. After some aggregation steps, however, the tenuous flocs may fill the system, thus forming a gel, whereas the only change of the coalescing system is a (small) increase of the particle size and a decrease of the total number of particles. Coalescence has to proceed for a much longer time before changes become visible and the aggregation time is thus much longer, up to several orders of magnitude.

Most of the fundamental work on colloid aggregation has dealt with the doublet formation step of monodisperse, smooth, spherical particles at low volume fractions. Many complications make the results that are thus obtained unsuitable to describe experimental results on aggregation kinetics. In this paper we will be dealing with the following complications:

- The hydrodynamic behaviour of fractal flocs which is different from that of smooth spherical particles [14-19]
- The effect of the floc size distribution [19-21]
- High effective volume fractions and gelation
- Velocity gradients
- Sedimentation of the aggregates
- The effect of slow, reaction limited aggregation [22, 23]
- Rearrangements and breakup of the flocs [11, 14, 22].

## 6.2 Diffusion limited aggregation

For the case of rapid perikinetic aggregation; i.e. aggregation due to Brownian motion where all encounters result in permanent contact, Smoluchowski has derived an approximate expression for the collision kernel [1, 2];

$$K_{i,j} = 4\pi(R_{c,i} + R_{c,j})(D_i + D_j) \quad (6.3)$$

$R_{c,i}$  is the collision radius which for flocs is rather ill-defined and  $D_i$  the diffusion constant of a cluster composed of  $i$  particles. An exact equation that relates the diffusion coefficient to the collision radius of a floc is not available, but we may define an effective hydrodynamic radius,  $R_{h,i}$ , according to

$$D_i = \frac{kT}{6\pi\eta R_{h,i}} \quad (6.4)$$

The factor  $(R_{c,i} + R_{c,j})(D_i + D_j)$  in equation (6.3) may then be replaced by  $kT/6\pi\eta (R_{c,i} + R_{c,j})(R_{h,i}^{-1} + R_{h,j}^{-1})$ . In the first stage of the aggregation of a monodisperse system of smooth, spherical particles the radii  $R_{c,i}$ ,  $R_{c,j}$ ,

$R_{h,i}$  and  $R_{h,j}$  are equal and the factor  $(R_{c,i} + R_{c,j})(R_{h,i}^{-1} + R_{h,j}^{-1})$  is thus equal to 4. Eqn. (6.1) then is well approximated by:

$$\frac{dc}{dt} = -\frac{4AkT}{3\eta}c^2 \quad \text{with } c = \sum_{i=1}^{\infty} c_i \quad (6.5)$$

$A$  is a constant factor which is for rapid, diffusion limited aggregation of order 1. The factor is affected by various complications like hydrodynamic interactions [16-19], polydispersity [19-21] and  $R_c$  being not equal to  $R_h$  [14];  $c$  is the total number concentration of aggregates and single particles. In this equation the collision kernel is constant, independent of the size of the clusters. The solution of this equation is

$$\frac{1}{c(t)} - \frac{1}{c_0} = \frac{4AkTt}{3\eta} \quad (6.6)$$

The time for the particle concentration to reach half its original value  $c_0$  is often called the coagulation or flocculation time. As we will see later on this time is not a good measure for the instability of the system (and as such flocculation time is a misnomer). In this paper we use the term 'aggregation time' for the time after which aggregation becomes visible, and 'flocculation time' for the time needed to reduce the particle number to half its initial value. Substitution of  $t = t_{1/2}$  and  $c(t) = c_0/2$  leads to

$$t_{1/2} = \frac{3\eta}{4AkTc_0} = \frac{\pi\eta a^3}{AkT\phi_0} \quad (6.7)$$

The flocculation time is thus very sensitive to the primary particle radius,  $a$ ; at constant volume fraction,  $t_{1/2}$  is proportional to  $a^3$ .

Smoluchowski also derived the complete time dependency of  $c_k$  in the case of a constant collision kernel [1, 2]:

$$c_k(t) = c_1(0) \frac{\left[ \frac{t}{t_{1/2}} \right]^{k-1}}{\left[ 1 + \frac{t}{t_{1/2}} \right]^{k+1}} \quad (6.8)$$

The resulting frequency of the number of clusters as a function of the number of particles in the clusters is monotonically decreasing. The distribution becomes broader during the aggregation process.

## 6.3 Complications

### 6.3.1 Flocs instead of smooth spheres

The assumption that the hydrodynamic radius is about equal to the collision radius is correct in the case of coalescence of spherical particles and in the first stage of the aggregation of spherical particles (formation of doublets). However, for tenuous flocs the hydrodynamic radius may be substantially smaller than the collision radius (fig. 6.1). In that case the factor  $A$  in eqn. (6.5) will increase by a factor  $B \equiv R_c/R_h$ .

Different radii can be defined in the case of flocs. Actually, eqn. (6.2) gives the number of particles in a sphere with radius  $R$  if fractal behaviour applies on length scales between  $a$  and  $R$ . The radial distribution function of the particles in a floc,  $g(r)$ , which is a measure of the probability to find a particle at a distance  $r$  from another particle in the centre of a floc, scales like  $r^{D-3}$  in that region. We assume the largest radius below which fractal behaviour applies to be equal to the collision radius,  $R_c$ , because the geometric structure of a floc will not change inside that radius after aggregation with another floc. In the case of rapid aggregation, the collision radius of a floc,  $R_c$ , will be little smaller than the radius of the smallest sphere that circumscribes the total floc,  $R_m$ , because rotational diffusion and diffusive motion of the protruding strands hinder deep interpenetration of flocs. An additional effect is the lateral diffusion of flocs with regard to each other. Smoluchowski considered a spherically symmetric approach of spherical particles along the line connecting their centres. In that case, lateral diffusion is not important because it does not bring spherical particles any closer to each other. However, for flocs, the lateral diffusion provides an additional increase of the collision radius because it also hinders interpenetration. In most computer simulations of aggregation lateral diffusion was taken into account, whereas rotational diffusion and diffusive motion of the protruding strands were not.

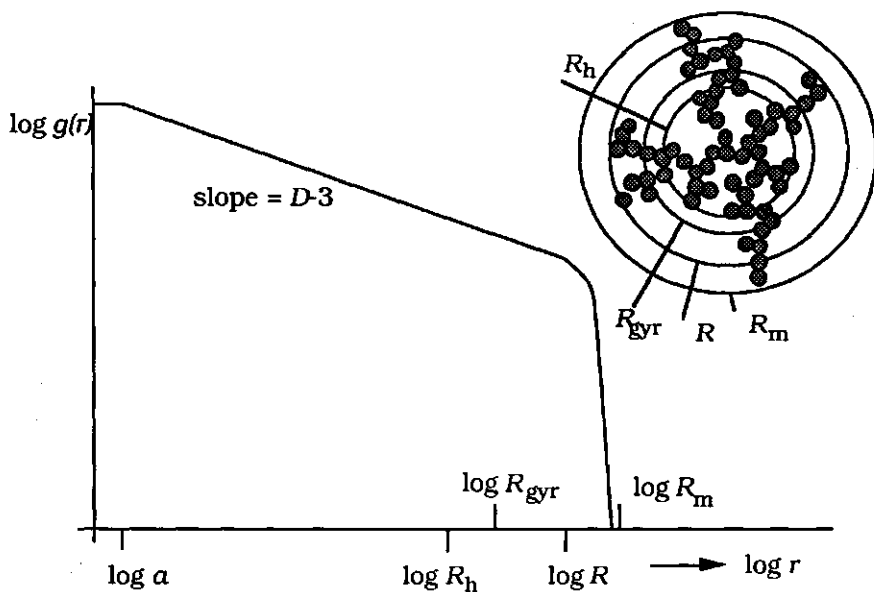


**Fig 6.1** Radial distribution function of the particles in a fractal floc. Indicated are the various radii: The hydrodynamic radius,  $R_h$ , the radius of gyration,  $R_{gyr}$ , the effective upper cut-off length  $R$  which is presumably about equal to the collision radius  $R_{c,b}$  and the radius of the smallest sphere that can contain the total floc,  $R_m$ .

Between  $R_c$  and  $R_m$  the radial distribution function of the particles in the floc is characterized by a sharp decay (fig. 6.1). Mathematically, this decay may be described by the introduction of a cutoff function,  $h(r)$ , in the radial distribution function of the particles in the floc;  $g(r) \propto r^{D-3} h(r)$ . This cutoff function should approach 1 if  $r < R_c$  and 0 if  $r > R_m$ . Lin et al. [12] reviewed different forms for the cutoff function and showed that forms that exhibit a sharp cutoff gave the best agreement with computer generated clusters.

The ratio between the collision radius and the hydrodynamic radius is expected to be constant for fractal flocs because they are scale invariant; i.e. small flocs resemble large flocs on another length scale. We expect all radii to be proportional to one another, independent of the size of the fractal floc (fig. 6.1). The diffusion coefficient of simulated clusters, and thus their effective hydrodynamic radius was calculated and

correlated to the cluster mass by Meakin et al. [15]. They obtained a scaling relation between the hydrodynamic floc radius and the number of particles in the floc,  $i$ ;  $R_{h,i} \propto i^\gamma$  with  $\gamma = 0.544 \pm 0.014$ . The resulting effective fractal dimensionality of the clusters,  $1.81 \pm 0.13$ , was not significantly different from  $1/\gamma = 1.84 \pm 0.05$  which indicates a roughly constant ratio  $R_{c,i}/R_{h,i}$ , independent of  $i$ .

For random polymer coils, the ratio between the hydrodynamic radius and the radius of gyration,  $R_h/R_{gyr}$ , calculated with the Kirkwood-Riseman theory, equals 0.665 [24]. For large, fractal flocs somewhat higher values, between 0.72 and approximately 1.0, have been reported [14]. These values were independent of the size of the flocs. In the first stages of the aggregation process  $R_h$  has to increase faster than  $R_{gyr}$  before the asymptotic value of  $R_h/R_{gyr}$  being roughly 0.8 will be reached. For the primary particles  $R_h = a$  and  $R_{gyr} = \sqrt{(3/5)} a$  and thus  $R_h/R_{gyr} = 1.29$ .

The radius of gyration of fractal flocs is smaller than  $R_c$ .  $R_{gyr}$  is defined as:

$$R_{gyr}^2 = c_v \int_0^{R_m} r^2 4\pi r^2 g(r) dr \quad (6.9)$$

where  $c_v$  is the average number concentration of particles in the floc. For an ideal fractal floc with fractal behaviour on all length scales smaller than  $R$  a relation between the radius of gyration and  $R$  can be obtained:

$$R_{gyr}^2 = \frac{\int_0^R r^2 4\pi r^2 r^{D-3} dr}{\int_0^R 4\pi r^2 r^{D-3} dr} = \frac{D}{2+D} R^2 \quad (6.10)$$

For fractal flocs  $R_{gyr}$  is thus roughly 0.7  $R$  for  $D = 1.7 - 2.5$ . We can estimate the ratio between the collision and the hydrodynamic radius,  $B = R_{c,i}/R_{h,i}$ , to be  $1/(0.7 \times 0.8) = 1.8$ , assuming the ratio between the hydrodynamic radius and the radius of gyration,  $R_h/R_{gyr}$ , to be 0.8. In practice,  $B$  will depend on the fractal dimensionality of the flocs.  $B = 1$  in

the case of coalescing particles ( $D = 3$ ) and in the first stage of the aggregation and according to calculations about 1.8 in the case of open fractal flocs ( $D = 2$ ). Permeability measurements of particle gels that consist of fractal clusters are, however, not in agreement with this high value of  $B$ . These measurements resulted in values of  $B = 1.15 \pm 0.05$  for flocs with a dimensionality  $D = 2.25$  (section 4.2 [25]).

### 6.3.2 Interactions between particles

Smoluchowski considered the diffusion to a particle with radius  $a$ . In practice, however, van der Waals attractive forces tend to make the collision radius larger than the particle radius. Another complication is the hydrodynamic interaction which decreases the diffusion of a particle in the direction of another particle. If van der Waals attraction and hydrodynamic interaction are taken into account [16, 17],  $K_{1,1}$  is calculated to be 20 - 65% of the value in (3) for smooth spherical particles, according to the Hamaker constant,  $A_H$ , but independent of the particle size. Such values were also obtained in measurements of the initial aggregation rate [18, 19].

An approximate equation for the diffusion coefficient of two smooth, spherical particles relative to each other,  $D_r$ , was given by Honig et al. [17]

$$D_r \approx 2 \left( \frac{6u^2 + 4u}{6u^2 + 13u + 2} \right) D_e \quad (6.11)$$

where  $u$  is equal to  $h/a$  where  $h$  is the distance between the particles (fig. 6.2) and  $D_e$  the diffusion coefficient of the individual particles.  $D_r$  approaches 0 if the particles approach each other. This implies that particles would never touch if there were no van der Waals attraction.

If there is some surface roughness,  $D_r$  and  $u$  are difficult to establish. The effect of hydrodynamic interactions will be smaller in that case because it is easier to squeeze the water out of the gap between the approaching particles. In that case  $K_{1,1}$  will be larger than the value of 20-65 % of the Smoluchowski value (eqn. 6.3). For later steps in an



aggregation process where flocs are formed, the hydrodynamic retardation of the aggregation is negligible.

If there is an activation energy that particles have to overcome before attachment, e.g. due to electrostatic repulsion, the aggregation rate slows down. To account for slow coagulation, Smoluchowski simply inserted a factor  $\alpha$ , the fraction of collisions which result in permanent contact. This concept of an efficiency of collisions was improved by Fuchs [7], who considered diffusion to take place in a force field. He defined a retardation factor,  $W$ , as the ratio between the rates of fast and slow aggregation. Spielman [16] and Honig et al. [17] incorporated the hydrodynamic drag and obtained

$$W = 2 \int_2^{\infty} \frac{D_r^{\infty}}{D_r} \exp\left(\frac{V(s)}{kT}\right) \frac{ds}{s^2} \quad (6.12)$$

where  $V$  is the interaction energy between the particles and  $s$  the relative mutual distance (fig. 6.2)



**Fig. 6.2** Schematic presentation of two approaching particles.

Eqn. 6.12 is only valid in the case of smooth spherical particles at low volume fractions. In the case of flocs, a repulsive barrier affects the aggregation kinetics in a complicated way. The resulting reaction limited aggregation will be dealt with later on.

### 6.3.3 Polydispersity

The factor  $(R_{c,i} + R_{c,j})(R_{h,i}^{-1} + R_{h,j}^{-1})$  that is used to obtain eqn. 6.5 from eqn. 6.3 becomes  $B(R_{c,i} + R_{c,j})(R_{c,i}^{-1} + R_{c,j}^{-1})$  for flocs. In the case of broad distributions, this factor will become larger than  $4B$  for most collisions. If the cluster size distribution is known, an average value can be determined. If  $R_i/a = i^{1/D}$  the average factor,  $P$ , can be calculated with [20, 21]:

$$P = \left[ 2 + 2 \sum_{i=1}^{\infty} i^{1/D} \psi(i) \sum_{i=1}^{\infty} i^{-1/D} \psi(i) \right] \quad (6.13)$$

where  $\psi(i)$  is the probability that a cluster consists of  $i$  particles. For the distributions in equation (6.8),  $\psi(i)$  can be determined:

$$\psi_k(t) = \frac{c_k(t)}{c(t)} = \frac{c_k(t)}{c_1(0) \left(1 + \frac{t}{t_{1/2}}\right)^{-1}} = \frac{\left(\frac{t}{t_{1/2}}\right)^{i-1}}{\left(1 + \frac{t}{t_{1/2}}\right)^i} \quad (6.14)$$

Values for  $P$  at different times after the beginning of aggregation, determined with these equations, and values for  $P$  in the case of fractal flocs with other dimensionalities (assuming that  $B = 1$ ,  $R_i/a = R_{h,i}/a = i^{1/D}$ ), are compiled in table 6.1. In practice, the cluster size distribution will be narrower because the collision rate for small with large particles is relatively high, which causes a faster decrease of the number of small clusters. Computer simulations of diffusion limited aggregation result in bell shaped distributions of  $c(i)$  in stead of the monotonically decreasing functions in eqn. 6.8 [22]. If  $t \gg t_{1/2}$ , the distribution of eqn. 6.8 becomes:  $c(i) \propto i^0$ .

Initially, the factor  $P$  increases somewhat during the aggregation process if the cluster size distribution is calculated assuming a constant collision kernel. In practice, the increase of  $P$  will be less because of the vanishing of the smallest clusters. After some time  $P$  becomes almost constant, the value of  $P$  depending on the dimensionality of the clusters. The factor  $A$  in eqn. 6.5 is thus almost constant and this equation

therefore gives a good approximation of the decrease of the total cluster concentration,  $c$ , throughout the aggregation process.

**Table 6.1.** Factor  $P$ , which is the average of  $(R_i + R_j)(R_i^{-1} + R_j^{-1})$ , at various times after the beginning of aggregation of a monodisperse system for various fractal dimensionalities.  $P$  was calculated with eqns. (6.13) and (6.14).

$t/t_{1/2}$	$P_{D=3}$	$P_{D=2.5}$	$P_{D=2}$	$P_{D=1.7}$
1	4.08	4.11	4.17	4.24
2	4.12	4.17	4.27	4.39
3	4.15	4.21	4.34	4.49
4	4.17	4.25	4.40	4.57
6	4.20	4.29	4.48	4.68
10	4.24	4.35	4.57	4.83
$\infty$	4.26	4.38	4.66	5.04

The small difference between  $P$  and 4 indicates that most attachments occur between approximately equal sized flocs. This is also reflected in computer simulations of diffusion limited aggregation [22]. The value of  $D$  in a three-dimensional simulation is 1.80 in the case of a constant kernel and 1.78 in the case of a hierarchical model. A higher  $D$  is expected if most attachments would occur between flocs with a large size difference, up to 2.5 in the case of diffusion controlled attachment of single particles to a large cluster.

The factor  $A$  (eqn. 6.5) is affected by polydispersity expressed by the factor  $P$ , particle interactions expressed by  $W$ , and the ratio  $R_c/R_h = B$ . Altogether  $A = BP/4W$ .

### 6.3.4 The effective volume fraction

So far we discussed aggregation of extremely dilute dispersions. However, in many situations the aggregation can only be observed at the moment the system is gelled, i.e. the moment at which the clusters occupy the total volume. In the case of immediate coalescence of the aggregating particles ( $D = 3$ ), the effective volume fraction  $\Phi$  stays constant, but for any smaller dimensionality,  $\Phi$  will increase during the aggregation up to 1 at the gelpoint. The 3D average size of the clusters at the gelpoint,  $R_g$ , is [26]

$$R_g = a\phi_0^{1/(D-3)} \quad (6.15)$$

The effective volume fraction may be related to the size of the aggregating clusters

$$\Phi = \phi_0 \left( \frac{R_{3D}}{a} \right)^{3-D} \quad (6.16)$$

Smoluchowski's approach is not valid at high  $\Phi$  because no stationary state can be reached in that case. Corrections for the lack of true stationarity can be neglected if  $t \gg 8\phi_0 t_{1/2}$  [27]. This implies that these corrections are unimportant long before  $t = t_{1/2}$  if  $\phi_0$  is smaller than a few percent.

At high volume fractions aggregation is no longer a second order reaction: the aggregation rate approaches infinity just before the gelpoint because the distance over which clusters have to diffuse in order to collide approaches zero. In a cubic lattice the distance between the centres of the flocs equals  $c^{-1/3}$  and that between their peripheries,  $X$ , can be defined via  $\frac{4}{3} \pi (R + X/2)^3 c = 1$ , leading to:

$$X = 2\phi_0^{-1/3} a \left( \frac{R}{a} \right)^{D/3} - 2R \quad (6.17)$$

This equation applies to a cubic lattice with monodisperse clusters. In practice the situation will be more complicated due to polydispersity and packing problems.

A first order approximation for a correction factor for the aggregation rate calculated by Smoluchowski's equation (eqn. 6.5) can be given by comparison of the distance over which particles without excluded volume have to diffuse ( $c^{-1/3}$ ) and the actual distance,  $X$ . Because the diffusion time is proportional to  $X^2$  we may write:

$$\frac{dc}{dt} \approx - \left( \frac{c^{-1/3}}{X} \right)^2 \frac{4AkTc^2}{3\eta} \quad (6.18)$$

At low effective volume fraction,  $c^{-1/3}$  is about equal to  $X$  and eqn. 6.18 equals eqn. 6.5. However, if  $\Phi$  increases during the aggregation the aggregation rate increases because the distance between the flocs,  $X$ , decreases to 0 at the gelpoint. In fig. 6.3,  $X$  and  $c^{-1/3}$  are plotted as a function of  $R$ .

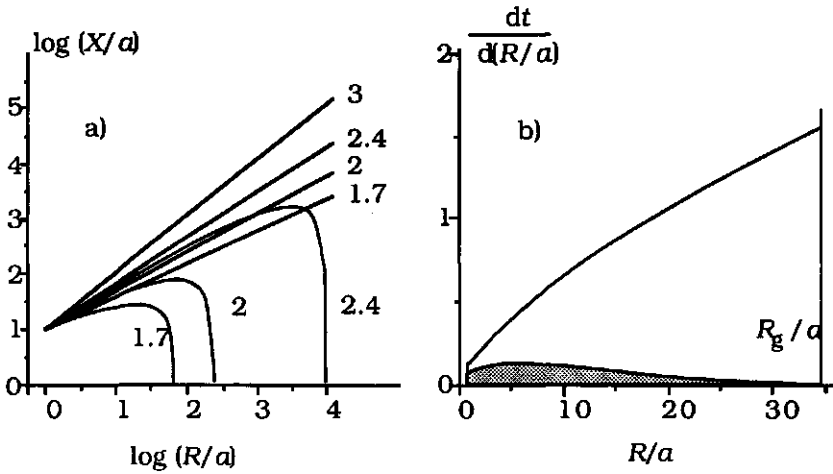


**Fig. 6.3a** The distance between the clusters as a function of the size of the clusters for various fractal dimensionalities and  $\phi_0 = 0.004$ . The straight lines represent the distance between the centres of the clusters and the curved lines the distance between the cluster peripheries calculated with eqn 6.17.  $D$  is indicated in the figure. The size of the clusters at the gelpoint,  $R_g$ , is 7, 25 and 992 times  $a$  for  $D = 1.7, 2$  and  $2.4$ , respectively.  
**Fig. 6.3b**  $dt/d(R/a)$  as a function of  $R/a$ . The area under the curve gives the gel time. The upper curve has been calculated without the correction factor for high effective volume fraction.  $D = 1.7, a = 100$  nm,  $\phi = 0.01, T = 298$  K and  $\eta = 1$  mPa s.

### 6.3.5 Velocity gradients

If the liquid is sheared, collisions will occur as a result of the velocity gradients. Aggregation in this manner is known as orthokinetic aggregation. An approximate expression for the collision kernel in the case of simple shear is given by

$$K_{i,j} = \frac{4}{3} \dot{\gamma} C (R_i + R_j)^3 \quad (6.19)$$

where  $\dot{\gamma}$  is the shear rate and  $C$  a numerical constant of order 1 that is affected by complications like hydrodynamic interactions [28]. Thus, for  $R_i \approx R_j$

$$\frac{dc}{dt} = -\frac{16\dot{\gamma}CR^3}{3}c^2 \quad (6.20)$$

The rate of aggregation in a shear field strongly depends on the size of the clusters. Since large clusters have a much higher collision rate than small clusters they will grow much faster leading, in first instance, to a polydisperse cluster size distribution. In some practical cases, however, the shear stress set up by the velocity gradient prevents further aggregation of clusters that have reached a certain critical size, depending on the strength of the bond that is formed and the shear rate (see later on). This then makes the final cluster size distribution more monodisperse. Shear forces may also cause rearrangement into more compact flocs.

Anisometric particles or flocs provide in simple shear a higher effective volume fraction because the particles rotate. Fractal flocs are on average spherical but each separate floc may be to some extent anisometric thus leading to  $R_c$  being relatively close to  $R_m$ . The aggregation kinetics of anisometric particles, in particular in a shear field, is an intricate subject, beyond the scope of this paper.

The ratio between ortho and perikinetic aggregation can be obtained from both aggregation rates (eqns. 6.5 and 6.20). If  $R_i \approx R_j$  and  $A \approx C$ , we may write:

$$\frac{\dot{c}_o}{\dot{c}_p} = \frac{4\dot{\gamma}R^3\eta}{kT} \quad (6.21)$$

where  $\dot{c}$  is  $dc/dt$ . If the ratio becomes larger than 1 the orthokinetic rate will exceed the perikinetic rate by a factor proportional to  $R^3$ . We may thus define a critical cluster radius above which, at a given shear rate,

perikinetic aggregation can be neglected compared with orthokinetic aggregation.

$$R_{cr} = \sqrt[3]{\frac{kT}{4\dot{\gamma}\eta}} \quad (6.22)$$

This results for a dispersion in water at room temperature in the following relation between the critical cluster size and the shear rate:

$$R_{cr} \approx \dot{\gamma}^{-1/3} \quad (6.23)$$

if  $R_{cr}$  is expressed in  $\mu\text{m}$  and  $\dot{\gamma}$  in  $\text{s}^{-1}$ . If the clusters become larger than a few  $\mu\text{m}$  the orthokinetic aggregation is in most cases more important than the perikinetic aggregation because, even in quiescent systems, small velocity gradients caused by small temperature gradients or vibrations will already cause a shear rate of  $0.1 \text{ s}^{-1}$  or more (in water). This can be illustrated by calculating the free-convection flow between two vertical plates with slightly different temperatures over a mutual distance  $2b$  [29]. The average shear rate equals  $\beta\rho gb\Delta T/16\eta$  where  $\beta$  is the coefficient of volume expansion. For water at room temperature and  $b = 0.1 \text{ m}$  the average shear rate would be roughly  $10 \Delta T$  which implies that a temperature difference of  $0.01 \text{ K}$  provides  $\dot{\gamma} = 0.1 \text{ s}^{-1}$ .

### 6.3.6 Sedimentation

If the aggregates grow in size, their sedimentation may become more and more prominent. At creeping flow conditions, and  $\Phi \ll 1$  the sedimentation velocity of a cluster can be written as:

$$v_i = \frac{F_i}{6\pi\eta R_{h,i}} \quad (6.24)$$

where  $F_i$  is the net force exerted on aggregate  $i$  due to gravity. In the case of fractal flocs  $F_i$  may be related to the difference in density of the particles composing the floc and the medium,  $\Delta\rho$ :

$$F_i = (R_i / a)^D \frac{4}{3} \pi a^3 \Delta\rho g \quad (6.25)$$

Substitution of eqn. (6.25) in eqn. (6.24) leads to:

$$v_t = \frac{2Bg\Delta\rho\alpha^2}{9\eta} \left( \frac{R_t}{\alpha} \right)^{D-1} \quad (6.26)$$

where  $B = R/R_h$ . Important is the ratio between the sedimentation and the diffusion rates. The times needed for a floc to diffuse over a distance equal to  $R$  ( $t = R^2/2D_e$ ) and to sediment over the same distance (according to eqn. 6.26) may be expressed as

$$t_{\text{dif}} = \frac{3\pi\eta R^3}{BkT} \quad (6.27a)$$

$$t_{\text{sed}} = \frac{9\eta R^{2-D}}{2Bg\Delta\rho\alpha^{3-D}} \quad (6.27b)$$

A critical value of  $R$ ,  $R_s$ , is reached when the ratio  $t_{\text{dif}}/t_{\text{sed}}$  equals 1. For aggregates larger than  $R_s$  the system will show appreciable sedimentation.

$$R_s = \left[ \frac{3kT}{2\pi\alpha^{3-D}\Delta\rho g} \right]^{1/(D+1)} \quad (6.28)$$

Sedimentation increases the aggregation rate [27] and the polydispersity. If large flocs start to sediment they aggregate with many smaller particles which increases the sedimentation velocity of the large cluster and thus the aggregation rate. If  $R_s$  is reached before  $R_{\text{cr}}$ , sedimentation determines the aggregation time because the time in which the floc size grows from  $R_s$  to visible or from  $R_s$  to  $R_g$  (gel formation) is short compared to the time needed to reach  $R_s$ . Values of  $R_s$  calculated by eqn. 6.28 are shown in fig. 6.4.

Whether formation of a sediment or a gel is the first sign of instability depends, among other things, on the initial volume fraction of the particles and on the fractal dimensionality of the flocs. At low volume fractions and high dimensionalities the clusters have to grow very large before they occupy the total volume and appreciable sedimentation is likely to occur.



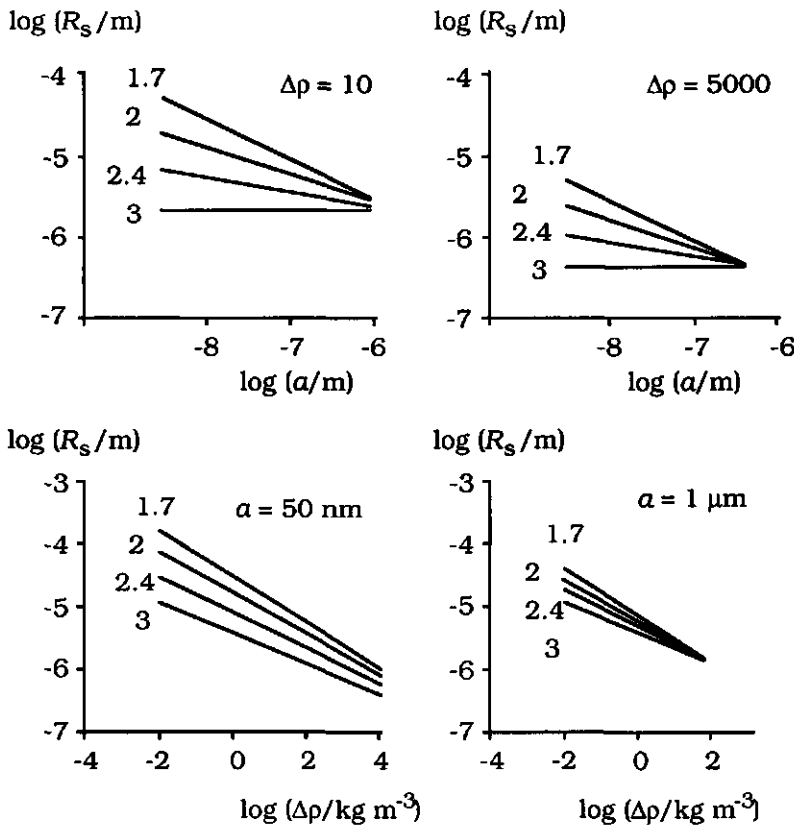


**Fig. 6.4** Critical cluster radius calculated with eqn. 6.28 for  $D = 1.7, 2, 2.4$  and  $3$  (indicated in the figure); a)  $\log R_s$  as a function of  $\log a$  for  $\Delta\rho = 10 \text{ kg m}^{-3}$  and  $\Delta\rho = 5000 \text{ kg m}^{-3}$  and b)  $\log R_s$  as a function of  $\log \Delta\rho$  for  $a = 50 \text{ nm}$  and  $a = 1 \mu\text{m}$ .  $3kT/2\pi g = 2 \times 10^{-22} \text{ N s}^2$ .

Small velocity gradients may prevent visible sedimentation of the aggregates. In that case the aggregation may become visible due to gelation or the formation of visible flocs, even if  $R_s$  from eqn. 6.28 is smaller than  $R_g$  and the radius of a just visible floc,  $R_v$ . Comparison of  $R_{cr}$  (eqn. 6.22) and  $R_s$  is therefore useful. In the case of  $D = 2$ , the critical shear rate below which  $R_s < R_{cr}$  is  $\pi a \Delta\rho g / 6\eta$  which is in water about  $5100 a \Delta\rho$ . If we assume an average shear rate of  $0.1 \text{ s}^{-1}$  in a 'quiescent' dispersion of particles with a radius of  $100 \text{ nm}$  then  $\Delta\rho$  has to be larger than  $200$  for visible sedimentation to occur.

#### 6.4 Some aggregation times for diffusion limited aggregation

Before aggregation,  $c_0$  equals  $3\phi_0/(4\pi a^3)$  (the initial volume fraction,  $\phi_0$ , relative to the volume of one particle,  $\frac{4}{3}\pi a^3$ ). As the aggregation proceeds  $c$  decreases. Because  $c$  equals  $c_0$  divided by the average number of particles in one aggregate it is possible to relate  $c$  to  $R$  in the case of fractal flocs;

$$c = \frac{3}{4\pi} \phi_0 a^{D-3} R^{-D} \quad (6.29)$$

Differentiation of this equation leads to

$$\frac{dc}{dR} = -\frac{3D}{4\pi} \phi_0 a^{D-3} R^{-D-1} \quad (6.30)$$

In the case of a distribution of clusters with various sizes we have to take the proper average for  $R$ , i.e.  $R_{D0}$ . We are interested in the time that has to pass before the aggregation can be observed. Whether or not the aggregation can be observed is mainly determined by the average size of the flocs  $R_{D0}$  and by the size distribution. Substitution of eqn. 6.29 and eqn. 6.30 in eqn. 6.5 provides, for perikinetic aggregation, the relation  $dt/dR$  which may be integrated from  $R = a$  to  $R = R_v$  to obtain the time elapsed before this cluster size has been reached.

$$\begin{aligned} t_c &= \int_a^{R_v} \frac{dt}{dR} dR = \int_a^{R_v} \frac{\pi\eta D}{AkT} \phi_0^{-1} a^{3-D} R^{D-1} dR \\ &= \frac{\pi\eta}{AkT} \phi_0^{-1} a^{3-D} (R_v^D - a^D) = t_{1/2} (q^D - 1) \end{aligned} \quad (6.31)$$

$R_v$  is the  $D0$  average cluster size at which the aggregation can be observed and  $q = R_v/a$ . During rapid aggregation the average cluster size scales like  $R \propto t^{1/D}$ .

Besides the bond formation rate, expressed by  $t_{1/2}$ , the structure of the flocs as expressed by the dimensionality, has a large effect on the time after which instability becomes visible. Because the factor  $q$  may be very large (e.g.,  $a = 100$  nm,  $R_v = 0.1$  mm provides  $q = 1000$ ), pure perikinetic aggregation would result in a very long aggregation time.

Whether aggregation is visible depends mainly on the largest clusters. In a polydisperse system the  $DO$  average  $R_v$  will therefore be smaller than the smallest floc that can be observed with the naked eye.

A similar relation may be obtained for orthokinetic aggregation:

$$t_c = \int_a^{R_v} \frac{dt}{dR} dR = \int_a^{R_v} \frac{\pi D}{4\dot{\gamma}C} \phi_0^{-1} a^{3-D} R^{D-4} dR$$

$$= \frac{\pi D}{4\dot{\gamma}C(3-D)} \phi_0^{-1} (1 - q^{D-3}) \quad D < 3 \quad (6.32a)$$

$$= \frac{3\pi}{4\dot{\gamma}C} \phi_0^{-1} \ln q \quad D = 3 \quad (6.32b)$$

In practice, the ortho and the perikinetic aggregation rates are additive and both aggregation rates can be combined to:

$$\frac{dc}{dt} = \frac{3\phi_0^2 a^{2D-6}}{4\pi^2 \eta R^{2D}} (4C\dot{\gamma}\eta R^3 + AkT) \quad (6.33)$$

Combination with eqn. 6.30 yields

$$t_c = \int_a^{R_v} \frac{dt}{dR} dR = \int_a^{R_v} \frac{\pi D \eta a^{3-D} R^{D-1}}{\phi_0 (4C\dot{\gamma}\eta R^3 + AkT)} dR \quad (6.34)$$

This equation can be solved analytically for some values of the fractal dimensionality; in the case of immediate coalescence ( $D=3$ )

$$t_c = \frac{\pi \ln(4C\dot{\gamma}\eta R_v^3 + AkT)}{4C\phi_0\dot{\gamma}} - \frac{\pi \ln(4C\dot{\gamma}\eta a^3 + AkT)}{4C\phi_0\dot{\gamma}} \quad (6.35)$$

If  $4\dot{\gamma}\eta a^3 \ll kT \ll 4\dot{\gamma}\eta R_v^3$  we may write

$$t_c = \frac{\pi}{4C\phi_0\dot{\gamma}} \ln \left( \frac{4C\dot{\gamma}\eta R_v^3}{AkT} \right) \quad (6.35a)$$

In fig. 6.5 the radius of the flocs is plotted as a function of time on a double logarithmic scale. Fig. 6.6 shows the aggregation time depicted as a function of  $a$ , for various shear rates and dimensionalities. Obvious effects that can be read from these figures are the large influence of the dimensionality and the shear rate on the aggregation time and the influence of the size of the primary particles. In the case of immediate coalescence after attachment ( $D = 3$ ) the aggregation time is almost independent of the size of the primary particles if these are small enough to be in the perikinetic regime ( $4\dot{\gamma}\eta a^3 \ll kT$ ).

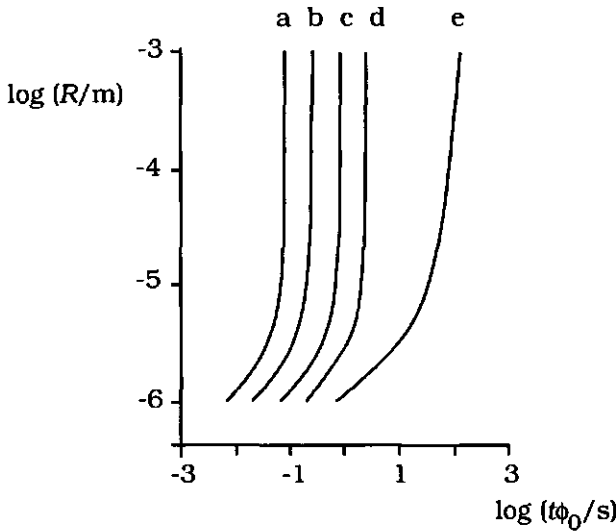


**Fig. 6.5**  $\log R$  as a function of  $\log t\phi_0$  for various initial particle sizes at a dimensionality,  $D = 2$ : a)  $a = 10$  nm, b)  $a = 30$  nm, c)  $a = 100$  nm and d)  $a = 300$  nm and e) at a dimensionality,  $D = 3$ ; curve is independent of  $a$  if  $4\dot{\gamma}\eta a \ll kT$ . The shear rate,  $\dot{\gamma}$ , is  $0.1 \text{ s}^{-1}$ ,  $\eta = 1 \text{ mPa s}$  and  $T = 298 \text{ K}$ .

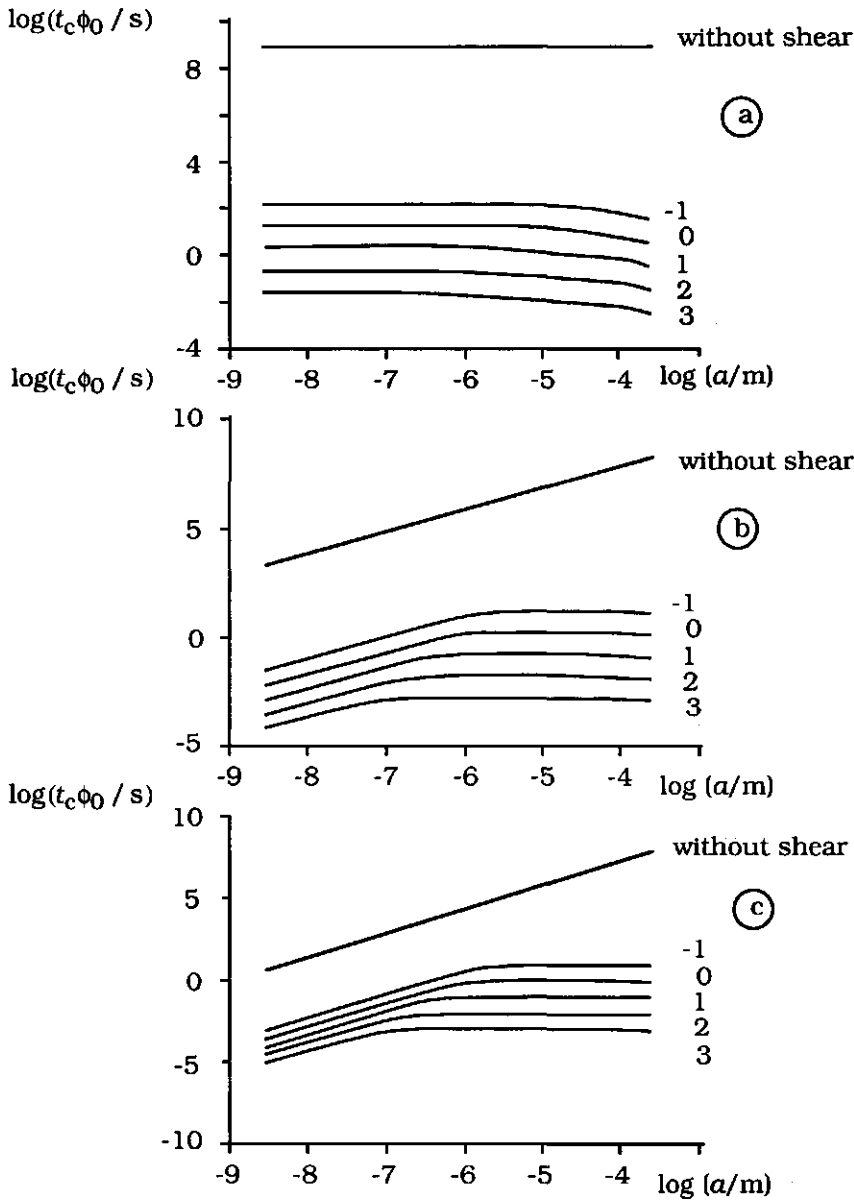


**Fig. 6.6**  $\log t_c \phi_0$  as a function of  $\log a$  for a)  $D = 3$ , b)  $D = 2$  and c)  $D = 1.5$ . The aggregation time is calculated using eqn. 6.34 with  $R_v = 1 \text{ mm}$ ,  $\log \dot{\gamma}$  is indicated near the curves,  $\eta = 1 \text{ mPa s}$  and  $T = 298 \text{ K}$ . Plots are valid if there is no gelation ( $R_g > 1 \text{ mm}$ ;  $\phi < (1000a)^{3-D}$ , ( $a$  in m)).

In the case of fractal flocs, small particles give a shorter aggregation time, scaling roughly like  $a^{3-D}$ . The value of  $R_v$  is of negligible importance for the aggregation time in the case of fractal flocs if  $4\dot{\gamma}\eta a^3 \ll kT \ll 4\dot{\gamma}\eta R_v^3$  (fig. 6.5). Once a certain floc size is reached further growth to  $R_v$  occurs almost instantaneous. The same phenomenon is found experimentally for the aggregation of colloidal nickel hydroxy carbonate [30]. For fractal aggregation eqn. 6.34 can be simplified to

$$t_c = \frac{K_6 D}{C\dot{\gamma}\psi_0} \left( \frac{4C\eta\dot{\gamma}a^3}{AkT} \right)^{(3-D)/3} \quad (6.36)$$

where  $K_6$  is a constant of order 1;  $D = 1.5$  gives  $K_6 = \pi^2/12$  and  $D = 2$  provides  $K_6 = \pi^2\sqrt{3}/18$ . Values of  $K_6$ , obtained from numerical solutions of eqn. 6.34 for various  $D$  values are plotted in fig. 6.7.

The time after which visible flocs are just formed,  $t_c$ , obtained with eqn. 6.36, is about equal to the time obtained by substitution of  $R_{cr}$  for  $R_v$  in eqn. 6.31. The aggregation time is shorter than calculated with eqn. 6.36 if  $R_s$  is smaller than  $R_{cr}$ . Instability becomes visible a short time after clusters reach size  $R_s$ . Once  $R_s$  is reached sedimentation will enhance the aggregation rate strongly and the aggregation time may therefore be estimated by substitution of  $R_s$  for  $R_v$  in eqn. 6.31. It is very complicated to calculate this aggregation time in a more precise way.

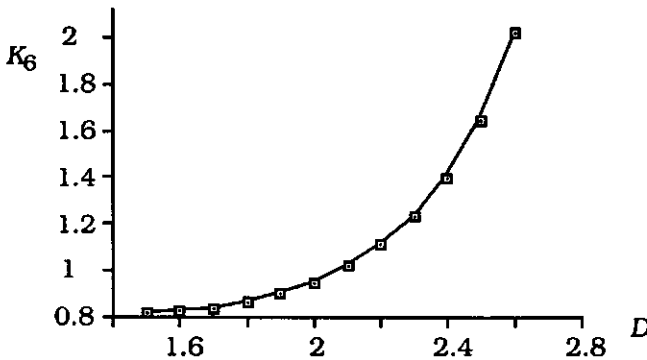


**Fig. 6.7** Value of the constant,  $K_6$ , in eqn. 6.36 as a function of the fractal dimensionality,  $D$ . The markers indicate results obtained by solving eqn. 6.34 numerically.

If perikinetetic aggregation goes up to visible gelation we may substitute  $zR_g$  for  $R_v$ . The factor  $z$  enters because  $R_g$  is a 3D average cluster size and  $R_v$  is a DO average size;  $R_{D0} = zR_{3D}$ . Because the effective volume fraction is high we use the correction of eqn. 6.18:

$$t_g = \int_{R_{3D}=a}^{R_{3D}=R_g} \frac{\pi D \eta a^2}{AkT\phi_0} \left( \left( \frac{R_{D0}}{a} \right)^{D-1} \left( 1 - \phi_0^{1/3} \left( \frac{R_{3D}}{a} \right)^{1-D/3} \right)^2 \right) dR_{3D}$$

$$\approx z^{D-1} \left( 1 - \frac{6D}{2D+3} + \frac{3D}{D+6} \right) \frac{\pi \eta a^3}{AkT} \phi_0^{3/(D-3)} \quad (6.37a)$$

In this integration  $a$  is assumed to be negligible compared to  $R_g$ . Because rapid aggregation results in self-preserving size distributions [20] the ratio  $R_{D0}/R_{3D}$ ,  $z$ , is constant. This ratio can be estimated if we approximate the cluster size distribution  $c(i) \propto i^D h(i, t)$  where  $h(i, t)$  is a cutoff function which is 1 if  $i$  is less than a certain number of particles in the flocs,  $i_c(t)$ , and 0 if  $i$  is more than  $i_c(t)$ . The largest clusters in the system have thus radius  $R_1(t) = i_c(t)^{1/D}$ . Values of  $z$  are compiled in table 6.2 for  $i_c = 1000$ , the ratio is almost constant at that value.

**Table 6.2.**  $z = R_{D0}/R_{3D}$  for various fractal dimensionalities, calculated for a cluster size distribution  $c(i, t) \propto i^D h(i, t)$ ,  $i_c = 1000$ .

D	z	D	z
1.7	0.853	2.2	0.899
1.8	0.865	2.3	0.906
1.9	0.875	2.4	0.912
2	0.884	2.5	0.917
2.1	0.892	2.6	0.922

A similar relation can be obtained for orthokinetic aggregation ( $4\dot{\gamma}\eta a^3 > kT$ ) by substitution of  $R_g$  in eqn. 6.32:

$$t_g = \frac{\pi D}{4C\dot{\gamma}(3-D)} (\phi_0^{-1} - 1) \quad (6.37b)$$

In this equation no correction has been made for the effect of the increasing effective volume fraction on the aggregation rate. In general,

such a correction is negligible in the case of orthokinetic aggregation unless the initial volume fraction,  $\phi_0$ , is very high. However, the effect of polydispersity may be important, because orthokinetic aggregation leads to a polydisperse cluster size distribution.

In the case of gelation after peri and orthokinetic aggregation eqn. 6.36 may be used, because the time during which the clusters grow from  $R_{cr}$  to  $R_g$  is negligible. In the figs. 6.8 - 6.11 various aggregation, gelation and sedimentation times are depicted as a function of  $a$ ,  $R_c$ ,  $D$  and  $\phi_0$ .

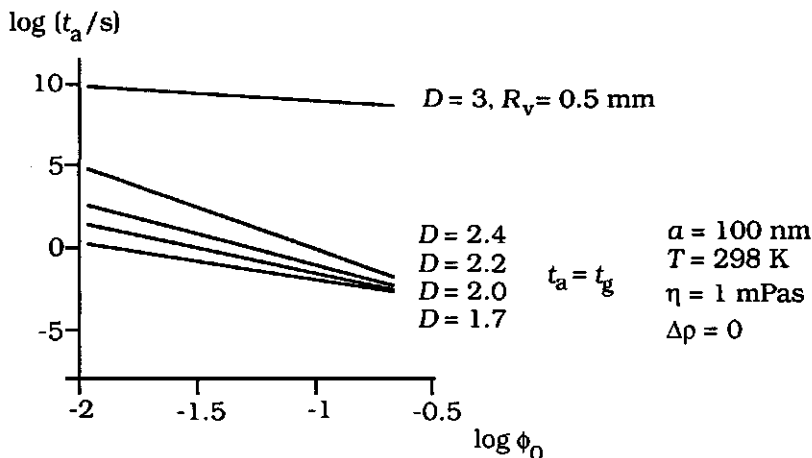


**Fig. 6.8** Aggregation and gel times in the absence of velocity gradients and sedimentation for various fractal dimensionalities.

Experimental results by Manegold [31] are given in table 6.3, plotted in fig. 6.9, and compared with eqn. 6.37a. To fit the experimental data a factor  $1/W$  was substituted for  $A$ . The value of  $D$  is in good agreement with computer simulations of slow aggregation.

**Table 6.3:** gel time for various volume fractions of silica particles [31].

$\phi_0$	$t_g$
12 %	a few hours
5 %	5 - 6 days
2 %	2 - 3 months
1 %	more than 2 years



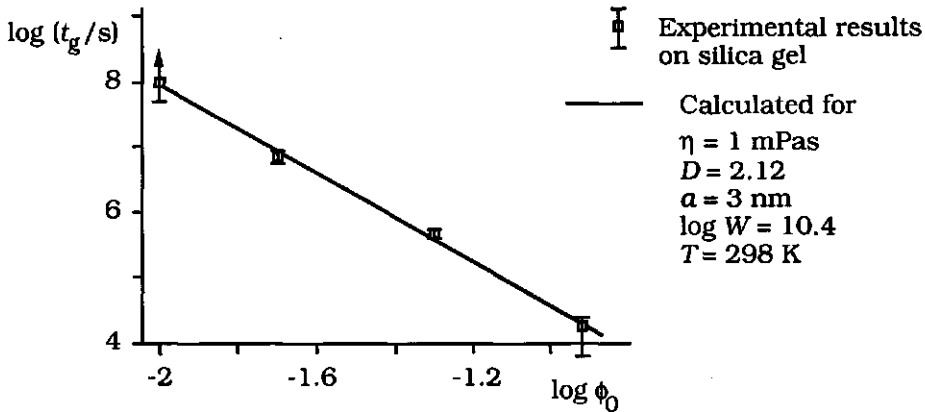


**Fig. 6.9** Gel time as a function of the volume fraction of silica particles (from [31], table 6.2). The experimental results are fitted to eqn. 6.37a

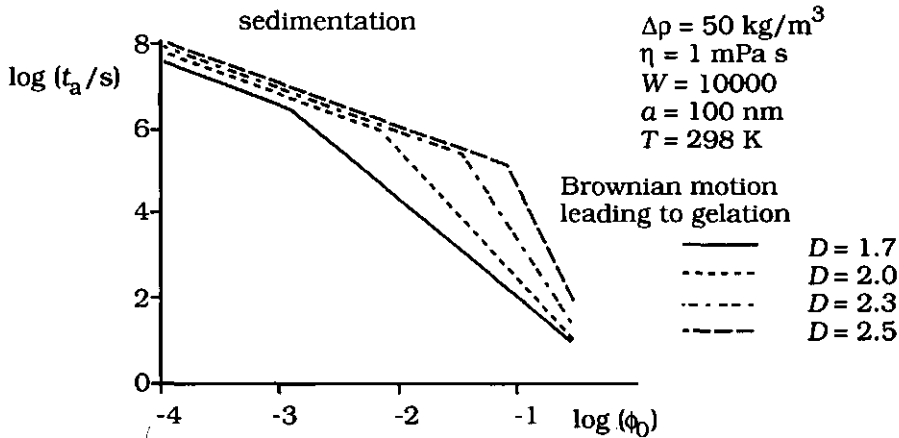


**Fig. 6.10** Logarithm of aggregation time,  $t_a$ , as a function of  $\log \phi_0$  in the absence of shear for various values of the fractal dimensionality  $D$ .

In fig. 6.10 the aggregation time is calculated with eqn. 6.37a and by substitution of  $R_s$  of eqn. 6.28 for  $R_v$  in eqn. 6.31. It was assumed that sedimentation occurs if  $R_s < R_g$ ; in that case eqn. 6.28 was used. At high volume fractions  $R_g$  decreases and gelation will occur before the clusters sediment. In practice, small velocity gradients in the dispersion may lead to gelation at volume fractions that are much smaller than those at which the transition from gelation to sedimentation occurs in fig. 6.10. The dependence of the aggregation time on the volume fraction is similar for

sedimentation and Smoluchowski type flocculation if the latter is due to small velocity gradients in the dispersion (eqn. 6.37b, fig. 6.11):  $t_a \propto \phi^{-1}$ . The aggregation time in fig. 6.10 that is obtained by substitution of  $R_s$  for  $R_v$  in eqn. 6.31 is therefore realistic if  $R_s < R_{cr}$ . If  $R_s > R_{cr}$  the aggregation time can be estimated with eqn. 6.37a if  $R_g < R_{cr}$  and with eqn. 6.36 if  $R_g > R_{cr}$ .

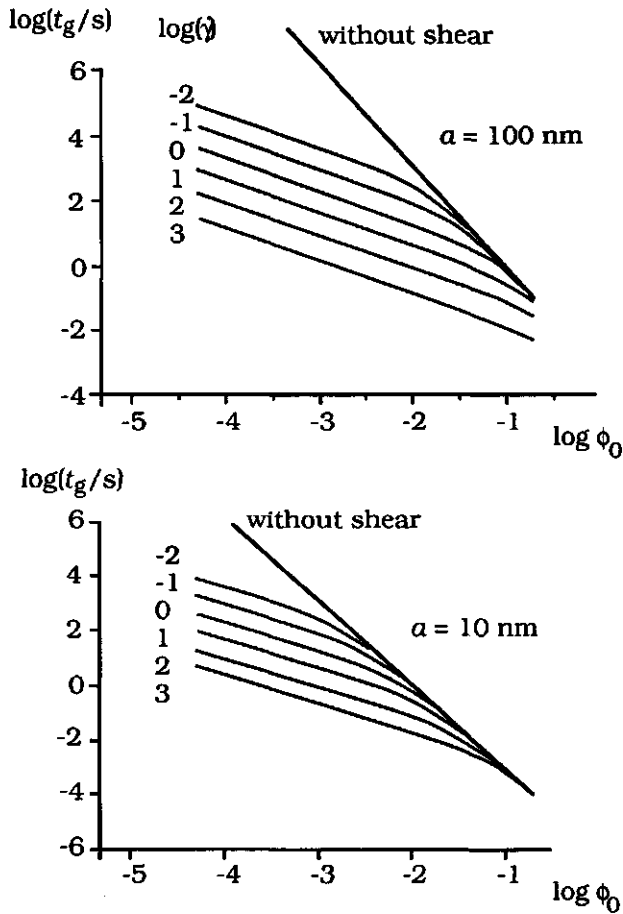


**Fig. 6.11**  $\log t_g$  as a function of  $\log \phi_0$  for various shear rates.  $D = 2$ ,  $T = 298 \text{ K}$ ,  $\eta = 1 \text{ mPa s}$ ,  $a$  and  $\dot{\gamma}$  are indicated. The curves were calculated by substitution of  $R_g$  for  $R_v$  in eqn. 6.34.

## 6.5 Reaction limited aggregation

In fig. 6.12 examples are given of curves of the logarithm of the stability ratio,  $W$ , as a function of the logarithm of the salt concentration,  $c_s$  for various particle sizes.  $W$  was obtained by substitution of the DLVO interaction energy [32, 33] in eqn. 6.12. According to DLVO theory, the interaction energy between two particles is about proportional to the particle radius. At similar Hamaker constants, the repulsive barrier is therefore higher for larger particles. The slopes of the  $\log W - \log c_s$  curves, calculated with DLVO, are proportional to the particle radius  $a$ . However, measurements of  $d \log W / d \log c_s$  result in slopes that are hardly dependent on the particle size [34]. Many attempts have been made to find an explanation for the stability ratio to be approximately independent of particle size in practice, whereas a strong dependence is expected within the framework of Fuchs and DLVO. Factors like surface roughness, shear and reeptization [34], a cross-over from primary to secondary minimum aggregation [35], relaxation retardation [36], or electroviscous forces [37] have been proposed.

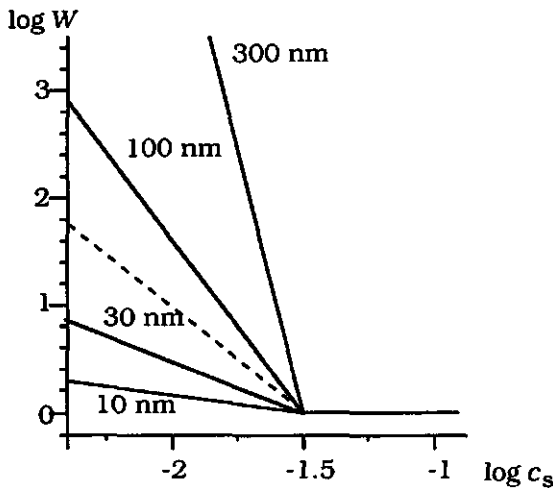


**Fig 6.12** Logarithm of  $W$  versus  $\log c_s$  plots calculated for various particle sizes with Fuchs/DLVO theory. The dashed line gives the approximate curve obtained experimentally for hematite sols with particle radii ranging from 86 to 352 nm [34].

If the Fuchs/DLVO approach would be applied to the kinetics of aggregation one would expect the activation free energy for aggregation,  $V_a$ , to be an increasing function of the floc size,  $R$ . In the case of immediate coalescence  $V_a$  is, just as in the case of solid spheres, approximately proportional to  $R$ . For flocs  $V_a$  will depend much less on  $R$ , because at most conditions interactions are active on length scales far smaller than the floc size, so that the effect of other particles than those forming the connection will be small if not zero. If we assume  $W$  to be independent of  $R$  it is possible to introduce the factor  $W$  by multiplying of the aggregation times by  $W$ . This approach gave reasonable aggregation and gel times (fig. 6.9), [38, 39].  $\log t_g$  versus  $\log c_s$  plots provide, just like the  $\log W - \log c_s$  plots, straight lines [31].

However, in computer simulations and also in some experiments, the size of the large clusters turns out to grow exponentially, which means that  $W$  decreases and finally equals 1, thus causing a transition from reaction limited to diffusion limited aggregation. An essential feature of reaction limited cluster-cluster aggregation is that the number of collisions, caused by diffusion, before aggregation of two clusters succeeds is sufficiently large to allow clusters to sample many possible mutual bonding configurations [23].

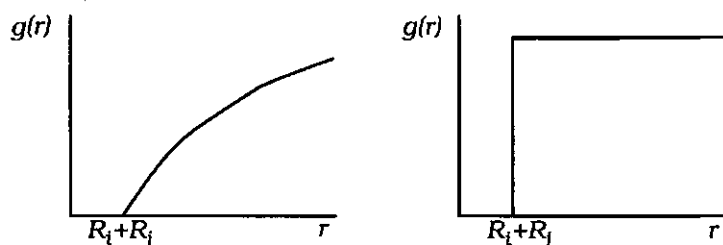


**Fig. 6.13** Radial distribution function of the clusters in a dispersion during (a) rapid, diffusion limited aggregation and (b) slow, reaction limited aggregation in the case of coalescing spheres.

The radial distribution function of the clusters throughout the dispersion,  $g(r)$ , then is (almost) independent of  $r$  (fig. 6.13). This difference of  $g(r)$  causes a difference in floc structure between diffusion and reaction limited aggregates. The latter have a more compact structure because all

bonding configurations have roughly the same probability, whereas in the case of rapid aggregation bonding configurations with a small degree of interpenetration are favoured. When two flocs approach and interpenetrate each other on Brownian trajectories, there will be many contacts due to the lateral diffusion of the flocs with regard to each other, rotational diffusion and diffusive motions of the protruding strands of the flocs. The probability that two flocs will stick thus increases rapidly with floc size, thereby causing a transition from reaction to diffusion limited aggregation. The effect of lateral, and to some extent rotational, diffusion is also important in the case of surface roughness of primary particles, as it also increases the mutual 'reaction' surface where sticking may occur and thereby the probability of bond formation.

Because the sticking probability of large clusters with other clusters is high, and that of small clusters with other small clusters low, the cluster size distribution becomes broad, with few large and many small clusters: see fig. 6.14. The attachment of small clusters to large clusters is therefore an important contribution to cluster growth. This typical cluster size distribution is, in addition to the deeper interpenetration of the flocs, responsible for the more compact flocs that are formed in the case of reaction limited aggregation as compared to the diffusion limited aggregation flocs. Computer simulations of reaction limited aggregation give a fractal dimensionality,  $D$ , equal to  $1.95 \pm 0.05$  for a hierarchical (mono-disperse) model and  $2.12 \pm 0.04$  for a, more realistic, poly-disperse model [40, 41].

A scaling relation for the collision kernel of reaction limited aggregation was derived by Ball et al. [23]. They argue that, since all mutual bonding configurations have similar probabilities, the mutual surface over which the flocs can come into contact determines the aggregation rate. For spherical, solid particles this would mean that the reaction kernel,  $K \propto R^2$ . For (reaction limited) fractal flocs they found:

$$K_{i,j} \propto i \quad i \gg j \quad \text{and} \quad K_{i,j} \propto i \quad i \approx j \quad (6.38)$$

This kernel led to exponential growth kinetics and a power-law cluster mass distribution,  $c(i) \propto t^{-3/2} h(i,t)$ , which is in excellent agreement with many experimental results [10, 12]. A power law cluster mass distribution

with a cutoff at large cluster sizes was also found in computer simulations [22]; the (absolute value of the) power was, however, somewhat higher, 1.69 in stead of 1.5. The cutoff size, i.e. the size of the largest clusters  $R_1$ , grows exponentially. In figure 6.14, cluster mass and size distributions are shown for reaction and diffusion limited aggregation.

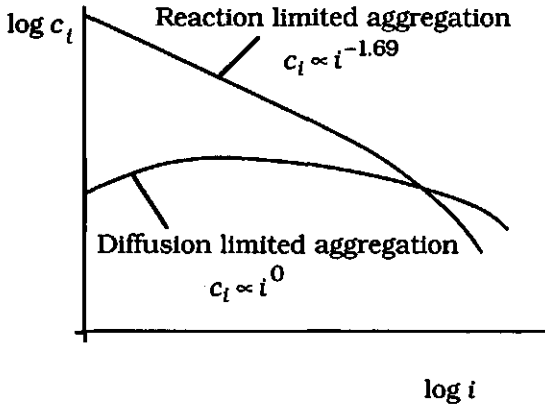


**Fig. 6.14** The number concentration of clusters as a function of the number of particles in the clusters. Distributions were obtained from computer simulations by Meakin [22] and can be approximated by  $c_i \propto i^{-1.69} h(i,t)$  for reaction and  $c_i \propto i^0 h(i,t)$  for diffusion limited aggregation.

In the case of slow orthokinetic aggregation, the force exerted on two flocs making contact is of the order of  $\dot{\gamma}\eta R^2$ . If there is an energy barrier for aggregation this force may easily be sufficient to overcome the barrier if the flocs are large enough. The aggregation rate will then show a stronger dependence on  $\dot{\gamma}$  and  $R$  than expected from eqn. 6.20. Systems may then be stable at low shear rate, but unstable at higher  $\dot{\gamma}$ .

Besides accelerating aggregation rates leading to a transition from slow to rapid aggregation, decelerating aggregation rates have been reported in the literature [42, 43]. In computer simulations, the repulsive barrier that slows down the aggregation, is assumed to be independent of the size of the clusters. It is also assumed that all mutual bonding configurations have equal probabilities; i.e. the surface is completely homogeneous. In the case of coalescence the aggregation rate may slow down because  $V_a \propto a$  and because the total particle surface becomes

smaller, which may result in an increase of the surface charge. If the surface is heterogeneous, bonds are more likely to be formed first at the most reactive places, thereby making the surface of the flocs, on average, less reactive.

### 6.6 Floc break up and rearrangements

Floc breaking and rearrangements affect both the net bond formation rate and the structure of the flocs. The extent of floc breaking and rearrangements depends on the total free energy of interaction between the clusters, the smoothness of the surface of the particles, ageing of the bonds (sintering) and the external forces exposed to the floc. Our understanding of floc disruption and rearrangement is much more qualitative and speculative than that of the kinetics of bond formation.

Bonds may occasionally spontaneously break if the activation free energy for bond breakage,  $V_b/kT$ , is not very high (fig. 6.15). The situation of diffusion limited aggregation occurs if  $V_b \gg kT$  and  $V_a \ll kT$  or if  $V_2 \gg kT$  and that of reaction limited aggregation if  $V_b \gg kT$ ,  $V_a > kT$ , and  $V_2 < kT$ . The situation becomes more complicated if  $V_b$  and  $V_2$  are not much larger than  $kT$  because spontaneous deflocculation may occur in that case.

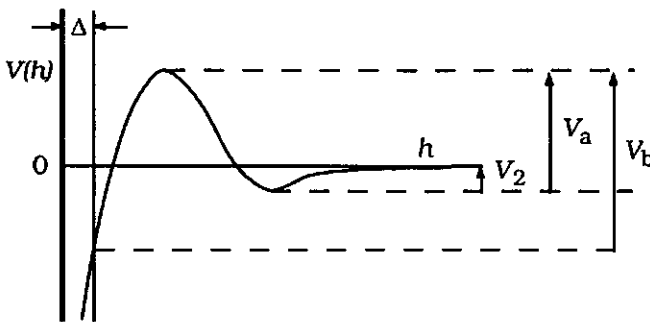


**Fig. 6.15** Interaction free energy between two particles as a function of distance  $h$  according to DLVO theory.  $\Delta$  is the distance of closest approach,  $V_2$  is the depth of the secondary minimum,  $V_a$  is the activation free energy for primary minimum aggregation and  $V_b$  is the activation free energy for bond breakage.

Floc disruption may be included in Smoluchowski's equations (eqn. 6.1) by means of additional terms;

$$\frac{dc_k}{dt} = \frac{1}{2} \sum_{t+j=k} K_{t,j} c_t c_j - c_k \sum_{j=1}^{\infty} K_{k,j} c_j + \sum_{j-t=k} k'_j c_j - \sum k'_k c_k \quad (6.39)$$

where  $k'_k$  is the rate constant for disrapture of flocs that contain  $k$  primary particles. Disruption of a floc is a first order process with a rate depending on  $V_b$  and a frequency factor for each floc independent of  $c$ . Bond formation is a second order process with a rate depending on  $V_a$  and another, presumably much smaller frequency factor proportional to  $c$ .  $V_b$  has, in practice, not just one fixed value but there are many different values, depending on the geometric structure of the floc and the position and age of the bond to be broken in the floc.  $V_b$  will often increase strongly with time after aggregation because the particles try to find the conformation with the lowest free energy. Moreover, sintering or fusion may occur and eventually reptization becomes impossible [44, 45].

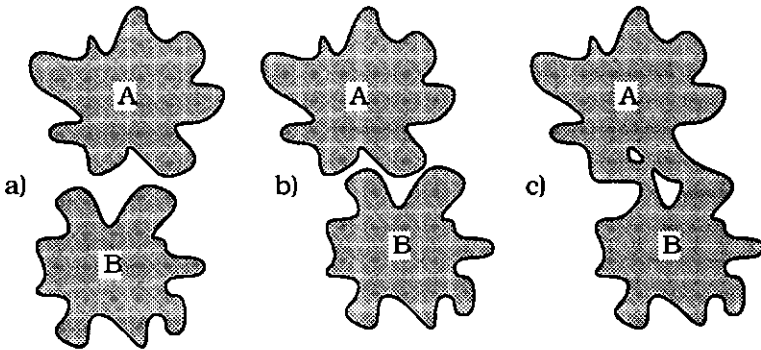


**Fig. 6.16** Schematic representation of processes that increase the strength of the bond between two (rough) particles, A and B. a) a short time after the aggregation, b) the particles have found a mutual position of low free energy, c) after fusion or sintering.

In addition to the effect at the level of the particle-particle bonds, rearrangement of the flocs causes  $V_b$  to increase. For compact flocs  $V_b$  is larger than for similar tenuous flocs. The rates of both processes that increase  $V_b$  are important for the geometric structure of the flocs. The faster the increase of  $V_b$  due to processes at the particle level and the



slower the increase due to rearrangement, the more open are the flocs. In the case of quiescent aggregation floc disruption is, in most cases, less important than floc rearrangement. The latter has no effect on the bond formation rate (eqn. 6.39) but is nevertheless important for the aggregation time, because it affects the floc structure. Computer simulations yield  $D = 1.8$  for cluster-cluster aggregation without rearrangements, if cluster approach via linear or Brownian trajectories. This value is thus expected, and found experimentally [14], for both peri and orthokinetic aggregation, if rigid bonds are formed soon after attachment. Reaction limited aggregation without restructuring results in  $D = 2.1$ . If clusters are allowed to rearrange their mutual position after attachment by rotation about the contacting particles,  $D$  increases up to 2.18 for diffusion and 2.25 for reaction limited aggregation [22].

In a shear field rearrangements and floc disruption become more pronounced. The disruption force exerted on a floc in a simple shear field scales like  $\dot{\gamma}\eta R_h^2$  which results in a maximum hydrodynamic radius,  $R_1$ , that a floc can obtain at a certain shear rate [14]. In addition to the shear rate, this size depends on the strength of the bonds between the particles and on the structure of the floc. An estimation of  $R_1$  was proposed by Torres et al. [14];

$$R_1 = \left( \frac{aA_H}{18\pi\eta\dot{\gamma}\Delta^2} \right)^{1/2} \quad (6.40)$$

If  $R_1$  is smaller than  $R_v$  no visible aggregation occurs and the system seems stable. Eqn. 6.40 is, in general, not useful to describe the disruption of flocs that have been formed previously in a quiescent system and exposed to shear later on, because  $V_b$  often increases after the attachment.

Sometimes flocs in a shear field rearrange rather than disrupt. Such a restructuring occurs at fairly long length scales, resulting in more dense flocs. The flocs maintain their original fractal correlations at short length scales [12]. Potanin has found that flocs attain a critical effective  $D$  at some critical shear rate [46], higher shear rates do not result in further contraction of the flocs.

## 6.7 Conclusions

Due to the large number of possible floc structures and the considerable variation that may occur in the evolution of the aggregation rate during the process of slow aggregation, it is impossible to derive general approximations for the time after which instability becomes visible. However, for many specific situations it is possible to derive good approximations of the aggregation time. In table 6.4 a summary is given of different situations and of the equation(s) that can be used to approximate the aggregation time.

**Table 6.4a.** Equations that may be used to estimate the aggregation time,  $t_a$ , at various conditions in the case of diffusion limited aggregation. C means coalescence ( $D = 3$ ), F fractal aggregation ( $D < 3$ ), O orthokinetic and P perikinetic aggregation. The smallest radius of either  $R_v$ ,  $R_{cr}$ ,  $R_s$  or  $R_g$  determines which equation should be used; see fig. 6.17 for examples.

Smallest radius	C or F	O or P	Eqn(s)	Factor(s)	Condition
$R_v$	F	P	6.31	$A = 1 - 2$	
$R_v$	C	P	6.31	$A = 0.2 - 1$	
$R_{cr} (< a)$	F	O	6.32a	$C = 1$	$R_v < R_g$
$R_{cr} (< a)$	C	O	6.32b	$C = 0.2 - 1$	
$R_{cr} (> a)$	F	P+O	6.36	$C = 1; A = 1 - 2$	
$R_{cr} (> a)$	C	P+O	6.35a	$C = 0.2 - 1; A = 0.2 - 1$	
$R_s$	F	P+O	6.28, 6.31	$q = R_g/\alpha; A = 1 - 2$	
$R_g$	F	P	6.37a	$A = 1 - 2$	
$R_{cr} (< a)$	F	O	6.37b	$C = 1$	$R_v > R_g$

**Table 6.4b** Eqns. that may be used to estimate the aggregation time,  $t_a$ , at various conditions in the case of slow (chemical limited) aggregation.

Smallest radius	C or F	O or P	Eqn(s)	Factor(s)	Condition
$R_v$	F	P	6.12, 6.31	$A = 1/W - 2/W$	for small $q$
$R_v$	C	P	6.12, 6.31	$A = 1/W$	for small $q$
$R_{cr} (< a)$	F	O	6.32a	$C = 1/W$ [47]	for small $q$
$R_{cr} (< a)$	C	O	6.32b	$C = 1/W$	for small $q$
$R_{cr} (> a)$	F	P+O	-		
$R_{cr} (> a)$	C	P+O	6.12, 6.35a	$C = 1/W; A = 1/W$	
$R_s$	F	P+O	-		
$R_g$	F	P	6.12, 6.37a	$A = 1/W - 2/W$	

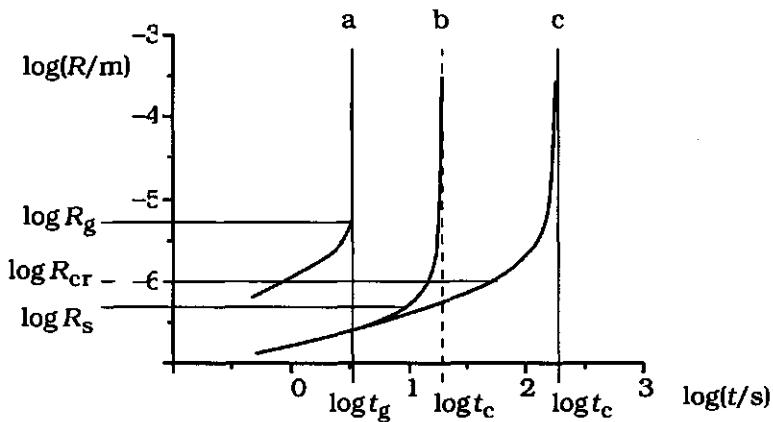


**Fig. 6.17** Logarithm of the radius of aggregating clusters as a function of  $\log t$  for three different situations:  $T = 298 \text{ K}$ ,  $\eta = 1 \text{ mPa s}$ ,  $D = 2$

a) polystyrene particles,  $a = 100 \text{ nm}$ ,  $\dot{\gamma} = 10^{-3} \text{ s}^{-1}$ ,  $\phi = 0.02$ , and  $\Delta\rho = 1 \text{ kg m}^{-3}$ . The resulting radii are:  $R_{\text{cr}} = 10 \text{ }\mu\text{m}$  (Eqn. 6.22),  $R_g = 5.0 \text{ }\mu\text{m}$  (Eqn. 6.15),  $R_s = 13 \text{ }\mu\text{m}$  (Eqn. 6.28) and  $R_v = 0.1 \text{ mm}$ .  $R_g$  is the smallest radius and Eqn. 6.37a may be used to estimate the gelation time. ( $t_g \approx 3 \text{ s}$ )

b) gold particles,  $a = 100 \text{ nm}$ ,  $\dot{\gamma} = 1 \text{ s}^{-1}$ ,  $\phi = 0.001$ , and  $\Delta\rho = 17800 \text{ kg m}^{-3}$ . The resulting radii are:  $R_{\text{cr}} = 1 \text{ }\mu\text{m}$ ,  $R_g = 0.1 \text{ mm}$ ,  $R_s = 0.5 \text{ }\mu\text{m}$  and  $R_v = 0.1 \text{ mm}$ .  $R_s$  is the smallest radius and may be substituted in Eqn. 6.31 to estimate the aggregation time. This estimation is less accurate because the enhancement of the aggregation rate due to sedimentation is unknown ( $t_c \approx 20 \text{ s}$ ).

c) polystyrene particles at the same conditions as b),  $\Delta\rho = 50 \text{ kg m}^{-3}$ . The resulting radii are:  $R_{\text{cr}} = 1 \text{ }\mu\text{m}$ ,  $R_g = 0.1 \text{ mm}$ ,  $R_s = 3.4 \text{ }\mu\text{m}$  and  $R_v = 0.1 \text{ mm}$ .  $R_{\text{cr}}$  is the smallest radius and Eqn. 6.36 may be used to estimate the aggregation time ( $t_c \approx 200 \text{ s}$ ).

The stability ratio,  $W$  or  $W'$ , is in most cases not constant during the aggregation process. This complicates the estimation of aggregation times in the case of reaction limited aggregation. It has been shown that the slope of  $\log W - \log c_s$  plots of polystyrene latex particles vary if  $W$  is measured at different stages of the aggregation process [42].  $W$  may thus also be different from the initial  $W$  for single particles if aggregation becomes visible due to gelation. It is somewhat puzzling why eqn. 6.37a fits experimental results of the gel time as a function of the initial volume fraction of slowly aggregating systems. If the results obtained for reaction limited aggregation apply to these systems – i.e. a power law cluster size

distribution and an exponential increase of the size of the largest particles - the gel time would be only slightly dependent on  $\phi_0$ . Probably, at high  $\phi_0$  the system is gelled before the mechanism of reaction limited aggregation applies, and the change of  $W$  during the aggregation may be small resulting in a slope of the  $\log t_g - \log \phi_0$  curve that can be fitted to Eqn. 6.37a.

Zhou and Chu [48] showed experimentally that  $R \propto t^{1/D}$  in the case of diffusion limited aggregation (high salt concentration). The dimensionality obtained from this relation,  $D = 1.89$ , was in fair agreement with the measured dimensionality. However, at lower  $c_s$  ( $W > 1$ ),  $R \propto t^{1/D}$  provided unrealistic low values for  $D$  because  $W$  decreased during the aggregation process. This decreasing  $W$  is responsible for the fact that eqns. 6.32 and 6.33 are only useful if  $q$  is small (table 6.4b) since at small  $q$  the change of  $W$  is small and  $W$  may be considered constant.

Finally, in table 6.5 examples are given for the aggregation time of a 'quiescent' system at various conditions in order to emphasize the large effect of floc structure and small velocity gradients. The existence of these gradients and the importance of small fluctuations in temperature can well be demonstrated in colloidal systems. The effective sedimentation velocity of a dispersion stored at room temperature is usually much lower than expected according to Stokes' law (Eqn. 6.24). The effective sedimentation velocity increases substantially if the temperature is kept constant. Especially in a refrigerator where the temperature is about 4 °C, implying a low coefficient of volume expansion of water (and thereby negligible convection currents), visible sedimentation may occur much faster than at room temperature.

**Table 6.5** Aggregation time for a 'quiescent' system with particles in water of 20 °C (no sedimentation,  $W = 1$ ,  $a = 20$  nm,  $\phi = 10^{-5}$ ) at various conditions. Visible aggregation if  $R_v = 0.2$  mm.

	Eqn.	$t_a$ (s)
Immediate coalescence, no velocity gradient	6.31	$6.2 \times 10^{11}$ (200 centuries)
Immediate coalescence, $\dot{\gamma} = 0.1 \text{ s}^{-1}$	6.35a	$1.1 \times 10^7$ (4 months)
Fractal aggregation $D = 2$ , no velocity gradient	6.31	$6.2 \times 10^7$ (2 years)
Fractal aggregation $D = 2$ , $\dot{\gamma} = 0.1 \text{ s}^{-1}$	6.36	$1.8 \times 10^4$ (5 hours)

## 6.8 References

- 1 M. von Smoluchowski, *Physik. Z.*, 1916, **17**, 557
- 2 M. von Smoluchowski, *Z. Physik. Chem.*, 1917, **92**, 129
- 3 P.G.J. van Dongen, *PhD Thesis*, (State University Utrecht, The Netherlands, 1987)
- 4 E.M. Hendriks and M.H. Ernst, *J. Coll. Int. Sci.*, 1984, **97**, 176
- 5 P.G.J. van Dongen and M.H. Ernst, *Phys. Rev. Lett.*, 1985, **54**, 1396
- 6 P.G.J. van Dongen and M.H. Ernst, *J. Coll. Int. Sci.*, 1987, **115**, 27
- 7 N. Fuchs, *Z. Physik*, 1934, **89**, 736
- 8 R.M. Ziff, E.D. McGrady, and P. Meakin, *J. Chem. Phys.*, 1985, **82**, 5269
- 9 F. Family and D.P. Landau (ed.), *Kinetics of Aggregation and Gelation* (North-Holland, Amsterdam, 1984)
- 10 D.A. Weitz and J.S. Huang, M.Y. Lin and J. Sung, *Phys. Rev. Lett.*, 1985, **54**, 1416
- 11 R.C. Sonntag and W.B. Russel, *J. Colloid Interface Sci.*, 1986, **113**, 399
- 12 M.Y. Lin, R. Klein, H.M. Lindsay, D.A. Weitz, R.C. Ball and P. Meakin, *J. Colloid Interface Sci.*, 1990, **137**, 263
- 13 R. Amal, J.A. Rapern and T. D. Waite, *J. Colloid Interface Sci.*, 1990, **140**, 158
- 14 F.E. Torres, W.B. Russel and W.R. Schowalter, *J. Colloid Interface Sci.*, 1991, **142**, 554
- 15 P. Meakin, Z.Y. Chen and J.M. Deutch, *J. Chem. Phys.*, 1985, **82**, 3786
- 16 L.A. Spielman, *J. Coll. Int. Sci.*, 1970, **33**, 562
- 17 E.P. Honig, G.J. Roeberson and P.H. Wiersema, *J. Coll. Int. Sci.*, 1971, **36**, 97
- 18 J.W.Th. Lichtenbelt, C. Pathmananoharan and P.H. Wiersema, *J. Coll. Int. Sci.*, 1974, **49**, 281
- 19 K. Higashitani, S. Miyafusa, T. Matsuda and Y. Matsuno, *J. Coll. Int. Sci.*, 1980, **77**, 21
- 20 D.L. Swift and S.K. Friedlander, *J. Coll. Sci.*, 1964, **19**, 621
- 21 S.K. Friedlander and C.S. Wang, *J. Coll. Sci.*, 1966, **22**, 126
- 22 P. Meakin, *Adv. in Colloid and Int. Sci.*, 1988, **28**, 249
- 23 R.C. Ball, D.A. Weitz, T.A. Witten and F. Leyvraz, *Physical Review Letters*, 1987, **58**, 274
- 24 C. Tanford, *Physical Chemistry of Macromolecules*, John Wiley, NY, 1961
- 25 L.G.B. Bremer, in preparation; Section 4.2
- 26 L.G.B. Bremer, T.van Vliet and P. Walstra, *J. Chem. Soc. Faraday Trans I*, 1989, **85**, 3359
- 27 J.Th.G. Overbeek, in *Colloid Science Vol. 1*, H.R. Kruyt, Ed., Chapt. 7, Elsevier, Amsterdam, 1952, 278
- 28 T.G.M. van de Ven and S.G. Mason, *J. Colloid Interface Sci.*, 1976, **57**, 517
- 29 R.B. Bird, W.E. Stewart and E.N. Lightfoot, *Transport phenomena*, John Wiley & Sons, New York - London (1960)
- 30 L.L. Hoekstra, R. Vrecker and W.G.M. Agterof, *J. Coll. Int. Sci.*, submitted
- 31 E. Manegold, *Allgemeine und angewandte Kolloidkunde*, Strassenbau, Chemie und Technik Verlagsgesellschaft m.b.h. Heidelberg (1958)
- 32 B.V. Deryagin and L.D. Landau, *Acta Physico Chm. U.R.S.S.*, 1941, **14**, 633

- 33 E.J.W. Verwey and J.Th.G. Overbeek, in *Theory of the Stability of Lyophobic Colloids*, (Elsevier, Amsterdam, 1948)
- 34 N.H.G. Penners and L.K. Koopal, *Colloids and Surfaces*, 1987, **28**, 67
- 35 A. Marmur, *J. Colloid Interface Sci.*, 1979, **72**, 41
- 36 S.S. Dukhin and J. Lyklema, *Faraday Discuss. Chem. Soc.*, 1990, **90**, 261
- 37 P. Warszyński and T.G.M. van de Ven, *Faraday Discuss. Chem. Soc.*, 1990, **90**, 313
- 38 P. Walstra, T. van Vliet and L.G.B. Bremer, in *Proc. Conf. Food Polymers, Gels and Colloids*, E. Dickinson, Ed., Royal Society of Chemistry, Cambridge, 1990
- 39 J.A.N. Nieuwenhuijse, T. van Vliet and P. Walstra, *Neth. Milk Dairy J.*, submitted
- 40 W.D. Brown and R.C. Ball, *J. Phys. A: Math. Gen.*, 1985, **18**, L517
- 41 W.D. Brown, PhD. Thesis, University of Cambridge, UK, 1987
- 42 A. Lips and R.M. Duckworth, *J. Chem. Soc. Faraday Trans I*, 1988, **84**, 1223
- 43 V.V. Klyubin, L.A. Kruglova and V.N. Sokolov, *Colloid Journal of the USSR*, 1990, **52**, 308
- 44 G. Frens and J.Th.G. Overbeek, *J. Coll. Int. Sci.*, 1971, **36**, 286
- 45 G. Frens and J.Th.G. Overbeek, *J. Coll. Int. Sci.*, 1972, **38**, 376
- 46 A.A. Potanin, *J. Coll. Int. Sci.*, 1991, **145**, 140
- 47 L. A. Spielman, in *The Scientific Basis of Flocculation*, K.J. Ives, Ed., NATO advanced study institutes; Series E: Applied Science-No. 27, (Sijthoff & Noordhof, Alphen aan den Rijn, The Netherlands 1978)
- 48 Zhou and Chu, *J. Coll. Int. Sci.*, 1991, **143**, 356

## VII Factors Disturbing Gelation and Altering Gel Structure

### 7.1 Introduction

The model of fractal aggregation (section 2.3) always implies the formation of a gel network if the size of the container is large enough compared to the size of the primary particles (section 2.4.1). In practice, however, aggregation often results in the formation of a precipitate or a cream layer, since various factors either disturb the gel formation, or the gel structure after it has been formed. In this chapter these factors are discussed. Some of them could be quantified, but in general the various factors affect each other which makes the total problem too intricate for general estimations. Especially the effect of forces between the particle surfaces is largely unknown. Measurements with the surface force apparatus can provide information about forces that are normal to the surface [1]. However, the lateral forces that may lead to or prevent rolling, slipping and rotation of particles with respect to each other, and the strength of the bonds between particles in touching contact are unknown.

### 7.2 Gravity; sedimentation or creaming and compression

#### 7.2.1 *Effects of sedimentation and creaming*

Sedimentation or creaming of the flocs during the aggregation process may hinder gel formation. A critical radius,  $R_s$ , above which sedimentation of clusters over a distance  $R$  takes less time than diffusion is derived in chapter 6 (eqn. 6.28). Because the sedimentation velocity increases and the diffusion decreases ever more rapidly as  $R$  increases, one may expect gelation if the radius of the clusters in the gel,  $R_g$ , is smaller than  $R_s$  and sedimentation if  $R_g > R_s$ . However, both the casein and the polystyrene particles form space-filling networks at volume fractions where  $R_g \gg R_s$ . Possible explanations for this observation are:

- 1- The settling rate in a concentrated system is much slower than in dilute systems
- 2- Sedimentation enhances the aggregation rate. The supernatant layer above the sediment may therefore be so thin that the sediment is considered to be a gel.
- 3- The dimensionality and size of the clusters at the moment that they just form a space filling network may be smaller than the size measured for aged gels. After the gel point the gel may be too weak to prevent rearrangements leading to a coarsening of the gel network; this would correspond to a higher  $R_g$  and consequently to an (apparently) higher value of  $D$ .
- 4- Velocity gradients in the solution may hinder settling of the flocs and lead to orthokinetic aggregation resulting in gelation.
- 5- A directionality in the interaction of the primary particles may lead to chains of particles rather than three-dimensional clusters.

All of these reasons may (partially) be responsible for the gel formation at very low volume fraction. If a gel network arises due to fractal aggregation of the 35 nm polystyrene particles with  $D = 2.2$  and  $\phi_0 = 0.0002$  the radius of the clusters in the gel is roughly 1.5 mm (experimental result) and  $R_s = 3.7 \mu\text{m}$  ( $\Delta\rho = 45 \text{ kg m}^{-3}$ ). The effective volume fraction of the flocs,  $\Phi$ , is 0.0083 when the size of the flocs equals  $R_s$  (Eqn. 6.16). At this low volume fraction the sedimentation is hardly hindered and Stokes' law is applicable. Even if fractal aggregation results in a very low fractal dimensionality, e.g.  $D = 1.7$ , the radius of the clusters when they just fill the volume would be 24.5  $\mu\text{m}$  and thus larger than  $R_s = 8.7 \mu\text{m}$  (explanation 3). The rearrangements that would lead to a coarsening of the network, and thus to an apparently higher value of  $D$  would probably affect the fractal nature of the gel. Rearrangements after gel formation may lead to a stretching of the strands in the network, and a type 1 gel that has lost its fractal nature. This was not found in practice for the type 2 gels at low  $\phi_0$ .

Velocity gradients hinder settling and enhance the aggregation rate due to orthokinetic aggregation thus leaving less time for visible sedimentation to occur (explanation 4). The distance,  $y$ , over which flocs settle or cream during their growth from  $R_s$  to  $R_g$  may be calculated from



a combination of Eqn. 6.26 and 6.32 (numerical constants of order 1 are neglected):

$$y = \int v dt \approx \frac{\pi D g \Delta \rho a^{6-2D}}{18 \dot{\gamma} \phi_0 \eta} \int_{R_s}^{R_g} R^{2D-5} dR =$$

$$\frac{\pi D g \Delta \rho a^{6-2D}}{18(2D-4) \dot{\gamma} \phi_0 \eta} (R_g^{2D-4} - R_s^{2D-4}) \quad D \neq 2$$

$$\frac{\pi g \Delta \rho a^2}{9 \dot{\gamma} \phi_0 \eta} \ln \left( \frac{R_g}{R_s} \right) \quad D = 2$$

(7.1)

In the case of polystyrene particles ( $a = 35 \text{ nm}$ ,  $\phi_0 = 0.0002$ ,  $\Delta \rho = 45 \text{ kg m}^{-3}$ ,  $\eta = 1 \text{ mPa s}$ ) even a velocity gradient ( $\dot{\gamma}$ ) as small as  $0.1 \text{ s}^{-1}$  causes  $y$  to be only  $1.7 \text{ mm}$ . These calculations show the importance of small velocity gradients for gelation at very low volume fractions. In many practical situations the term 'orthokinetic aggregation' is used for the break up of a particle network due to mechanical disturbances.

Linear aggregation (explanation 5) would lead to an elastic modulus that is roughly proportional to  $\phi_0$  [2] and a pore size proportional to  $\phi_0^{-0.5}$  [3]. Because this is not found experimentally, directionality of the interactions and linear aggregation do probably not apply to the polystyrene and casein gels studied in this thesis.

The creaming velocity of flocs formed by agglutination of milk-fat globules ( $a \approx 2 \mu\text{m}$ ) in the cold has been studied by Troy and Sharp [4]. They plotted the velocity of the flocs as a function of their size and compared these data with calculations based on Stokes' law. Flocs were compared with spheres of the same size but with various densities corresponding to the volume fraction of the fat globules in the sphere (fig. 7.1). It was found that the rate of rising of the nearly spherical flocs roughly agrees with Stokes' law assuming, flocs containing 10 - 70% fat, the remainder being plasma. As shown in fig. 7.1, the fat globule concentration in the flocs decreased with increasing floc size, as expected for fractal flocs.

Recently Adachi and Kamiko [5] conducted similar experiments using uniform polystyrene spheres coagulated in a 3.5 M KCl solution, and a video camera connected to a microscope to measure the size and creaming velocity of the flocs. Individual flocs were rezeptized and the number of particles in the floc was counted in a hemocytometer [6]. The radius of the smallest sphere that circumscribes a floc,  $R_m$ , was obtained from the video images. The experimental creaming velocity,  $v_t$ , was found to be equal to  $v = 19.1 R_{m,t}^{1.40}$  and  $v = 16.2 R_{m,t}^{1.43}$  for  $a = 1010$  nm,  $\Delta\rho = 126$  kg m<sup>-3</sup>, and  $a = 465$  nm,  $\Delta\rho = 102$  kg m<sup>-3</sup>, respectively. Assuming fractal dimensionalities of 2.40 and 2.43 (cf. Eqn. 6.26) their results on the number of particles in a floc as a function of  $R_m$  can be fitted to  $N_p = (0.6R_m/a)^{2.40}$ , and  $(0.5R_m/a)^{2.43}$  for the 1010 and 465 nm particles, respectively.

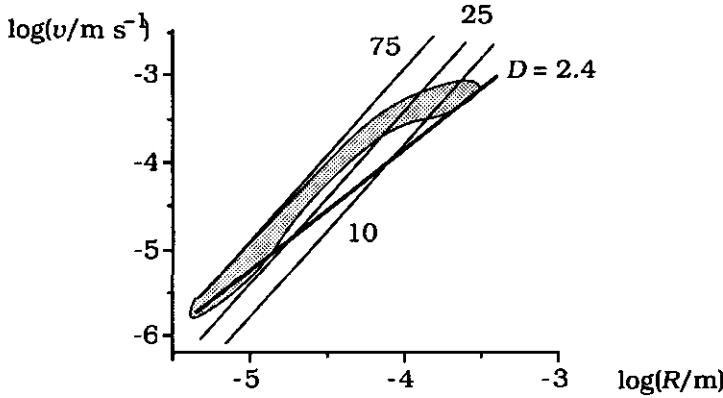


**Fig. 7.1** *Logarithm of the creaming velocity,  $v$ , of a floc of fat globules as a function of the radius of the floc,  $R$ . The lines are theoretical for spherical impenetrable flocs assuming 10, 25 and 75 % fat in the flocs and for fractal flocs of fractal dimensionality  $D = 2.4$ . The grey area gives the position of the experimental results by Troy and Sharp [4].*

Adachi and Kamiko [5] fitted their data to another equation in which they essentially assume fractal behaviour on all length scales between  $a$  and  $R_m$ :  $N_p = (R_m/a)^D$ . With this equation a fractal dimensionality of 2.20 was obtained. However, both equations fit the experimental results (fig. 7.2).

The creaming velocity can be estimated if we assume that  $R_h \propto R_m$ . For this purpose  $R_{h,t} = B^*R_{m,t}$  and  $F_t = N_{p,t} \frac{4}{3}\pi a^3 \Delta\rho g$  may be substituted in

Eqn. 6.24. For  $a = 465 \text{ nm}$ ,  $\Delta\rho = 102 \text{ kg m}^{-3}$ ,  $N_{p,i} = (0.5R_{m,i}/a)^{2.43}$  substitution leads to  $v = 10.1 (B^*)^{-1}R_m^{1.43}$ .  $B^*$  is the ratio between the hydrodynamic radius,  $R_h$ , and the smallest radius that circumscribes a floc  $R_m$ ;  $B^* = R_h/R_m$ . Comparison with the experimental results of Adachi and Kamiko results in  $B^* = 0.63$ .

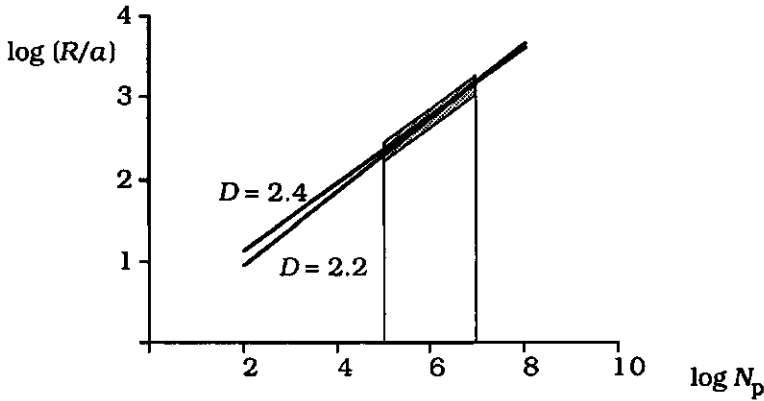


**Fig 7.2** Logarithm of the radius of a floc, i.e., the largest distance in a projected floc divided by 2, as a function of the logarithm of the number of primary particles in the floc. Both lines,  $N_p = (0.5R_m/a)^{2.43}$  and  $N_p = (R_m/a)^{2.2}$ , fit experimental results (grey area) of 465 nm particles over the range considered [5].

### 7.2.2 Collapse of the network under its own weight

After a gel is formed gravitational forces may lead to uniaxial compression of the network under its own weight causing visible segregation. The extent of the compression depends on the balance between the gravitational force exerted on the network,  $\phi_0\Delta\rho gh$ , and the product of the uniaxial compression modulus,  $E_y$ , and the effective strain  $\epsilon$  defined as  $\ln(h_0/h)$ , where  $h_0$  is the height that the sediment would approach in the absence of gravity. As most gels and sediments are viscoelastic to some extent and as  $\epsilon$  may be high,  $E_y$  depends on the strain  $\epsilon$  (non-linear behaviour) and on the time scale of the observation [7].

$$E_y(\epsilon, t)\epsilon(t) = \phi_0 \Delta \rho g h \quad (7.2)$$

As the compression may be to some extent irreversible - i.e., yielding occurs, leading to a decrease of what should be taken as  $h_0$  - the effective strain is also time dependent. The velocity of segregation depends on the time scale at which particle-particle bonds break (yielding), but also on the permeability of the network [7]. Slow segregation has been observed in the case of polystyrene latex and haematite sediments (section 4.1), the sediment volume decreasing over a wide time range. The segregation velocity decreased as a function of time, but even after 3 weeks segregation proceeded.

An important factor determining whether segregation occurs is adherence of the network to the wall of the container. Adherence reduces the effective value of  $h$  in Eqn. 7.2. If a gel is poured out of the container, the network is subjected to much larger stresses due to the weight of the entire gel, i.e. the network and the serum.

Particle networks have, by definition, a yield stress at all volume fractions, but it may be lower than the stress set up by gravity if the volume fraction is lower than a critical value; moreover, the yield stress is mostly smaller for longer time scales. Buscall et al. have shown that aggregated spherical polystyrene particles at volume fractions exceeding a critical value,  $\phi_g$ , of about 5 % develop a yield stress  $P_y$  below which viscoelasticity can be observed [8, 9]. Above the yield stress limited irreversible compression occurs [10]. However, the study of the rheological properties of polystyrene networks (section 5.4) shows that viscoelasticity can also be observed at volume fractions far below the  $\phi_g$  of Buscall et al. A reason for this discrepancy may be that casein and palmitate/polystyrene networks adhere strongly to the inner surface of the container. This drastically reduces the effective height,  $h$ , in Eqn. 7.2 and thus prevents segregation of the network. Probably the network would be irreversibly compressed under its own weight if no adherence occurred, i.e. the stress caused by gravity would be larger than the yield stress.

The shear modulus,  $G$ , may be related to the uniaxial compression modulus  $E_y$  as  $E_y = 2G$  (Eqn. 5.18). At  $\phi_0 = 0.01$  the palmitate-covered

polystyrene particle gels had a shear modulus of  $0.2 \text{ N m}^{-2}$  (fig. 5.21) and thus  $E_y = 0.4 \text{ N m}^{-2}$ . Assuming  $\Delta\rho$  to be  $50 \text{ kg m}^{-3}$ , the stress that is exerted on the network by its own weight,  $\phi_0\Delta\rho gh$  can be obtained for any value of  $h$ . The compression of the network under its own weight may be estimated using Eqn. 7.2. In a 1% polystyrene network with a total height of 8 cm the stress varies from 0 at the top to  $0.4 \text{ N m}^{-2}$  at the bottom of the gel. This would result in an average strain,  $\epsilon$ , of 0.5, and thus segregation leading to a 'gel layer' of about 5 cm and a supernatant layer of roughly 3 cm. Uniaxial deformation of the particle network may be the reason for the occurrence of stretched strands at volume fractions below 1 % as observed for the polystyrene gels measured in a floating disk rheometer in section 5.4.3. Because the gel is fixed to the floating disk (fig. 5.11), collapse of the entire network is impossible. The gravitational force may however stretch the strands that stick the network to the floating disk, and cause a higher volume fraction of particles closer to the bottom of the container. In practice  $\Delta\rho$  was probably smaller than  $50 \text{ kg m}^{-3}$  because of the palmitate layer on the polystyrene particles. This small density difference and a small value of the effective height,  $h$ , caused by adherence of the network to the wall of the container may be the reasons why these particles form networks at extremely low  $\phi_0$ .

### *7.2.3 Changes of the rheological properties of the gel due to mechanical disturbances*

In order to describe rearrangements of gel networks and flocs of colloidal particles in touching contact, it is useful to distinguish between junctions and bonds. The term junction denotes the sum of the bonds between two particles, while bond is used for each single interaction. An important difference between compression of a network under its own weight, causing visible segregation, and simple shear deformations is that the latter occur at a constant network volume. Compression of a network will result in the formation of numerous new junctions because the strands in the network become pressed together. In the case of deformation in shear the number of additional junctions will be smaller (section 5.4.4). Formation of additional junctions may cause irreversible compression without breaking of 'old' bonds. After release of the stress

the old bonds try to give the network its original shape whereas new junctions try to keep the gel in the shape it had when the stress was applied. The measurements discussed in section 5.4.4 show that junctions become stronger during ageing, the increase of the strength being relatively faster for fresh junctions. This implies that the irreversible part of the deformation increases with time. The balance between the tendency to recover the old shape, caused by old bonds and that to irreversible deformation, caused by new junctions, depends on the volume fraction (fig. 7.3): networks with a small volume fraction, and therefore large clusters, have a larger tendency to deform irreversibly than those with small clusters. The force that is exerted on a new junction by the tendency of the old strand to recover its original shape is proportional to the elastic constant of the strand,  $C_e$ , and thus to  $R_g^{-1}$  in the case of the model with curved strands, and proportional to  $R_g^{-2-x}$  for the model of Brown and Ball (Table 5.1).

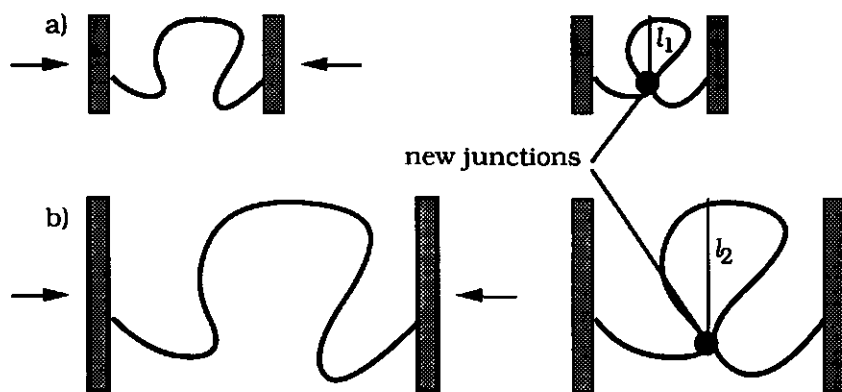


**Fig. 7.3** Schematic presentation of the compressive deformation of two strands. After release of the stress the old strands try to recover their original shape but the new junctions do hinder this. This causes a force on the new junction that is larger for small flocs (a) because  $l_1$  is smaller than  $l_2$ . The macroscopic strain,  $\epsilon$ , was similar in both cases.

The effect illustrated in fig. 7.3 may also be the reason for the dependency of the loss tangent,  $\tan \delta = G''/G'$ , on  $\phi_0$  in the case of type 2 gels, whereas it is independent of  $\phi_0$  in the case of type 1 gels (section

5.3.6 and 5.4.4). For both gel-types the number of new junctions that are formed due to a certain macroscopic deformation scales like  $R_g^{-2}$  because the number of stress-carrying strands per unit area in a cross-section perpendicular to the direction of the applied force scales like  $R_g^{-2}$ . However, the stiffness of the gel scales like  $R_g^{-2}$ , and  $R_g^{-3}$  in the case of type 1 and 2 gels, respectively. This implies that the dissipation of energy due to formation and breaking of new junctions and bonds, respectively the stiffness of the gel, have the same dependency on  $R_g$  (and thus on  $\phi_0$ ) in the case of type 1 gels. For these gels  $\tan \delta$  is roughly independent of  $\phi_0$ . In the case of type 2 gels, the formation and breaking of new junctions and bonds becomes relatively more important as the size of the clusters in the gel increases, and thus as  $\phi_0$  decreases. The dissipation of energy expressed as  $G''$  is therefore relatively high at low  $\phi_0$ . This causes the slope of the  $\log G'' - \log \phi_0$  plot to be less steep than the  $\log G' - \log \phi_0$  plot and thus  $\tan \delta$  to be a decreasing function of  $\phi_0$ .

Gels that were formed while a large oscillating deformation was applied had presumably relatively long stress carrying strands because only long strands have junctions which are aged, and thus strong. After decreasing the amplitude of the strain in these gels the storage modulus decreased. The energy dissipation, expressed in  $G''$ , was roughly similar for gels formed at small and large strain. This causes  $\tan \delta$  to be much higher in the case of gels formed at small strain (fig. 5.24). Probably, the long and tortuous 'old' strands provide little resistance against small deformations leading to a low storage modulus. The dissipation of energy depends on the number of bonds that relax due to the applied deformation. This number was apparently roughly independent of the strain history of the gel. After decreasing the amplitude of the strain in gels that are formed while a large oscillating deformation is applied there are several new junctions formed due to the deformations, convection currents and heat movement of the strands. These new junctions shorten the stress carrying strands but they are still weak and break easily. This is presumably the reason why  $G'$  increases strongly at a large strain where the aged, strong strands become stretched (fig. 5.24).

### 7.3 Velocity gradients

In section 7.2 is illustrated that small velocity gradients may hinder settling or creaming of flocs and thereby promote gelation. However, larger velocity gradients may also hinder gelation. The force exerted on the flocs due to velocity gradients may rearrange them into more compact structures or cause the floc to break up. Rearrangement into compact flocs in the case of a flow field has been reported for various practical situations (e.g. [11 - 13]). Because the force exerted on a cluster is of the order of  $\dot{\gamma}\eta R_h^2$ , rearrangement occurs on length scales that exceed a certain critical value, dependent on the strength of the floc and on  $\dot{\gamma}\eta$ . Rearrangement may be restricted to a change of the conformation of rigid clusters due to rotation with respect to each other. After collision this will lead to the formation of more junctions between the two flocs. This situation has been simulated on a computer [14] and with table-tennis balls [6] and an increase of the fractal dimensionality to about 2.2 - 2.3 is found. But, in many situations rearrangement is not limited to rotation or rolling of rigid clusters with respect to each other and the whole floc may be forced into an almost homogeneous structure ( $D = 2.8$  [13]). Denser flocs, i.e., flocs with a higher fractal dimensionality, have a smaller probability to form a gel network because they settle or cream faster ( $v \propto R^D$ , Eqn. 6.26), they grow slower ( $t_c \propto D/(3-D)$ , Eqn. 6.32a) and they have to grow larger in order to form a gel network (Eqn. 2.6).

In addition to rearrangements, break up of the flocs may occur. Torres et al. [15] obtained fractal flocs with a dimensionality of 1.8 with polystyrene particles in a simple shear field. The force exerted on the flocs did not cause rearrangement, but break up after the flocs reached a critical size (Eqn. 6.40). Whether rearrangement or break up occurs depends presumably on the properties of the bonds between the particles. The resistance of bonds against deformation due to forces normal to the surface, causing break up, may be different from that against lateral forces causing rolling, slipping and rotation and thereby rearrangement. The radius of the flocs at the gel point,  $R_g$ , and thus  $\phi_0$ , and the maximum radius that a floc can obtain at a certain shear rate,  $R_1$  (Eqn. 6.40), may be important. Three different situations may be distinguished: 1) If  $R_1 > R_g$  the flocs form a network that may bend or



break due to the mechanical disturbances (fracture mechanics). 2) If  $R_1 \approx R_g$  rearrangements may lead to denser flocs and an increase of  $D$  because a high effective volume fraction of the flocs results necessarily to compression (fig. 7.4b), whereas 3) only break up may occur if  $R_1 < R_g$  because flocs have the opportunity to rotate around each other without being compressed too much (fig. 7.4a). In addition to the volume fraction of the particles and their interactions the nature of the velocity gradients is important. An elongational flow field favours break up, whereas simple shear may favour rearrangements.

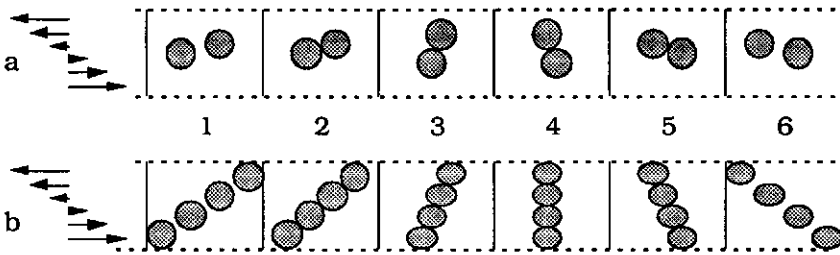


**Fig. 7.4** Schematic picture of possible effects of simple shear on the floc structure. a)  $R_1 < R_g$ , flocs with radius  $R_1$  approach each other due to the flow field (1,2), they stick and rotate around each other (2-5), and disrupt again (6). b)  $R_1 \approx R_g$ , Flocs approach and form a connection, i.e. a network, (1,2), the network is disturbed (2-5), resulting in denser, compressed flocs (6).

After a gel has been formed macroscopic velocity gradients, i.e. gradients that persist over a length scale larger than the size of the pores in the gel, become impossible without disruption of the gel; the gel may bend or break. The break up of gel and flocs cause the shear thinning behaviour of strongly aggregated systems. An increase of the shear rate results in more break up, smaller clusters and thereby a lower effective volume fraction and viscosity. Shear thinning behaviour might be quantified using a fractal model because both the strength of individual flocs and their effective volume fraction in the dispersion can be related to the floc size. After being disrupted, the flocs may gel again, but the structure of the new gel is found to be more coarse which implies that the flocs have been rearranged (section 4.1.2). Often the flocs are so dense that they settle or cream rather than gel after disruption of the gel.

The intensity of the velocity gradients and the stiffness of the gel determine the extent of the rearrangement of the flocs. Gels of 35 nm polystyrene particles could be broken up into flocs that showed shear thinning behaviour at volume fractions below roughly 10 % if they were stirred violently. At higher  $\phi_0$  the gel was not broken up into individual flocs but in granules containing a homogeneous part of the gel, and thus many flocs. ( $R_g \approx 620$  nm if  $\phi_0$  is 10 %)

## 7.4 Rearrangements

### 7.4.1 Rearrangement of clusters of colloidal particles

A ramified floc is thermodynamically unstable because many more junctions and bonds can be formed if the particles would assume a denser packing. In order to become more closely packed, junctions have to be broken or lateral movement of particles along each others surface has to occur. Lateral movement causes breaking of bonds on one side of the junction, and formation of new bonds on the other side. If the junctions between the particles are strong and stiff because they consist of several bonds, junction breaking or lateral movement may require several  $kT$  units and is therefore unlikely (without applying external forces). A high activation free energy for disaggregation or rearrangement does not imply that these processes never occur since the rate constant for disaggregation,  $k' = \nu_b \exp(-V_b/kT)$ , also contains a frequency factor,  $\nu_b$ . The highest possible frequency factor is the natural frequency,  $kT/h_P$  ( $\approx 6 \times 10^{12} \text{ s}^{-1}$ ), where  $h_P$  is Planck's constant. In the case of colloidal particles,  $\nu_b$  will be much lower than the natural frequency, but it may still be high and the activation free energy for junction breakage should be many times  $kT$  to prevent disaggregation on a short time scale. Ramified flocs may thus be meta-stable, i.e., the time scale of rearrangement due to thermal motion may be extremely long if  $V_b \gg kT$ .

Colloidal dispersions are known to exhibit a variety of apparent phases and phase transitions, resembling those observed in pure atomic or molecular systems. Adhesive hard spheres may assume a closest packed ordering in a crystalline phase and exhibit melting and freezing behaviour [16]. But in most practical situations, colloidal particles behave

differently from atoms or small molecules; in the presence of attractive interactions, they aggregate into more or less ramified flocs which may form a gel. The most obvious difference between molecular and colloidal systems is the size of the particles. Since the entropical part of the Gibbs energy due to translation of any particle equals  $\frac{3}{2}kT$  whereas the interaction energy is proportional to the size of the particles (Deryagin approximation [17]), colloidal particles are more static. In most situations, the depth of the primary Gibbs energy minimum of aggregating colloidal particles attains a value of many  $kT$  units and it becomes deeper as the particle size is larger. This means that disaggregation due to Brownian motion becomes ever more unlikely as the particles become larger.

Another important difference between small molecules and colloidal particles is that the range,  $\Delta_i$ , of the interaction forces relative to the particle size  $a$ , is relatively much larger for the former ( $\Delta_i/a \gg 1$ ) than for the latter ( $\Delta_i/a \approx 10^{-2}$ ). Ideally, e.g. in the DLVO theory, the Gibbs energy of two interacting particles changes only if their mutual distance changes; lateral movement by slipping, rolling or rotation is unrestricted. In practice this may be the case for homogeneous spherical particles if the separation between the edges of the particles that are aggregated into a Gibbs energy minimum,  $H_0$ , is sufficiently large. However, the length scale of irregularities on the surface of a colloidal particle is usually larger than this separation, especially in the case of primary minimum aggregation. This hinders lateral movement of the particles with respect to each other and thus rearrangement of flocs. For a particular system, the resistances against lateral and normal movements are presumably coupled, but among various systems large variation in the ratio between both resistances may occur, depending on the surface roughness, the deformability of the particles and  $H_0$ .

If the activation free energy for disaggregation,  $V_b$ , or for lateral movement,  $V_l$ , is small, the flocs will rearrange into densely packed aggregates. If the primary particles are large this will soon lead to sedimentation rather than gelation, unless the volume fraction is so high as to cause aggregation being fast compared to the rate of rearrangement. The latter rate decreases during the aggregation process: This is because lateral movement and rearrangement lead to a high coordination number,

i.e., number of junctions per particle, and dense flocs (as long as they are small). Further aggregation of these dense flocs results in larger flocs in which the small flocs are connected by several junctions. Rearrangement on a longer length scale and break up are thus unlikely and large flocs will thus be ramified; they have a dimensionality of about 2.2 according to the models of Meakin [14] and Adachi and Ooi [6]. The strength and stiffness of the connection between two clusters increases as a function of time because more and more junctions are formed. Rearrangement may result in an increase of the lower cut-off length (fig. 7.5), and in gels with strands that are several particles thick. The formation of a rennet-induced skim-milk gel from paracasein micelles occurs in such a way, leading to strands that are one to four micelles thick. Usually, large dense flocs will settle too fast for gelation to occur. For example, the experimental results of Troy and Sharp [4] for flocs of milk fat globules (average radius about  $2\ \mu\text{m}$ ) show dense flocs containing roughly 50 % fat globules until their radius is about  $100\ \mu\text{m}$ . Larger flocs became more open, containing less than 10 % fat globules for flocs with a radius of  $350\ \mu\text{m}$ .

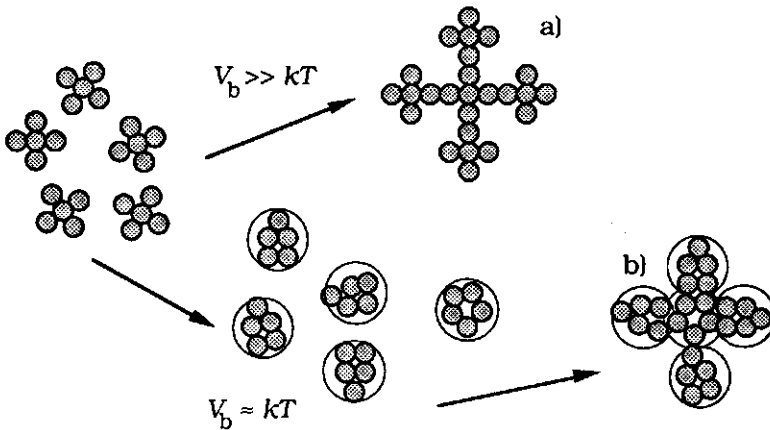


**Fig. 7.5** Schematic presentation of the increase of the lower cut-off length, of two-dimensional flocs due to rearrangement in the first stage of aggregation. For both flocs the fractal dimensionality,  $D$ , is  $(\log 5)/(\log 3)$  but floc b) has a larger lower cut-off length and is therefore more dense.

The activation free energy for disaggregation of flocs increases as a function of time due to two processes: 1) an increase in the strength of the junctions between the particles due to an increase in the number of bonds, e.g. due to some kind of sintering, and 2) an increase in the number of junctions, caused by rearrangement. The geometric structure of the aggregates is determined by the relative contribution of these effects to the increase of the activation free energy for disaggregation of flocs, and by the aggregation rate. Fast aggregation and some kind of sintering results in ramified flocs. Increase of the strength of flocs in a gel is observed experimentally in chapter V via the increase of the modulus of a gel with ageing time. The effect is shown more directly by Frens and Overbeek, [18, 19], who found rezeptization to become less complete for aged flocs of AgI particles.

In general, slow aggregation results in dense, settling flocs rather than a gel. The flocs are more dense because of the reaction limited aggregation process (section 2.2), but also because slow aggregation allows the flocs a longer time to rearrange. Rather ramified flocs may be formed by slow aggregation if rearrangement is hindered. Slow aggregation occurs if the activation free energy for aggregation,  $V_a$ , is high but the activation free energy for junction breaking or rearrangement may also be high (fig. 6.15). Particles with a heterogeneous surface displaying only a few reactive areas form ramified flocs because rearrangement is hindered. Frens argued that in the case of slow coagulation of lyophobic particles by mono-valent counterions rearrangements of a floc may be strongly hindered due to the high potential energy barrier caused by electrostatic repulsion [20]. At these conditions the flocs may be even more open than in the case of rapid aggregation and a gel can easily be formed at low particle concentrations. In the case of higher counter-ion valencies and slow aggregation the repulsion is weaker, but of a longer range. The weaker repulsion offers less resistance against rearrangement and slow coagulation by polyvalent counterions led to denser flocs with a high coordination number [20].

Rapid aggregation may lead to ramified flocs because of a diffusion-limited aggregation mechanism and rapid growth of the flocs allowing little time for rearrangement. Diffusion limited aggregation is, however, no guaranty for tenuous flocs to form. Polystyrene and haematite sols had

a relatively low sediment volume at the critical coagulation concentration, and a turbidity plateau that attained a relatively high maximum. This indicates rather dense flocs, in spite of the aggregation being diffusion-limited. At higher (mono-valent) salt concentrations the sediment volume increased and the turbidity maximum decreased (section 4.1), indicating more ramified flocs. The reason why flocs become more open at higher  $c_s$  is probably an increase in stiffness of the junctions as a function of the salt concentration. Stiffer junctions lead to less rearrangements and thus to more ramified flocs. Stiff junctions occur if the (van der Waals) attraction between the surfaces of the particles is high, if the particles are soft and deformable thus causing a large contact area [1], or if some kind of sintering or fusion occurs. The latter two factors apply probably to the palmitate covered polystyrene, and to the casein gels studied in this thesis. Palmitate and casein molecules may dissolve and condensate in the gap between the particles.

Bridging flocculation due to adsorbing macromolecules may lead to several polymer loops and tails (bonds) forming junctions between the particles. The free activation energy for disaggregation is thus presumably high, but some lateral movement may occur since  $\Delta$  is relatively large. This leads to a high coordination number and dense flocs as long as they are small. Rearrangement on a longer length scale is unlikely and large flocs may be ramified and have, again, a fractal dimensionality of about 2.2 [6, 14]. Measurements of the sediment volume of flocculated (bridging) and coagulated silver iodide sols [21] showed that of the former to remain almost constant during 500 h. This may be due to rapid small scale rearrangements followed by very slow rearrangement on long length scales. The sediment volume of the coagulated AgI, on the contrary, was initially higher, presumably because small scale rearrangements are slower in this case. Here the sediment volume decreased over the whole time span (500 h).

#### 7.4.2 Rearrangements after gelation, (micro-) syneresis

At the moment that the flocs occupy the total available volume a gel is formed. This is however not the end of the aggregation and rearrangement process; at the gel point the gel is still very weak and disaggregation and rearrangements may still occur. Rearrangements, and ageing of the junctions, increase the activation free energy for disaggregation of flocs and thereby decrease the rate of further rearrangements. This results in an increasing stiffness and a decreasing ratio between the loss,  $G''$ , and the storage,  $G'$ , modulus ( $\tan \delta$ ), of particle gels as a function of time. Gels of very small particles that are formed by rapid aggregation may still be very dynamic, i.e., subject to rearrangement due to thermal motion, because the flocs may not have had enough time to rearrange into a (meta-) stable conformation before the gel point. However, for gels of colloidal particles the ageing is mainly due to an increase of the number of bonds per junction. Rearrangement due to thermal motion now becomes unlikely because many bonds have to break simultaneously for breaking or rearrangement of a junction to occur [22]. This is confirmed by permeability measurements showing a constant permeability coefficient, whereas the modulus increases with time (chapters IV and V). Particle gels have in general an enthalpic nature (chapter I), i.e., deformations lead mainly to enthalpic changes (e.g. to extension of atomic or physical bonds). This implies that many properties that characterize the entropic nature of polymer gels do not apply to particle gels; the modulus of particle gels is not proportional to  $kT$  (rubber theory), and they never swell and show, in general, no endogenous syneresis. Disturbance of a particle gel by (gravitational) forces or velocity gradients may lead to an irreversible shrinkage of the network (syneresis).

Rennet-induced casein gels are particle gels [23], but nevertheless show endogenous syneresis. This phenomenon has received much attention. Van Dijk et al. [24 - 26] developed a model based on the transport of whey inside the gel. The model enabled the endogenous syneresis pressure to be estimated from the velocity of one-dimensional syneresis, and the permeability of the gel. They also described a possible mechanism of syneresis. After the gel is formed, those parts of the

particle surfaces that are not in contact with each other are still reactive. By Brownian motion or deformation these areas may locally approach each other and stick, thus causing a higher stress in the strands leading to a syneresis pressure. This results in shrinkage of the gel, or, if shrinkage is impossible because the network is fixed to the walls of the container, to local condensation of the network and formation of wider pores elsewhere. The latter process is called microsineresis and may create the stretched strands of type 1 gels. Extensive microsineresis may occur if strands in the gel can break due to the internal stress in the gel network. This resulted in the considerable increase of the permeability and pore size during ageing which was found for rennet-induced casein gels (chapter IV). Microsineresis may also occur if the liquid cannot be expelled because it has to move over a long distance through a gel network with a low permeability.

Rearrangements on long length scales caused by thermal motion are unlikely in the case of (enthalpic) particle gels. The reason for the endogenous syneresis must probably be sought on a shorter length scale than that of the paracasein micelles, i.e., that of the casein molecules or that of submicelles. Paracasein micelles fuse during ageing; gradually more protein-protein bonds are formed in each junction between the particles [23, 27]. Fusion must lead to rearrangements inside the paracasein micelle. Probably, little resistance exists against lateral movement of the submicelles (or casein molecules) inside the paracasein. Fusion of the micelles, and a zipperlike cross-linking of the strands [24, 25] cause the endogenous syneresis. Two different mechanisms that cause an increase in the number of bonds per junction are illustrated in fig. 7.6. A kind of sintering occurs if molecules condensate preferentially in the gap between the particles thus causing an increase of the contact region. This mechanism resembles Ostwald ripening of particles and may cause an increase in stiffness of networks like those of hematite or AgI particles during ageing. If the particles are to some extent visco-elastic another mechanism which resembles coalescence of particles may occur (fig. 7.6b). This mechanism may cause shrinkage of the strands. In the case of casein gels both mechanisms may occur simultaneous.



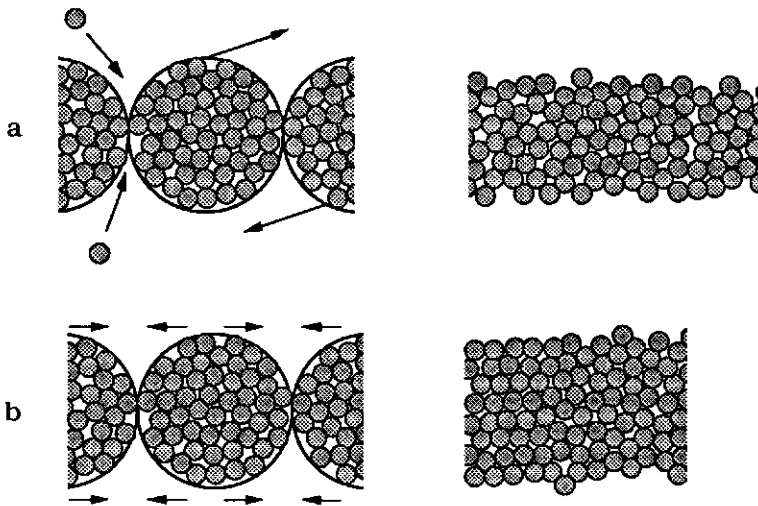


**Fig. 7.6** Mechanisms causing an increase of the number of bonds per junction. a) Small particles (or molecules) dissolve and condensate preferentially in the gap between the particles. b) Little resistance against lateral movement of the small particles or molecules exists and rearrangements inside the large particles enable the formation of new bonds. These new bonds close the gap between the particles in a zipperlike way and may cause shrinkage of the strand.

Fusion occurs presumably relatively faster for small particles than for larger ones. This may be the reason why small particles form often stronger and stiffer gels after a certain ageing time (cf. fig 5.21). The solubility of the material of the particles and their viscoelastic properties determine the course of the curve of the shear modulus as a function of ageing time. If the solubility is high the ageing occurs presumably faster and the modulus of the gel will increase more rapidly. In the case of viscoelastic particles the increase of the contact area of the junctions will lead to some kind of flow inside the particles. The rate of growth of the junction zone is thus also dependent on the apparent viscosity of the material inside the particles and thus on the relaxation spectrum of the bonds.

Recently the rheological properties of casein gels have been related to syneresis [22]. It has been shown that low fracture stresses and high  $\tan \delta$  correlate with an increased tendency to exhibit syneresis. This tendency may be expressed as the rate of change of the permeability [25].

(section 4.2). Results are shown in table 7.1. An essential feature for syneresis of particle gels may be the possibility of lateral movement of molecules or 'subparticles' along each others surface due to thermal motion (fig. 7.6b). This possibility enables some kind of flow and leads to a short relaxation time of the bonds and thus to a high  $\tan \delta$  and a low fracture stress.

Lateral movement of the submicelles or casein molecules along each others surfaces is presumably easier as the temperature is higher in rennet-induced casein gels. A small resistance against lateral movement leads to fast fusion, and thus to a shorter time after which  $G'$  attains its maximum value. At 20 °C lateral movement due to thermal motion may become almost impossible and fusion is thus slow. Microsyneresis hardly occurs at this condition and  $\tan \delta$  is relatively low.

pH of the gel	6.65	6.65	6.65	6.65	4.60
temperature (°C)	20	25	30	35	30
$\frac{dB}{dt}$ (nm <sup>2</sup> s <sup>-1</sup> )	0	5	19	55	0
$\tan \delta$ ( $\omega = 0.05$ rad s <sup>-1</sup> )	0.30	0.40	0.47	0.56	0.25
Ageing time after which $G'$ attains maximum (h)	>100	~50	~9	~5	>170

**Table 7.1** Rate of change of the permeability coefficient ( $dB/dt$ ) and the relaxation behaviour of the bonds in rennet-induced casein gels and in an acid casein gel of pH 4.6. Data from [28, 29].

The possibility of lateral movements has also a clear effect on the fracture behaviour of the gels. Acid casein gels fractured at a constant strain,  $\gamma_f$  being roughly 0.6 and 1.2 for type 1 and 2 gels, respectively. The strain at which fracture occurred was independent of the stress that had been applied (fig. 5.10). For rennet induced gels  $\gamma_f$  was higher, and increased as the stress decreased,  $\sigma_f = 30$  N m<sup>-2</sup> provided  $\gamma_f = 2.8$  after 600 s, whereas  $\sigma_f = 160$  N m<sup>-2</sup> resulted in  $\gamma_f = 1.3$  within 1 s [22]. Lateral movement of the particles enables the formation of new bonds which are, at least momentarily, stress free. This process will cause a slow yielding of

the strand as depicted in fig. 7.7. If lateral movement due to thermal motion is hindered, or if the deformation is so fast that there is not enough time for lateral movement, the submicelles or casein molecules have no opportunity to form new bonds and the gel fractures at a relatively small strain that is independent of the applied stress. This was found for the acid casein gels in which lateral movement due to thermal motion of the submicelles or casein molecules may thus be restricted. Also in the case of rennet-induced casein gels at 20 °C lateral movement is expected to be restricted. The deformation at which fracture occurs is therefore expected to be independent of the applied stress for these gels. It would be interesting to check this.

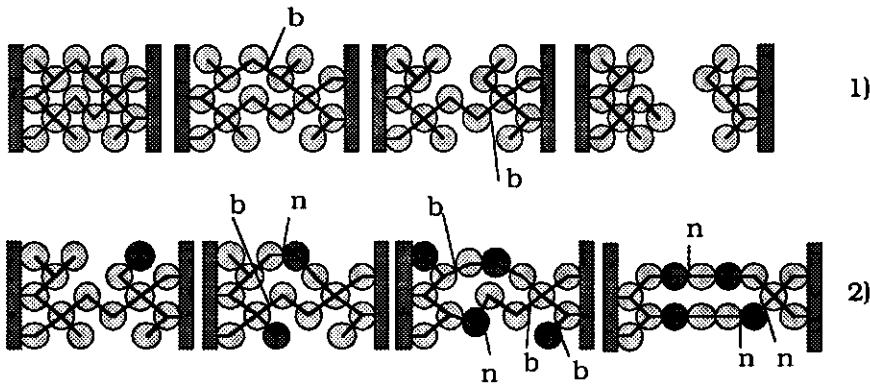


**Fig. 7.7** Schematic representation of the elongation and fracture of a junction between casein particles. 1) Acid casein gels: lateral movement of the submicelles is hindered, 2) rennet induced gels, the strand slowly yields due to new bonds formed after lateral movement of the submicelles. b indicates a bond that will break and n a newly formed bond. Submicelles that have rearrange(d) are dark grey.

All systems studied in this thesis that gel at low volume fraction show probably some sintering or fusion which may be described as an increase in the number of bonds per junction. This may be a prerequisite for aggregation of colloidal particles leading to a gel at low  $\phi_0$ .

## 7.6 References

- 1 J.N. Israelachvili, *Intermolecular and Surface Forces* (Academic Press, London, 1985)
- 2 C.J. Nederveen, *J. Colloid Sci.*, 1963, **18**, 276
- 3 M.P. Tombs, *Faraday Discussions of the Chemical Society*, 1974, **57**, 158
- 4 H.C. Troy and P.F. Sharp, *J. Dairy Sci.* 1928, **11**, 189
- 5 Y. Adachi and M. Kamiko, *Proc. World Congress of Chem. Eng.*, Karlsruhe, 1991
- 6 Y. Adachi and S. Ooi, *J. Coll. Int. Sci.* 1990, **135**, 375
- 7 T. van Vliet and P. Walstra, in *Food Colloids*, eds. R.D. Bee, P. Richmond and J. Mingins (Royal Soc. of Chem., Cambridge, 1989)
- 8 R. Buscall, P.D.A. Mills and G.E. Yates, *Colloids and Surfaces*, 1986, **18**, 341
- 9 R. Buscall, I.J. McGowan, P.D.A. Mills, R.F. Stewart, D. Sutton and G.E. Yates, *J. Non-Newtonian Fluid Mech.*, 1987, **24**, 183
- 10 R. Buscall and R. White, *J. Chem. Soc. Faraday Trans. 1*, 1987, **83**, 873
- 11 R.C. Sonntag and W.B. Russel, *J. Colloid Interface Sci.*, 1986, **113**, 399
- 12 M.Y. Lin, R. Klein, H.M. Lindsay, D.A. Weitz, R.C. Ball and P. Meakin, *J. Colloid Interface Sci.*, 1990, **137**, 263
- 13 L.L. Hoekstra, R. Vreeker and W.G.M. Agterof, *J. Coll. Int. Sci.*, submitted
- 14 P. Meakin, *Adv. in Colloid and Int. Sci.*, 1988, **28**, 249
- 15 F.E. Torres, W.B. Russel and W.R. Schowalter, *J. Colloid Interface Sci.*, 1991, **142**, 554
- 16 P.W. Rouw, *PhD. Thesis*, Utrecht University, The Netherlands, 1988
- 17 B.V. Deryagin, *Kolloid Z.*, 1934, **69**, 155
- 18 G. Frens and J.Th.G. Overbeek, *J. Coll. Int. Sci.*, 1971, **36**, 286
- 19 G. Frens and J.Th.G. Overbeek, *J. Coll. Int. Sci.*, 1972, **38**, 376
- 20 G. Frens, *Faraday Disc. Chem. Soc.*, 1990, **90**, 143
- 21 G.J. Fleer, *PhD. Thesis*, Wageningen Agricultural University, The Netherlands, 1971
- 22 T. van Vliet, H.J.M. van Dijk, P. Zoon and P. Walstra, *Colloid Polym. Sci.*, 1991, **269**, 620
- 23 P. Walstra and T. van Vliet, *Neth. Milk Dairy J.*, 1986, **40**, 241
- 24 P. Walstra, H.J.M. van Dijk and T.J. Geurts, *Neth. Milk Dairy J.*, 1985, **39**, 209
- 25 H.J.M. van Dijk and P. Walstra, *Neth. Milk Dairy J.*, 1986, **40**, 3
- 26 H.J.M. van Dijk and P. Walstra and J. Schenk, *Chem. Eng. J.*, 1984, **28**, B43
- 27 P. Zoon, T. van Vliet and P. Walstra, *Neth. Milk Dairy J.*, 1988, **42**, 241
- 28 P. Zoon, T. van Vliet and P. Walstra, *Neth. Milk Dairy J.*, 1988, **42**, 271
- 29 H.J.C.M. van den Bijgaart, *PhD. Thesis*, Wageningen Agricultural University, The Netherlands, 1988

## VIII General Reflections and Suggestions for Further Research

Although the work described in this thesis contributes to the understanding of the formation of a gel network from colloidal particles, it does not give a definite answer to the question why some systems gel and others precipitate. The lack of knowledge relates mainly to the field of interactions between the particles. Interactions may prevent rearrangement of the flocs which may be a result of lateral movement of the primary particles with respect to each other, or of disaggregation of the flocs. The possibility for lateral movement disaggregation varies widely among different colloidal systems. Rearrangements, and thus normal and lateral interaction forces, are very important for the geometric structure of the flocs. Moreover, the resistance against uniaxial compression of the gel under its own weight is dependent on the interaction forces. In order to predict whether a particular system will gel or not, knowledge on the interaction forces, both normal and lateral to the surface is required.

Colloidal systems in which the activation free energy for lateral movement of particles with respect to each other is low compared to  $kT$  resemble molecular liquids. The syneresis pressure in rennet-induced skim-milk gels may be considered to be caused by a phenomenon analogous to surface tension in a molecular system. The magnitude of this 'surface tension' is determined by the normal interaction forces, i.e., the 'stickiness' of the submicelles. An order of magnitude estimation of the 'surface tension',  $\gamma_s$ , may be obtained from the endogenous syneresis pressure,  $P_s$ , of the skim-milk gels which is of order  $1 \text{ N m}^{-2}$  [1]. The length of the stress carrying strands that cause the endogenous syneresis pressure,  $N$ , is about  $10^{13} \text{ m per m}^3$  for these gels. In an isotropic system the syneresis pressure can be calculated with the same kind of model as used for the Young modulus in section 5.2.3. The energy involved in the creation of a larger surface area due to extension of the strands over a distance  $\Delta L$  is roughly  $2\pi a \Delta L \gamma_s$ , where  $a$ , the radius of the strands is roughly  $70 \text{ nm}$ . The energy involved in a macroscopic uniaxial syneresis deformation,  $\epsilon$ , is  $\epsilon P_s V$  or  $\epsilon P_s L/N$ , analogous to Eqn. 5.3. Because  $\epsilon P_s L/N =$

$2\pi a\Delta L\gamma_s$  the apparent surface tension may be related to the syneresis pressure leading to (Eqn. 5.17)

$$\gamma_s = \frac{\epsilon L}{\Delta L} \frac{P_s}{N2\pi a} = \frac{\pi}{4 - \pi} \frac{P_s}{N2\pi a} \quad (8.1)$$

substitution of the values for rennet-induced skim-milk gels yields  $\gamma_s \approx 0.8 \mu\text{N m}^{-1}$ . The contribution of each individual submicelle to the surface free energy is expected to be of the order of  $kT$ . This implies a surface area of roughly  $kT/\gamma_s \approx 5 \times 10^{-15} \text{ m}^2$  per submicelle, and thus a diameter of roughly 70 nm which is higher than expected; submicelles have a size of 10 to 20 nm [2].

In this thesis, the geometric structure of casein gels was investigated by confocal scanning laser microscopy. A problem with casein is that the particles are polydisperse, too small to be observed individually, and that they may swell and shrink and thus have an uncertain volume fraction. A better picture of the geometry of fractal gels may be obtained by using monodisperse polystyrene particles that are larger than the resolution limit of the microscope. This may enable to elucidate the structure of the network and provide information about length scales smaller than the resolution of the microscope, because the particles are spherical and connected and because their size and volume fraction are known. Consequently, permeability, rheological properties, and light scattering could be predicted directly from the image. Especially for studying the permeability, 3-dimensional analysis of the gel is necessary. Values found for the permeability (chapter IV) are at least ten times smaller than expected on the basis of present ideas of the ratio between the hydrodynamic radius and the radius of gyration of clusters. This may be due to insufficiencies in the theory, but also to the larger holes in the gel being cavities rather than pores. It is impossible to distinguish between cavities and pores in a 2-dimensional image. For instance, a foam looks highly permeable in a cross-section.

Also the ageing of gels may be studied by CSLM. Permeability measurements could only be performed after the gels were aged for some time. Especially during the period between the gelpoint and the time at which the gel geometry could be studied by permeability, large changes

may be expected. The microsineresis of rennet-induced gels may be studied 'live'. The gels in fig. 4.5 were aged at 30 °C, and observed at room temperature where no syneresis occurred. It would be interesting to observe microsineresis directly, i.e. in a fresh gel at 30 °C.

## References

- 1 T. van Vliet, H.J.M. van Dijk, P. Zoon and P. Walstra, *Colloid Polym. Sci.*, 1991, **269**, 620
- 2 P. Walstra and R. Jenness, *Dairy chemistry and physics*, John Wiley & Sons, New York, 1984

## List of symbols

$a$	radius of the primary particles	m
$A$	numerical factor in Eqn. 6.5	-
$A_c$	pore size area of the gel	m <sup>2</sup>
$A_H$	Hamaker constant	J
$B$	ratio between the collision and the hydrodynamic radius of the clusters; $B = R_c/R_h$	-
$B^*$	$R_h/R_m$	-
$B_p$	permeability coefficient	m <sup>2</sup>
$c$	total number concentration of aggregates and single particles	m <sup>-3</sup>
$c_0$	initial number concentration of primary particles	m <sup>-3</sup>
$c_k$	number concentration of clusters containing $k$ primary particles	m <sup>-3</sup>
$c_v$	number concentration of primary particles inside a cluster	m <sup>-3</sup>
$c_s$	salt concentration	mol l <sup>-1</sup>
$\dot{c}$	aggregation rate, $dc/dt$	m <sup>-3</sup> s <sup>-1</sup>
$C$	mass concentration	kg m <sup>-3</sup>
$C$	chapter V, characteristic length relating the deformation of the strands in the gel to the macroscopic shear strain, $\gamma$	m
$C$	chapter VI, numerical factor in Eqn. 6.19	-
$C_e$	elastic constant of a strand	N m <sup>-1</sup>
$C(r)$	density-density correlation function (Eqn. 2.13)	-
$D$	fractal dimensionality	-
$D_2$	fractal dimensionality of a cross section through a fractal aggregate	-
$D_e$	diffusion coefficient	m <sup>2</sup> s <sup>-1</sup>
$D_i$	diffusion coefficient of a cluster containing $i$ primary particles	m <sup>2</sup> s <sup>-1</sup>
$D_r^s$	diffusion coefficient of two particles relative to each other at a relative separation $s$	m <sup>2</sup> s <sup>-1</sup>
$D_r^\infty$	diffusion coefficient of two particles relative to each other at a relative separation $\infty$ , $D_r^\infty = 2 D_e$	m <sup>2</sup> s <sup>-1</sup>
$E$	section 5.2.2 amount of energy	J
$E$	Young modulus	N m <sup>-2</sup>
$f$	chapter V, force exerted on a strand in the gel	N
$F$	chapter V, force exerted on a gel	N
$F$	ratio between the resistance experienced by an impermeable and a permeable sphere	-
$g$	acceleration due to gravity	m s <sup>-2</sup>
$g(r)$	radial distribution function of the particles in a floc	-
$G$	shear modulus, $\sigma/\gamma$	N m <sup>-2</sup>



$G'$	storage modulus	$N\ m^{-2}$
$G''$	loss modulus	$N\ m^{-2}$
$h$	separation between the edges of 2 particles (fig. 6.2)	$m$
$h_P$	Planck constant ( $6.626 \cdot 10^{-34}$ )	$N\ m\ s$
$h(r)$	cut-off function	-
$H$	optical constant in Eqn. 2.20	$kg^{-2}mol^{-1}m^{-2}$
$H_0$	inter-particle distance at which attractive and repulsive forces are cancelled out	$m$
$I$	intensity of the transmitted beam	$W\ m^{-2}$
$I_0$	intensity of the incident beam	$W\ m^{-2}$
$i, j, k$	the number of primary particles, or a subscript referring to that number	-
$k$	Boltzmann constant ( $1.381 \cdot 10^{-23}$ )	$J\ K^{-1}$
$k'$	rate constant for disruption of clusters	$s^{-1}$
$K$	numerical constant in eqn. 2.11	-
$K_6$	numerical constant in eqn. 6.36	-
$K_{ij}$	reaction kernel for the aggregation of clusters containing $i$ and $j$ primary particles	$m^3\ s^{-1}$
$l$	(optical) path length through the gel	$m$
$L$	length of a cubic or square part of the gel	$m$
$L$	chapter V, length of a stress carrying strand	$m$
$M_w$	molecular weight	$kg/mol$
$n_0$	refractive index of the medium	-
$n_{i,L}$	number of particles in a square or cube of gel with edge length $L$	-
$N$	length of the stress carrying strands per unit volume	$m^{-2}$
$N_a$	total number of lattice sites taken up by a fractal floc	-
$N_A$	Avogadro's number ( $6.022 \cdot 10^{23}$ )	$mol^{-1}$
$N_p$	number of lattice sites that contain a particle	-
$N_t$	total number of lattice sites in the gel	-
$p$	characteristic pore radius	$m$
$P$	numerical factor affected by the polydispersity $P$ is the average value of $(R_i + R_j)(R_i^{-1} + R_j^{-1})$	-
$P_s$	endogenous syneresis pressure	$N\ m^{-2}$
$q$	wave vector	$m^{-1}$
$q$	(in chapter 6) ratio between $R_v$ and $a$	-
$Q$	dissipation function, ratio between the actual scattering and that calculated according to Rayleigh	-
$Q_f$	flow rate	$m^3\ s^{-1}$
$r$	length scale	$m$
$R_c$	collision radius of a cluster	$m$
$R_{cr}$	critical radius of clusters above which the rate of orthokinetic aggregation exceeds the rate of perikinetic aggregation	$m$
$Re$	Reynolds number	-
$R_g$	3D average radius of the clusters in a gel	$m$

$R_{gyr}$	radius of gyration of a cluster	m
$R_h$	hydrodynamic radius of a cluster	m
$R_l$	radius of the largest flocs that occur in a dispersion	m
$R_m$	radius of the smallest sphere that circumscribes a cluster	m
$R_s$	critical radius of clusters above which sedimentation over a distance $R$ takes less time than diffusion	m
$R_v$	radius of a just visible cluster	m
$R_{xy}$	$x, y$ average cluster radius;	m

$$R_{xy} = \left[ \frac{\sum c(t)R_i^x}{\sum c(t)R_i^y} \right]^{\frac{1}{x-y}}$$

$s$	dimensionless distance between the centres of two particles (fig. 6.2)	-
$S$	distance between centres of two particles (fig. 6.2)	m
$S_2$	$\langle n_i L^2 \rangle$ , Eqn. 3.5	-
$S(q)$	structure factor	-
$t_{1/2}$	time needed to reduce the number of particles to half its initial value	s
$t_a$	aggregation time, time in which aggregation becomes visible due to visible flocs, sedimentation or gelation.	s
$t_c$	time in which visible flocs are just formed	s
$t_g$	time in which gelation occurs	s
$T$	absolute temperature	K
$u$	dimensionless separation between two particles $u = h/a$ (fig. 6.2)	-
$v$	voluminosity	$\text{cm}^3 \text{g}^{-1}$
$v_s$	relative sediment volume (fig. 4.2)	-
$V$	section 5.2.2 volume of the gel	$\text{m}^3$
$V_a$	activation free energy for aggregation (fig. 6.15)	J
$V_b$	activation free energy for junction breakage	J
$V_2$	depth of the secondary minimum	J
$V(s)$	total free energy of interaction between two clusters on distance $s$ from each other	J
$W$	stability ratio	-
$W'$	stability ratio for orthokinetic aggregation	-
$X$	average distance between the peripheries of the flocs	m
$z$	$R_{D0}/R_{3D}$	-
$\alpha$	acceptance angle of the spectrophotometer	rad
$\beta$	chapter II - IV, coefficient in Eqn. 2.21	-
$\beta$	coefficient of volume expansion	$\text{K}^{-1}$
$\gamma$	chapter II - IV, coefficient in Eqn. 2.21	-

$\gamma$	chapter V, shear strain	-
$\gamma_f$	shear strain at which macroscopic fracture occurs	-
$\dot{\gamma}$	shear rate	$s^{-1}$
$\Delta$	distance of closest approach of two particles	m
$\varepsilon$	compressive strain	m
$\phi_0$	volume fraction of the primary particles	-
$\phi_a$	volume fraction of the primary particles in a floc	-
$\phi_{fs}$	surface fraction of the primary particles in a floc	-
$\phi_s$	surface fraction of the primary particles in a cross section through a gel	-
$\phi_{sed}$	volume fraction of particles in a sediment	-
$\Phi$	effective volume fraction of the flocs	-
$\Phi_s$	effective surface fraction of flocs in a cross section through the gel	-
$\eta$	viscosity of the liquid phase	$N m^{-2} s$
$\lambda$	wavelength in air	m
$\mu$	coefficient relating the modulus of a fractal network to the volume fraction of the particles: $G = \phi_0^\mu$	-
$\mu_p$	Poisson ratio	-
$\rho_0$	mass density of the liquid phase	$kg m^{-3}$
$\rho_p$	mass density of the primary particles	$kg m^{-3}$
$\Delta\rho$	$\rho_p - \rho_0$	$kg m^{-3}$
$\rho(x)$	local mass concentration of the primary particles at position $x$	$kg m^{-3}$
$\bar{\rho}$	average mass concentration of the primary particles, equal to $\phi_0\rho_p$	$kg m^{-3}$
$\theta$	scattering angle	rad
$\sigma$	shear stress	$N m^{-2}$
$\sigma_f$	shear stress at which fracture occurs	$N m^{-2}$
$\tau$	turbidity, $\ln(I_0/I)/l$	$m^{-1}$
$\tau_{max}$	maximum turbidity attained by an aggregating system	$m^{-1}$
$\omega$	angular frequency	$rad s^{-1}$
$\psi(i)$	probability that a cluster consists of $i$ particles, $c_i/c$	-

### Some terms and abbreviations used in this study

CSLM	confocal scanning laser microscopy
DLCA	diffusion limited cluster aggregation
RLCA	reaction limited cluster aggregation
GDL	glucono- $\delta$ -lactone
ccc	critical coagulation concentration; for $c_s \geq ccc$ the aggregation is diffusion limited
gel	continuous 3-dimensional network of connected molecules or particles filling the whole volume of a continuous liquid phase
gel point	moment at which the sol-gel transition occurs
type 1 gel	fractal particle gel in which the stress carrying strands are stretched (due to rearrangements after the gel point)
type 2 gel	gel built of interconnected fractal flocs (no significant rearrangement)
coagulation	aggregation due to destabilisation of a sol caused by electrolytes only
junction	the sum of the bonds between two particles
bond	each single interaction or bond in a junction
syneresis	shrinking of the gel network not caused by external forces
microsyneresis	syneresis on a microscopic scale occurring if macroscopic shrinking of the gel is impossible
perikinetic	caused by Brownian motion of the particles
orthokinetic	caused by velocity gradients in the liquid

## Summary

The purpose of this study is to gain insight into the conditions determining whether small particles in a liquid are able to jointly occupy the total volume thus forming a gel network. In order to build a network the colloidal particles have to be 'sticky', unstable. In the unassociated state the particles move at random through the liquid due to collisions with solvent molecules. This movement, called thermal or Brownian motion or diffusion, depends on the temperature and on the size of the particles. By thermal motion particles may meet and subsequently stick, thus forming clusters or flocs. This process is called perikinetic aggregation. Other transport mechanisms that lead to aggregation involve velocity gradients in the dispersion (orthokinetic aggregation) or sedimentation of the flocs.

A model describing the formation of a gel out of aggregating flocs is derived in chapter II. Flocs that are formed by aggregation have in general a fractal geometry. This implies that repetitive levels of detail exist on all length scales between the size of the primary particles and the size of the floc. A floc is built up of smaller flocs that, on their turn, are built of still smaller flocs, etc. Each separate fractal floc has its own geometry, different from that of any other floc. However, all flocs share a similar average structure characterized by a stochastic fractal nature, and are in this respect scale invariant. The efficiency with which flocs fill the available space is expressed by the fractal dimensionality,  $D$ , which is the exponent in the power-law relation between the number of particles in a floc and the size of the floc. A low value of  $D$  implies a small number of particles needed to build up a floc of certain size, and thus a high space-filling efficiency. In a three-dimensional system,  $D$  may attain values between 1 and 3. Computer simulations of the aggregation process yield  $D = 1.8$  if all collisions lead to attachment (diffusion-limited cluster aggregation) and  $D = 2.1$  if the sticking probability is very low (reaction-limited cluster aggregation). Rearrangement of the flocs during aggregation results in higher fractal dimensionalities.

Since  $D$  is generally smaller than 3 the volume fraction of the particles in a fractal floc decreases as the size of the floc increases. When the flocs jointly become space-filling a gel is formed; now the overall volume fraction of particles in the system equals the average volume fraction of particles in the flocs. This implies that fractal flocs have the ability to become space-filling at any volume fraction of primary particles if the flocs have enough space to grow large enough, i.e., if the container is large enough. In section 2.3 a model is derived that describes the relation between the average size of clusters in a gel and the overall volume fraction of the particles.

Gels formed at high and low volume fractions will have similar geometric structures, be it on different length scales, if the relative size distribution of the clusters remains constant during the aggregation process. This is shown experimentally in section 4.3 where micro-graphs of gels at various volume fractions and magnifications are compared. Scale invariance enables the derivation of scaling relations between gel properties and the volume fraction of the particles or the length scale on which the gel is studied. Relations between the permeability and the correlation length versus the volume fraction, and the correlation function and the turbidity versus length scale (wavelength), are derived in section 2.4. These relations can be used to obtain the fractal dimensionality from experimental results.

In chapter III materials and methods are described that have been used to make and study the gels. For the preparation of the gels it is essential that aggregation occurs under quiescent conditions, because velocity gradients may lead to rearrangement of the flocs into more compact clusters with a lower space-filling efficiency. Different methods of destabilisation that have been used to obtain quiescent aggregation, are described: 1) slowly warming up a dispersion that is stable at low, but unstable at higher temperatures, 2) acidification of a dispersion that is unstable at low pH by a slowly hydrolyzing acid precursor, and 3) addition of an enzyme that removes stabilizing compounds from the surface of the particles. The permeability of these gels was studied by measuring the flow rate, caused by a certain pressure gradient, through tubes in which a gel was constrained. The geometry of the network was studied by confocal

scanning laser microscopy. A small spot inside the gel, that is provided with a suitable fluorescent label, is illuminated by a focused laser beam and the fluoresced light that stems from the spot is detected via a microscope in a photon multiplier. Many positions in the gel are scanned in this way and optical sections and three-dimensional images are obtained.

In chapter IV results of the gelation and coagulation studies are described. At quiescent conditions dispersions of small particles may gel at extremely low volume fractions. Spherical, palmitate covered polystyrene particles ( $a = 35$  nm) formed space-filling networks even at volume fractions below 0.1 %! Aggregation caused by electrolyte addition to polystyrene or haematite sols (coagulation) may also result in continuous networks. The mixing of the electrolyte and the sol leads presumably to rearrangement of the flocs into more compact clusters. The volume fraction of particles that was necessary for gel formation turned out to be roughly 5 % at high NaCl concentrations. A relative measure for the coagulation rate is the initial rate of change of the turbidity after electrolyte addition. It is found that at some critical salt concentration, the ccc, this rate attains a maximum; here, the aggregation rate is diffusion limited. In the case of coagulation by NaCl, flocs of polystyrene or haematite particles were relatively compact at the ccc. This resulted in high values of the turbidity plateau that an aggregating system approaches, and in small sediment volumes. At higher NaCl concentration the flocs become more ramified. Presumably, high salt concentrations cause stronger inter-particle junctions and less rearrangement, leading to more ramified flocs.

The fractal dimensionalities obtained from permeability studies were 2.34 and 2.21 for acid casein and palmitate covered polystyrene gels, respectively (section 4.2). From the absolute value of the permeability the ratio between the radius of the clusters in the gel and their effective hydrodynamic radius was estimated to be 1.13. This value is substantially lower than expected from calculations on fractal flocs obtained by computer simulation. The permeability of most gels did not change during ageing, indicating that no large scale rearrangements occur. However, the permeability of rennet-induced casein gels increased during ageing, because microsineresis causes a coarsening of the gel.

Microsyneresis occurs if a gel tends to synerese whereas shrinkage is impossible. The process leads to local condensation of the network and the formation of large pores elsewhere.

Changes in rennet-induced casein gels during ageing are shown on micrographs in section 4.3. The mesh-sizes of fresh rennet induced casein gels and acid casein gels with the same casein concentration are similar, but after ageing the mesh size of rennet-induced gels increases dramatically whereas that of acid gels is constant. Close to the glass surface the density of the gel is relatively high because particles stick to the surface during aggregation. Sections were taken at a depth larger than the diameter of the clusters to ensure the observation of a bulk gel. The fractal dimensionality obtained from the relation between the correlation length in micrographs of acid casein gels and the volume fraction of the particles was 2.35. A similar value was obtained from the relation between the correlation function and the length scale. Results of turbidity measurements as a function of wavelength yielded a value of  $D$  for acid casein gels of roughly 2.3.

Various models may be derived to relate rheological properties of particle gels to the volume fraction of the particles. In addition to the geometric structure of the network, the interactions between and rheological properties of the particles are important. In chapter V two models are derived for gels built up of fractal clusters. One model applies to type 1 gels in which the stress carrying strands in a gel gradually get stretched, e.g. due to microsyneresis. The other model applies to type 2 gels in which no large scale rearrangements occur after the gel point. Rennet induced casein gels and acid casein gels made by slowly warming up a cold (4 °C) casein dispersion of pH 4.6 to 30 °C turned out to be type 1 gels, whereas GDL-induced casein and palmitate covered polystyrene gels were type 2 gels. At the same volume fraction, type 1 casein gels were much stiffer than type 2 gels but the strength, i.e. the stress at which fracture occurs, was roughly similar. The strain at which the gels fracture was larger for type 2 gels. The values of  $D$  obtained by applying the models to results on the shear modulus versus the volume fraction, were 2.24 and 2.36 for type 1 and 2 casein gels, respectively, and 2.26 for palmitate-covered polystyrene gels. The stiffness of all gels studied



increased during ageing. Since permeability studies show that no large scale rearrangements occurred during ageing (except in rennet gels), the increase in stiffness must be due to an increase of the strength of the inter-particle junctions, e.g. due to some kind of sintering.

The aggregation time of an unstable colloidal dispersion, defined as the time after which aggregation becomes visible, depends both on the bond formation rate and on the way the structure of the aggregates develops. The latter is not taken into account in the traditional theory of aggregation kinetics where only the bond formation rate is considered. In chapter VI it is shown that the structure of colloid aggregates has a large effect on the aggregation rate and an even larger one (up to several orders of magnitude) on the aggregation time. Approximate expressions for the aggregation time at different conditions are derived. Due to the intricacy of the subject it is mostly impossible to derive exact expressions. For many situations it is possible, though, to roughly predict the aggregation time. Complications, due to deviations from the ideal case of spherical, smooth, monodisperse particles at low volume fractions, are compiled and their effects on the aggregation rate and time are estimated. It is shown that small velocity gradients often cause a huge decrease of the aggregation time. Small velocity gradients occur also in 'quiescent' systems, e.g. due to convection.

Fractal aggregates will always fill the entire volume if they are allowed to grow without being disturbed. Factors that can disturb the gelation, or change the gel structure, are described in chapter VII. It is argued that small velocity gradients are essential for the formation of networks at very low volume fractions because the flocs forming the network are so large that the time needed for diffusion over a distance equal to the radius of the floc is much longer than the time needed to settle over that distance. Larger velocity gradients may cause compaction or breakup of the flocs, thus hindering gelation. All systems studied in this thesis that gel at low volume fraction show some sintering or fusion, which may be ascribed to an increase in the number of bonds per junction. This may be a prerequisite for aggregation of colloidal particles leading to a gel at low volume fraction.

## Samenvatting

Het doel van dit onderzoek is inzicht te krijgen in de factoren die bepalen of kleine deeltjes in een vloeistof in staat zijn om gezamenlijk het totaal beschikbare volume op te vullen en zodoende een gel netwerk te vormen. Om een netwerk op te bouwen moeten de deeltjes 'plakkerig', instabiel zijn. De deeltjes bewegen kris-kras door de vloeistof door botsingen met vloeistofmoleculen. Deze beweging wordt diffusie, Brownse-, of warmtebeweging genoemd en hangt af van de temperatuur en de grootte van de deeltjes. Door de warmtebeweging kunnen de deeltjes elkaar ontmoeten, plakken en op die manier clusters of vlokken vormen. Dit proces noemt men perikinetische aggregatie. Andere transport-mechanismen die tot aggregatie leiden worden veroorzaakt door stromingen in de dispersie (orthokinetische aggregatie) of door sedimentatie van de vlokken.

De term 'gel' wordt van oudsher gebruikt voor veel verschillende substanties. In dit proefschrift is sprake van een gel wanneer het totale volume van een dispersie opgevuld wordt met een netwerk van gevlokte deeltjes. Een neerslag of precipitaat (of een roomlaag) ontstaat wanneer de vlokken uitzakken of opromen, of als het netwerk niet sterk genoeg is om de zwaartekracht te weerstaan. Hoewel ook neerslagen of roomlagen strikt genomen een gel zijn worden ze hier niet als zodanig aangemerkt. Een ander soort gel bestaat uit een netwerk van lange flexibele macromoleculen die plaatselijk verknoopt zijn. Dit soort gellen heeft een aantal eigenschappen die verschillen van die van gevlokte deeltjesgelen. Het duidelijkste verschil in ruimtelijke structuur is de verhouding tussen de lengte en de dikte van de strengen. In een macromoleculair gel zijn de strengen veel dunner en ze bewegen onder invloed van de warmtebeweging in het wilde weg door de vloeistof. De warmtebeweging zorgt ervoor dat het netwerk het vloeistofvolume op blijft vullen. Het netwerk kan zelfs zwellen wanneer er extra vloeistof aan het gel toegevoegd wordt. Als de aantrekkende kracht tussen de strengen onderling toeneemt (of die tussen de strengen en de vloeistof afneemt) dan zullen er meer knooppunten ontstaan waardoor het netwerk zal inkrimpen en vloeistof uitstoten. Dit proces noemt men synerese. Omdat de structuur van een

macromoleculair gel vooral door de warmtebeweging in stand blijft, wordt zo'n gel een entropisch gel genoemd.

Een gel dat ontstaat uit gevlokte kolloïdale deeltjes heeft in het algemeen veel dikkere, stijve strengen die nauwelijks bewegen onder invloed van de warmtebeweging. Hier blijft het netwerk de ruimte vullen doordat de strengen stevig genoeg zijn om niet in elkaar te zakken door de zwaartekracht, dat wil zeggen door stevige bindingen tussen de deeltjes. Zo'n gel noemt men een enthalpisch gel. Door de starre opbouw zal een enthalpisch gel in het algemeen niet zwellen of synereren onder invloed van de warmtebeweging.

Vlokken gevormd door aggregatie hebben in het algemeen een fractale opbouw. Dit betekent dat steeds dezelfde structuurelementen terugkomen, op alle lengteschalen tussen die van de deeltjes en die van de vlok. Een vlok bestaat uit kleinere vlokken, die op hun beurt uit nog kleinere vlokken bestaan enz. Dit betekent dat grote en kleine vlokken, gemiddeld genomen, op elkaar lijken, alleen de lengteschalen zijn anders. De effectiviteit waarmee vlokken de ruimte vullen kan worden uitgedrukt in een getal, de fractale dimensionaliteit,  $D$ . Het verband tussen de straal van de vlok,  $R$ , de deeltjesstraal,  $a$ , en het aantal deeltjes in de vlok,  $N_p$ , wordt gegeven door de vergelijking  $N_p = (R/a)^D$ . Hiermee wordt ook de term fractale (gebroken) dimensionaliteit duidelijk; een lijn is één- en een vlak twee-dimensionaal omdat een  $x$  maal zo grote lijn  $x^1$  maal zo veel punten bevat en er in een  $x$  maal zo groot vlak  $x^2$  maal zo veel punten zitten. Analooft bevat een  $x$  maal zo grote vlok  $x^D$  maal zo veel deeltjes. Een lage waarde voor  $D$  betekent dat er weinig deeltjes nodig zijn om een vlok van een zeker formaat op te bouwen, en dus een hoog ruimtevullend vermogen. In een 3-dimensionaal systeem kan  $D$  waarden tussen 1 en 3 aannemen. Computer simulaties van het aggregatieproces resulteren in  $D = 1.8$  als alle botsingen effectief zijn, de aggregatiesnelheid van de vlokken wordt door hun Brownse beweging bepaald, en  $D = 2.1$  als de reactiviteit van de clusters bepalend is voor de vloksnelheid. Tijdens de aggregatie kan herstructurering van de vlokken tot een hogere  $D$  (compactere vlokken) leiden.

Omdat  $D$  in het algemeen kleiner is dan 3 neemt de volumefractie van de deeltjes in een vlok af naarmate deze groeit. Op het moment dat

de vlokken ruimtevullend worden (het gelpunt) is de volumefractie van de deeltjes in het systeem gelijk aan de gemiddelde volumefractie in de vlokken. Dit betekent dat fractale vlokken altijd, bij elke volumefractie, in staat zijn ruimtevullend te worden als de vlokken voldoende ruimte hebben om groot genoeg te worden, d.w.z., als de ruimte groot genoeg is. In sectie 2.3 is een model ontwikkeld dat de relatie beschrijft tussen de gemiddelde grootte van de clusters in een gel en de volumefractie van de deeltjes. Simpel gezegd komt deze afleiding erop neer dat het aantal deeltjes in een fractale vlok gelijk is aan  $(R/a)^D$  terwijl het totale volume dat de vlok inneemt, uitgedrukt in het aantal volumina gelijk aan het volume van de primaire deeltjes, gelijk is aan  $N_a = (R/a)^3$ . De volumefractie van de deeltjes in een vlok is dus  $N_p/N_a = (R/a)^{D-3}$  en omdat de volumefractie van de deeltjes in het systeem,  $\phi_0$ , gelijk is aan de gemiddelde volumefractie in de vlokken op het moment dat deze ruimtevullend worden is de gemiddelde grootte van de vlokken in het gel,  $R_g$ , gelijk aan  $a\phi_0^{1/(D-3)}$ .

Als de grootteverdeling van de clusters constant van vorm blijft gedurende de aggregatie dan zullen gelen die bij lage en hoge volumefracties gevormd zijn op elkaar lijken, alleen de lengteschalen zullen anders zijn. Dit is aangetoond in sectie 4.3 waar microscopische opnamen van gelen met verschillende volumefracties en vergroting zijn vergeleken. Schaalinvariantie maakt de afleiding mogelijk van allerlei schalingsrelaties tussen geleigenschappen en de volumefractie van de deeltjes of de lengteschaal waarop het gel bestudeerd is. In sectie 2.4 zijn de doorstroombaarheid en de correlatie-afstand berekend als functie van de volumefractie, en de correlatiefunctie en de troebelheid als functie van de lengteschaal (golflengte). Deze relaties kunnen gebruikt worden om de waarde van  $D$  uit experimentele resultaten af te leiden.

In hoofdstuk III zijn de materialen en methoden die werden gebruikt beschreven. De gelen moeten gemaakt worden zonder dat er (sterke) stromingen in de vloeistof optreden, omdat deze kunnen leiden tot veranderingen in de ruimtelijke structuur van de vlokken waardoor er compactere vlokken ontstaan met een geringer ruimtevullend vermogen. Verschillende methoden hiertoe zijn beschreven in sectie 3.2: 1) Het langzaam opwarmen van een dispersie die stabiel is bij lage, maar

instabiel bij hogere temperatuur, 2) verzuring van een dispersie die instabiel is bij een lage pH met een stof die in water langzaam hydrolyseert tot een zuur en 3) toevoegen van een enzym dat stabiliserende bestanddelen van het deeltjesoppervlak verwijdert. De ruimtelijke structuur van het gel netwerk is onderzocht via doorstroombaarheidsmetingen, die informatie geven over de grootte van de poriën in het gel, en door middel van confocale scanning microscopie. Bij deze laatste techniek wordt aan de dispersie een aan de deeltjes adsorberende fluorescerende stof toegevoegd voordat er een netwerk ontstaat. Na gatering wordt een klein punt in het gel verlicht door een gefocusseerde laserbundel en het gefluoresceerde licht afkomstig van die plek wordt, via een microscoop, gedetecteerd door een fotomultiplicator. Op deze manier worden vele posities in het gel afgetast teneinde optische doorsneden of drie-dimensionale informatie over het gel te verkrijgen.

De resultaten van deze metingen zijn beschreven in hoofdstuk IV. De doorstroombaarheid en de ruimtelijke structuur van de gellen blijven nagenoeg constant. Alleen met leb gestremde caseïne gellen ondergaan veranderingen gedurende veroudering hetgeen te zien is in microscopische opnamen in sectie 4.3. De poriegrootte van verse met leb gestremde en zure gellen met dezelfde caseïneconcentratie zijn ongeveer gelijk, maar na veroudering is de poriegrootte van lebgellen aanzienlijk toegenomen. Dit resulteerde ook in een toename van de doorstroombaarheid tijdens bewaren van het gel. De reden van deze structuurverandering wordt toegeschreven aan zogenaamde microsinerese, hetgeen op treedt als gellen tot synerese neigen terwijl krimp van het netwerk in zijn totaliteit onmogelijk is. Dit leidt tot het straktrekken van de strengen en een lokale verdichting van het netwerk en het ontstaan van grotere gaten elders doordat de strakgetrokken strengen kunnen breken.

De waarde van de effectieve fractale dimensionaliteit lag voor alle gellen die bestudeerd zijn op  $2.3 \pm 0.1$ , nagenoeg onafhankelijk van de methode die gebruikt werd om  $D$  te bepalen. In afwezigheid van verstoringen kunnen deeltjes bij uiterst lage volumefracties nog een netwerk vormen. Bolvormige, met palmitaat bedekte polystyreen deeltjes

met een straal van 35 nm vormden zelfs bij volumefracties lager dan 0.1 % nog een ruimtevullend netwerk.

Voor de reologische eigenschappen zijn, behalve de ruimtelijke structuur van het netwerk ook de interacties tussen de deeltjes en de reologische eigenschappen van de deeltjes zelf van belang. De stevigheid van alle onderzochte gellen bleef toenemen tijdens bewaren. Deze toename moet toegeschreven worden aan een stijging van de sterkte van de bindingen tussen de deeltjes, bijvoorbeeld door een soort sintering, omdat de ruimtelijke structuur van het gel niet veranderde. In hoofdstuk V zijn twee modellen gepresenteerd voor gellen die zijn ontstaan uit fractale clusters. Het ene model geldt voor gellen waarin de strengen zijn rechtgetrokken, bijvoorbeeld door microsinerese. Deze gellen worden hier type 1 gellen genoemd. Het andere model slaat op type 2 gellen waarin geen grote veranderingen hebben plaatsgevonden na de vorming van het gel. Onder gelijke omstandigheden (soort en volumefractie van de deeltjes) zijn gellen van type 1 veel steviger dan die van type 2, maar de sterkte, d.w.z. de spanning waarbij het gel breekt kan ongeveer gelijk zijn. De vervorming waarbij het gel breekt is groter bij type 2.

In hoofdstuk VI is geprobeerd om onder verschillende omstandigheden de aggregatietijd, de tijd waarna aggregatie zichtbaar wordt, uit te rekenen. Hiervoor is, behalve de snelheid waarmee de vlokken elkaar ontmoeten en een binding vormen, ook de manier waarop de vlokstructuur zich ontwikkelt van belang. Als de fractale dimensionaliteit van de vlokken laag is dan bevat een vlok met een zekere grootte relatief weinig deeltjes, en zijn er dus relatief weinig botsingen nodig geweest om de vlok te vormen. Een lage  $D$  leidt dus tot een korte aggregatietijd. Wanneer de vlokken eenmaal een kritieke grootte bereikt hebben dan wordt aggregatie snel zichtbaar. Deze kritieke grootte kan de vloggrootte zijn waarbij de vlokken ruimtevullend worden en een gel vormen, maar ook de grootte waarbij vlokking onder invloed van sedimentatie of stromingen belangrijker wordt dan perikinetische vlokking. Als deze vloggrootte bereikt is zal de verdere aggregatie steeds sneller verlopen en zullen er binnen korte tijd zichtbare vlokken, een ruimtevullend netwerk of een precipitaat ontstaan. Kleine stromingen blijken tot een enorme

vermindering van de aggregatietijd te leiden. Deze stromingen ontstaan ook in een systeem 'in rust', bijvoorbeeld door convectie (temperatuurverschillen).

Fractale aggregaten zullen altijd het geheel beschikbare volume opvullen wanneer de aggregatie niet verstoord wordt. Factoren die de gelering kunnen verstoren of de gelstructuur veranderen zijn beschreven in hoofdstuk VII. Kleine stromingen zijn essentieel voor de vorming van netwerken bij heel lage volumefractie, doordat de vlokken hierin zo groot zijn dat ze al lang uitgezakt zouden zijn voordat ze door de warmtebeweging een netwerk gevormd zouden hebben. Sterkere stromingen kunnen de vlokken samendrukken of opbreken en dus de gelering verstoren.

Een netwerk met een lage volumefractie is vaak niet in staat om te voorkomen dat het onder invloed van de zwaartekracht in elkaar gedrukt wordt. Alleen als het netwerk aan de wanden van het potje blijft plakken zal het niet in elkaar zakken. Hiervoor zijn sterke bindingen tussen de deeltjes nodig die kunnen ontstaan wanneer deze een groter contactoppervlak krijgen, bijvoorbeeld door een soort sintering. Dit is waarschijnlijk een essentiële voorwaarde voor de vorming van gelen bij lage volumefracties.

## Curriculum Vitae

De schrijver van dit proefschrift werd op 23 juni 1963 in Bommel geboren. In 1981 behaalde hij het diploma Atheneum B aan het Canisius College te Nijmegen waarna hij begon met zijn studie moleculaire wetenschappen aan de Landbouw Universiteit.

In september 1985 legde hij het kandidaatsexamen af en in september 1987 het doctoraal met als hoofdvakken kolloïdchemie en microbiologie. Stages werden vervuld aan het Institute for Surface Chemistry in Stockholm en bij Akzo corporate research in Arnhem.

Op 1 juni 1987 trad hij in dienst bij de vakgroep Fysische en Kolloïd Chemie waar hij, in samenwerking met de sectie Zuivel en Levensmiddelen natuurkunde, het in dit proefschrift beschreven onderzoek uitvoerde.

Per 1 januari 1992 begint hij aan een door DSM gesponsord onderzoek aan de Vrije Universiteit Brussel waarna hij in dienst zal treden bij DSM Research in Geleen.



## Nawoord

Graag wil ik iedereen die op enigerlei wijze aan de totstandkoming van dit proefschrift heeft meegewerkt bedanken. Ik ga hier niet iedereen met name noemen omdat het proefschrift al dik genoeg is. Enkele groepen, paren of personen komen echter niet onder een vermelding uit.

Allereerst wil ik mijn ouders bedanken omdat ze mij de gelegenheid gaven om te studeren, maar ook voor hun morele financiële en logistieke steun. In de laatste fase van de promotie heb ik thuis een werkkamer ingericht die een welhaast magische aantrekkingskracht op papier bleek te hebben. Ondanks al die kubieke meters papier, die ongetwijfeld een doorn in het oog van mijn moeder waren, bleef de bovengenoemde steun onverminderd bestaan.

De zeer hoog geleerde (co-)promotoren Pieter Walstra, Bert Bijsterbosch en Ton van Vliet zijn van essentieel belang geweest voor dit proefschrift. Door hun kritische bestudering en grondige correctie van mijn teksten is dit boekje enigszins leesbaar geworden. Behalve voor bovengenoemde, niet onbelangrijke, bijdrage ben ik zeer dankbaar voor de vrijheid die ik heb gekregen in de uitwerking van het onderzoek. Ik denk dat wij ruim vier jaar lang als een goed team hebben gefunctioneerd. Het enthousiasme en de ideeën-rijkdom van Pieter Walstra hebben mij gestimuleerd terwijl Bert Bijsterbosch de grote lijnen goed in het oog hield. Door de ideale positie van mijn bureau op de sectie zuivel had ik een goed overzicht over de werkzaamheden van Ton van Vliet. Op de weinige momenten waarop Ton niet ontzettend druk was kon ik daarom gemakkelijk binnenstappen om te profiteren van zijn reologisch vakmanschap.

I am grateful to Yasuhisa Adachi for helpful discussions which have led to many new ideas (I hope for both of us). Some of these ideas have been inserted on various places in this thesis. (e.g. section 4.2, chapter VI and section 7.2.1)

De samenwerking met Robert Schrijvers is zeer vruchtbaar gebleken. Het grootste gedeelte van sectie 5.3 is overgenomen uit zijn doctoraalverslag. William Kloek heeft in zijn vrije tijd nogal wat programmeerwerk verricht, onder andere om op een snelle manier

correlatie-functies uit te rekenen. Resultaten hiervan zijn gebruikt in sectie 4.3 en 4.4. Met veel genoegen heb ik, onder het genot van een van Williams zelf gebrouwde bieren, mogen ervaren hoe de grens tussen computerspel en wetenschappelijk onderzoek vervaagde.

Een prettige werksfeer draagt naar mijn mening bij tot de kwaliteit van het onderzoek. Daarom ben ik blij dat ik meerdere prettige werksferen heb mogen ervaren: Zuivel en levensmiddelen natuurkunde, fysische en kolloïd chemie op het Dreyenplein en de onderwijsgroep op het Transitorium. Hiervoor wil ik iedereen die gedurende mijn promotie-onderzoek als medewerker of student bij Fysko of ZLMN werkzaam was hartelijk bedanken. Met plezier denk ik terug aan het hardlopen voor en tijdens de Veluweloop, het zwemmen, het squachen, het gourmetten op Trans, de uitstapjes, feestjes enz.

Ook van buiten de vakgroep Fysko en de sectie zuivel en levensmiddelen natuurkunde (ZLMN) heb ik veel hulp ondervonden. Met plezier denk ik terug aan de samenwerking met Siebe Henstra, en later met El Bouw van TFDL. Verder worden Dr. M.H. Hendriks van de vakgroep wiskunde en Dr. J.W.Th. Lichtenbelt en Dr. B. Reuvers van Akzo corporate research in Arnhem in dit proefschrift bedankt voor hun bijdrage. Vele anderen hebben via (voor mij) interessante discussies meer of minder directe bijdragen geleverd. Bedankt.